PB92-176973

NATIONAL CENTER FOR EARTHQUAKE
ENGINEERING RESEARCH
State University of New York at Buffalo

Experimental and Theoretical Study of a Sliding Isolation System for Bridges

by

M. C. Constantinou, A. Kartoum, A. M. Reinhorn and P. Bradford
Department of Civil Engineering
State University of New York at Buffalo
Buffalo, New York 14260

Technical Report NCEER-91-0027

November 15, 1991

This research was conducted at the State University of New York at Buffalo and was partially supported by the National Science Foundation under Grant No. ECE 86-07591.

NOTICE

This report was prepared by the State University of New York at Buffalo as a result of research sponsored by the National Center for Earthquake Engineering Research (NCEER). Neither NCEER, associates of NCEER, its sponsors, State University of New York at Buffalo, nor any person acting on their behalf

a. makes any warranty, express or implied, with respect to the use of any information, apparatus, method, or process disclosed in this report or that such use may not infringe upon privately owned rights; or

b. assumes any liabilities of whatsoever kind with respect to the use of, or the damage resulting from the use of, any information, apparatus, method or process disclosed in this report

50272-101

REPORT DOCUMENTATION PAGE	1. REPORT NO. NCEER-91-0027	2.	3 PB92-176973

4. Title and Subtitle Experimental and Theoretical Study of a Sliding Isolation System for Bridges	5. Report Date November 15, 1991 6.
7. Author(s) M.C. Constantinou, A. Kartoum, A.M. Reinhorn, P. Bradford	8. Performing Organization Rept. No.
9. Performing Organization Name and Address Department of Civil Engineering State University of New York at Buffalo Buffalo, New York 14260	10. Project/Task/Work Unit No. 11. Contract(C) or Grant(G) No. (C) CES-8857080 (G) ECE 86-07591
12. Sponsoring Organization Name and Address National Center for Earthquake Engineering Research State University of New York at Buffalo Red Jacket Quadrangle Buffalo, N.Y. 14261	13. Type of Report & Period Covered Technical Report 14.

15. Supplementary Notes
This research was conducted at the State University of New York at Buffalo and was partially supported by the National Science Foundation under Grant No. ECE 86-07591.

16. Abstract (Limit: 200 words) A seismic isolation system for bridges has been tested on a shake table. The system consisted of Teflon disc bridge bearings and displacement control devices. These devices provided restoring force for re-centering the bridge during earthquake excitation, additional energy dissipation capacity and rigidity for service loading. The tests were carried out with a 51-kip (227 kN) model which was subjected to strong recorded earthquake motions with a wide range of frequency content and to simulated motions compatible with CALTRANS 0.6g design spectra. In all tests the isolated deck responded with peak acceleration less than the peak table acceleration and peak displacement less than the peak table displacement. Furthermore, results are presented on a parametric study of the response of bridges supported by this isolation system. The isolated bridges are subjected to simulated earthquake motions which are compatible with CALTRANS design spectra. The effects of isolation system properties, deck flexibility, pier flexibility, pier strength, distribution of isolation elements and earthquake type are investigated. Finally, simplified, code-type analysis methods for sliding isolated bridges are presented and evaluated.

17. Document Analysis a. Descriptors

b. Identifiers/Open-Ended Terms

EARTHQUAKE ENGINEERING. BRIDGES. SLIDING ISOLATION SYSTEMS. VIBRATION ISOLATION. TEFLON DISC BRIDGE BEARINGS. DISPLACEMENT CONTROL DEVICES. SHAKING TABLE TESTS. BASE ISOLATION. ENERGY DISSIPATION. SEISMIC RESPONSE ANALYSIS.

c. COSATI Field/Group

18. Availability Statement	19. Security Class (This Report)	21. No. of Pages
Release Unlimited	Unclassified	[redacted]
	20. Security Class (This Page) Unclassified	22. Price

Experimental and Theoretical Study of a Sliding Isolation System for Bridges

by

M.C. Constantinou[1], A. Kartoum[2], A.M. Reinhorn[3] and P. Bradford[2]

November 15, 1991

Technical Report NCEER-91-0027

NCEER Project Numbers 89-2101 and 90-2101

and

NSF Grant Number CES-8857080

NSF Master Contract Number ECE 86-07591

1 Associate Professor, Department of Civil Engineering, State University of New York at Buffalo
2 Research Engineer, Imbsen Associates, Inc., Sacremento, California; former Graduate Student, Department of Civil Engineering, State University of New York at Buffalo
3 Professor, Department of Civil Engineering, State University of New York at Buffalo
4 Engineer, Watson Bowman Acme Corp., Amherst, New York

NATIONAL CENTER FOR EARTHQUAKE ENGINEERING RESEARCH
State University of New York at Buffalo
Red Jacket Quadrangle, Buffalo, NY 14261

PREFACE

The National Center for Earthquake Engineering Research (NCEER) is devoted to the expansion and dissemination of knowledge about earthquakes, the improvement of earthquake-resistant design, and the implementation of seismic hazard mitigation procedures to minimize loss of lives and property. The emphasis is on structures and lifelines that are found in zones of moderate to high seismicity throughout the United States.

NCEER's research is being carried out in an integrated and coordinated manner following a structured program. The current research program comprises four main areas:

- Existing and New Structures
- Secondary and Protective Systems
- Lifeline Systems
- Disaster Research and Planning

This technical report pertains to Program 2, Secondary and Protective Systems, and more specifically, to protective systems. Protective Systems are devices or systems which, when incorporated into a structure, help to improve the structure's ability to withstand seismic or other environmental loads. These systems can be passive, such as base isolators or viscoelastic dampers; or active, such as active tendons or active mass dampers; or combined passive-active systems.

Passive protective systems constitute one of the important areas of research. Current research activities, as shown schematically in the figure below, include the following:

1. Compilation and evaluation of available data.
2. Development of comprehensive analytical models.
3. Development of performance criteria and standardized testing procedures.
4. Development of simplified, code-type methods for analysis and design.

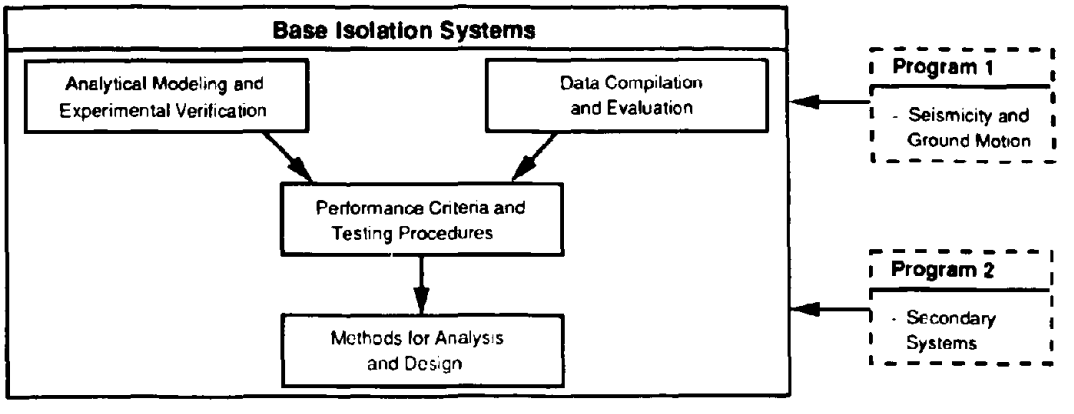

Presented in this report are the results of an analytical and experimental study of a seismic isolation system for bridges. The system, consisting of Teflon disc bearings and displacement control devices, provides restoring force for re-centering, added energy dissipation capacity and rigidity for service loads. The tests were conducted on a shaking table using a quarter-scale 51 kip model. The effects of pier flexibility and strength, deck flexibility and distribution of isolation elements on the dynamic response of sliding isolated bridges were studied analytically.

ABSTRACT

A seismic isolation system for bridges has been tested on a shake table. The system consisted of Teflon disc bridge bearings and displacement control devices. These devices provided restoring force for re-centering the bridge during earthquake excitation, additional energy dissipation capacity and rigidity for service loading. The tests were carried out with a 51-kip (227 kN) model which was subjected to strong recorded earthquake motions with a wide range of frequency content and to simulated motions compatible with CALTRANS 0.6g design spectra. In all tests the isolated deck responded with peak acceleration less than the peak table acceleration and peak displacement less than the peak table displacement. Analytical techniques are presented that provide interpretation of the experimental results.

Furthermore, results are presented on a parametric study of the response of bridges supported by this isolation system. The isolated bridges are subjected to simulated earthquake motions which are compatible with CALTRANS design spectra. The effects of isolation system properties, deck flexibility, pier flexibility, pier strength, distribution of isolation elements and earthquake type are investigated. Results are presented in a form that is useful in the design of sliding isolation systems for two-span continuous deck bridges. Comparisons with the response of conventionally built bridges demonstrate the significant benefits of seismic isolation.

Finally, simplified, code-type analysis methods for sliding isolated bridges are presented and evaluated.

ACKNOWLEDGEMENTS

Financial support has been provided by the National Center for Earthquake Engineering Research (contracts 89-2101, 90-2101), the National Science Foundation (Grant CES 8857080) and Watson Bowman Acme Corporation, Amherst, New York.

TABLE OF CONTENTS

LIST OF ILLUSTRATIONS

LIST OF TABLES

SECTION 1

INTRODUCTION

Seismic isolation systems are typified by use of either elastomeric or sliding bearings. Elastomeric systems reduce the fundamental frequency of the isolated structure so that the isolation effect is produced by primarily deflecting rather than absorbing the earthquake energy (Kelly 1991). This results in-phase response with low accelerations and large bearing displacements. Reduction of bearing displacements is accomplished by use of either damping-enhanced rubber or by use of additional energy dissipating elements like mild steel dampers, lead plugs in the bearings (Buckle 1990) or frictional elements (Chalhoub 1989). The introduction of significant hysteretic type of damping may create out-of-phase response and larger response acceleration in flexible, tall structures (Chalhoub 1989). However, the story shear forces and drifts are maintained at values comparable to those of purely elastomeric isolation systems because of the out-of-phase response (Constantinou 1991a; Mokha 1991b).

In bridges, which have squatty and stiff superstructures, this behavior does not occur and a significant isolation effect may be produced with both low acceleration and displacement response. This has been demonstrated by Kelly et al. (1986b) in shake table tests of an isolated bridge deck supported by elastomeric bearings with and without lead plugs. Hence, elastomeric bearings/mild steel devices and lead-rubber bearings found application in bridge

isolation in New Zealand, United States and elsewhere (Buckle 1990).

Sliding isolation systems produce the isolation effect by limiting the transfer of force across the isolation interface and by absorbing earthquake energy. They are characterized by insensitivity to the frequency content of earthquake excitation, stability, and low bearing displacements. The insensitivity to the frequency content of input motion results from the tendency of sliding isolation systems to reduce and spread the earthquake energy over a wide range of frequencies. Sliding isolation systems have found several applications in buildings and bridges. Most notably, Italian engineers designed several bridges on sliding isolation bearings with restoring force devices. Section 2 of this report presents a review of applications of sliding isolation systems.

Sliding seismic isolation systems for bridges consist of multi-directional sliding bridge bearings and restoring force devices. These devices are useful in re-centering the bridge during earthquakes, in absorbing further earthquake energy and in providing rigidity to service loads. Recently, Constantinou et al. (1991b) described a seismic isolation system for bridges which utilizes bridge Teflon bearings and displacement control devices. The system relies on the combination of strong frictional force and weak restoring force to produce significant isolation effect with low bearing displacements. The advantages that are realized from this result are:

(a) Significant reduction of the seismic forces that are transferred to the bridge substructure,

(b) Ability of the designer to direct the seismic loads to those elements of the substructure that are most capable of resisting them,

(c) Ability to accommodate multi-directional non-seismic movement as that of horizontally curved bridges, and

(d) Use of short modular expansion joints.

The implications of the reduction of the seismic forces that are transferred to the substructure become evident in an examination of the recently developed AASHTO Seismic Isolation Design Requirements (AASHTO 1991; Mayes 1991). In non-essential bridges, the same Response Modification Factors (R-Factors) as in non-isolated bridges may be used. This option provides the same level of seismic safety in the two types of construction. In this case the advantage of the seismic isolation design is to realize substantial cost savings, provided that seismic forces govern the bridge design (Mayes 1991).

In essential bridges, in which significant damage and disruption of traffic are unacceptable, an R-Factor of 1.5 is recommended for the seismic isolation design. In this case the substructure of the isolated bridge is designed for the same order of magnitude of seismic forces as a conventional bridge. However, the isolation design ensures essentially elastic behavior in the substructure with potential for substantial life-cycle cost savings for the bridge.

The distribution of the seismic forces to the elements of the substructure is accomplished by proper positioning of the restoring force devices and by use of low friction sliding bearings at the elements with low strength and ductility capacity. This ability is particularly useful in the retrofit of bridges with inadequate strength and ductility capacity.

The sliding isolation system described by Constantinou et al. (1991b) is the subject of the experimental and analytical study reported herein. The experimental study consisted of shake table testing of a quarter-scale, 51 kip (227.4kN) bridge deck supported by this isolation system. The model was subjected to a large number of real and artificial earthquake motions. The tests demonstrated good isolation effectiveness with both the deck peak acceleration and displacement being less than the table peak acceleration and displacement, respectively. Analytical techniques are presented which reproduce the recorded response with good accuracy.

The experiments were conducted with a rigid bridge deck model with the isolation system supported by rigid supports. The possible significant effects of pier flexibility, pier strength, deck flexibility and distribution of isolation elements could not be studied in the experimental program. A study of these effects was attempted by resorting to analytical methods. These methods utilized the experimentally calibrated model of the isolation system.

The analytical study primarily concentrated on the dynamic response of a two-span continuous deck bridge with a pier at its center. The bridge was excited in its longitudinal and transverse directions by motions compatible with the California Department of Transportation (CALTRANS) bridge design spectra (Gates 1979). Results on bearing displacements, accelerations above and below the isolation interface and pier displacement ductility demand were obtained. Comparison of these results to corresponding results of conventional non-isolated bridges demonstrated the significant benefits of isolation. These benefits are significant reduction or elimination of ductility demand in the pier and reduction of the deck displacement with respect to the ground.

While isolation systems for bridges found wide application with more than 200 bridges already on sliding systems (see Section 2), large scale testing of bridge sliding isolation systems has not been conducted. The tests reported herein represent the first such attempt. Earlier large scale shake table testing of isolated bridge structures has been restricted to elastomeric systems. The earliest of these tests were conducted with a 96 kip (427 kN) rigid deck model at U.C. Berkeley (Kelly 1986b). Very recently, shake table tests of a 88 kip (392.4 kN) rigid deck model on elastomeric bearings were conducted at the Public Works Research Institute (PWRI) in Japan.

SECTION 2

APPLICATIONS OF SLIDING SEISMIC ISOLATION SYSTEMS

Historical reviews of seismic isolation clearly indicate that sliding systems represent a conceptually simple method of seismic isolation (Kelly 1986a; Buckle 1990). Purely sliding systems impose a limit to the transfer of force across the sliding interface and, thus, they provide an isolation mechanism which is completely insensitive to the characteristics of the earthquake excitation. However, purely sliding systems lack restoring force capability (are not self-centering) and large permanent displacements following an earthquake are possible (Constantinou 1991a). Modern sliding isolation systems combine sliding bearings of quantifiable and controlled frictional properties and restoring force devices. Applications of sliding isolation systems are numerous.

Some important applications of sliding isolation systems are presented in the sequel in chronological order of construction:

1. **Twelve Buildings in Sevastopol, U.S.S.R.**

Built since 1972 these 5-story to 9-story large panel buildings have a total area of 75000m^2. They are supported by ellipsoidal bearings which utilize the weight of the structure to provide restoring force. Three of these buildings were constructed prior to the March 4, 1977 Sevastopol earthquake. All three performed well during the earthquake (Eisenberg 1990).

2. **Bridges for Shinkansen, Japan**

Since the late 1970's over 100 prestressed concrete railway bridges for the Shinkansen (bullet train) were built on sliding isolation systems. The bridges consist of long continuous deck on top of several piers which are strong in their transverse direction. Isolation in the transverse direction could not provide any benefits so that only the longitudinal direction was isolated. The isolation system consists of sliding bearings and shear keys embedded in viscous fluid. This device, called the KP-stopper, restricts displacements within certain limits (Buckle 1990).

3. **Koeberg Nuclear Power Plant, S. Africa**

Built in the late 1970's, this structure represents the world's largest isolated structure. Two thousand sliding bearings on top of 600 pedestals support the 100m by 150m raft of two 900 MWe nuclear power units. The weight of the isolated structure is 364000 metric tons. The sliding bearings which consists of an elastomeric and a sliding leaded bronze-stainless steel part were developed by Electricite de France (EDF). This isolation system lacks self-centering capability (Gueraud 1985).

4. **Bridges in Italy**

Italian engineers employed seismic isolation for the first time in 1974. Following the devastating earthquakes of 1976 at Fruili and 1981 at Irpinia the application of the concept in bridges accelerated. Today about 150 bridges with total length exceeding 150 Km are isolated by systems which utilize sliding bearings and energy dissipating-restoring force devices in the form

of either liquid spring-dampers or elastoplastic devices made of steel (Medeot 1991). A large number of these bridges are isolated only in their longitudinal direction because the piers have adequate transverse force capacity so that isolation in the transverse direction is not necessary.

One of the most recent applications of sliding isolation systems in Italy is in the Mortaiolo double viaduct on the Livorno-Civitavecchia highway. It is 9.6 Km long and is divided into continuous sections of 10 spans each with each span having 30 to 50m length. Each section is supported by several multi-directional sliding bearings with hysteretic steel energy dissipators integrated in most of the bearings. Construction of the viaduct was completed in 1990 (Marioni 1991).

5. **Buildings in Frunze, Middle Asia, U.S.S.R.**

Eighteen 5-story to 8-story brick-masonry and large panel buildings of total floor area of 90000m^2 were constructed in the late 1980's. All are supported by sliding stainless steel-Teflon bearings with restoring force devices (Eisenberg 1990).

6. **Buildings in Japan**

Three buildings in Japan are isolated by the so-called TASS system which was developed by TAISEI Corporation (Kawamura 1988). The isolation system consists of TFE-elastomeric sliding bearings and rubber springs for providing the restoring force. The first building was constructed in 1988 and it is a 4-story office building in Yokohama. In 1989 and 1990 two more buildings were constructed in Kamo-gun and Yokkaichi-shi.

7. Applications of Friction Pendulum (FPS) Bearings, U.S.A.

A water tank of Dow Chemicals and an apartment building in San Francisco are isolated by FPS bearings (Zayas 1987; Mokha 1991b). In these bearings the sliding surface is spherically shaped so that restoring force is produced during rising of the structure along the spherical surface. Construction of the apartment building was completed in early 1991.

The large number of isolated bridges by sliding systems demonstrates the popularity of sliding seismic isolation for bridges for a number of years. The reason for this popularity may be found in the fact that bridges are typically constructed on sliding bearings for accommodating thermal movements and creep and shrinkage of concrete. Seismic isolation is easily achieved by replacing the fixed and guided bearings used in conventional bridge construction with multidirectional sliding bearings and with the addition of restoring force devices. If the restoring force devices are capable of providing rigidity under service loads, the function of the isolated bridge under loading other than seismic remains essentially the same as that of the conventional non-isolated bridge (Constantinou 1991b).

SECTION 3

DISPLACEMENT CONTROL DEVICE FOR ISOLATED BRIDGES

Restoring force devices for sliding isolated bridges are useful in re-centering the bridge during earthquakes, in absorbing further earthquake energy and in providing rigidity to service loads. One implemented form of such devices relies on the reliable yielding properties of mild steel to produce these functions (Medeot 1991, Marioni 1991).

The restoring force device used in the work described in this report carries the name displacement control device (or DCD) and its design and function has been described by Constantinou et al. (1991b). Its behavior is bilinear hysteretic and it is produced by purely mechanical means so that its fatigue life is unlimited. A brief description of this device is presented herein.

Figure 3-1a shows a possible configuration of a single span conventionally built bridge. Uni-directional disc sliding bearings are used on one side to allow for thermal expansion and fixed bearings are used on the other side. Seismic and service horizontal loads are transferred to the abutments by the shear restriction mechanism of the bearings. In providing a seismic isolation system to this bridge deck, multidirectional sliding bearings may be used together with displacement control devices as illustrated in Figure 3-1b. The displacement control devices act only in their longitudinal direction and are connected to the deck and abutments by universal joints. They exhibit a behavior which

is bilinear hysteretic with high initial and unloading stiffnesses and characteristic strength F_c. An idealized force-displacement relation of the displacement control device is shown in Figure 3-2. The isolated bridge behaves in a manner identical to the conventional bridge for forces less than the combined characteristic strength of the displacement control devices.

Another configuration of an isolated two-span continuous deck bridge is shown in Figure 3-3. The displacement control devices in this bridge are intentionally placed at the abutments so that the force transmitted to the presumably weak pier is minimized. This, together with proper selection of the frictional properties of sliding bearings, enables a designer to direct the seismic loads to the strongest elements of the bridge substructure.

Each displacement control device consists of the spring and frictional assemblies which are connected in series as shown in Figure 3-4. On loading of the device no motion occurs as long as the force is less than the characteristic strength of the device which is equal to the frictional force, F_c, that may be mobilized in the frictional assembly. When the force exceeds the limit F_c, sliding at the frictional assembly occurs and the spring assembly is compressed. On unloading the frictional force reverses direction and the spring is decompressed resulting in the force-displacement loop shown in Figure 3-2. The slope of the curve, K, is equal to the spring constant of the spring assembly. Accordingly, the device provides rigidity for forces up to the

limit of its characteristic strength and flexibility and energy dissipation capacity for strong forces which exceed this limit.

3.1 Frictional Assembly

The frictional assembly is shown in Figure 3-5. It consists of a stainless steel shaft machined flat and with a slotted hole. Two bronze plates are compressed against the stainless steel part by a high strength bolt which runs through the assembly. The bronze plates are recessed in backing plates which are supported by two steel plates (parts 4P7 in Figure 3-4). A load cell is used to measure the normal load (bolt tension or preload) on the sliding interface and belleville washers are used to control the bolt tension.

The bronze plates are impregnated with graphite along lines at 45° angle with the longitudinal axis. The graphite provides continuous lubrication of the rubbing parts which results in extremely low wear rate, stable frictional properties and silent operation.

3.2 Spring Assembly

Figure 3-6 shows the spring assembly. A helical steel spring is bounded on top by a spring hook. Guide bars (parts 2M1 and 2P3) are used to support the sides and bottom of the spring. When the bottom plate (part 2P1) moves downwards, load is transferred to the hook by the central bolt (part 4B4) and the spring is compressed between the hook and plates 2P3 which are supported by the guide bars. On return the spring is decompressed until the hook reaches the top plate (part 2P2). At that time the central bolt

disconnects from the hook, it moves in the open space provided by the hook and the bottom plate (part 2P1) compresses the spring. It should be noted that the guide bars and the spring hook are placed at right angle so that there is no interference.

The spring is always in compression. There are two important advantages when the spring is subjected to only compression. First the stiffness of the assembly is the same when the bottom plate moves up or down as shown in Figure 3-6. It should be noted that helical steel springs exhibit different stiffness when they are in tension than when they are in compression. The compression stiffness of the spring is practically constant to displacements of about 0.3 times the free length of the spring. Beyond this limit the stiffness increases rapidly to a very large value when solid height is reached. This represents the second advantage. Stiffness increases at large displacements so that fail-safe action is provided. It should be noted that helical springs which are subjected to tension become softer at large displacements, a behavior which is undesirable.

Alternatively, a rubber spring may be used in place of the helical steel spring. The rubber spring has the advantages of low weight, large displacement capacity in comparison to size and wide range of stiffnesses for constant spring volume. Furthermore, a rubber spring exhibits gradual increase of its stiffness during compression due to bulging.

3.3 Operation of Displacement Control Device

The spring and frictional assemblies are connected in series as shown in Figure 3-4. The backing plates housing the graphite impregnated bronze plates of the frictional assembly are press fitted between two steel plates (parts 4P7) and compressed by the tension bolt of the frictional assembly. The steel plates (parts 4P7) transfer the mobilized frictional force to the skin of the device (part 4M3) which in turn transfers the force to the end plate (part 2P2). When the outer shaft moves to the right the spring is compressed by the spring hook and the spring force is transferred to the end plate (part 2P2) by the guide bars (part 2M1). When the outer shaft moves to the left the spring is compressed by plate 2P1 and the spring force is transferred to plate 2P2 by the spring hook as illustrated in Figure 3-6.

The force-displacement relation produced by the displacement control device is illustrated in Figure 3-2. Upon loading the force increases without any movement in the device until the characteristic strength of the frictional assembly is reached. The characteristic strength is the mobilized frictional force at the graphite-bronze-stainless-steel interface when sliding occurs. It is given by:

$$F_c = 2\mu N \qquad (3\text{-}1)$$

in which μ is the coefficient of friction at the sliding interface of bronze and steel and N is the tension force in the bolt of the

frictional assembly. When sliding occurs the spring is compressed and the force increases beyond the value F_c by the product of the spring stiffness, K, and displacement. Upon unloading the frictional force changes direction and the total force drops by an amount equal to $2F_c$, resulting in the loop shown in Figure 3-2.

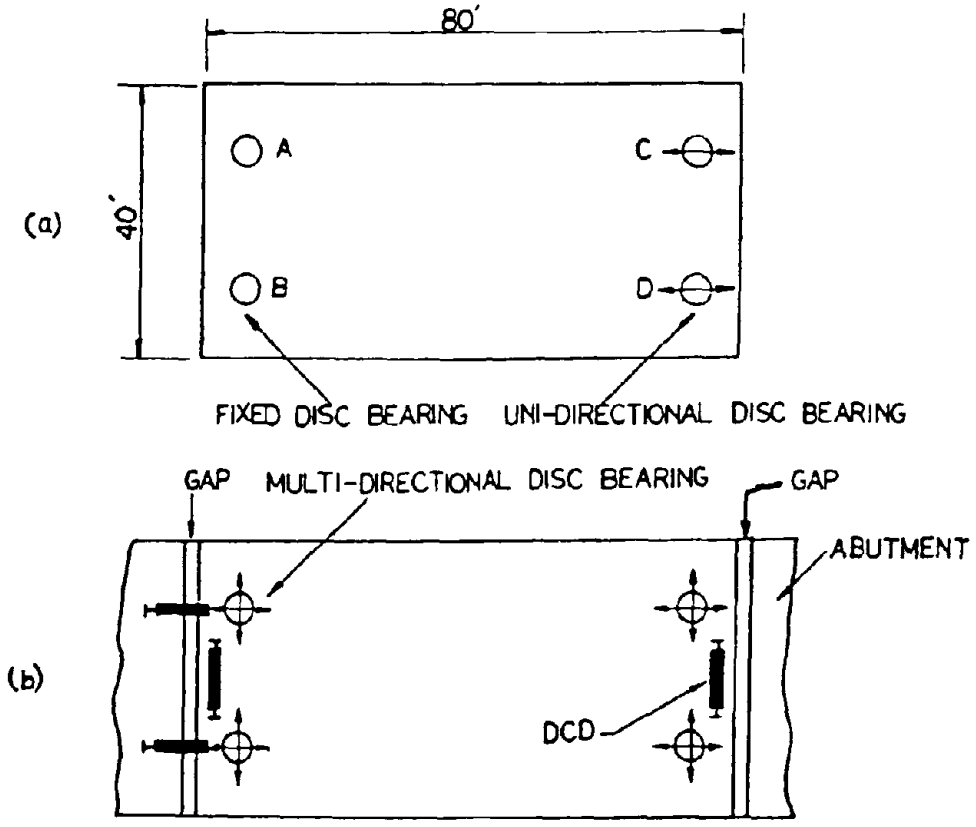

Fig. 3-1 Single Span Bridge on Sliding Bearings (a) Conventional Bridge (b) Base-isolated Bridge.

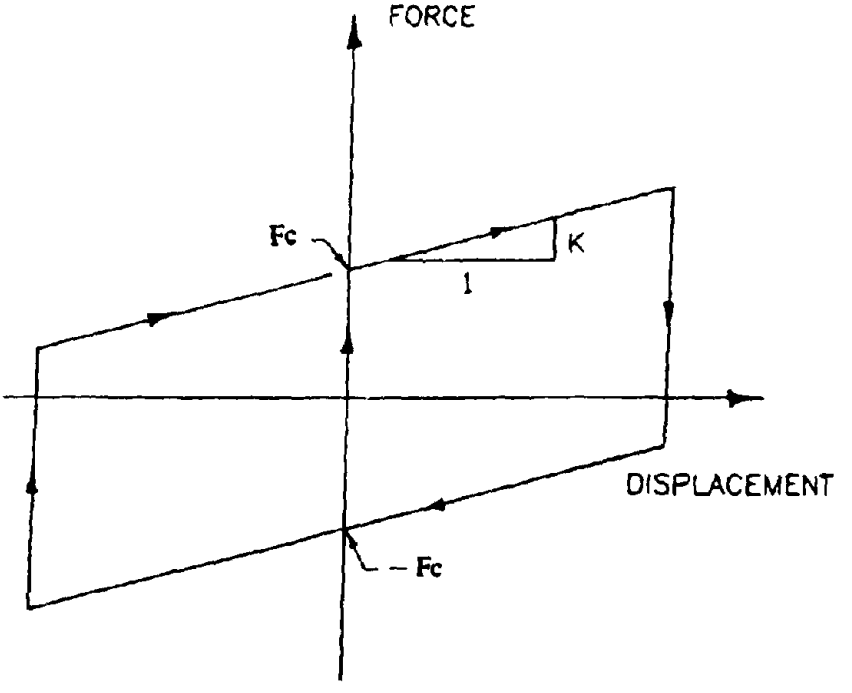

Fig. 3-2 - Idealized Force-displacement Loop of Displacement Control Device.

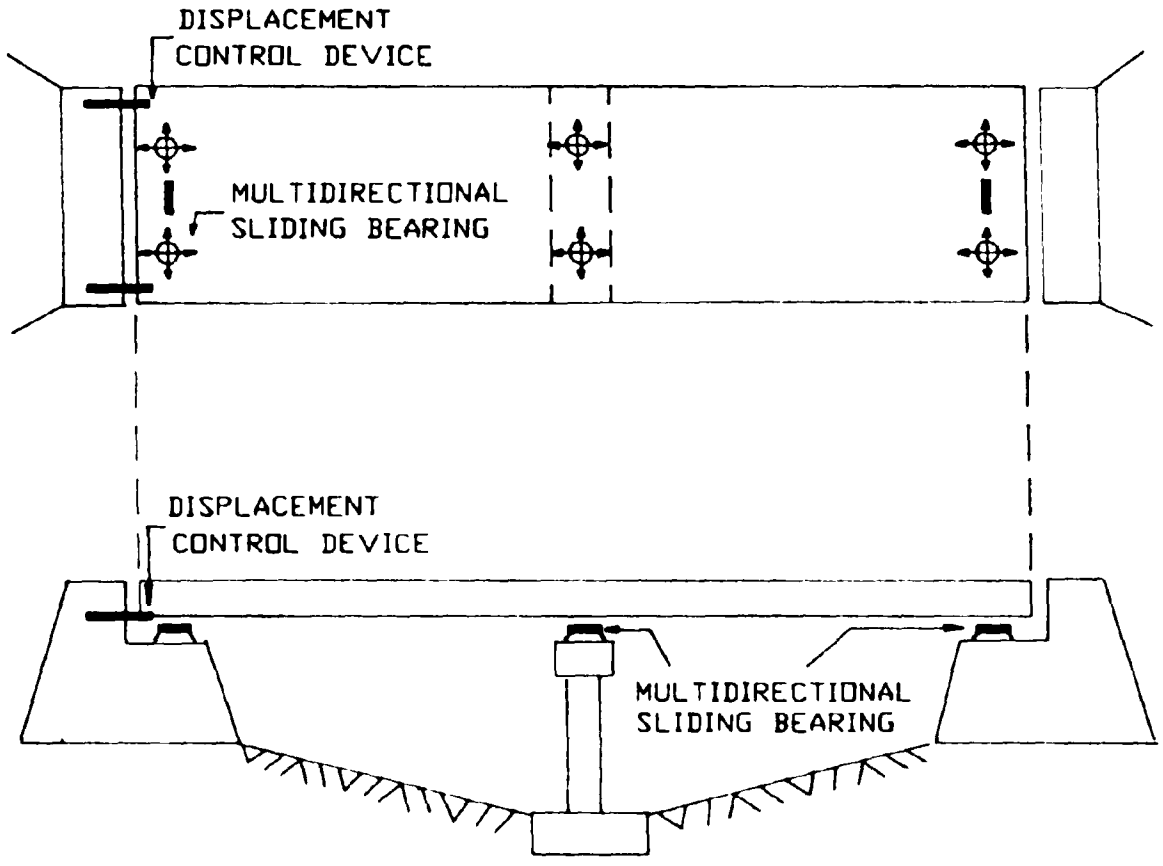

Fig. 3-3 - Two-span Continous Deck Isolated Bridge.

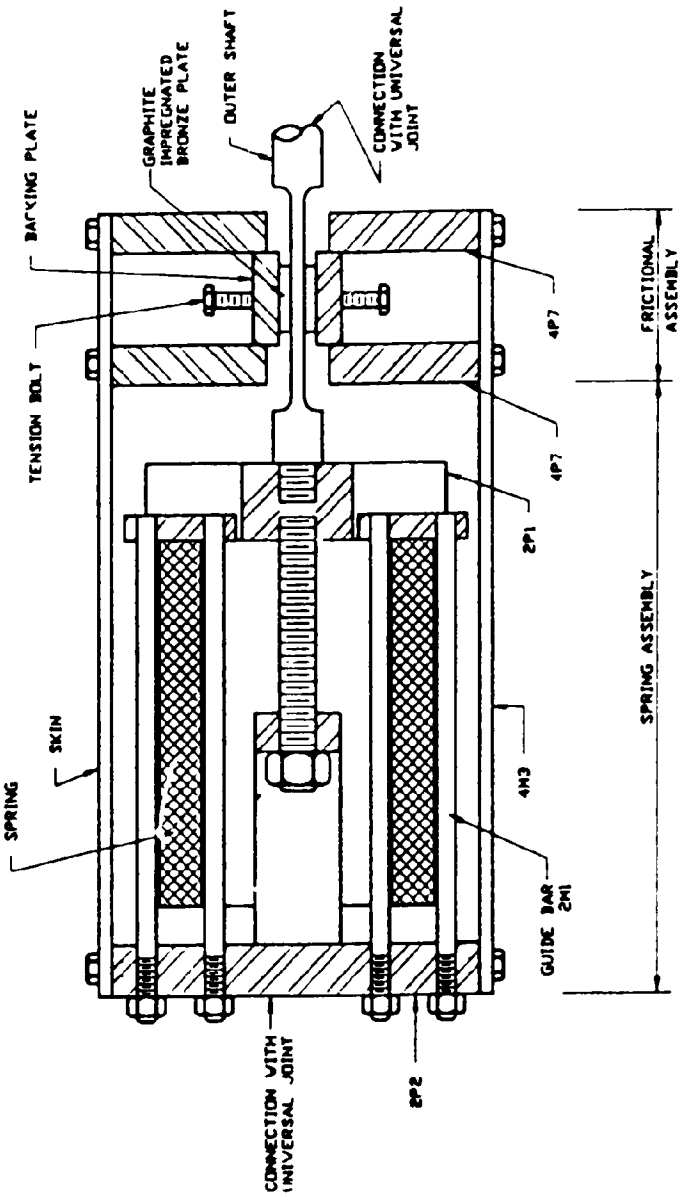

Fig. 3-4 - Displacement Control Device.

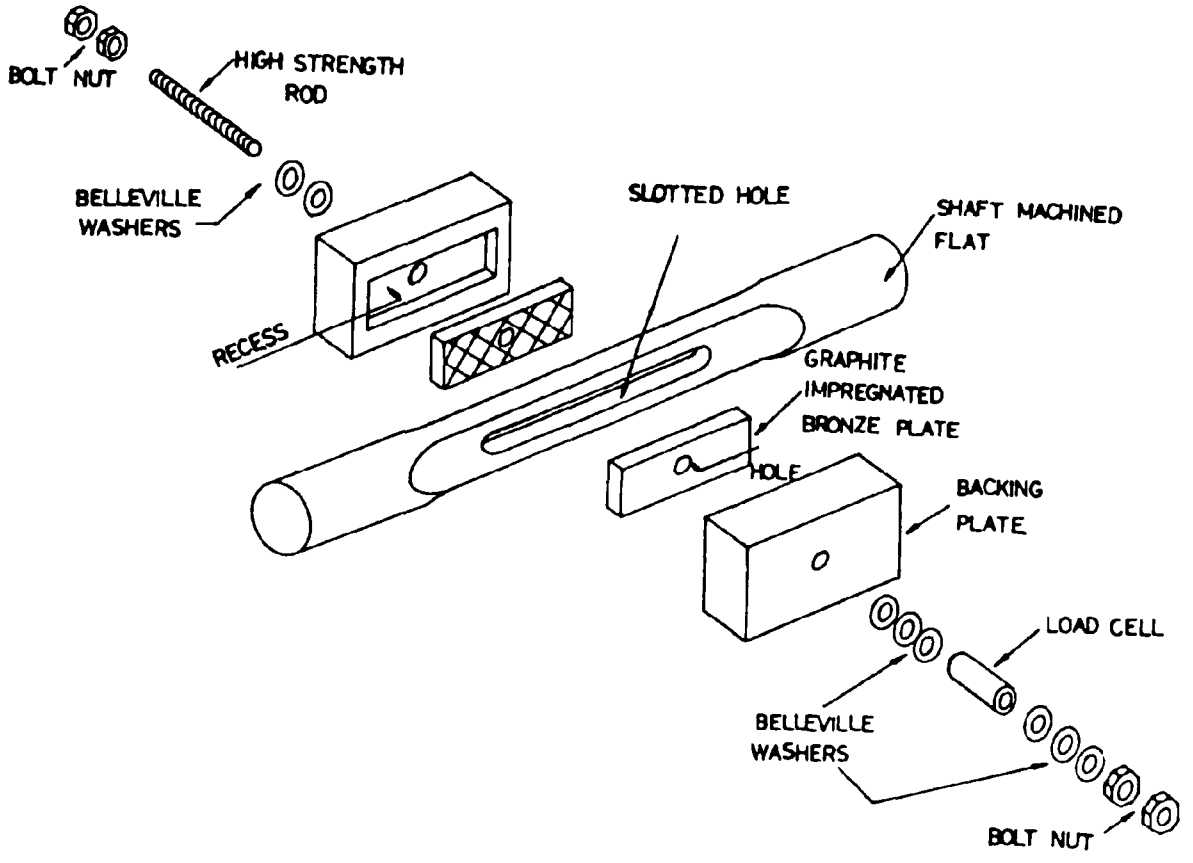

Fig. 3-5 - Frictional Assembly in Displacement Control Device.

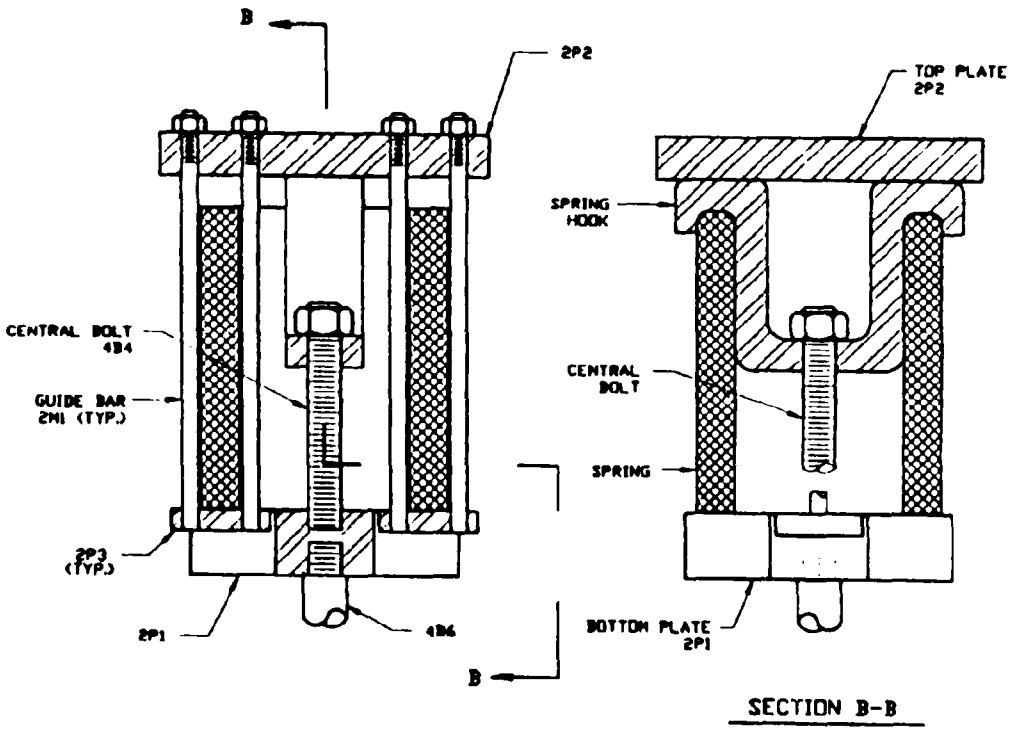

Fig. 3-6 - Spring Assembly in Displacement Control Device.

SECTION 4

EXPERIMENTAL MODEL AND ISOLATION SYSTEM

The model of the bridge deck consisted of two twenty foot (6.1 m) long, 24 in. by 10 in. (610 mm by 305 mm) reinforced concrete girders spaced 9.4 feet (2.85 m) apart and transversely connected by a 6 in. (152.4 mm) reinforced concrete slab and cross beams. Steel weights were added to bring the total deck weight to 51 kip (227.4 kN). Figure 4-1 shows an elevation of the model.

The isolation system consisted for four Teflon disc sliding bearings which supported the weight of the model with a clear span of 8.4 feet (2.56 m) with overhangs of 5.8 feet (1.77 m) on each end. One displacement control device(DCD) was placed in the longitudinal (testing) direction of the model. The device was connected to the deck at its center and to the shake table at a point along its center line.

The construction of the Teflon disc bearing is shown in Figure 4-2. It consisted of an Adiprene (urethane rubber) disc which allowed for limited rotation about a horizontal axis, a shear restriction mechanism to prevent shear deformation of the disc and the Teflon-stainless steel sliding interface. This interface consisted of a Teflon sheet recessed in its backing plate and a highly polished stainless steel plate. The plate was commercially polished to degree 8 which corresponds to a measured surface roughness of 1.6 μ-in (0.04 μ m) in the arithmetic average scale (Mokha 1988). Two bearing materials were used:

(a) Unfilled Teflon at pressure of 2000 psi (13.8 MPa) which gave a coefficient of friction at high velocity of sliding equal to 0.12, and

(b) A Teflon-based plastic (called Techmet-B) at pressure of 7000 psi (48.3 MPa) which gave a coefficient of friction at high velocity of sliding equal to 0.07.

The displacement control device was a replica of the prototype device described by Constantinou et al. (1991b) and in Section 3 herein. It consisted of frictional and spring assemblies connected in series as shown in Figure 4-3. The frictional assembly was identical to the prototype one (Constantinou 1991b). Two small size helical steel springs comprised the spring assembly. The springs operated only in compression with a combined stiffness of 3.85 kip/in (675.9 N/mm). Their free length of 4.5 in. (114.3 mm) allowed for a displacement of 1.12 in. (28.5 mm) at initiation of stiffening and a displacement of 1.26 in. (32 mm) at solid height. After solid height in the springs was reached the device was designed to initiate yielding at about 30% of the deck weight, dissipate further energy and prevent the deck from further motion. In case of failure of the displacement control device, an ultimate displacement restraint could be provided by the connecting bolts of the top bearing plate which allowed for a maximum of 2.8 in. (71.1 mm) displacement in each direction. This represented the fail-safe mechanism of the isolation system.

Figure 4-4 shows the force-displacement characteristics of the displacement control device. In the first test, five cycles of

sinusoidal motion of 1 in. (25.4 mm) amplitude and 0.5 Hz frequency were imposed. The load in the frictional assembly was set at 10.4 kips (46.4 kN) and the resulting characteristic strength, F_c, was 3.7 kips (16.5 kN). The device exhibited the desired bilinear hysteretic behavior with very high initial stiffness and stiffness after sliding, K, equal to 3.85 kip/in (675.9 N/mm). The second test was a slow force-controlled test in which the displacement amplitude reached the spring solid height limit of 1.26 in. (32 mm). The device exhibited the desired stiffening characteristics up to a force of about 17 kips (75.8 kN) where yielding occurred. The characteristic strength of the device could be adjusted at any desired level. In the shake table tests it was varied between about 2.5 and 5 kips (11.2 to 22.3 kN).

The frictional characteristics of the sliding bearings were determined by the test procedure described in Mokha et al. (1991b). The model deck was rigidly connected to a nearby reaction wall while the shake table below was driven at harmonic motion of specified amplitude and frequency. The motion of the table was the motion experienced by the sliding bearings and the frictional force mobilized at their sliding interface was measured by the supporting load cells (Fig. 4-1). Measurements of the frictional force in a range of velocities of sliding resulted in the coefficient of sliding friction which could be approximated by the following equation (Constantinou 1990):

$$\mu = f_{max} - (f_{max} - f_{min}) \exp(-a|\dot{U}|) \qquad (4\text{-}1)$$

in which $\dot{U}$ is the velocity of sliding; f_{max} and f_{min} are the maximum and minimum coefficients of friction, respectively; and a is a constant which controls the variation of friction with velocity. The parameters of the model of eq. 4-1 were $f_{max}=0.12$, $f_{min}=0.06$, a = 0.6 sec/in. (23.62 sec/m) for the interface of unfilled Teflon-stainless steel at 2000 psi (13.8 MPa) pressure and $f_{max}=0.07$, $f_{min}=0.035$, a = 1.5 sec/in. (59.1 sec/m) for the Techmet-B material at 7000 psi (48.3 MPa) pressure.

The peak value of the total frictional force at the isolation system (from sliding bearings and DCD) is

$$F_f = f_{max} W + F_c \qquad (4\text{-}2)$$

where F_c is the characteristic strength of the displacement control device and W is the deck weight (51 kip or 227.4 kN). In the shake table tests the peak value of the total frictional force was between about 6.3 and 9.4 kips (28 and 42 kN). In all tests, except one in which the displacement restraint mechanism of the isolation system was activated, the bearing displacement did not exceed 1 in. (25.4 mm) so that the peak restoring force in the displacement control device did not exceed 3.8 kips (17 kN). Accordingly, all tested configurations had a peak frictional force that was stronger than the peak restoring force. Earlier experimental work with building models (Constantinou 1991a) demonstrated that this isolation condition is appropriate for

strong earthquake excitations with wide range of frequency characteristics.

The configuration of the isolation system could produce a lateral force at the design displacement (1.12 in. or 28.5 mm) at least 0.04 W greater than the lateral force at 50 percent of the design displacement. This satisfies the requirements (0.025 W) imposed by the recently developed guide specifications for seismic isolation design of bridges (AASHTO 1991).

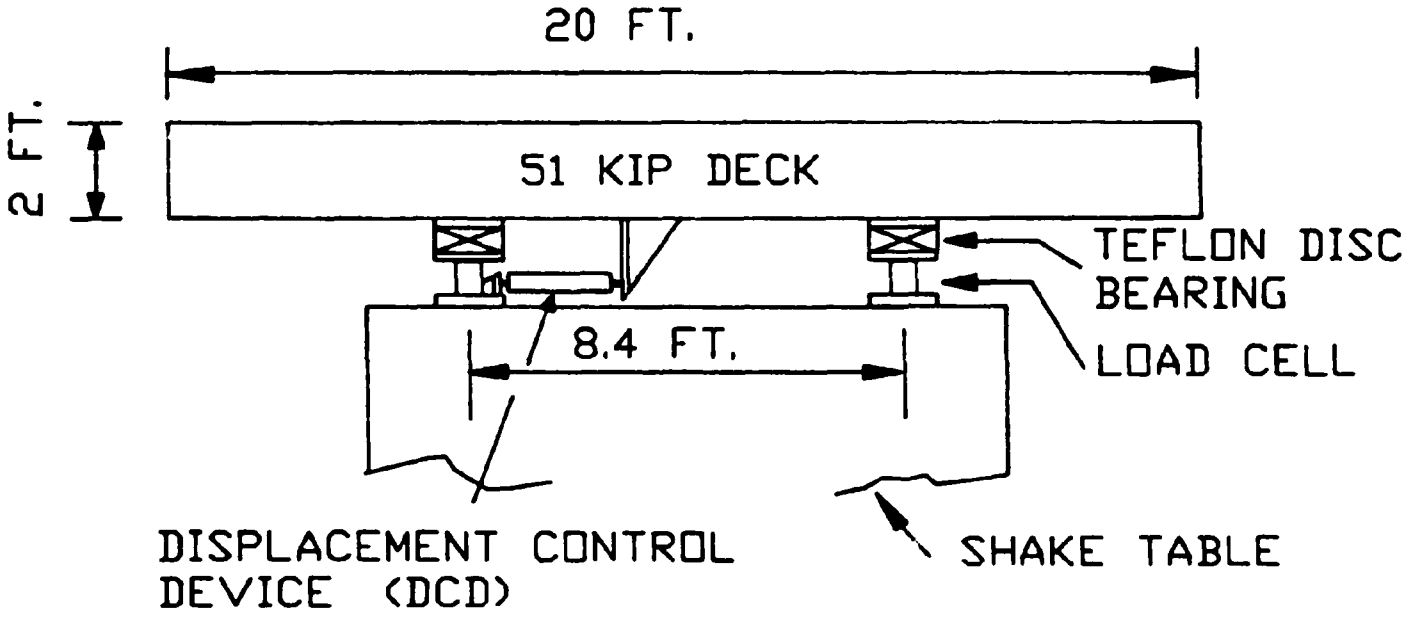

Fig. 4-1 - Elevation of Bridge Deck Model (1 Kip = 4.46 KN, 1 ft = 0.3 m).

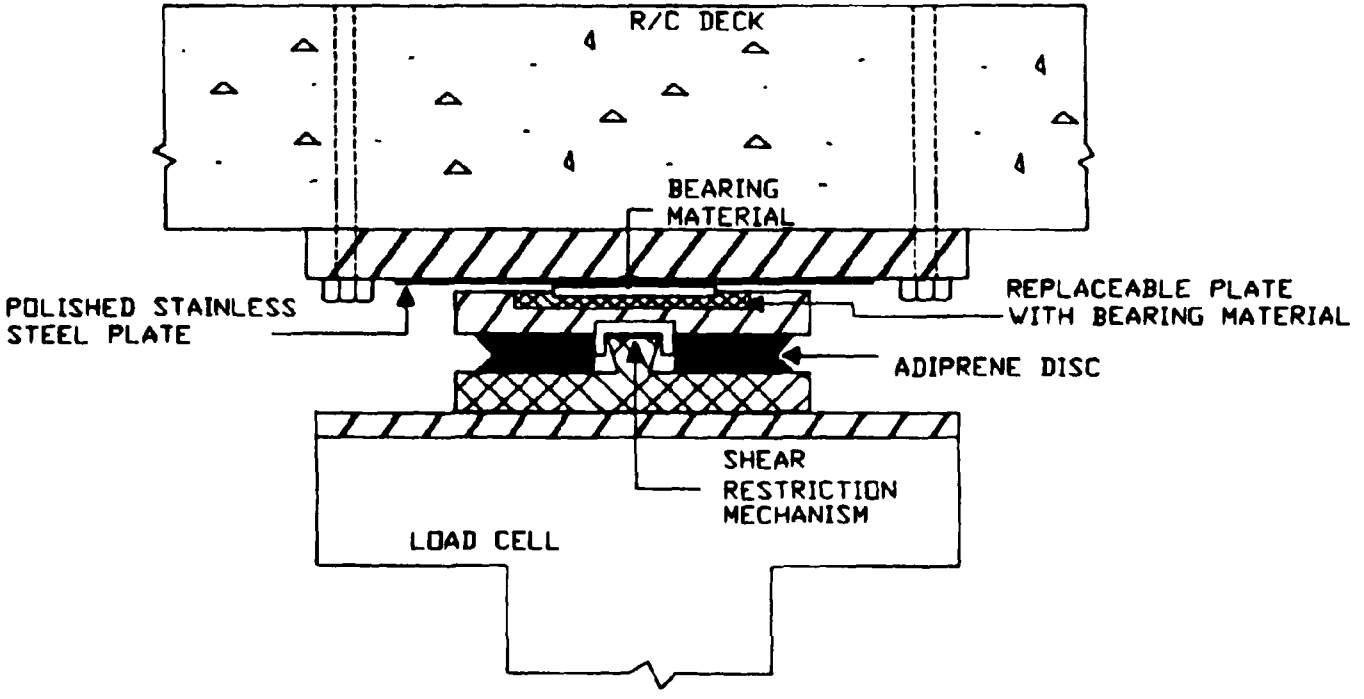

Fig. 4-2 - Construction of Sliding Disc Bearing.

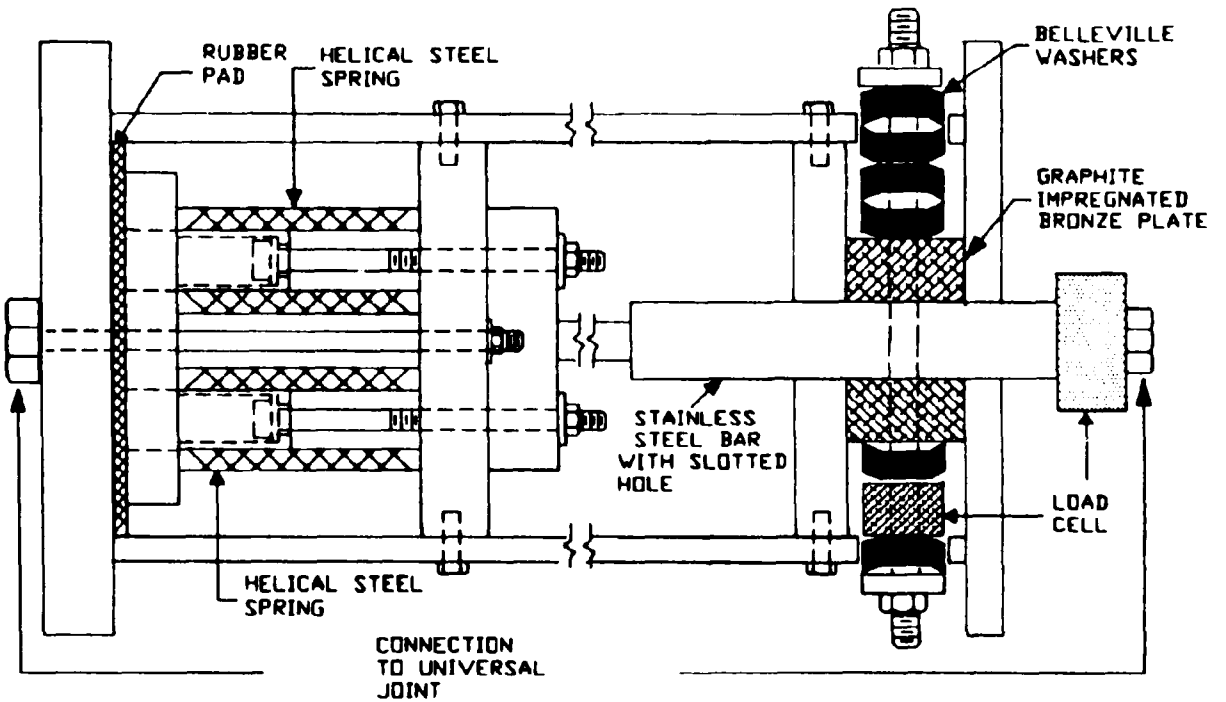

Fig. 4-3 - Construction of Scaled Displacement Control Device.

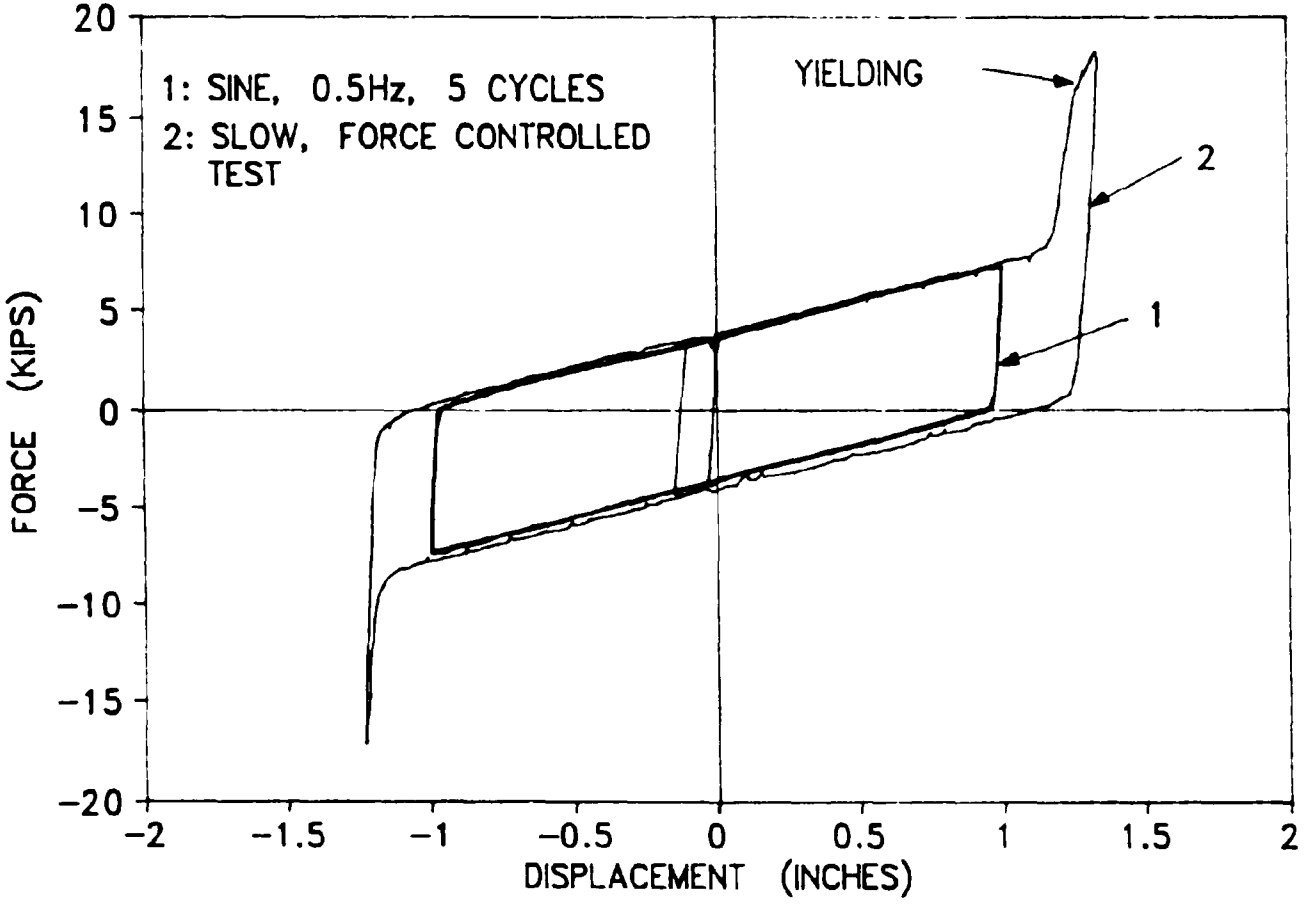

Fig. 4-4 - Hysteresis Loops of Scaled Displacement Control Device.

SECTION 5

TEST PROGRAM

The isolated model bridge deck was tested with seven actual earthquake motions and six simulated motions which were compatible with the California Department of Transportation (CALTRANS) bridge design spectra (Gates 1979). The characteristics, in prototype scale, of these earthquake motions are listed in Table 5-I. Of these records, the Hachinohe, Mexico City and the artificial Caltrans Alluvium motions are rich in long period components.

The artificial motions were created by the procedure described by Gasparini and Vanmarke (1976). The generated time histories of acceleration were 20 secs long for the Caltrans Rock spectrum compatible motions and 25 secs long for the Caltrans Alluvium spectrum compatible motions. The characteristics of these motions which are listed in Table 5-I were determined by using the analog integrator of the shake table, specifying as input the acceleration signal and obtaining the velocity and displacement command signals. The peak motion parameters of the artificial motions indicate strong excitations with large ground displacements.

All earthquake motions were time compressed by a factor 2 to satisfy the similitude requirements of the quarter scale model. Furthermore, each earthquake signal was ran at a modified level of peak table acceleration (either increased or decreased) so that it resulted in either a severe earthquake excitation or an excitation

with peak displacement within the shake table limitations (5 in. or 127 mm).

In addition to the earthquake motion test program, one test with sinusoidal table motion was conducted. The sinusoidal wave had a frequency of 1 Hz. The test was conducted in order to observe the characteristics of the isolation system over a large number of cycles (about 100) of motion.

Table 5-1 - Characteristics in Prototype Scale of Earthquake Motions Used in Test Program (1 in=25.4mm, 1ft=0.3m)

Motion (1)	Record (2)	Peak Acceleration (g) (3)	Peak Velocity (in/s) (4)	Peak Displacement (in) (5)
El Centro	Imperial Valley, May 18, 1940 component S00E	0.34	13.17	4.28
Taft	Kern County, July 21, 1952 component N21E	0.16	6.19	2.64
Pacoima Dam S74W	San Fernando, February 9, 1971 component S74W	1.08	22.73	4.26
Pacoima Dam S16E	San Fernando, February 9, 1971 component S16E	1.17	44.58	14.83
Miyagiken-Oki	Miyaki, Japan, June 12, 1978 Ofunato-Bochi, component EW	0.16	5.55	2.00
Hachinohe	Tokachi, Japan, May 16, 1968 Hachinohe, component NS	0.23	14.06	4.68
Mexico City	Mexico City, September 19, 1985 SCT building, component N90W	0.17	23.82	8.35
Caltrans Rock No.1	Artificial compatible with CALTRANS 0.6g rock spectrum	0.60	20.9	17.08
Caltrans Rock No.2	Artificial compatible with CALTRANS 0.6g rock spectrum	0.60	20.08	10.80
Caltrans Rock No.3	Artificial compatible with CALTRANS 0.6g rock spectrum	0.60	22.48	13.48
Caltrans Alluvium No.1	Artificial compatible with CALTRANS 0.6g 10'-80' alluvium spectrum	0.60	38.00	23.72
Caltrans Alluvium No.2	Artificial compatible with CALTRANS 0.6g 10'-80' alluvium spectrum	0.60	30.12	9.80
Caltrans Alluvium No.3	Artificial compatible with CALTRANS 0.6g 10'-80' alluvium spectrum	0.60	30.64	17.28

SECTION 6

TEST RESULTS

Table 6-I lists the input signals of the shake table test program, the isolation conditions, the peak table motion parameters, and the response of the model bridge in terms of peak deck acceleration, peak bearing displacement and permanent bearing displacement at the end of free vibration response. The table acceleration and displacement were directly measured, whereas the table velocity was obtained by differentiation of the recorded displacement history. Time histories of the recorded response are presented in Appendix A.

The isolation conditions identified in Table 6-I are T2 and TB which correspond, respectively, to sliding bearings with unfilled Teflon at 2000 psi (13.8 MPa) pressure and material Techmet-B at 7000 psi (48.3 MPa) pressure. The maximum value of the sliding coefficient of friction, f_{max} (eq.4-1), was 0.12 for condition T2 and 0.07 for condition TB. The characteristic strength of the displacement control device was measured by the load cell shown in Figure 4-1 and is included in Table 6-I. The tests were conducted in the order they appear in Table 6-I.

The earthquake excitation is presented with a percentage figure that applies to the peak ground acceleration of the actual record. For example, the case El Centro 200% corresponds to an increase in acceleration of the actual El Centro record (Table 5-I)

by a factor of approximately 2. The velocity and displacement were also increased by the same factor.

During the entire testing program the shake table was driven in its acceleration controlled mode without any off-line compensation for improving the simulation fidelity. Nevertheless, the table reproduced well the input signal except in certain peak values. A comparison of the recorded peak response of the shake table (Table 6-I) to the earthquake peak parameters (Table 5-I) provides evidence for this. For example, the Pacoima S74W record has peak parameters: acceleration 1.08g, velocity 22.73 in./sec (577.4 mm/sec) and displacement 4.26 in. (108.2 mm). The table response when extrapolated to prototype scale was: acceleration 1.07g, velocity 19.42 in./sec (493.3 mm/sec) and displacement 4.64 in. (117.9 mm). In general, the table peak velocity was less than that of the actual earthquake motions.

Details of the recorded earthquake (table) motion are presented in Figures 6-1 to 6-13. Each figure shows time histories of recorded (in the scale of experiment) table acceleration, displacement and velocity. The velocity history was not directly measured but rather obtained by differentiation of the displacement record. Furthermore, each figure shows the 5%-damped acceleration spectrum of each motion in prototype scale. In the case of simulated motions, the spectrum is compared to the target spectrum (Gates 1979). It may be observed that the spectrum of the simulated motions is in good agreement with the target spectrum.

6.1 Effectiveness of Isolation System

The effectiveness of isolation system, as determined from a comparison of the isolated deck response to the motion of the shake table, is apparent in the experimental results of Table 6-I. In all tests the peak deck acceleration and bearing displacement are less than the peak table acceleration and displacement. Excluding the single test in which the displacement restraint mechanism of the displacement control device was activated (Pacoima Dam S16E 75%), the isolated deck responded with a peak acceleration of about or less than 0.22 g regardless of the intensity and content in frequency of the earthquake motion. This good behavior is achieved with bearing displacements being less than 1 in. (25.4mm) or 4 in. (101.6 mm) in prototype scale. Such small displacements are of particular importance in bridges because they require short expansion joints. Short joints are less costly, produce less noise and vibration during automobile crossing and are easier to maintain than long expansion joints.

To illustrate the action of the isolation system with increasing earthquake intensity Figure 6-14 shows the peak table displacement and peak model response versus the peak table acceleration for the Taft and Pacoima S74W inputs. The results shown are for the T2 system. Evidently, the isolation effectiveness increases with increasing earthquake intensity.

The demonstrated good behavior of the isolation system in strong earthquake excitation was a result of its design to deliver a combination of strong frictional force and weak restoring force.

This was apparent in the tests with the lower bearing friction TB system in which the characteristic strength of the displacement control device was increased so that the total friction force in the two systems was of the same order.

6.2 Behavior of Displacement Control Device

In the test with Pacoima Dam S16E 75% input the deck displacement reached the spring solid height limit of 1.26 in. (32 mm) and the displacement restraint mechanism of the displacement control device was activated. Yielding of the device occurred at a force of about 40% of the deck's weight. The recorded deck displacement (bearing) history and loops of force in DCD and base shear versus displacement are shown in Figure 6-15. The base shear loop shows that the energy dissipated during yielding of the displacement control device amounts to about 15% of the energy dissipated by friction during the main cycle of motion. This was not sufficient to provide any significant reduction of the acceleration response. Lower acceleration response could be easily accomplished by simply increasing the characteristic strength of the displacement control device as it was done in the tests with the Mexico City motion.

6.3 Behavior at Resonance

In the series of tests with Mexico City motion the isolated deck was driven at resonance. The fundamental period of the isolated deck, in the absence of friction, is determined from the

spring stiffness in the displacement control device and the deck weight to be 1.16 secs (or 2.33 secs in prototype scale). This value coincides with the predominant period in the Mexico City motion. Despite this the isolated deck responded with small displacement amplitude without amplifying the table acceleration. Of particular interest are the tests with Mexico City 120% motion in the T2 system. A minor increase in the characteristic strength of the displacement control from 2.60 to 2.91 kips (11.6 to 13 kN), which amounts to only 0.6% of the deck's weight, resulted in reduction of displacements to about half with a simultaneous decrease in acceleration response. These experimental results agree very well with analytical predictions of the behavior of harmonically excited sliding isolation systems at resonance (Den Hartog 1931; Makris 1989 and 1991).

Makris (1989) has shown that harmonically excited sliding systems with velocity dependent friction (eq. 4-1) build up infinite displacement amplitude if driven at resonance for sufficiently long time and provided that the ratio of peak frictional force, F_f, to amplitude of driving force, P_o, is less than $\pi/4$:

$$\epsilon = \frac{F_f}{P_o} < \frac{\pi}{4} \qquad \textbf{(6-1)}$$

For values of ϵ larger than but close to $\pi/4$, the displacement amplitude is small but very sensitive to changes of either the value of ϵ or the variation of the friction force with velocity of

sliding. This would explain the significant changes in the displacement response of the system in the Mexico City tests when small changes were made in either the input acceleration or the characteristic strength of the displacement control device.

Furthermore, the significant differences in the displacement response between systems T2 and TB in the Mexico City 120% tests are explained by the differences in the variation of friction with velocity. For example, system T2 with F_c = 2.6 kips (11.6kN) and system TB with F_c = 5.03 kips (22.4 kN) (see table 6-I) have both peak frictional force F_f (eq. 4-2) equal to 0.17W but respond with significantly different displacements. The TB system, with its friction derived primarily from the displacement control device, behaves almost as a Coulomb frictional system for which displacements at resonance are lower than the velocity dependent frictional T2 system (Makris 1989).

6.4 System Adequacy

(a) The adequacy of the isolation system was assessed by (a) repeating tests and observing changes in the response of isolated deck, and

(b) performing a test with large displacement amplitude response and with over 100 cycles of motion.

The tests on the T2 system with Caltrans Rock No. 1 100% and Taft 300% motions were repeated having first conducted a number of other tests (see Table 6-I). The response of the system in the

repeated tests was almost identical to that in the first tests with some very small differences explained by the small difference in the characteristic strength of the displacement control device (see Table 6-I). Of interest is to note that the second test with Taft 300% motion was conducted after yielding of the displacement control device. Apparently, this had no effect on the performance of the device.

A single test was conducted on the T2 system with sinusoidal input motion of 1 Hz frequency. The system, driven essentially at resonance, responded with large displacement amplitude which varied between 0.2 and 0.86 in. (5.1 and 21.8 mm) over 106 cycles. In 72 of these cycles the bearing displacement exceeded 0.5 in. (12.7 mm) or 45% of the system's displacement limit. The input acceleration varied only between 0.15 and 0.19g in this test and the large variability in the displacement response has been a result of sensitivity at resonance (Makris 1989). The deck (bearing) displacement history and loops of base shear versus displacement are shown in Figure 6-16. The loops demonstrate stable characteristics over a very large number of cycles.

6.5 Permanent Displacement

Permanent displacements were recorded at the conclusion of each test and reported in Table 6-I. The model bridge deck was not re-centered prior to conducting each test. This did not have any adverse effect on the performance of the isolation system and permanent displacements were not cumulative.

The recorded permanent displacements were one order of magnitude less than the upper limit calculated on the assumption of zero inertia forces. This limit is

$$U_p = \frac{f_{min}W+F_c}{K} \qquad (6\text{-}2)$$

where K is the stiffness of the displacement control device. For the tested T2 system this limit is about 1.5 in. (38 mm). Apparently the inertial forces play an important role in re-centering the system.

Table 6-I - Summary of Experimental Results (1 in.=25.4mm, 1 kip=4.46kN)

Excitation	Isolation Condition	Fc (kips)	Table Peak Motion			Peak Deck Accel. (g)	Peak Bearing (Deck) Displ. (in)	Permanent Displ. (in)
			Displ. (in)	Veloc. (in/s)	Accel. (g)			
(1)	(2)	(3)	(4)	(5)	(6)	(7)	(8)	(9)
Taft 100%	T2	2.46	0.61	2.49	0.150	0.148	0.060	0.027
Taft 200%	T2	2.50	1.16	4.93	0.260	0.170	0.172	0.092
Taft 300%	T2	2.80	1.70	7.28	0.544	0.187	0.337	0.002
Taft 400%	T2	2.69	2.30	9.78	0.747	0.207	0.657	0.029
El Centro 100%	T2	2.77	0.87	5.87	0.330	0.175	0.214	0.104
El Centro 200%	T2	2.75	1.80	11.84	0.747	0.221	0.913	0.130
Hachinohe 100%	T2	2.56	1.20	6.42	0.304	0.167	0.270	0.172
Hachinohe 150%	T2	2.69	1.80	9.36	0.445	0.205	0.661	0.041
Miyagiken-Oki 300%	T2	2.62	1.43	8.65	0.521	0.186	0.252	0.060
Miyagiken-Oki 500%	T2	2.68	2.39	12.75	0.662	0.210	0.691	0.038
Caltrans Rock No.1 100%	T2	2.88	4.70	10.64	0.587	0.220	0.750	0.035
Caltrans Rock No.2 100%	T2	2.82	2.85	9.85	0.600	0.206	0.410	0.097
Caltrans Rock No.3 100%	T2	2.84	3.67	12.09	0.850	0.191	0.700	0.164
Caltrans Rock No.1 100%	T2	2.95	4.70	10.64	0.587	0.215	0.756	0.005
Caltrans 10'-80' Alluvium No.1 75%	T2	2.95	4.70	14.43	0.520	0.191	0.431	0.003
Caltrans 10'-80' Alluvium No.2 75%	T2	2.97	2.04	11.31	0.593	0.206	0.750	0.021
Caltrans 10'-80' Alluvium No.3 75%	T2	3.07	3.36	12.02	0.600	0.199	0.747	0.152
Pacoima Dam S74W 50%	T2	2.75	0.62	4.72	0.497	0.193	0.300	0.041

Fc: characteristic strength of DCD

Table 6-I - Continued

Excitation	Isolation Condition	Fc (kips)	Table Peak Motion			Peak Deck Accel. (g)	Peak Bearing (Deck) Displ. (in)	Permanent Displ. (in)
			Displ. (in)	Veloc. (in/s)	Accel. (g)			
(1)	(2)	(3)	(4)	(5)	(6)	(7)	(8)	(9)
Pacoima Dam S74W 75%	T2	2.94	0.90	7.18	0.860	0.204	0.406	0.013
Pacoima Dam S74W 100%	T2	2.82	1.16	9.71	1.070	0.215	0.847	0.008
Pacoima Dam S16E 50%	T2	2.82	1.62	9.36	0.430	0.202	0.511	0.019
Pacoima Dam S16E 75%	T2	2.95	2.34	14.22	0.695	0.636	1.278	0.154
Taft 300%	T2	2.48	1.70	7.23	0.546	0.180	0.360	0.050
Mexico City 100%	T2	2.24	1.99	11.70	0.174	0.156	0.295	0.026
Mexico City 120%	T2	2.60	2.34	14.15	0.203	0.205	0.913	0.032
Mexico City 120%	T2	2.91	2.37	14.17	0.209	0.190	0.540	0.001
Mexico City 120%	T2	3.32	2.37	14.17	0.209	0.190	0.430	0.013
Sine Wave 1 Hz	T2	2.75	0.87	6.40	0.192	0.191	0.860	0.039
El Centro 100%	TB	2.77	0.86	5.86	0.347	0.150	0.330	0.013
El Centro 100%	TB	5.00	0.86	6.00	0.304	0.189	0.260	0.065
El Centro 200%	TB	5.12	1.77	11.97	0.608	0.221	0.934	0.059
Hachinohe 150%	TB	4.98	1.80	9.60	0.347	0.215	0.902	0.271
Taft 300%	TB	5.12	1.70	7.32	0.508	0.198	0.430	0.081
Taft 400%	TB	5.06	2.26	9.78	0.634	0.215	0.860	0.078
Miyagiken-Oki 500%	TB	5.14	2.40	12.90	0.616	0.221	0.804	0.282
Mexico City 100%	TB	5.02	1.97	11.63	0.189	0.171	0.121	0.069
Mexico City 120%	TB	5.03	2.37	13.90	0.208	0.189	0.429	0.043
Mexico City 130%	TB	4.99	2.56	15.28	0.221	0.215	0.740	0.152

Fc: characteristic strength of DCD

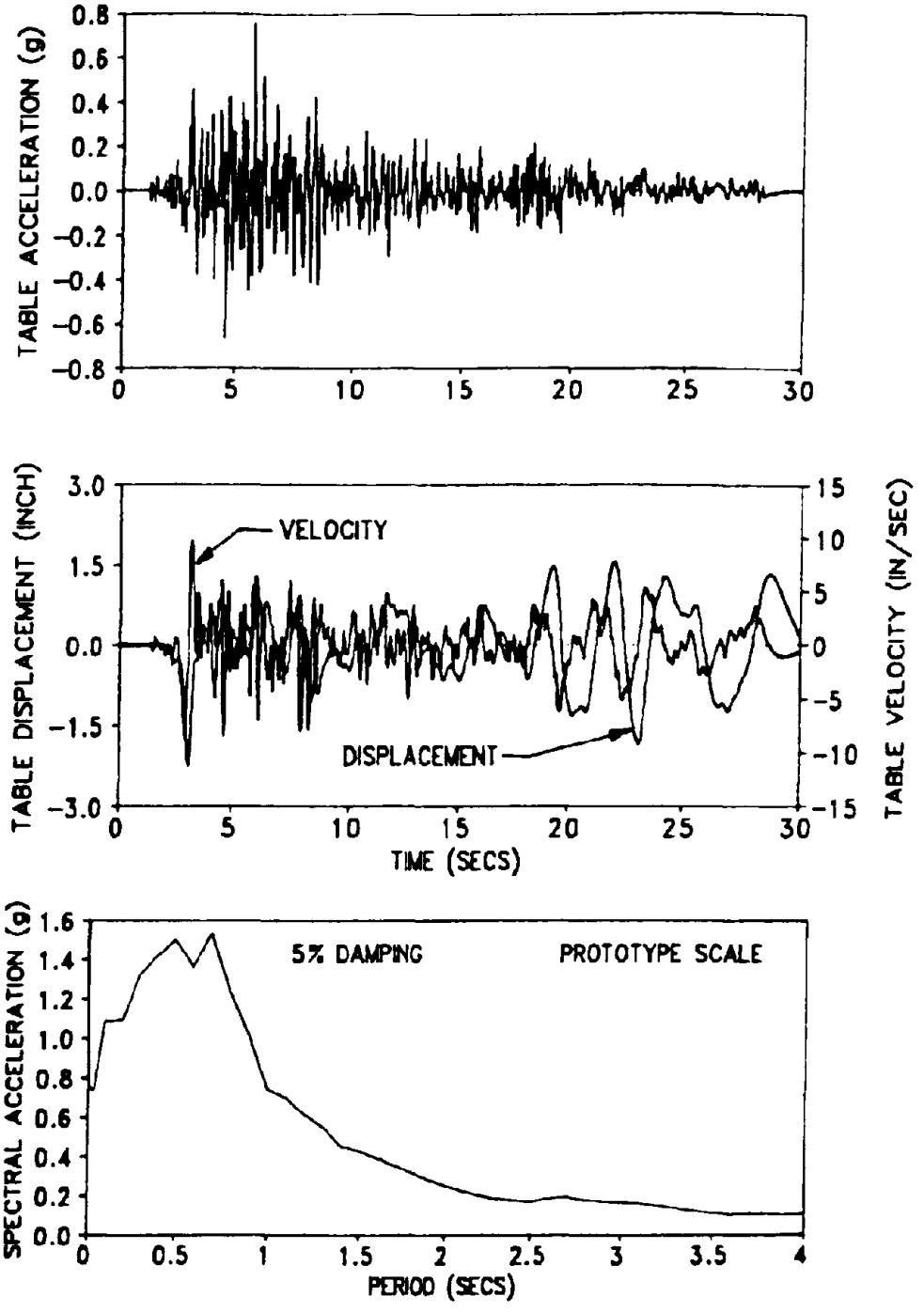

Fig. 6-1 - Recorded Table Motion and Response Spectrum of Taft N21E 400% (1 in. = 25.4 mm).

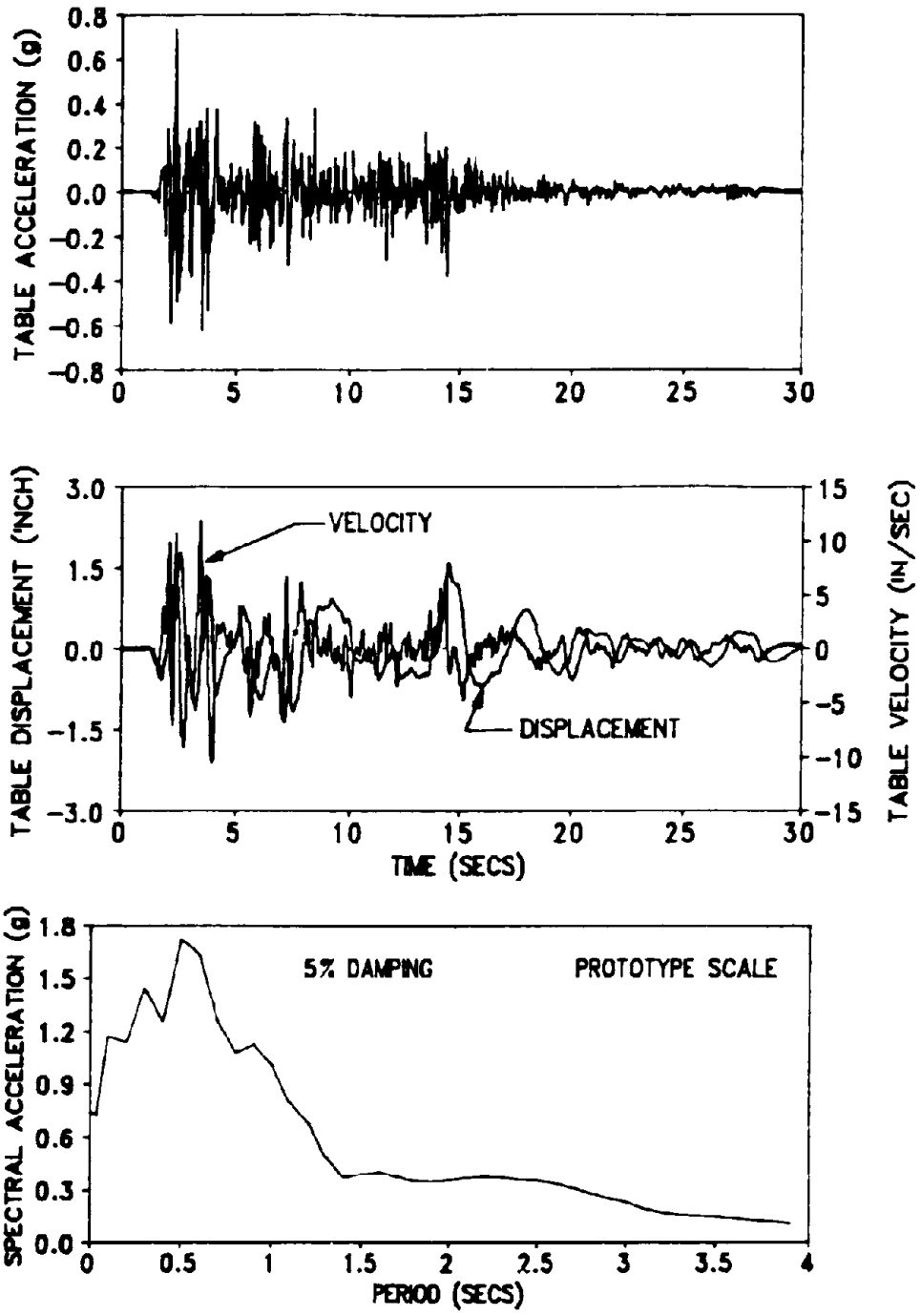

Fig. 6-2 - Recorded Table Motion and Response Spectrum of El Centro S00E 200% (1 in. = 25.4 mm).

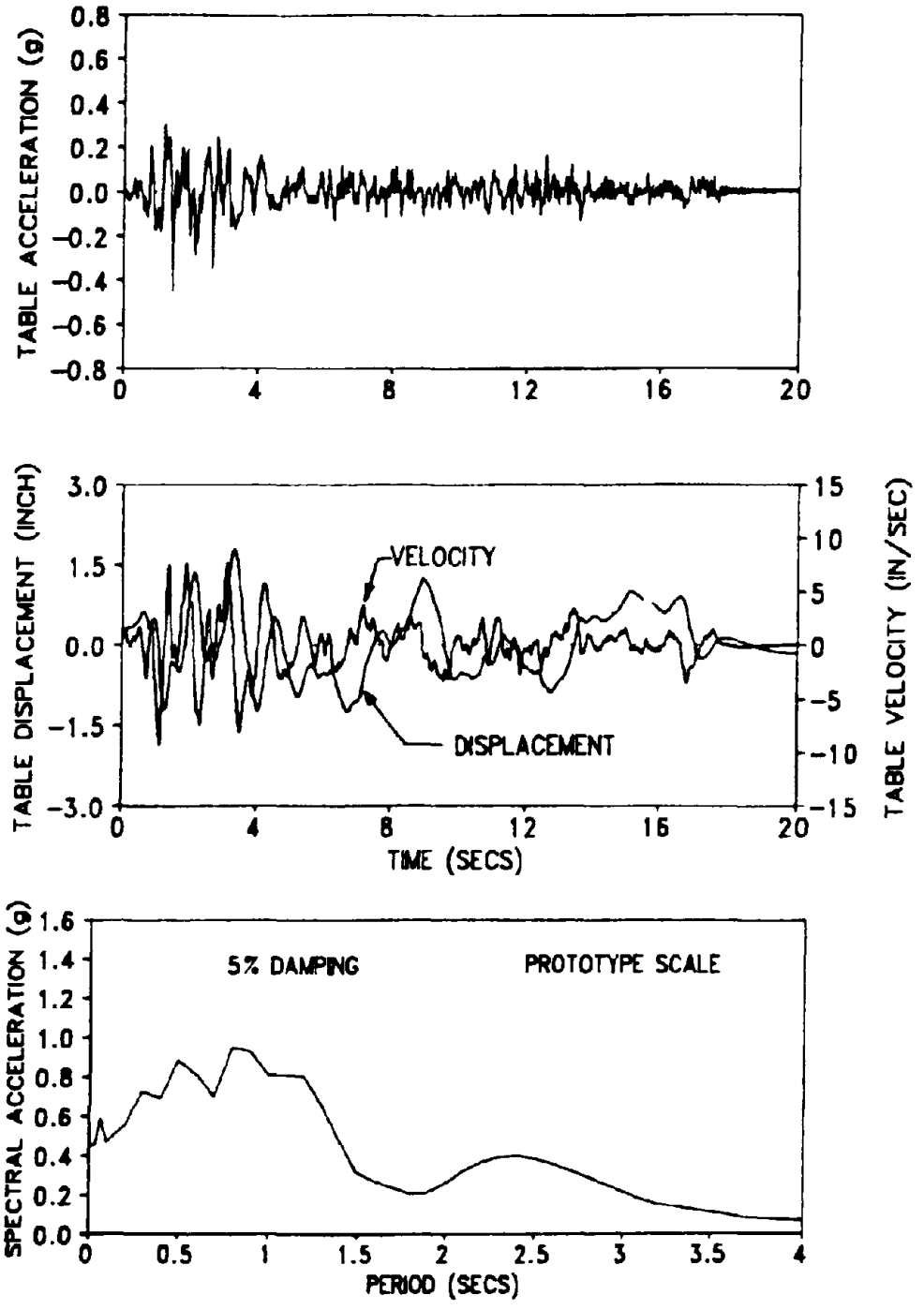

Fig. 6-3 · Recorded Table Motion and Response Spectrum of Hachinohe NS 150%(1 in. = 25.4 mm).

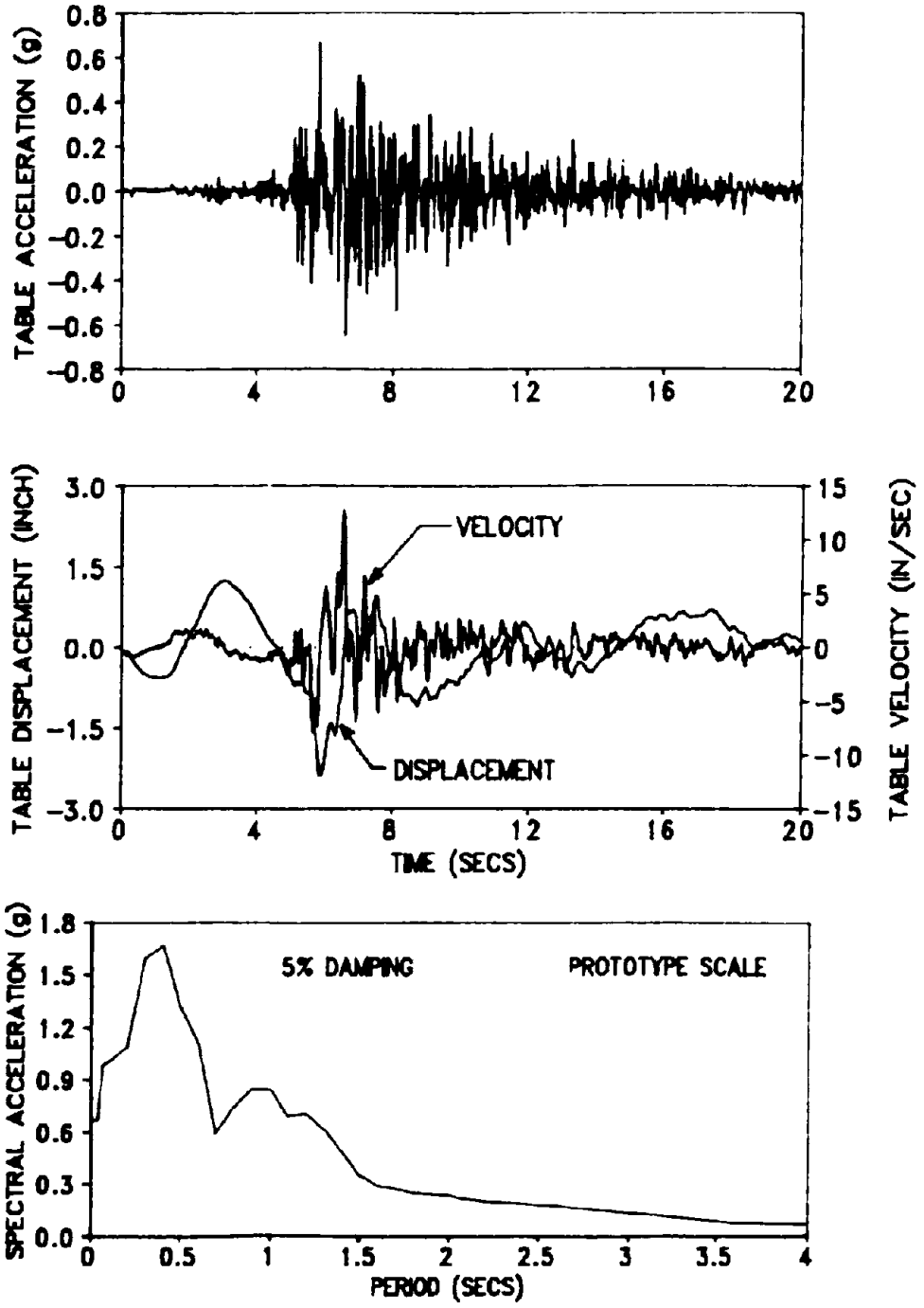

Fig. 6-4 - Recorded Table Motion and Response Spectrum of Miyagiken-Oki EW 500% (1 in. = 25.4 mm).

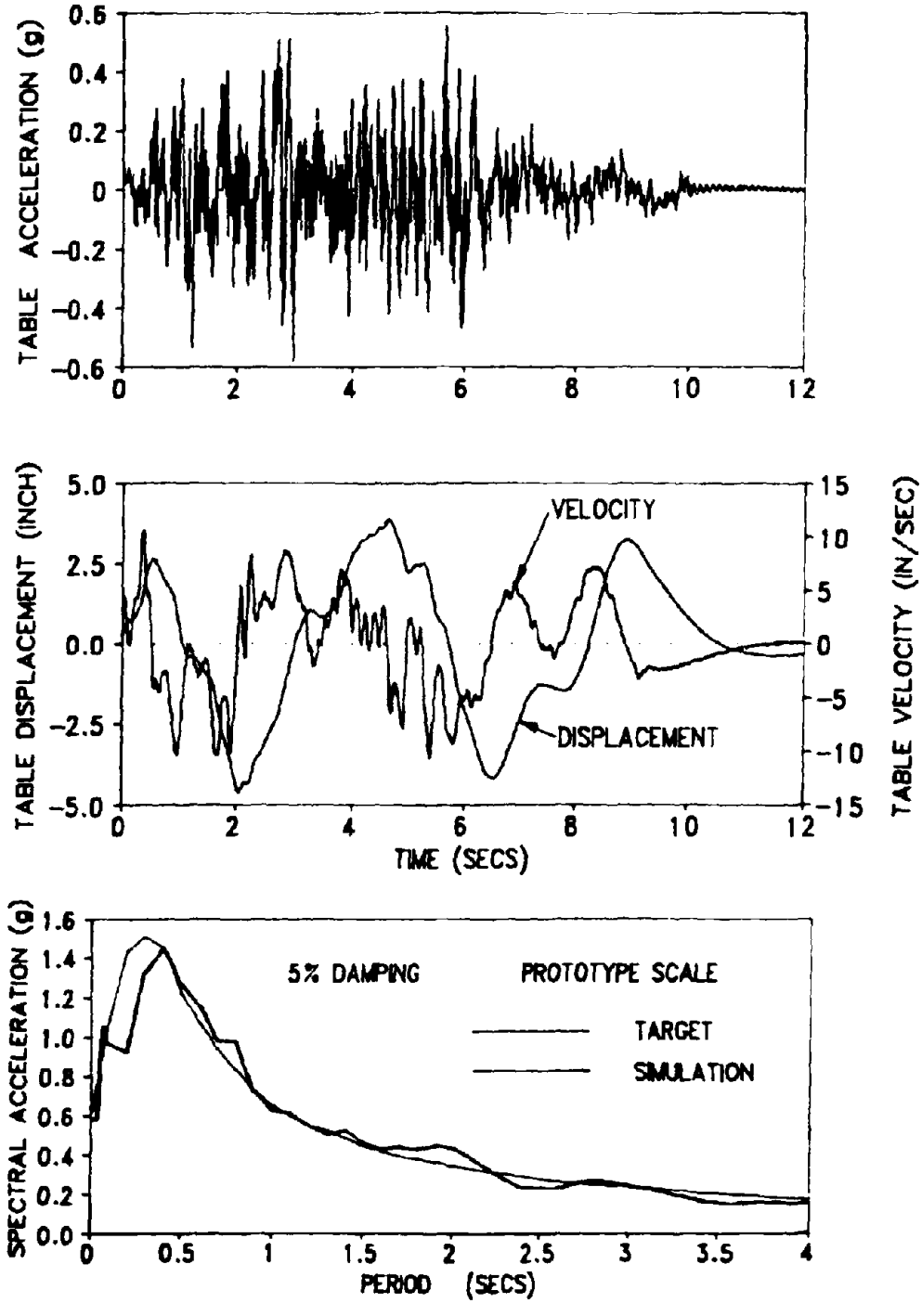

Fig. 6-5 - Recorded Table Motion and Response Spectrum of Caltrans Rock No. 1, 100% Spectrum Compatible Earthquake (1 in. = 25.4 mm).

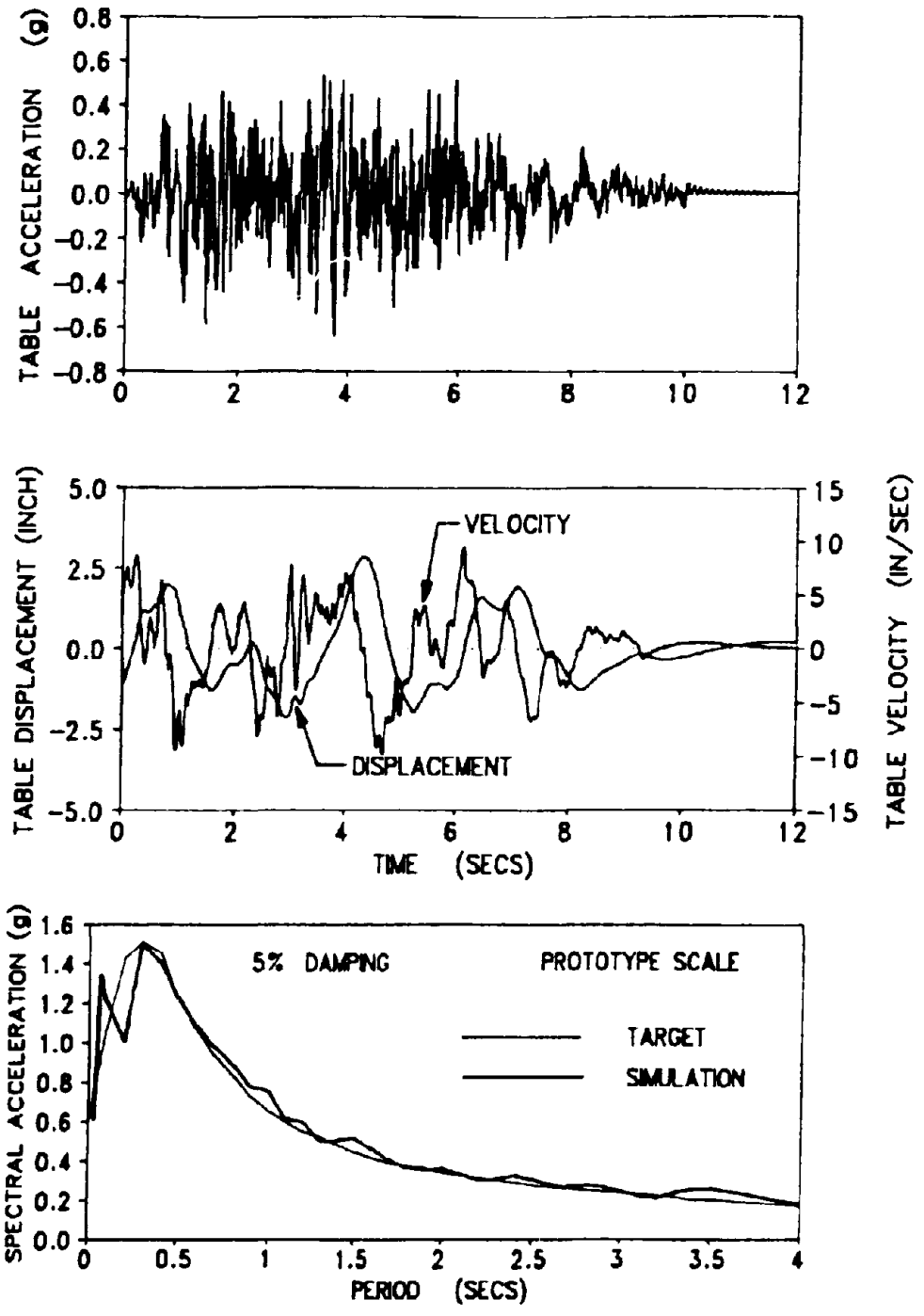

Fig. 6-6 - Recorded Table Motion and Response Spectrum of Caltrans Rock No. 2, 100% Spectrum Compatible Earthquake (1 in. = 25.4 mm).

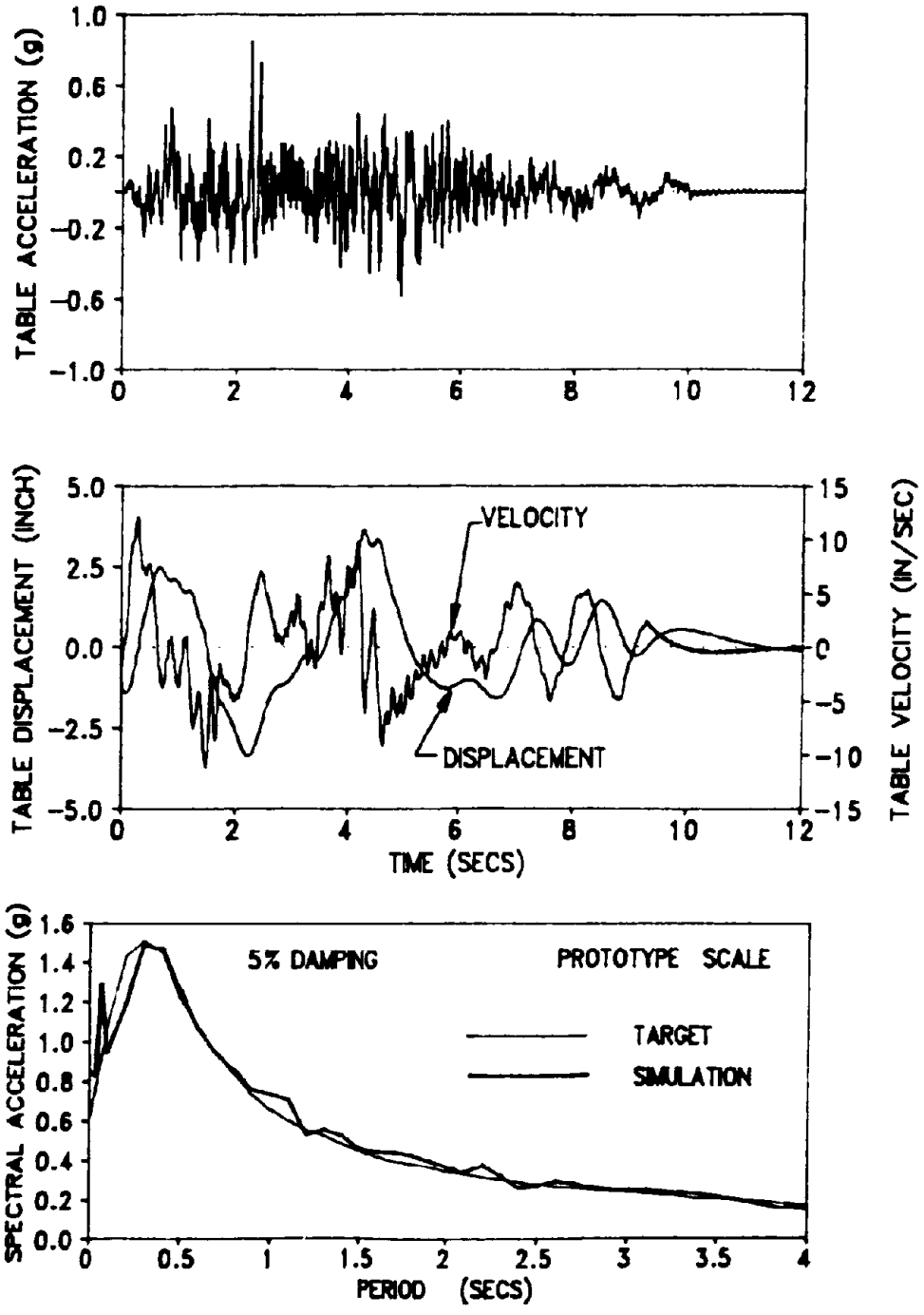

Fig. 6-7 - Recorded Table Motion and Response Spectrum of Caltrans Rock No. 3, 100% Spectrum Compatible Earthquake (1 in. = 25.4 mm).

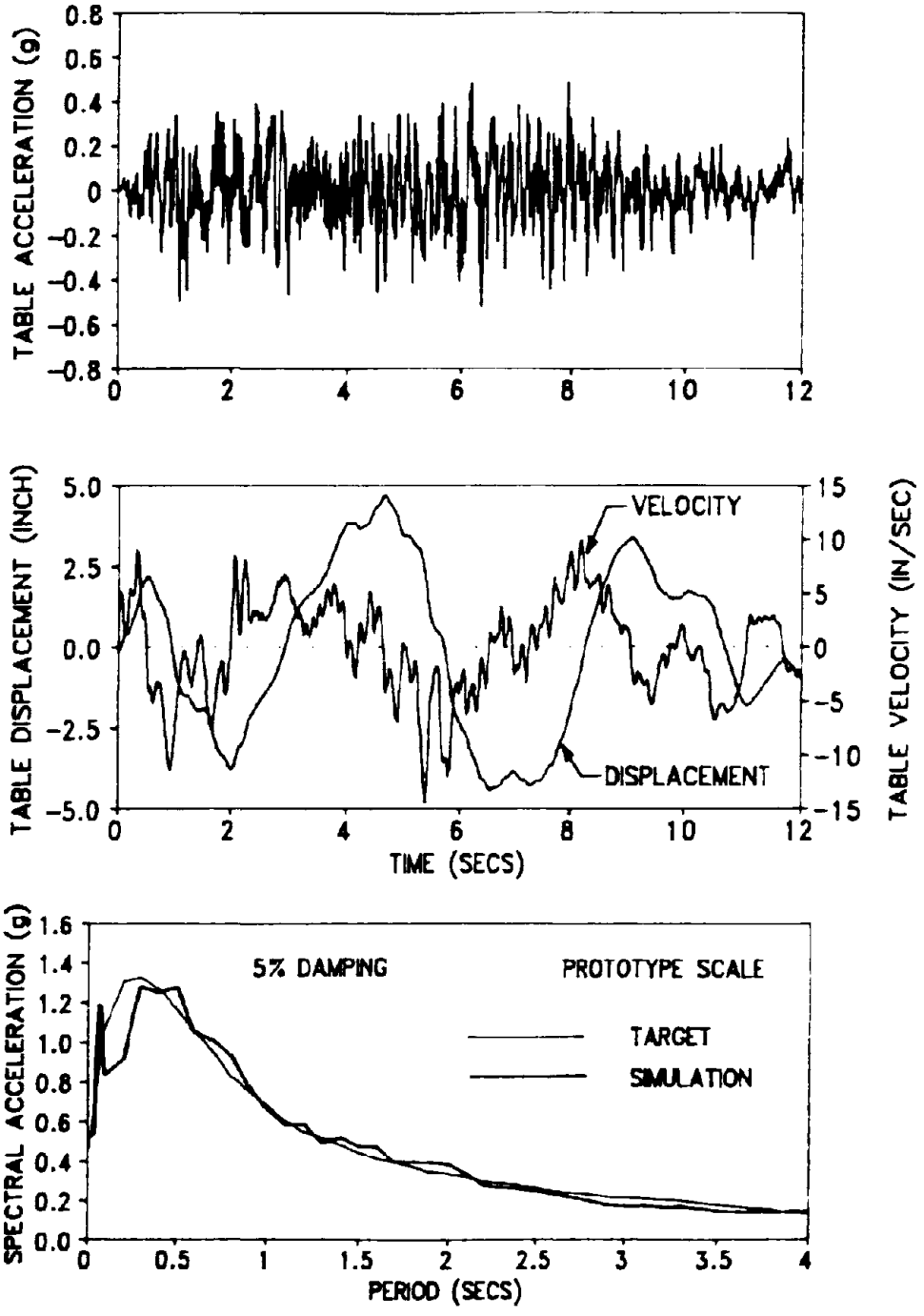

Fig. 6-8 - Recorded Table Motion and Response Spectrum of Caltrans 10'-80' Alluvium No. 1, 75% Spectrum Compatible Earthquake (1 in. = 25.4 mm).

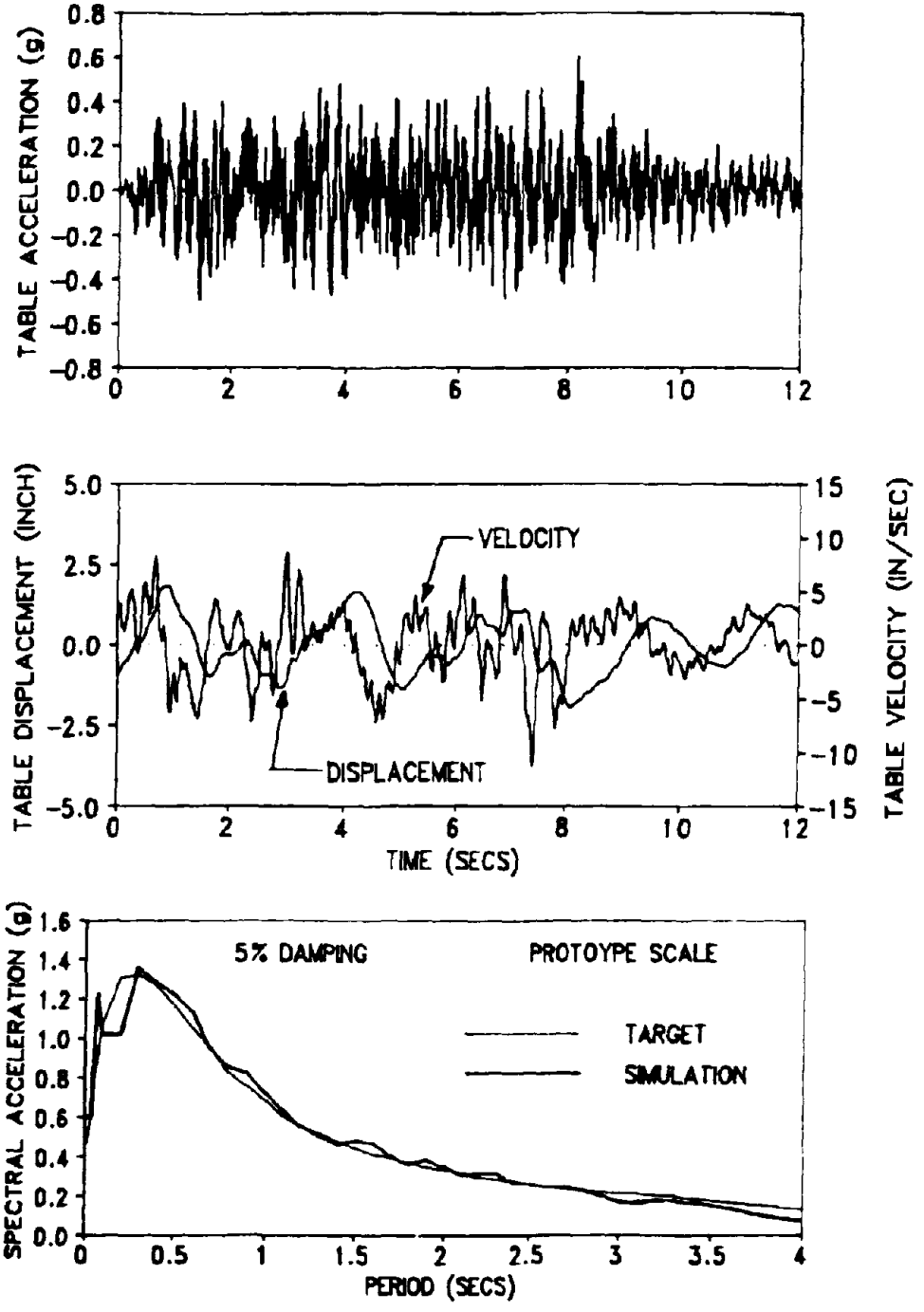

Fig. 6-9 - Recorded Table Motion and Response Spectrum of Caltrans 10'-80' Alluvium No. 2, 75% Spectrum Compatible Earthquake (1 in. = 25.4 mm).

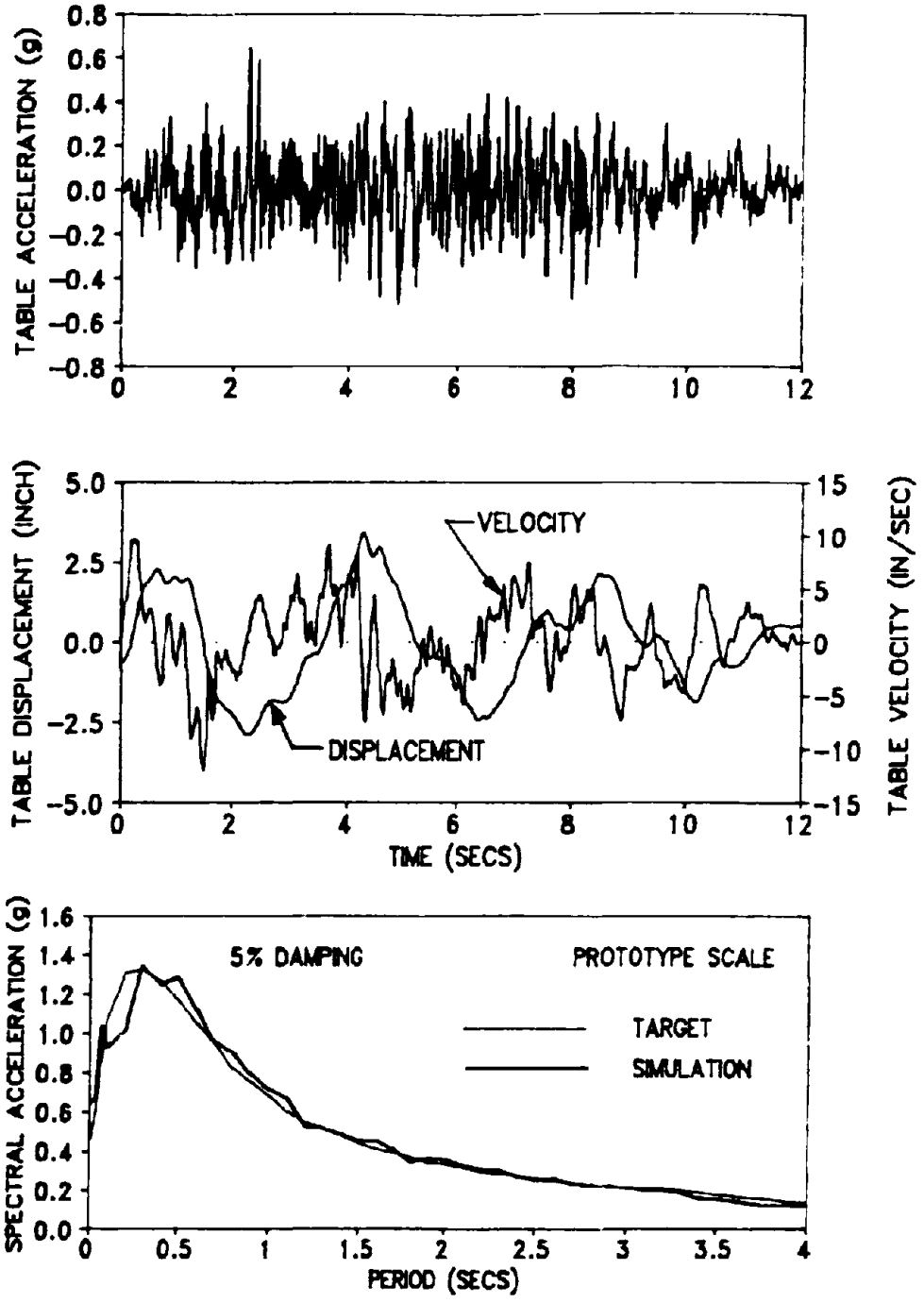

Fig. 6-10 - Recorded Table Motion and Response Spectrum of Caltrans 10'-80' Alluvium No. 3, 75% Spectrum Compatible Earthquake (1 in. = 25.4 mm).

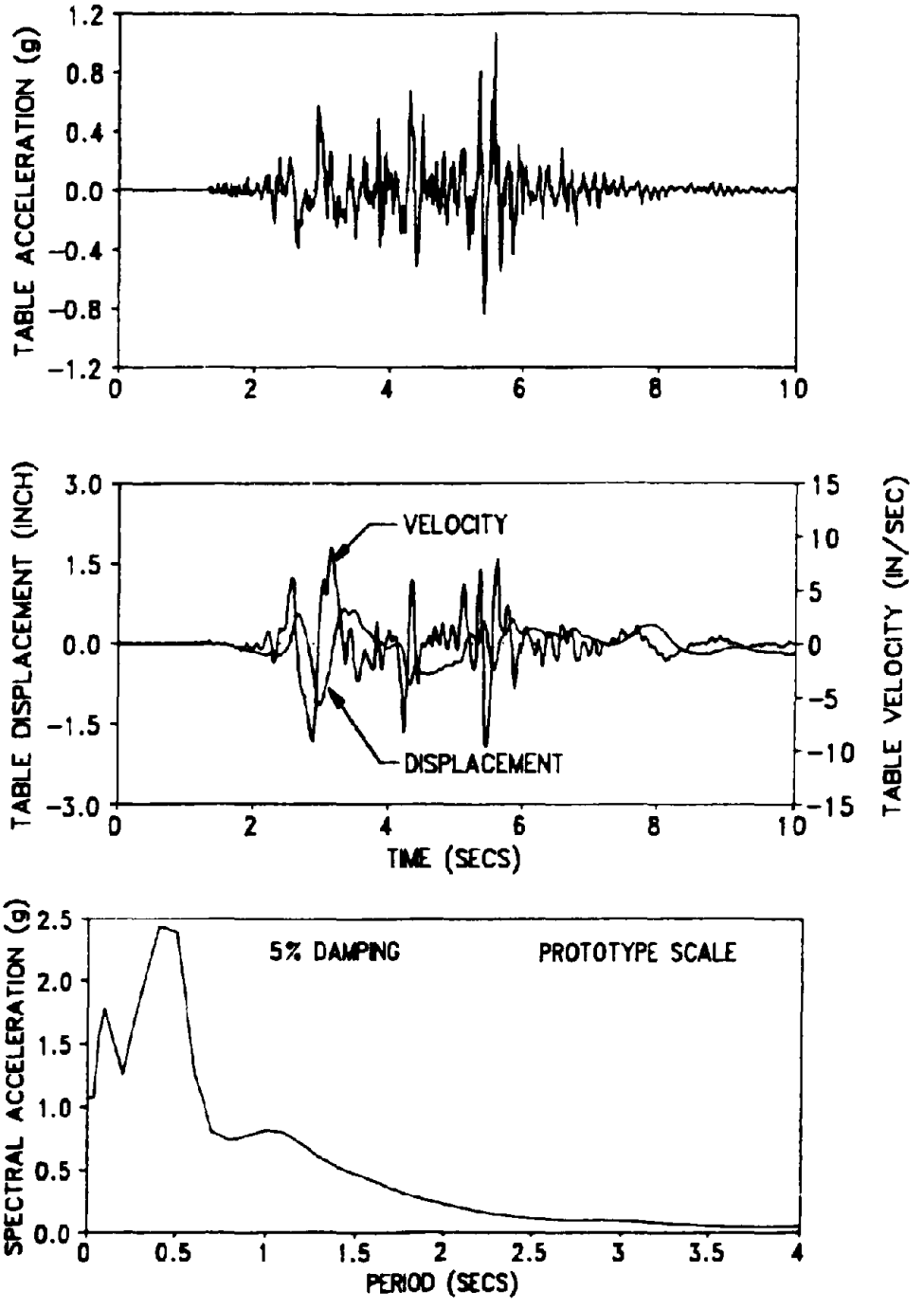

Fig. 6-11 - Recorded Table Motion and Response Spectrum of Pacoima Dam S74W 100% (1 in. = 25.4 mm).

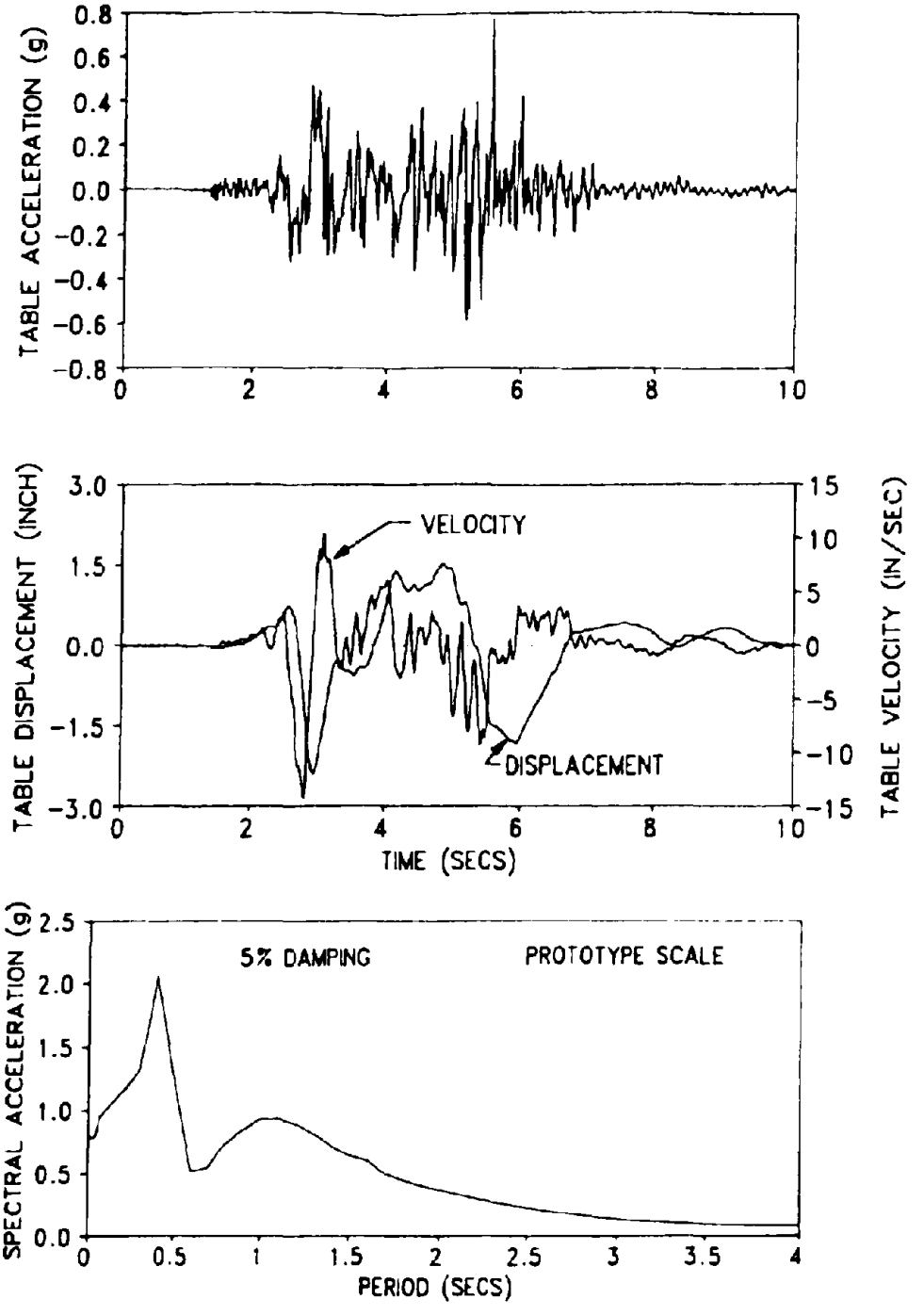

Fig. 6-12 - Recorded Table Motion and Response Spectrum of Pacoima Dam S16E 75% (1 in. = 25.4 mm).

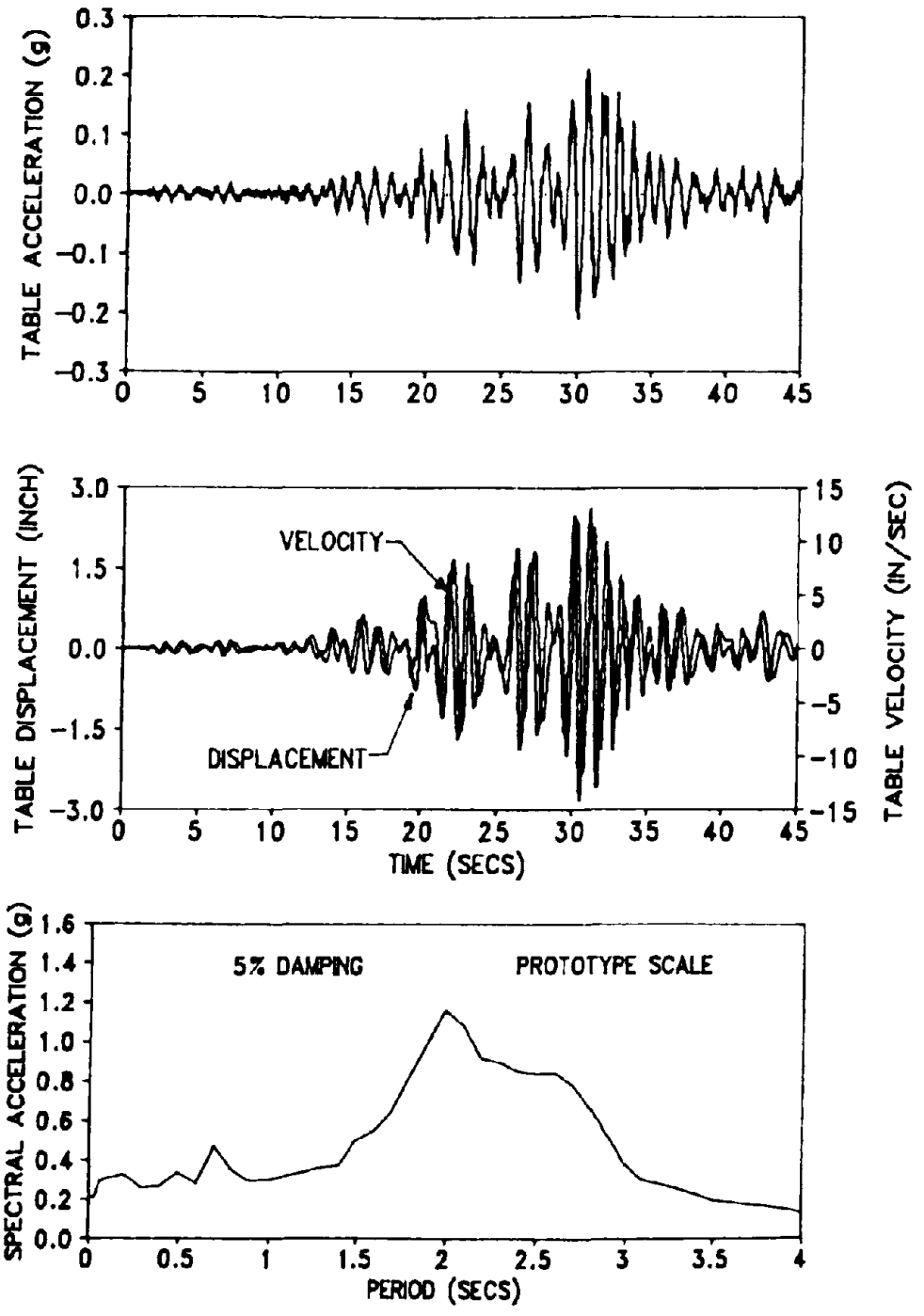

Fig. 6-13 - Recorded Table Motion and Response Spectrum of Mexico City N90W 120% (1 in. = 25.4 mm).

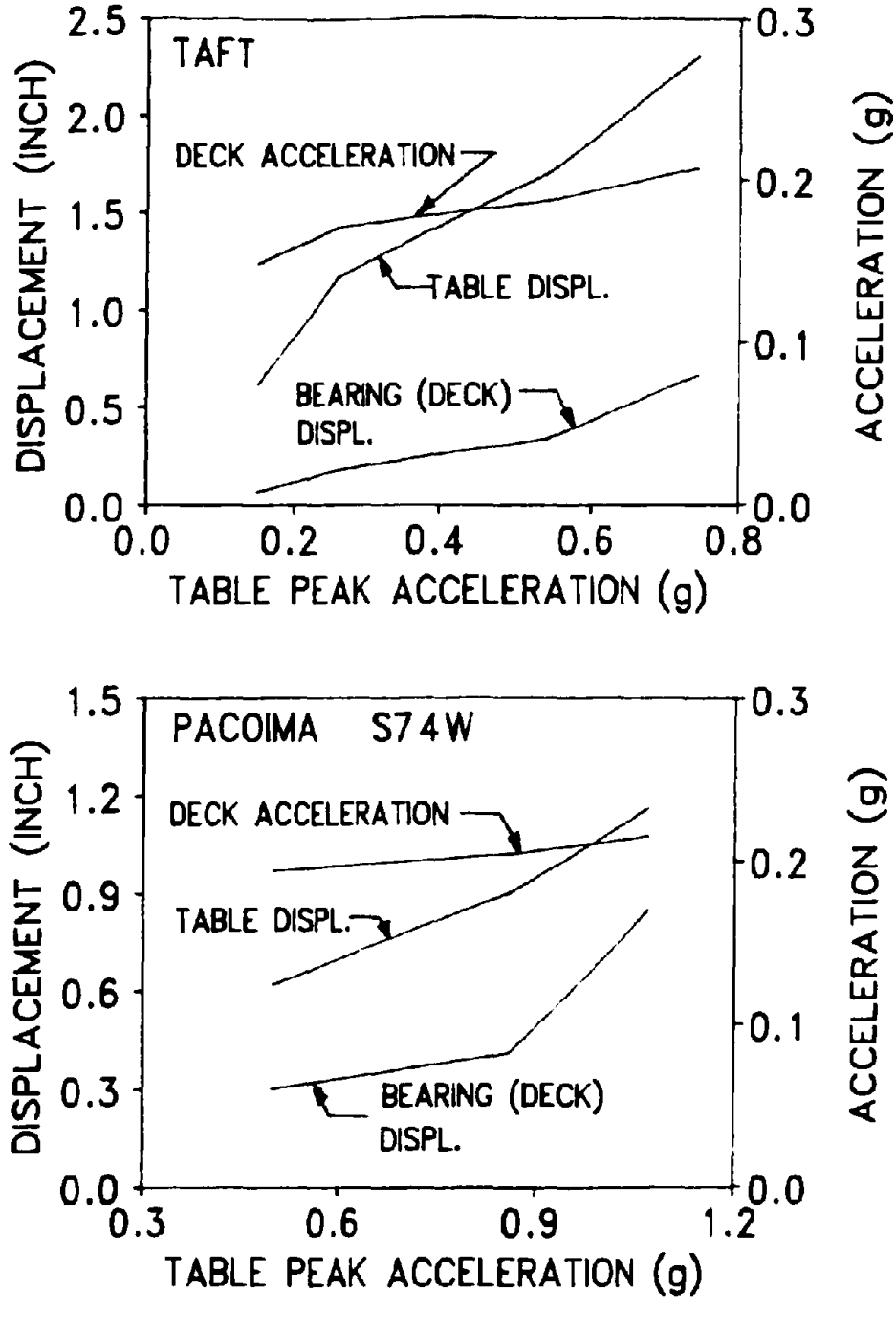

Fig. 6-14 - Response of T2 System under Increasing Earthquake Intensity (1 in. = 25.4 mm).

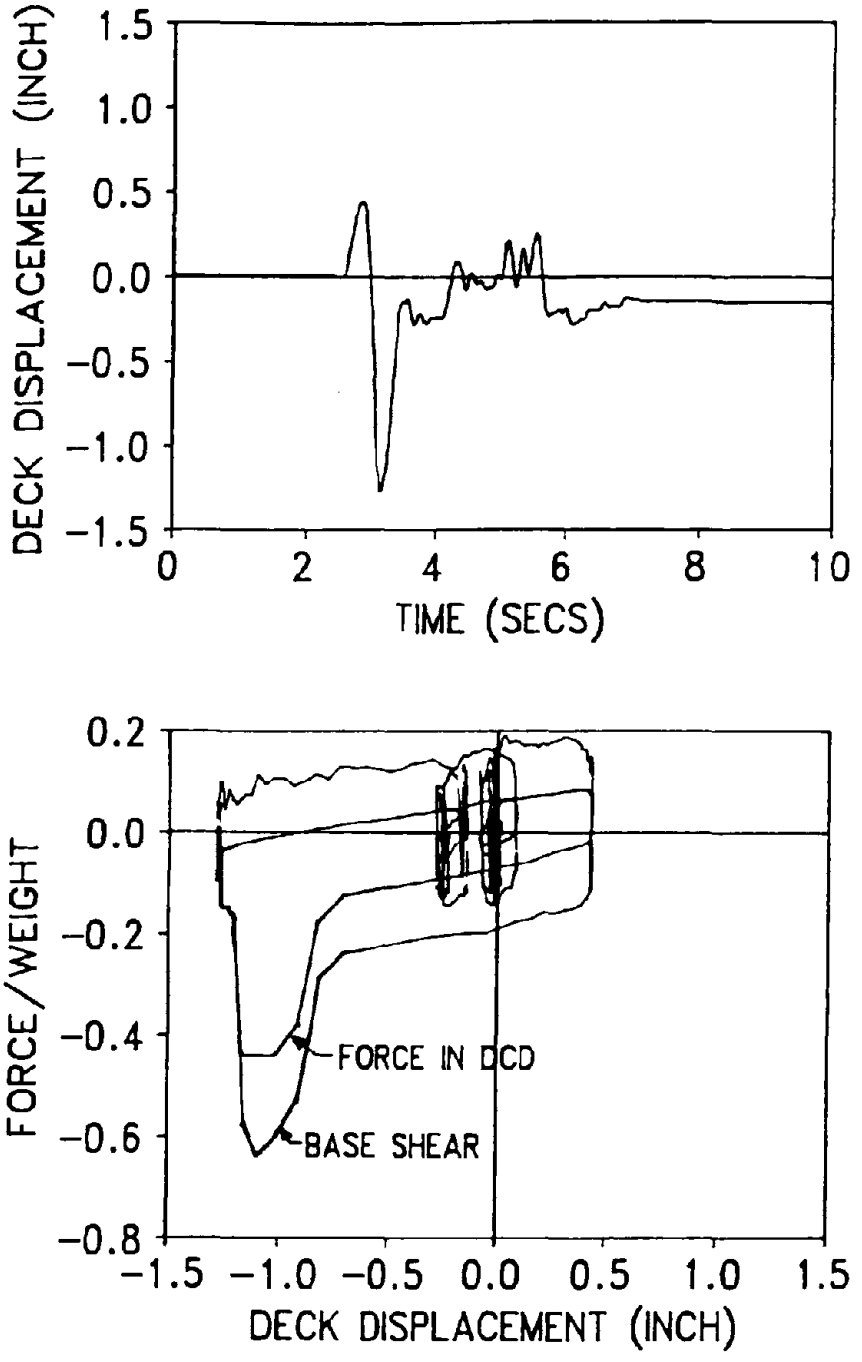

Fig. 6-15 - Recorded Response of T2 System in Pacoima Dam S16E 75% Test (1 in. = 25.4 mm).

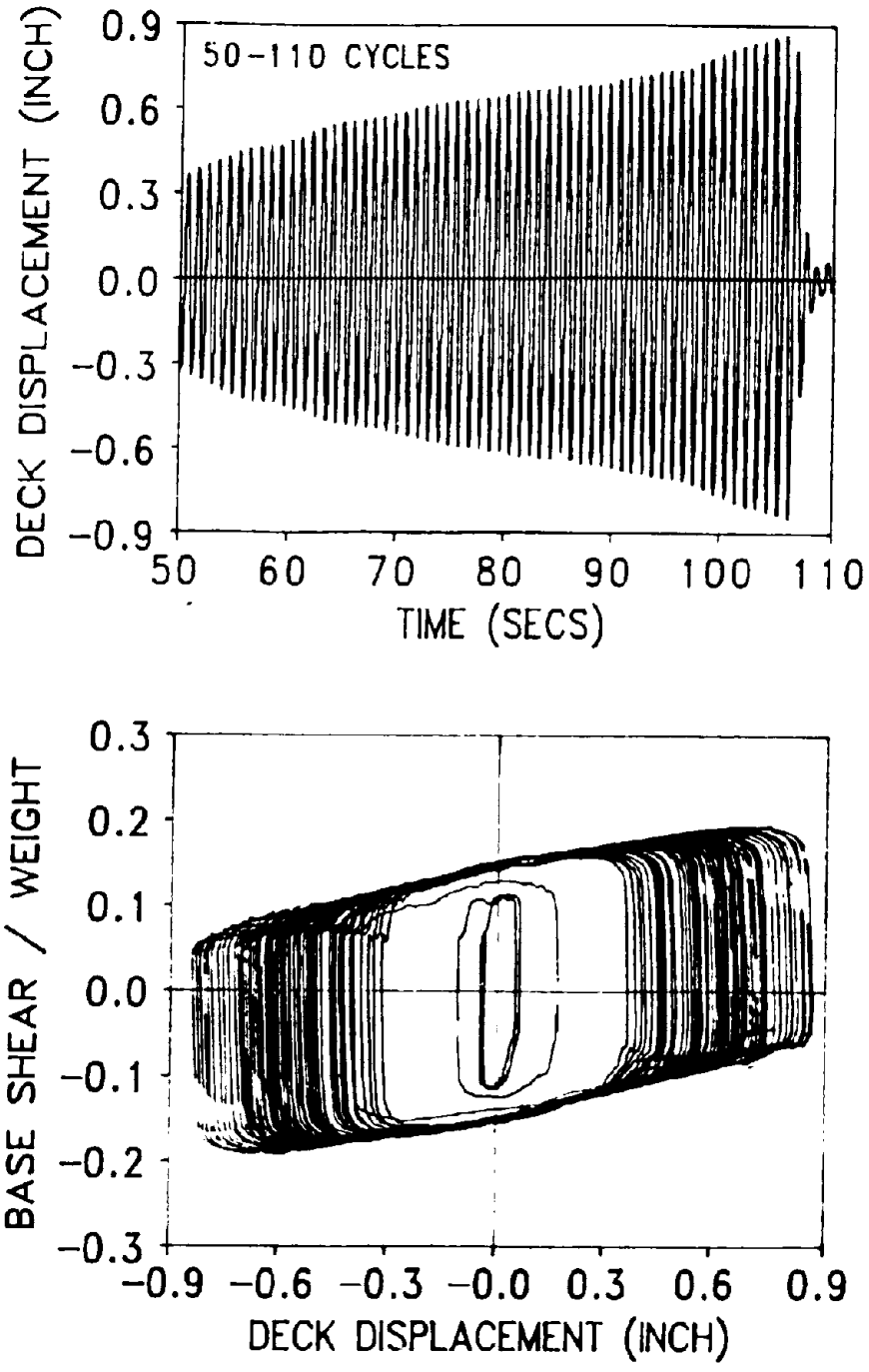

Fig. 6-16 · Recorded Response of T2 System in Test with over 100 Cycles of Motion (1 in. = 25.4 mm).

SECTION 7

ANALYTICAL PREDICTION OF RESPONSE

Reliable analytical techniques for predicting the dynamic response of sliding isolation systems are available (Mokha 1991b; Constantinou 1991a; Mostaghel 1991). This is demonstrated by comparing analytical and experimental responses in several cases.

The isolated model deck is idealized as a rigid block of mass m. Its equation of motion is

$$m\ddot{U}+F_b+F_d = -m\ddot{U}_g \qquad (7\text{-}1)$$

where U is the deck (bearing) displacement with respect to the table; $\ddot{U}_g$ is the table acceleration; F_b is the frictional force from the sliding bearings; and F_d is the force from the displacement control device. Force F_b is given by

$$F_b = [\mu(\dot{U})\cos\delta - sgn(\dot{U})\sin\delta]WZ_b \qquad (7\text{-}2)$$

where sgn stands for the signum function; $\mu(\dot{U})$ is the coefficient of sliding friction of the sliding bearings, which depends on the velocity of sliding (eq. 4-1); and δ is the accidental inclination of the sliding interfaces. Constantinou et al. (1991a) demonstrated that the accidental bearing inclination may be important in predicting bearing displacements of sliding systems with strong frictional force and weak restoring force.

The force in the displacement control device consists of its characteristic strength, F_c and the spring restoring force, F_r

$$F_d = F_c Z_d + F_r \qquad (7\text{-}3)$$

The spring restoring force is elastic nonlinear with the characteristics illustrated in Figure 7-1. Displacement D_1 is the limit beyond which stiffening of the spring of the displacement control device occurs. Displacement D_2 is the spring solid height limit. Stiffness K_2 represent the stiffness of the device when solid height is reached. An analytical description of force F_r is

$$F_r = \begin{cases} K\,U & |U| \le D_1 \\ \dfrac{K_2 - K}{(D_2 - D_1)} \dfrac{(|U| - D_1)^2}{2} sgn(U) + KU, & D_1 < |U| \le D_2 \\ \dfrac{(K - K_2)(D_1 + D_2)}{2} sgn(U) + K_2 U, & |U| > D_2 \end{cases} \qquad (7\text{-}4)$$

One should note that equations 7-3 and 7-4 do not account for the finite strength of the displacement control device.

Variables Z_b and Z_d are used to account for the conditions of separation and reattachment (Constantinou 1990) and are governed by the following equation:

$$Y_i \dot{Z}_i + \gamma |\dot{U}| Z_i |Z_i| + \beta \dot{U} Z_i^2 - \dot{U} = 0, \quad i = b, d \qquad (7\text{-}5)$$

where $\beta + \gamma = 1$ and Y_i is a displacement quantity.

The parameters in equations 7-1 to 7-5 were as follows for the T2 system: $f_{max} = 0.12$, $f_{min} = 0.06$, a = 0.6 sec/in. (23.62 sec/m), $\delta = 0.15°$, W = 51 kips (227.4 kN), K = 3.85 kip/in (675.9 N/mm),

K_2=200 kip/in(35.1 kN/mm), $Y_b = Y_d$ = 0.005 in. (0.127 mm), D_1 = 1.12 in. (28.4 mm) and D_2=1.26 in. (32mm).

Comparisons of analytical and experimental results are presented in Figures 7-2 to 7-8 for the T2 system subjected to Pacoima Dam S74 W 100%, Hachinoche 150%, Caltrans Rock No. 1 100%, Taft 400%, El Centro 200%, Miyagiken-Oki 500% and Mexico City 120% (case of F_c=2.6 kips) motions. The figures demonstrate that the analytical model predicts well the experimental response.

Finally, Figure 7-9 compares the experimental and analytical responses in the test with Pacoima Dan S16E 75% motion in which the displacement restraint mechanism of the displacement control device was activated. The analytical model, which does not account for yielding of the displacement control device, overpredicts the force at the isolation interface. Despite the rather limited additional energy dissipated by yielding (see discussion in Section 6.2), the results of Figure 7-9 demonstrate that yielding had the effect of reducing the base shear from 0.77W to 0.63W. Thus, yielding reduced the impact effect and prevented the deck from bouncing as seen in the analytical time history of deck displacement. Clearly, yielding was beneficial.

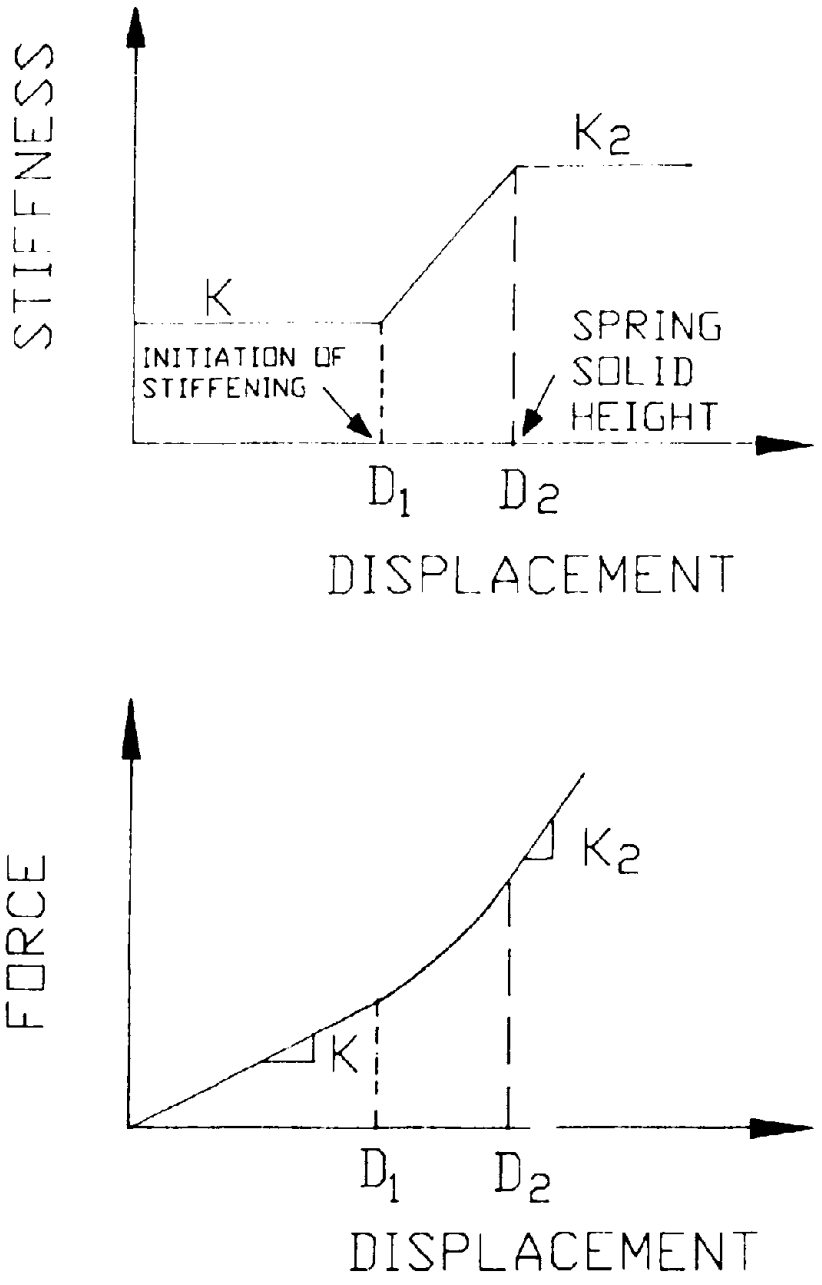

Fig. 7-1 - Stiffness and Force in Analytical Model of Displacement Control Device.

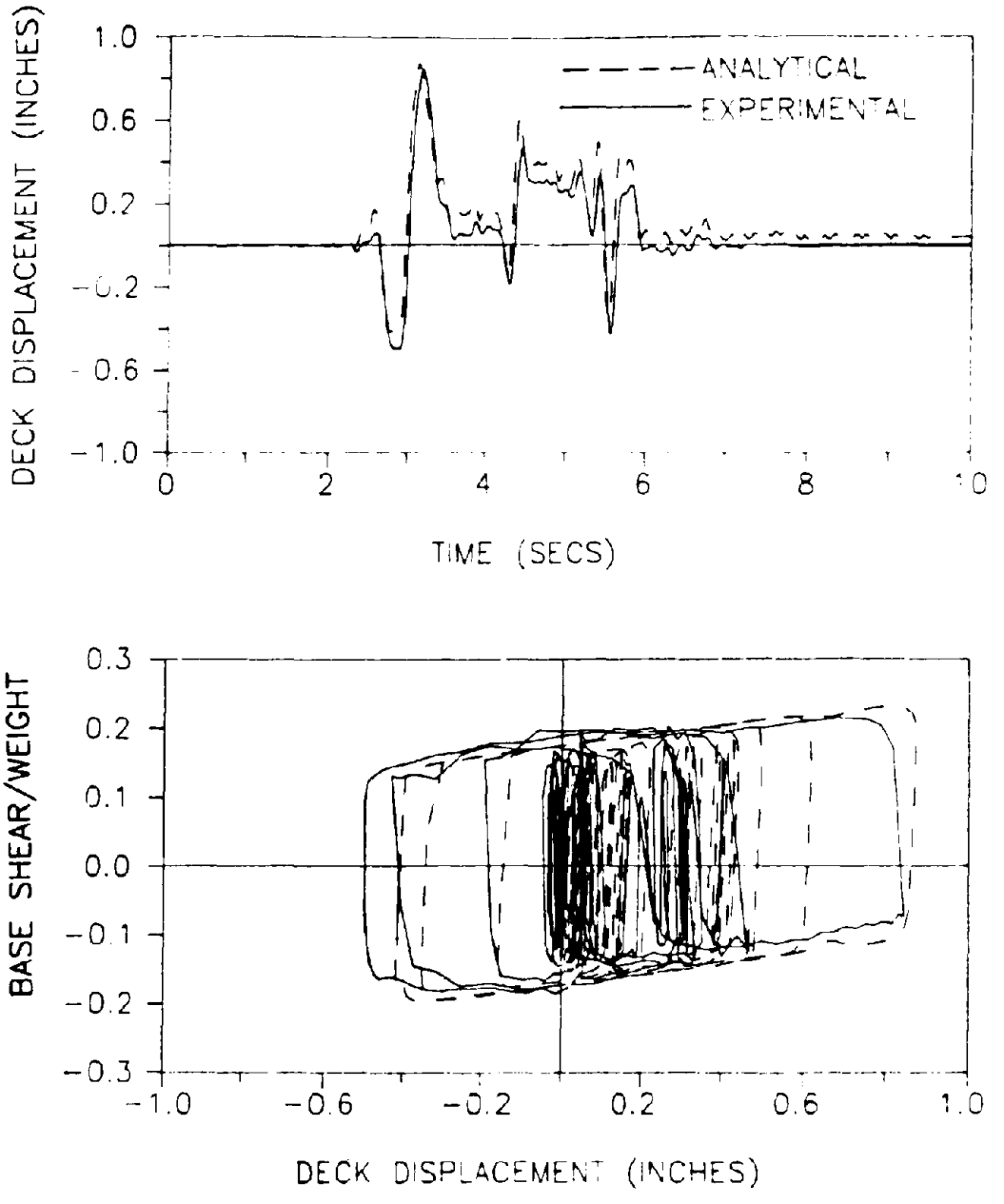

Fig. 7-2 - Comparison of Experimental and Analytical Response of T2 System for Pacoima Dam S74W 100% Input (1 in. = 25.4 mm).

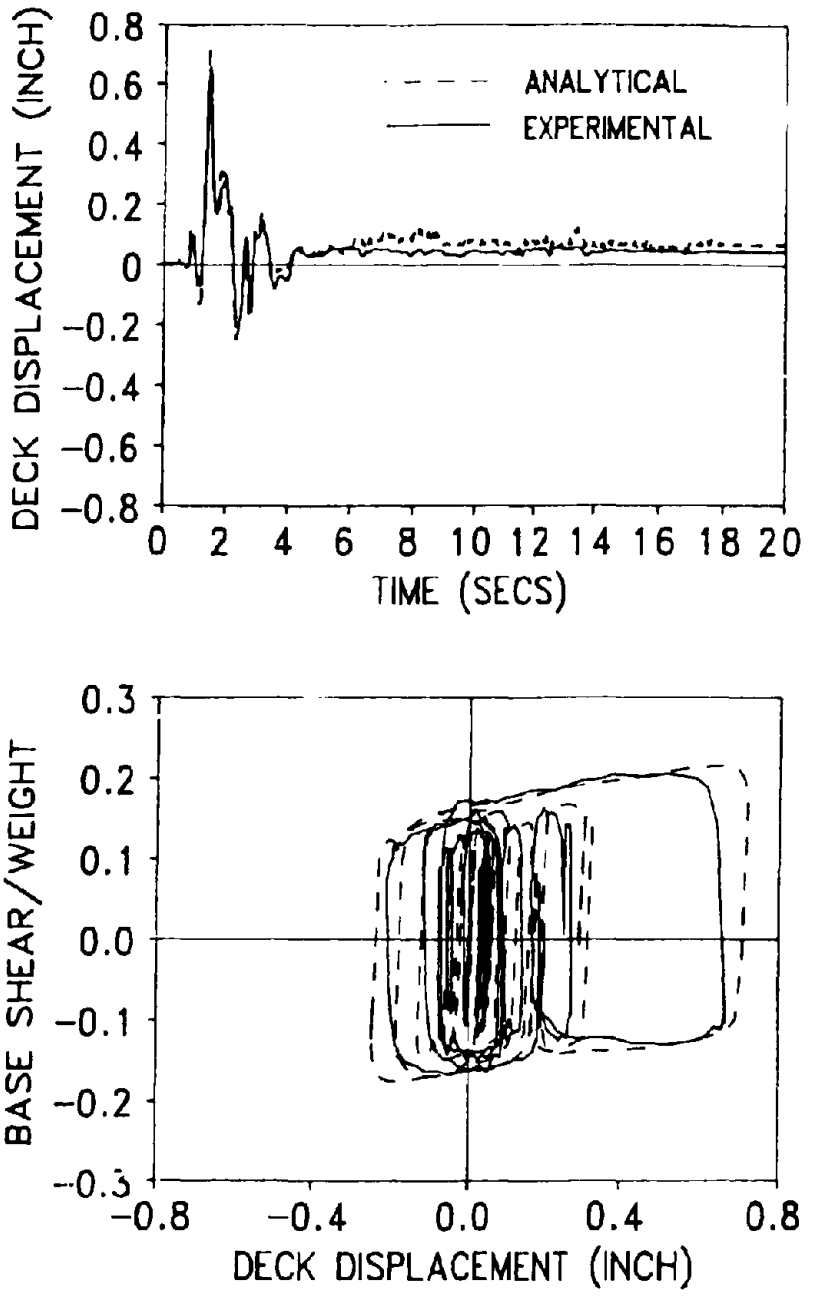

Fig. 7-3 - Comparison of Experimental and Analytical Response of T2 System for Hachinohe NS 150% Input (1 in. = 25.4 mm).

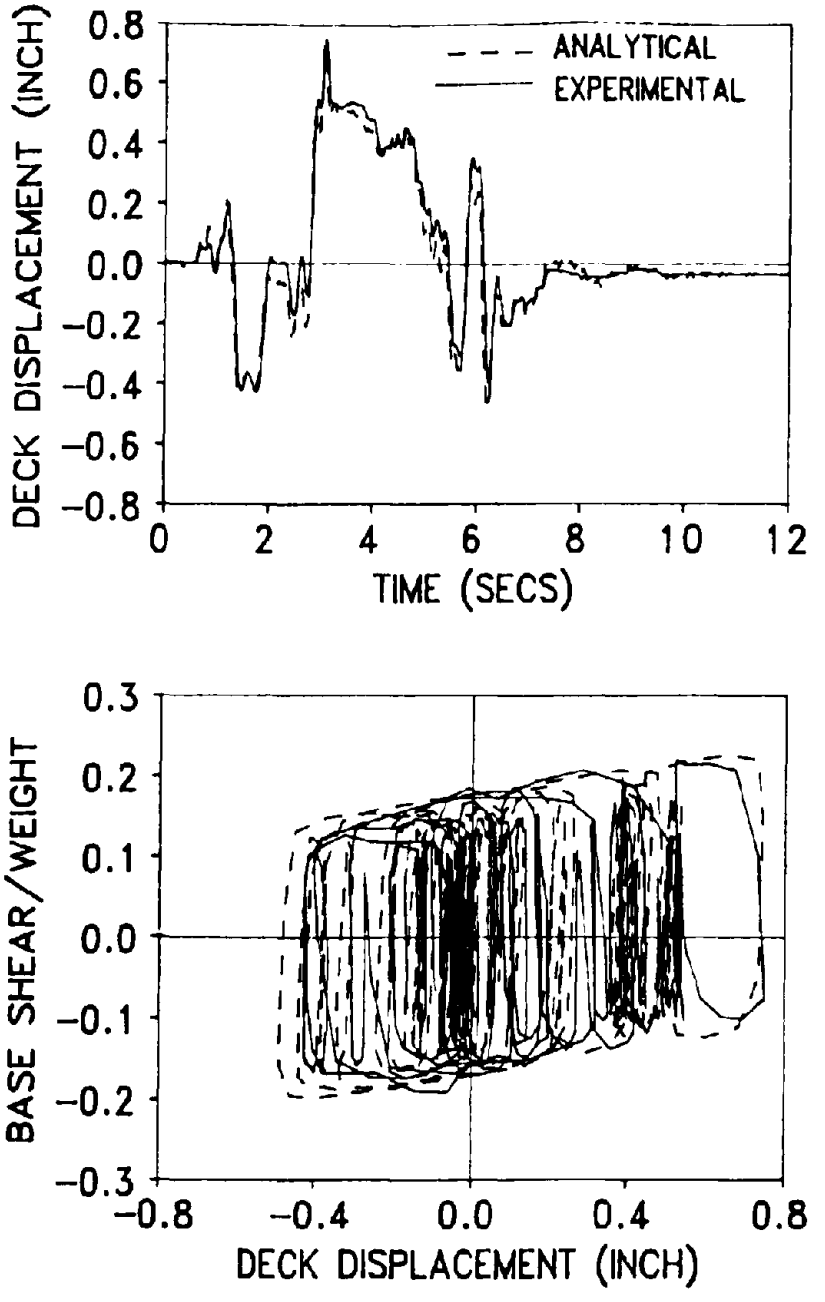

Fig. 7-4 - Comparison of Experimental and Analytical Response of T2 System for Caltrans Rock No. 1 100% Input (1 in. = 25.4 mm).

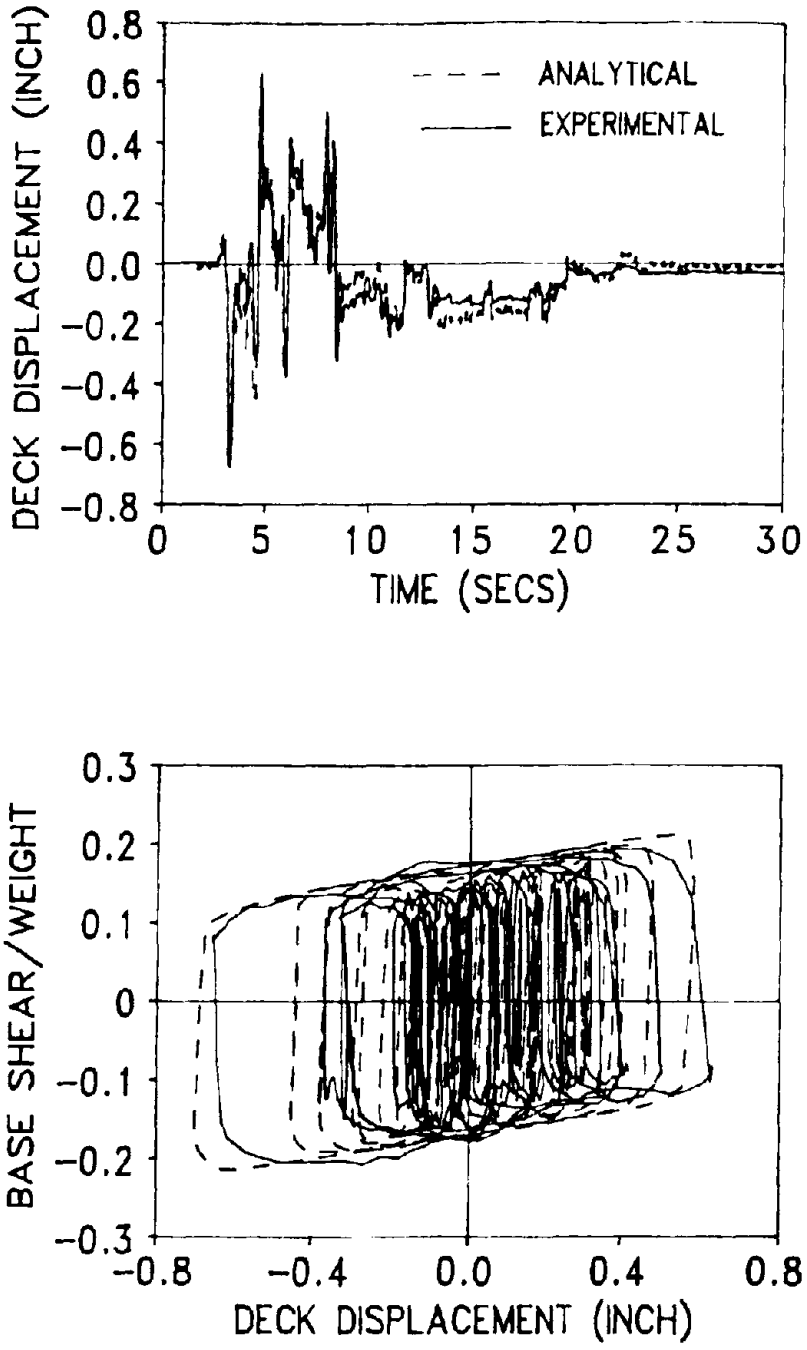

Fig. 7-5 - Comparison of Experimental and Analytical Response of T2 System for Taft N21E 400% Input (1 in. = 25.4 mm).

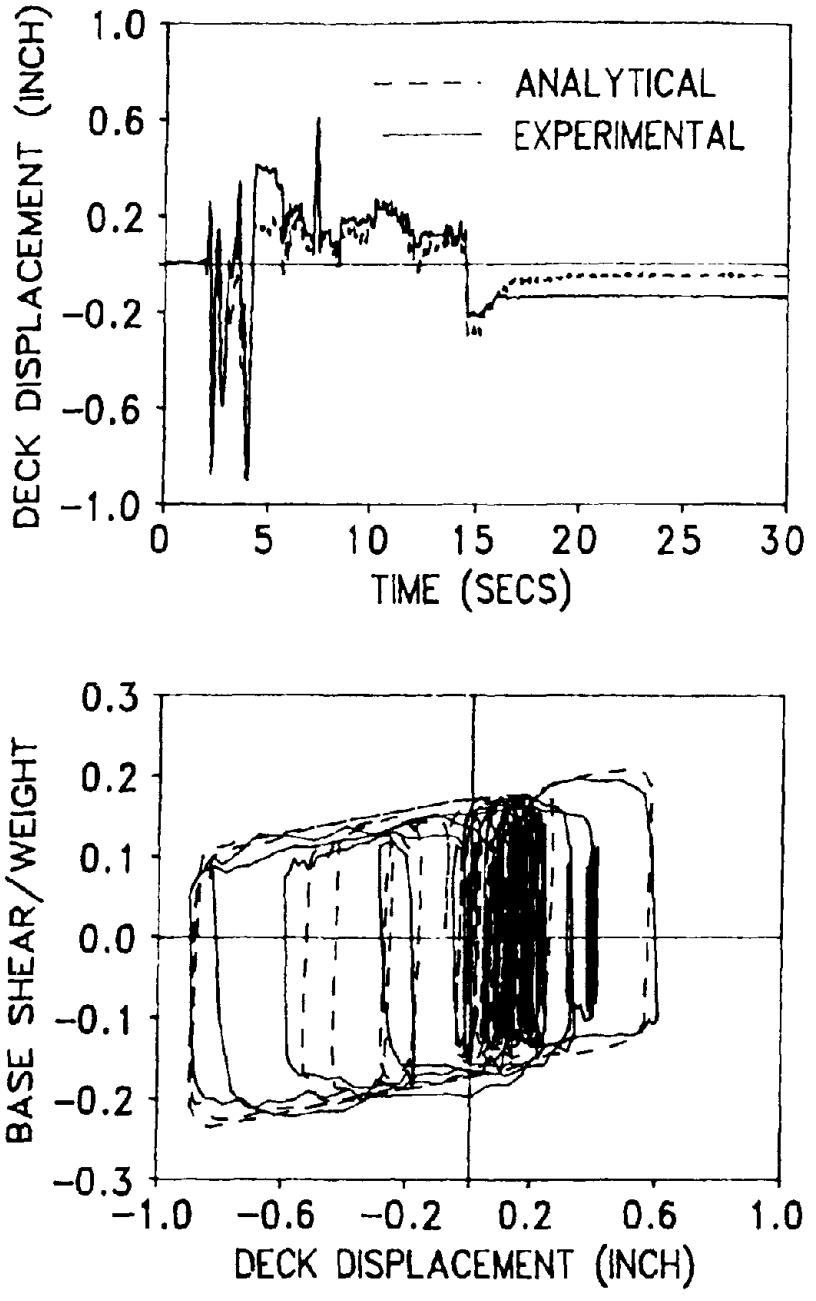

Fig. 7-6 - Comparison of Experimental and Analyti ' Response of T2 System for El Centro S00E 200% Input (1 in. = 25.4 mm).

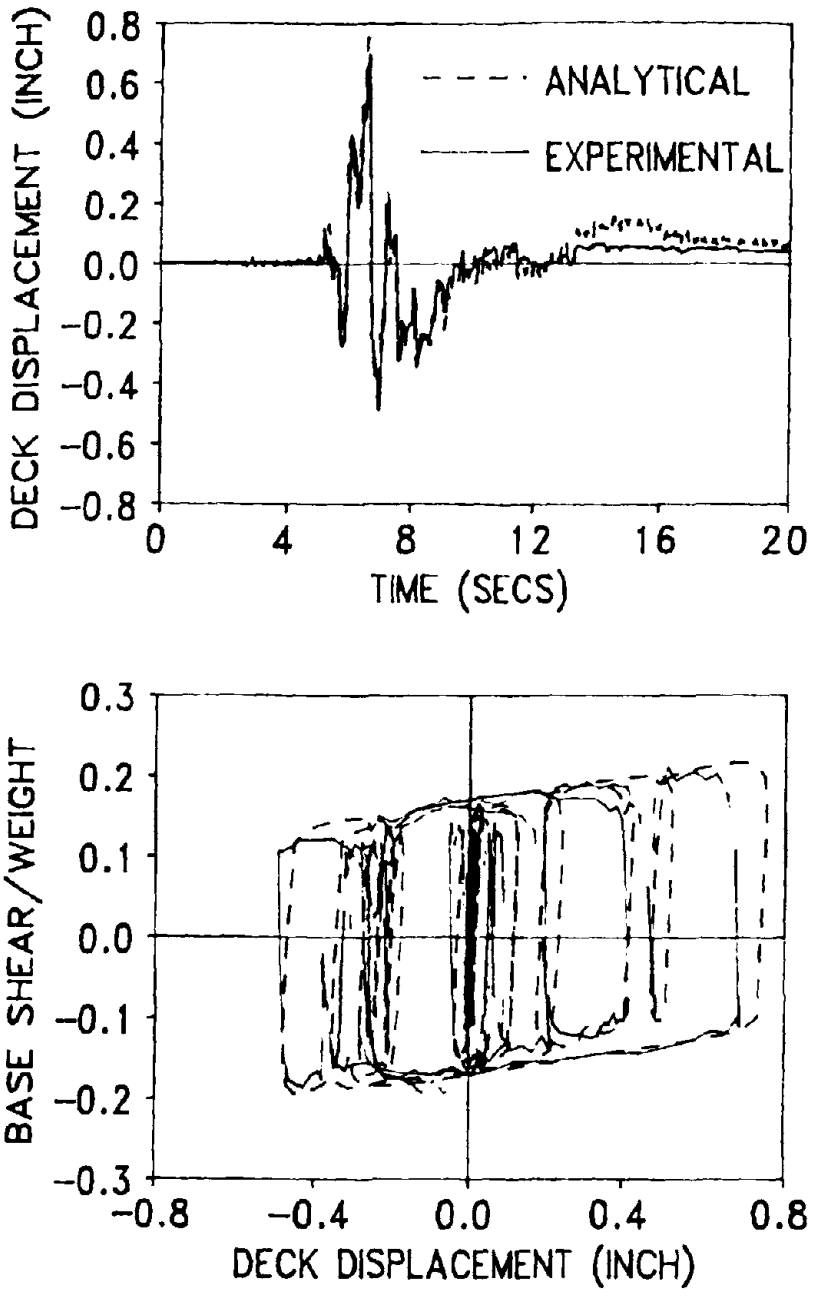

Fig. 7-7 - Comparison of Experimental and Analytical Response of T2 System for Miyagiken-Oki EW 500% Input (1 in. = 25.4 mm).

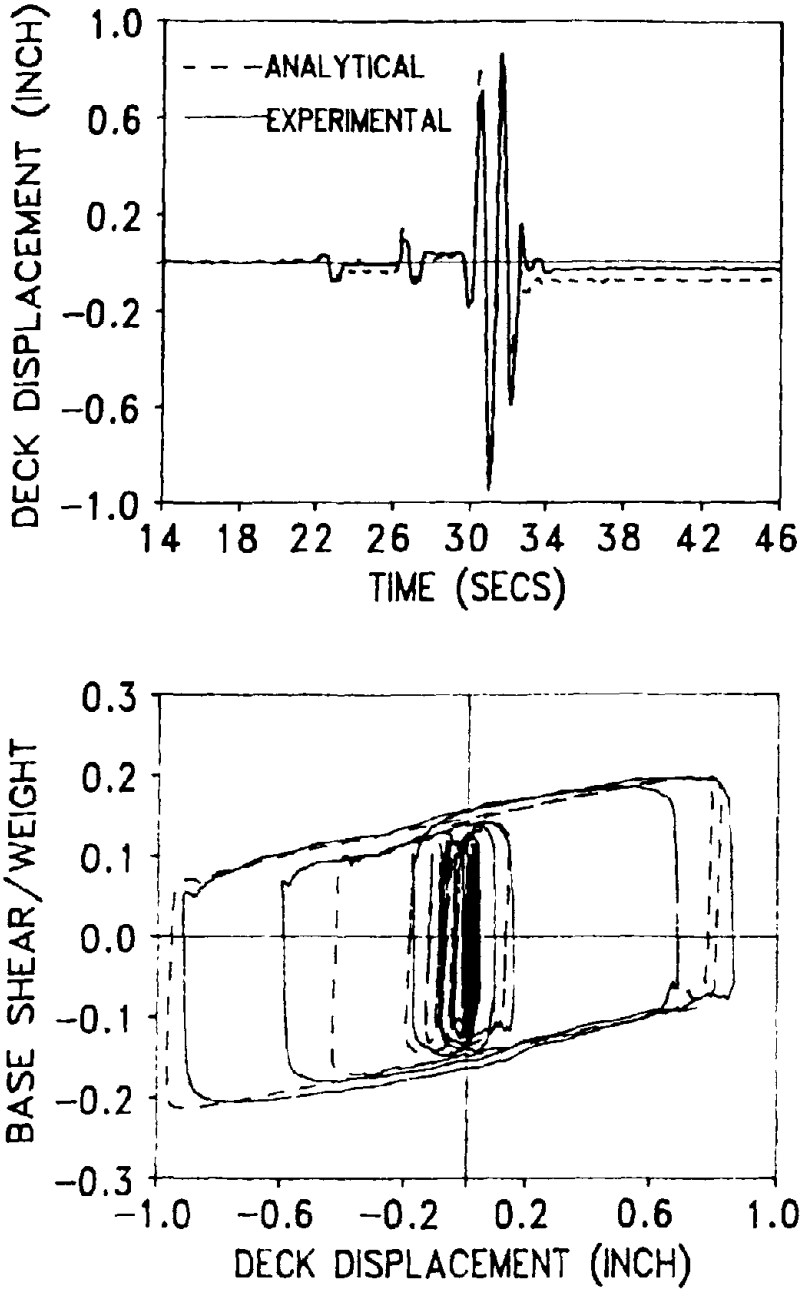

Fig. 7-8 - Comparison of Experimental and Analytical Response of T2 System for Mexico City N90W 120% Input (1 in. = 25.4 mm).

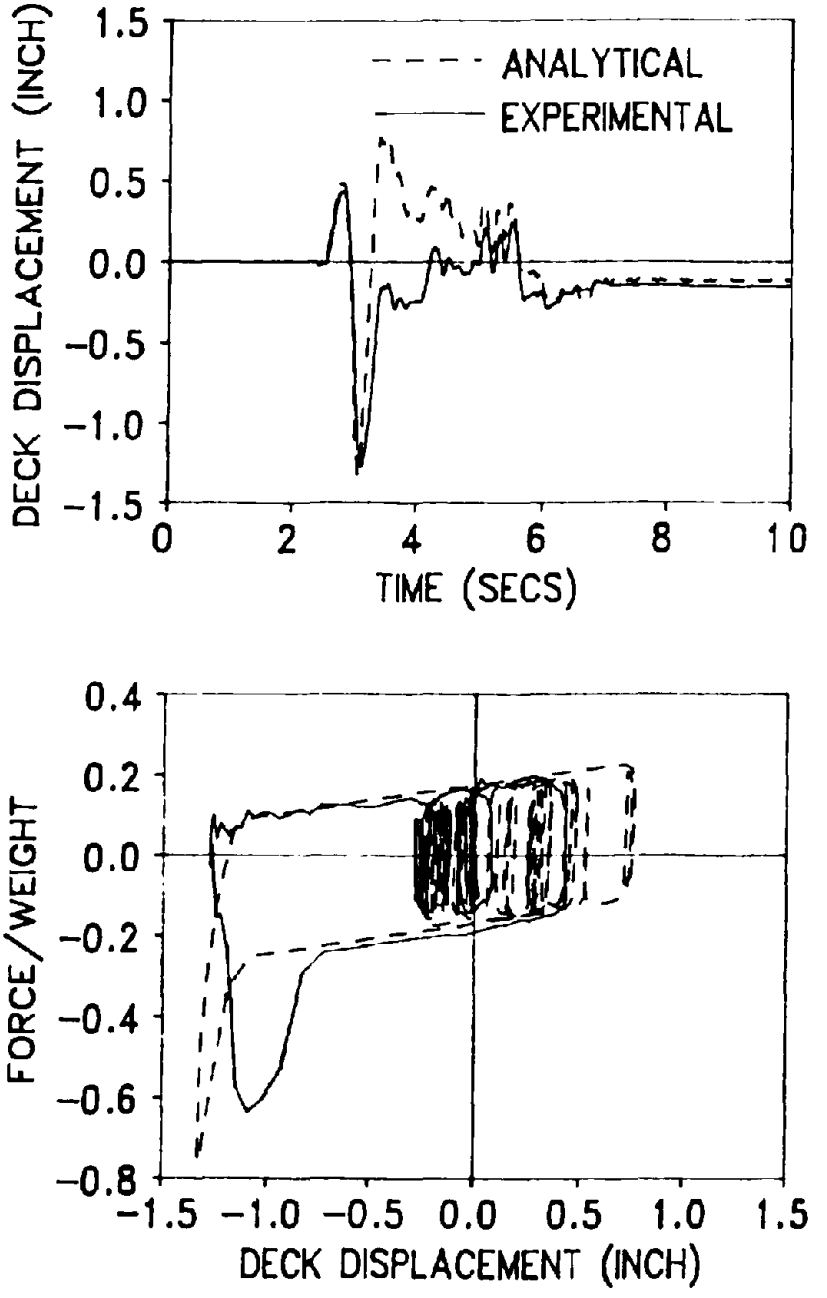

Fig. 7-9 - Comparison of Experimental and Analytical Response of T2 System for Pacoima Dam S16E 75% Input (1 in. = 25.4 mm).

SECTION 8

BRIDGE MODEL IN ANALYTICAL STUDY

The experimental study demonstrated the effectiveness of the isolation system in reducing the acceleration response of the isolated deck while allowing bearing displacements less than those of the ground. Analytical methods were shown to be capable of accurately predicting the experimental response.

The experiments were conducted with a rigid deck model with the isolation system supported by rigid supports. The possible significant effects of pier flexibility, pier strength, deck flexibility and distribution of isolation elements could not be studied in the experimental program. Rather, these effects are studied by analytical techniques which utilize the experimentally calibrated model of the isolation system.

The analytical study primarily concentrates on the dynamic response of two-span continuous deck isolated bridges as the one shown in Figure 3-3.

8.1 Model in Transverse Direction

A model for dynamic analysis of the two-span bridge in its transverse direction is shown in Figure 8-1. The abutments are idealized as rigid elements. The pier is idealized as a single-degree-of-freedom bilinear hysteretic oscillator with mass m_p. The deck is modelled as a three-mass system with one half of its mass, m_d concentrated above the pier and the rest of its mass equally concentrated above the abutments. The three masses are

interconnected by spring and viscous elements that represent the deck flexibility. The deck is connected to the abutments and pier by sliding and bilinear hysteretic elements which represent the behavior of the sliding bearings and displacement control devices, respectively.

Owing to symmetry in the model, the dynamic response is described by three degrees of freedom. These are the deck displacement at the abutments, U_{d2}, the deck displacement at the pier, U_{d1}, and the pier top displacement, U_p. All displacements are with respect to the ground. The frictional force in the sliding bearings at the abutment is described by

$$F_{ba} = \mu_a(\dot{U}_{d2})\, W_a Z_a \qquad \textbf{(8-1)}$$

whereas the force in the sliding bearings at the pier is described by

$$F_{bp} = \mu_p(\dot{U}_{d1} - \dot{U}_p)\, W_p Z_p \qquad \textbf{(8-2)}$$

In (8-1) and (8-2), μ_a and μ_p are the coefficients of friction of the sliding bearings at the abutment and pier locations, respectively. They depend on the velocity at the sliding interface (Constantinou, 1990) in accordance to

$$\mu(\dot{U}) = f_{max} - (f_{max} - f_{min})\exp(-a|\dot{U}|) \qquad \textbf{(8-3)}$$

Parameters f_{max}, f_{min} and a depend on the materials which form the sliding interface and on the bearing pressure (Mokha 1990 and 1991a). Values of these parameters for the materials and conditions assumed in this study are presented in Table 8-I.

Furthermore, W_a and W_p are the weights carried by the sliding bearings at the abutment and pier locations, respectively.

The force in each displacement control device is given by (Constantinou et al. 1991b)

$$F_d = F_c Z_d + K U_{d2} \qquad \textbf{(8-4)}$$

in which F_c is the characteristic strength of the device and K is the constant of the spring assembly of the device. Equation (8-4) describes bilinear hysteric behavior with very large initial and unloading stiffness and with yield force equal to F_c. It reproduces well the behavior of displacement control devices (Constantinou et al. 1991b).

Variables Z_i, i = a, p and d in (8-1), (8-2) and (8-4) are used to account for the conditions of separation and reattachment (Constantinou 1990) and are governed by the following equation:

$$Y_i \dot{Z}_i + \gamma |\dot{U}_i| Z_i |Z_i| + \beta \dot{U}_i Z_i^2 - \dot{U}_i = 0 \qquad \textbf{(8-5)}$$

where $\beta + \gamma = 1$, Y_i = 0.005 in. (0.127 mm). Furthermore, when i = a, $\dot{U}_i = \dot{U}_{d2}$, when $i = p$, $\dot{U}_i = \dot{U}_{d1} - \dot{U}_p$, and when $i = d$, $\dot{U}_i = \dot{U}_{d2}$.

The pier behavior is described by a smooth bilinear, non-degrading hysteretic element of initial stiffness K_{in}, yield force F_y and post-yielding stiffness of $\alpha_p K_{in}$. Furthermore, a viscous element of constant C_p is used in parallel to the hysteretic element. The viscous element is needed to account for energy dissipation in the pier when essentially elastic behavior occurs.

The dynamic behavior of the model in the transverse direction is described by the following parameters:

a) Period of free vibration when deck and pier are assumed rigid

$$T_b = 2\pi\left(\frac{m_d}{\Sigma K}\right)^{1/2} \qquad \textbf{(8-6)}$$

b) Characteristic strength of displacement control devices as portion of the deck weight

$$\epsilon = \frac{\Sigma F_c}{m_d g} \qquad \textbf{(8-7)}$$

In (8-6) and (8-7) the sum Σ extends over all devices in the transverse direction.

c) Pier period of free vibration for elastic behavior and in its cantilever position

$$T_p = 2\pi\left(\frac{m_p}{K_{in}}\right)^{1/2} \qquad \textbf{(8-8)}$$

d) Damping ratio of pier

$$\xi_p = \frac{C_p}{2\,(K_{in} m_p)^{1/2}} \qquad \textbf{(8-9)}$$

e) Strength of pier as portion of the weight it carries

$$e_p = \frac{F_y}{W_p} \qquad \textbf{(8-10)}$$

f) Period of free vibration of deck when assumed pinned at the abutments

$$T_d = 2\pi\left(\frac{m_d}{2K_d}\right)^{1/2} \qquad \textbf{(8-11)}$$

g) Damping ratio of deck

$$\xi_d = \frac{C_d}{(2K_dM_d)^{1/2}} \qquad \textbf{(8-12)}$$

h) Ratio of pier mass to deck mass

$$\nu = \frac{m_p}{m_d} \qquad \textbf{(8-13)}$$

i) Ratio of weight carried by abutment to weight of deck

$$\ell = \frac{W_a}{m_d g} \qquad \textbf{(8-14)}$$

The model accounts in a simplified way for the flexibility of deck and pier and for the limited strength and possible inelastic behavior of the pier. However, it does not account for the possible higher mode effects of the pier and the rotational inertia effects of the deck.

8.2 Model in Longitudinal Direction

The model is further simplified for analysis in the longitudinal direction by assuming the deck to be rigid in its own plane. This model is consistent with the bridge models used by Ghobarah and Ali(1988) and Turkington et al. (1989a and 1989b) in seismic analyses of bridges on lead-rubber bearings.

8.3 Earthquake Excitation

The earthquake excitation consists of simulated motions compatible with the California Department of Transportation bridge design spectra of 0.6g acceleration for rock and deep alluvium of 80 to 150 ft (24 to 46 m) depth (Gates 1979). Three artificial records were simulated for each design spectrum with a duration of 20 secs in the case of rock spectrum and 30 secs in the case of deep alluvium spectrum. Each record was applied in the longitudinal and transverse directions of the model. The maximum response of the parameters of interest calculated by the three time-history analyses in each direction is reported.

The three motions which are compatible to 0.6g rock spectrum are identical to those used in the experimental program (see Figures 6-5 to 6-7 and apply scales to displacement and velocity). As an example of deep alluvium motion, Figure 8-2 shows the ground motion histories of one of the three artificial records used in the study. The figure shows also the acceleration spectrum of the record which closely matches the corresponding CALTRANS spectrum (Gates 1979).

8.4 Parametric Study

The range of values of the parameters in (8-8), (8-11) and (8-13) has been studied for some bridges. Lam and Martin (1986) reported detailed information on some conventionally built bridges in the United States. In four of these bridges the pier period, T_p (8-8), was calculated by modeling the reinforced concrete piers as cantilever beams with moment of inertia equal to 0.3 times their gross moment of inertia. This gave values for period T_p in the range 0.1 to 0.5 secs. In two 2-span bridges the deck was modeled as simply supported beam with moment of inertia equal to 0.5 times the gross moment of inertia. Deck transverse period, T_d (8-11), was found to be about 0.4 secs, whereas the mass ratio, ν (8-13), was found to be about 1/20. Table 8-II lists the calculated properties of these bridges. Furthermore, typical values of parameters T_b, (8-6) and ϵ, (8-7) for sliding isolation systems are: T_b = 1.5 to 3 secs and ϵ = 0 to about 0.1. For example, the tests were conducted with parameters T_b = 2.33 secs (in prototype scale) and ϵ = 0.04 to 0.1.

Accordingly, the values of parameters in the study were selected to be: T_p = 0.2 and 0.4 secs, T_d = 0.3 and 0.6 secs, ν = $\frac{1}{10}$ and $\frac{1}{20}$, T_b = 1.5 to 3 secs and ϵ = 0.05. Furthermore, the ratio of post-yielding stiffness to initial stiffness, α_p, of the pier was set at 0.05 and damping ratios ξ_p, (8-9) and ξ_d, (8-12),

were both set at 0.05. The ratio of pier strength to load carried by the pier, e_p (8-10), was assigned values of 0.1, 0.2 and 0.3. The case e_p = 0.1 corresponds to a pier of inadequate strength. The results obtained in this case are of interest in the seismic retrofit of bridges with piers of inadequate strength and ductility capacity.

The frictional properties of sliding bearings are selected in such a way as to maximize energy dissipation and to minimize the transfer of force to the pier which is assumed to be the weakest element of the bridge substructure. The frictional properties of sliding bearings used in the study are presented in Table 8-I. The case of sliding interface consisting of unfilled Teflon and polished stainless steel represents a design with commonly used bridge sliding bearings. The sliding interface of woven Teflon and stainless steel (referred to as the lower friction case) is used at the pier location only in the case of pier with inadequate strength (e_p = 0.1).

Table 8-1 - Frictional Properties of Sliding Bearings
(1 in. = 25.4mm, 1000 psi = 6.9 MPa)

Sliding Interface	Bearing Pressure (psi)	fmin	fmax	a (sec/in.)	Bearing Location
Unfilled Sheet Teflon-Polished Stainless Steel of Ra = 1.6 μin	1000	0.027	0.120	0.60	Abutment
	3000	0.015	0.070	0.80	Pier
Woven Teflon-Polished Stainless Steel of Ra = 1.6 μin	10000	0.012	0.045	1.60	Pier (case of lower friction

Table 8-II - Properties of Some Bridges

Bridge	Superstructure	Pier	Pier Period Tp (secs)		Deck Transverse Period Td (secs)	$\nu = \frac{m_p}{m_d}$
			Longitudinal	Transverse		
Meloland Rd. Overcrossing 58-215, CA.	2-span, R/C Box Girder 208 ft. Length	Single Circular R/C Column	0.26	0.26	0.40	1 / 23
Painter Str. Overcrossing 4-236, CA.	2-span, R/C Box Girder 265 ft. Length	2 Octagonal R/C Columns	0.21	0.11	0.36	1 / 21
East Connector Separation, 56-748F, CA.	3-span, R/C Box Girder, 362 ft. Length	Single Octagonal R/C Column	0.48	0.48	-	-
Rose Creek Interchange, I-862, NV	5-span, R/C Box Girder, 400 ft. Length	Single Octagonal R/C Column	0.25	0.13	-	-

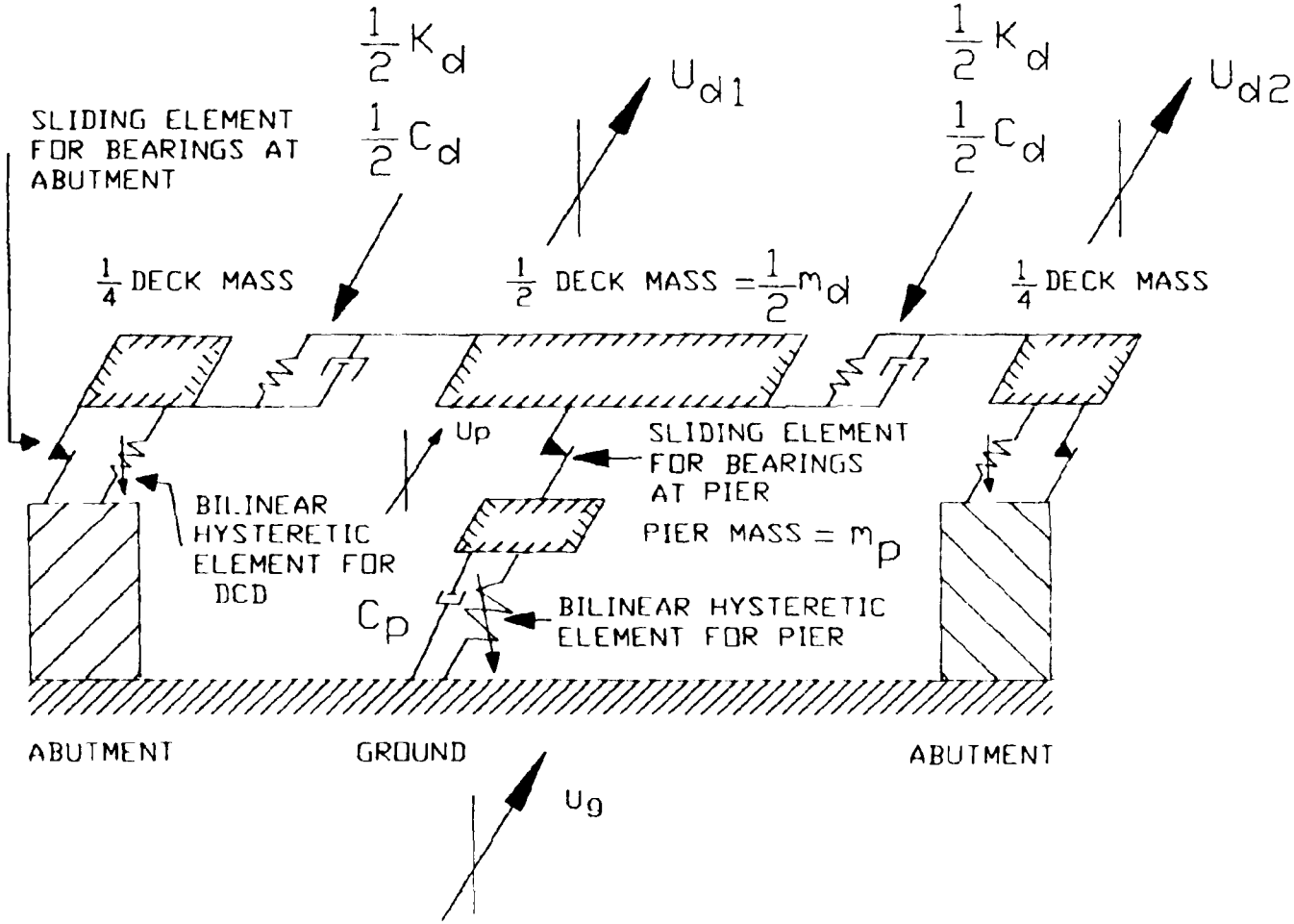

Fig. 8-1 - Transverse Direction Model of Two-span Isolated Bridge.

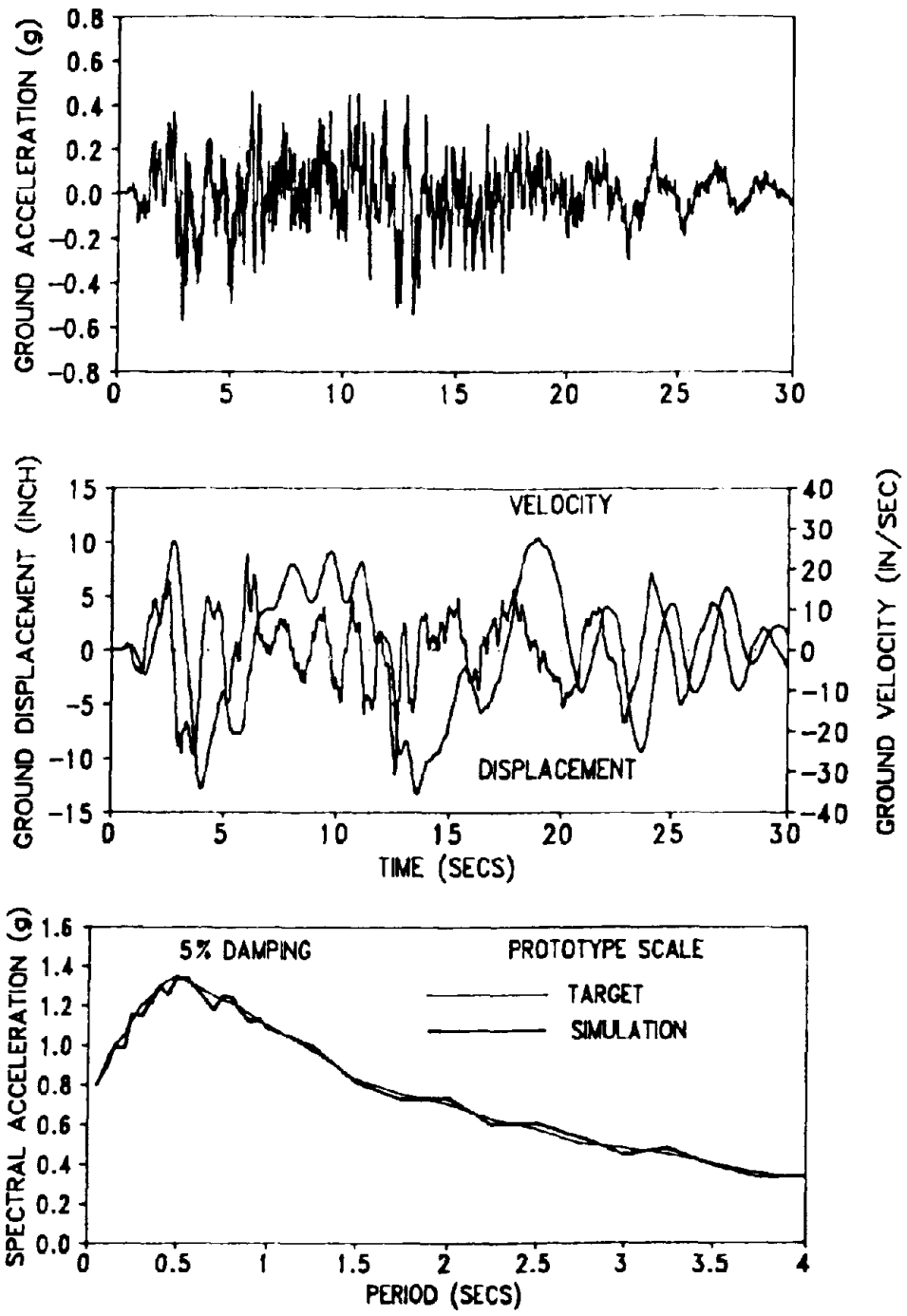

Fig. 8-2 - Time Histories of Ground Motion and Response Spectrum of Simulated Earthquake Compatible with Caltrans 0.6g, 80'-150' Alluvium Spectrum (1 in. = 25.4mm).

SECTION 9

RESULTS OF ANALYTICAL PARAMETRIC STUDY

Results of the analytical parametric study are presented in graphical form. These results are the deck (bearing) displacements at the abutment and pier locations, deck acceleration, pier top acceleration, pier displacement ductility, and transverse deck bending moment.

The pier displacement ductility is the pier top peak displacement divided by its yield displacement Y

$$Y = \frac{4\pi^2 e_p (1 - 2\ell)\, g T_p^2}{v} \qquad (9\text{-}1)$$

The transverse deck bending moment is the maximum bending moment about a vertical axis due to transverse motion of the deck. It was computed from the distributed inertia forces and concentrated bearing and displacement control device forces using standard methods of statics (Clough and Penzien 1975). The bending is normalized by the product of deck weight ($W_d = m_d g$) and length L of one span.

The results for longitudinal excitation are presented in Figures 9-1 to 9-10 and the results for transverse excitation are presented in Figures 9-11 to 9-34. All results are for the typical case of $v = \frac{1}{20}$ and $\ell = \frac{3}{16}$ (equal length spans).

9.1 Effectiveness of Isolation System

The effectiveness of the isolation system is first demonstrated by comparison of responses of isolated bridges with T_b = 2 secs (a typical case) to that of comparable non-isolated bridges. The pier of the conventionally built bridges is assumed to be connected to the deck above by a fixed bearing, that is a bearing allowing for rotation but no displacement. The bearings at the abutment location are guided (allow only longitudinal movement) sliding bearings having the same frictional properties as those of the isolated bridge. In this respect the isolation design consists of replacing the fixed and guided bearings by multidirectional bearings and with displacement control devices added.

The results of the comparison study are presented in Tables 9-I and 9-II for the cases of rock and deep alluvium input applied in the longitudinal direction. The results demonstrate a marked reduction in the displacement ductility demand of the pier of the isolated bridge. In the case of the severely under-designed pier (ϵ_p = 0.1) the ductility demand is excessive and clearly indicates the possibility of collapse or severe damage. In contrast, the pier of the isolated bridge experiences limited ductility demand and in the case of lower friction at the pier it experiences nearly elastic behavior. Furthermore, the isolated bridge with pier strength of $\epsilon_p \geq 0.2$ remains elastic.

This very good performance is achieved with bearing displacements being less than 4 in. (101.6 mm) in the case of rock

input and less than 9 in. (228.6 mm) in the case of deep alluvium input. Even more interestingly, the displacements of the isolated bridge are less than those of the non-isolated bridge by a factor as high as 2.

9.2 Effect of Pier Flexibility

Increases in the pier flexibility (period of cantilever pier T_p) result in increases in the deck displacement with respect to the abutment (bearing displacement at abutment) which are more pronounced in the rock type input. Differences in the deck displacements with respect to abutment between 5 and 20% are noted. Furthermore, the pier flexibility has an effect on the bearing displacement at the pier location which is in general less pronounced than that on the bearing displacement at the abutment location.

Increases in the pier flexibility have also mixed effects on the pier displacement ductility and pier top acceleration. In the case of rock input both quantities are substantially reduced when the pier flexibility increased. In the case of deep alluvium input the differences are much smaller and for some combinations of parameters even increases in these quantities are noted.

Furthermore, the pier flexibility has an insignificant effect on the shear force across the isolation interface. This is apparent in the figures showing the deck acceleration for longitudinal excitation (Figs. 9-3 and 9-8). In this case, the deck is rigid and the deck acceleration is proportional to the shear force across the isolation interface. This was expected as

friction contributes a major portion of the isolation interface shear force.

9.3 Effect of Deck Flexibility

Deck flexibility has a minor effect on bearing displacements, pier displacement ductility and pier top acceleration. However, it has a significant effect on the distribution of transverse acceleration along the length of the bridge. Flexible decks respond with out-of-phase accelerations in a fashion very similar to that observed in shake table tests of flexible buildings on sliding isolation systems (Constantinou 1991a; Mokha 1991b). For evidence of this behavior observe Figures 9-3, 9-13 and 9-19. In the transverse direction the deck responds with higher peak acceleration than it does in the longitudinal direction. Furthermore, the peak deck acceleration, which occurs at the abutment location, increases with increasing deck flexibility.

While accelerations were larger in the flexible deck, the internal stresses (as expressed by the bending moment about a vertical axis of the deck) are only marginally affected. Comparison of Figures 9-16 to 9-22 reveals even a decrease in bending moment as flexibility increases. This, of course, is explained by the out-of-phase acceleration response. This behavior is illustrated in Figure 9-35 which shows profiles of deck acceleration (solid line) and bearing displacement (dashed line) in the case of one of the rock type motions. The system is characterized by parameters T_p = 0.2 secs, T_d = 0.3 secs, T_b = 2 secs, ϵ_p = 0.1, ϵ = 0.05 and ν = 1/20. The profiles are shown at

times at which certain response quantities attain their maximum values. Similarly, Figure 9-36 shows profiles of the response of the same system for another of the rock type motions.

9.4 Effect of Pier Mass to Deck Mass Ratio

The results presented so far are for the case of pier mass to deck mass ratio $\nu = 1/20$. The effect this ratio has on the bridge response is investigated herein. Larger values of ratio ν, up to 1/5, are possible in the case of massive piers (e.g. walls) or in the case low weight decks. In both cases a large value of ν is associated with a large value of ratio of pier characteristic strength to weight carried by the pier, ϵ_p. Accordingly, the effect of the mass ratio is investigated only for the case of $\epsilon_p = 0.2$. Results are presented in Figures 9-37 to 9-41 for the bridge excited by rock type motion in its longitudinal direction. The results demonstrate that the mass ratio has a minor effect on the isolated bridge response.

9.5 Pier Behavior

In addition to the previously discussed substantial reduction in the pier displacement ductility demand, two other aspects of the pier behavior are worthy of discussion. First we note that an upper limit to pier shear force over axial load ratio, V_p/W_p, may be estimated by the following equation:

$$\frac{V_p}{W_p} = \frac{a_p \nu}{g(1-2\ell)} + f_{max} \qquad (9\text{-}2)$$

in which a_p is the top of pier peak acceleration. Equation (9-2) was derived by assuming that the peak pier inertia force and the peak frictional force occur at the same time. Calculations of the pier shear force by (9-2) give values which are 10 to 20% larger than those predicted by nonlinear dynamic analysis (e.g. Table 9-II, case $\epsilon_p = 0.1$, $T_p = 0.2$ secs). For a yielding pier such difference in the shear force results in a multifold difference in displacement ductility. This suggests that nonlinear dynamic analysis should be used for accurate prediction of the pier nonlinear behavior.

The criterion used in this report for evaluating the performance of the isolation system is the degree of reduction of the pier displacement ductility in comparison to the corresponding non-isolated bridge. For example, the reduction of pier ductility of the system with $T_p = 0.2$ secs, $\epsilon_p = 0.1$ and 0.3 for deep alluvium input (Table 9-II) is about 11.5 for both cases. This indicates excellent performance. Another criterion, which was used in evaluating base isolated buildings (e.g. Griffith 1988), is based on the acceleration above the isolator in comparison to the acceleration below the isolator. Using this criterion the aforementioned two systems exhibit different performances with reduction factors of 2.4 and 3.6, respectively, which are much less than those achieved for the pier displacement ductility. The

writers believe that the acceleration above the isolator is not necessarily the best, and is not the only measure of performance. In this respect, the direct use without analysis of acceleration records of instrumented isolated bridges for evaluating performance in an earthquake may give misleading results. This, of course, would apply for all isolation systems, not only sliding systems.

Table 9-1 - Comparison of Response of Isolated and Non - Isolated Bridge for CALTRANS 0.6g - Rock Input (1 in. = 25.4mm)

ISOLATED BRIDGE WITH Tb = 2 SECS

ε_p	Tp (sec)	Bearing Displacement (in)		Deck Accel. (g)	Pier Accel. (g)	Pier Displ. Ductility	Pier Shear/ Axial Load
		At Abutment	At Pier				
0.1	0.2	3.15	2.88	0.21	0.82	2.15	0.109
0.1	0.4	3.84	2.49	0.23	0.43	1.51	0.105
0.2	0.2	3.23	3.15	0.21	1.26	0.88	0.171
0.2	0.4	3.75	2.72	0.23	0.83	0.66	0.130
0.3	0.2	3.23	3.15	0.21	1.20	0.52	0.155
0.3	0.4	3.80	3.74	0.23	0.84	0.44	0.132

ISOLATED BRIDGE WITH Tb = 2 SECS AND LOWER FRICTION AT PIER

0.1	0.2	3.56	3.53	0.21	1.01	1.53	0.105
0.1	0.4	3.97	3.68	0.22	0.87	1.11	0.099

NON-ISOLATED BRIDGE

0.1	0.2	4.87	0	0.15	0.15	9.94	0.174
0.1	0.4	9.95	0	0.12	0.12	5.07	0.142
0.2	0.2	4.64	0	0.20	0.20	4.73	0.257
0.2	0.4	7.54	0	0.18	0.18	1.92	0.232
0.3	0.2	4.23	0	0.25	0.25	2.87	0.350
0.3	0.4	7.02	0	0.22	0.22	1.19	0.307

Table 9-II - Comparison of Response of Isolated and Non - Isolated Bridge for CALTRANS 0.6g - Deep Alluvium Input (1 in. = 25.4mm)

ISOLATED BRIDGE WITH Tb = 2 SECS

ε_p	Tp (sec)	Bearing Displacement (in)		Deck Accel. (g)	Pier Accel. (g)	Pier Displ. Ductility	Pier Shear/ Axial Load
		At Abutment	At Pier				
0.1	0.2	7.80	7.21	0.33	0.78	2.81	0.112
0.1	0.4	8.45	7.85	0.35	0.74	2.29	0.109
0.2	0.2	7.77	7.62	0.33	1.16	0.79	0.157
0.2	0.4	8.23	7.48	0.34	1.38	0.83	0.163
0.3	0.2	7.77	7.64	0.33	1.18	0.53	0.158
0.3	0.4	8.23	7.70	0.34	1.43	0.55	0.166

ISOLATED BRIDGE WITH Tb = 2 SECS AND LOWER FRICTION AT PIER

0.1	0.2	8.97	8.86	0.35	0.95	1.72	0.103
0.1	0.4	9.15	8.69	0.35	1.06	1.81	0.107

NON-ISOLATED BRIDGE

0.1	0.2	16.20	0	0.22	0.22	33.04	0.293
0.1	0.4	22.17	0	0.15	0.15	11.31	0.178
0.2	0.2	9.83	0	0.23	0.23	10.03	0.322
0.2	0.4	23.40	0	0.20	0.20	5.97	0.277
0.3	0.2	8.84	0	0.29	0.29	6.01	0.415
0.3	0.4	23.34	0	0.26	0.26	3.97	0.373

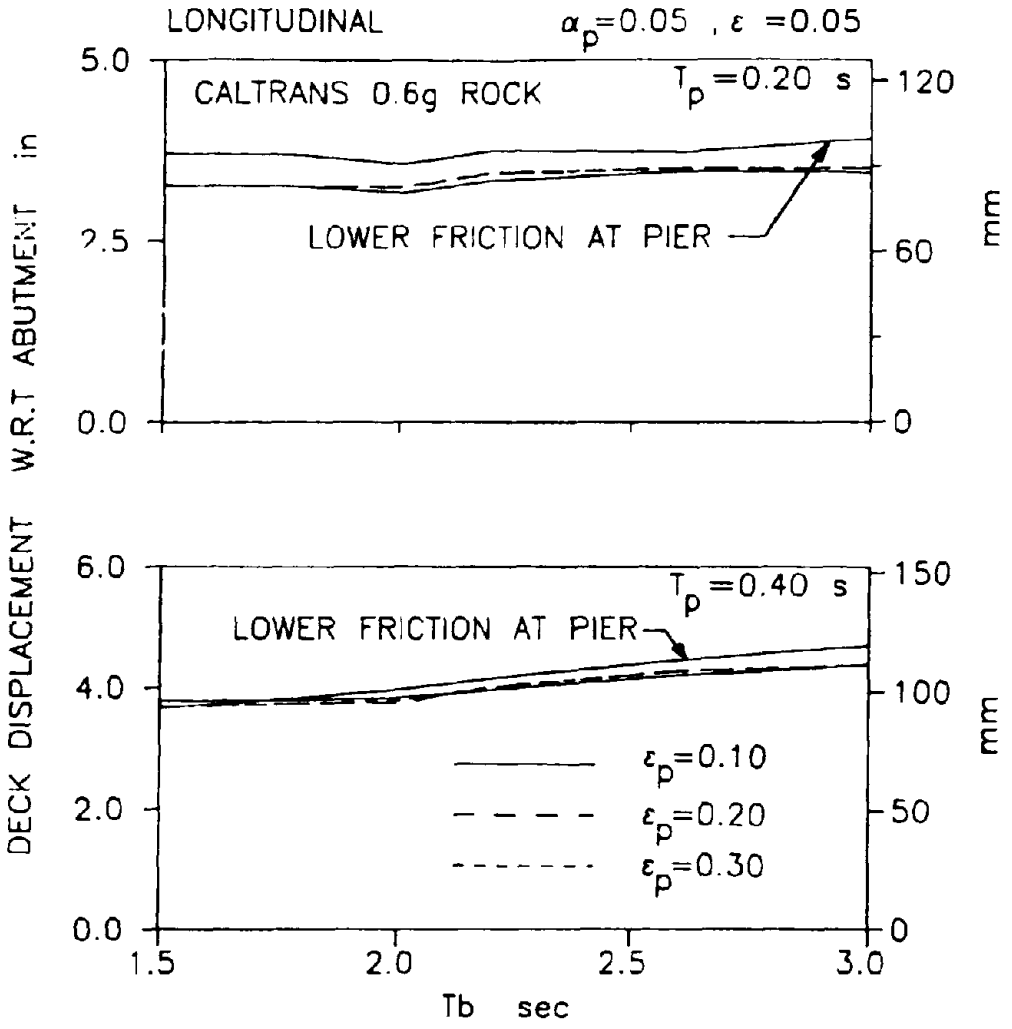

Fig. 9-1 - Deck (Bearing) Displacement at Abutment of Isolated Bridge for Caltrans 0.6g Rock Motion Applied in Longitudinal Direction.

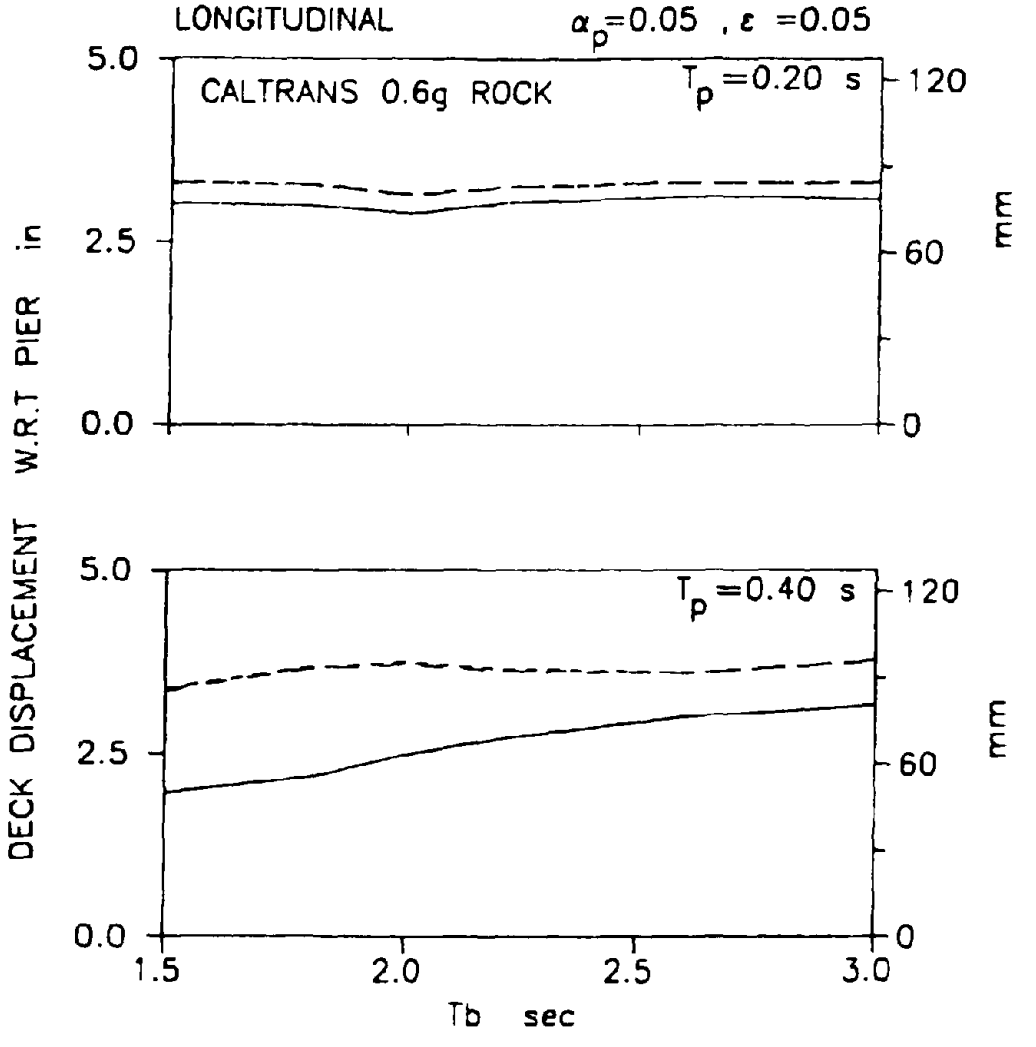

Fig. 9-2 - Deck (Bearing) Displacement at Pier of Isolated Bridge for Caltrans 0.6g Rock Motion Applied in Longitudinal Direction.

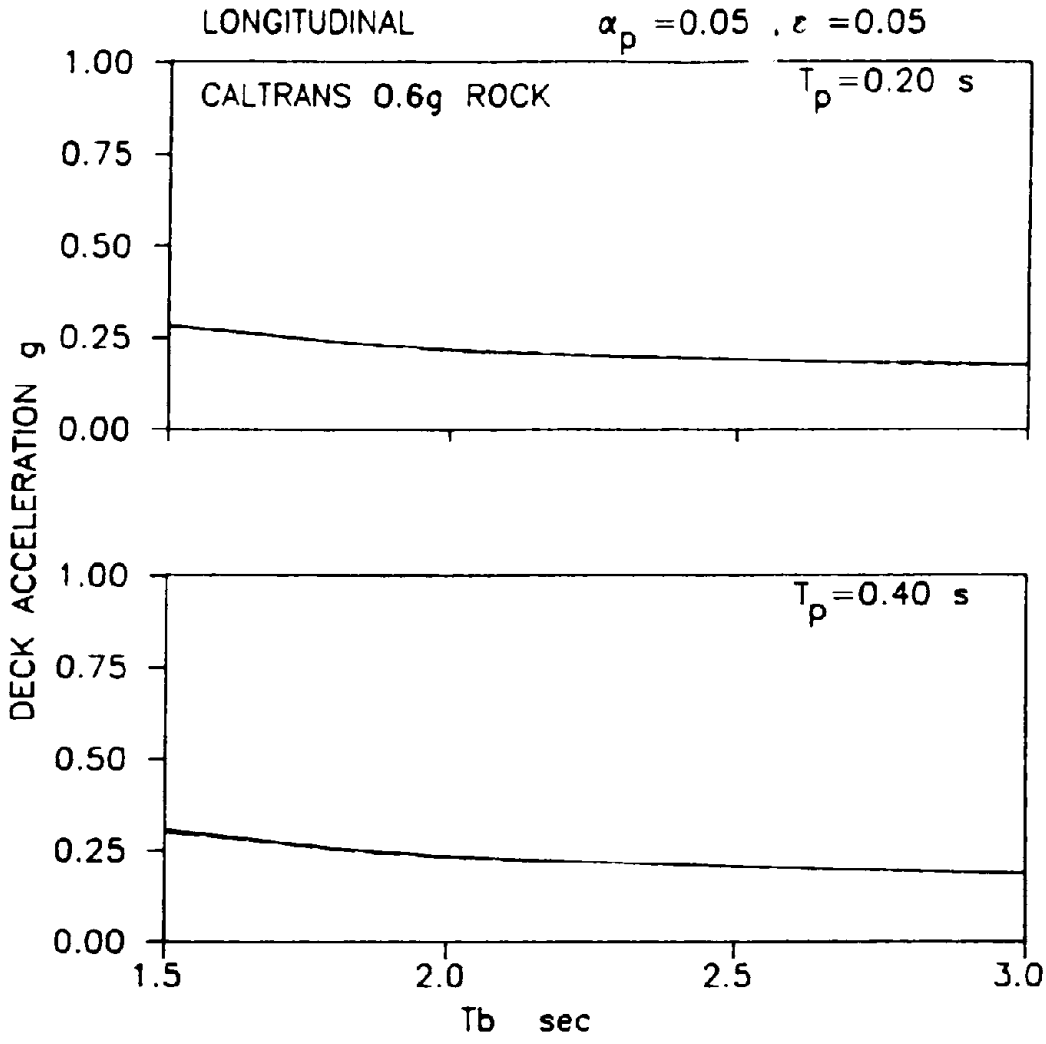

Fig. 9-3 - Deck Acceleration of Isolated Bridge for Caltrans 0.6g Rock Motion Applied in Longitudinal Direction.

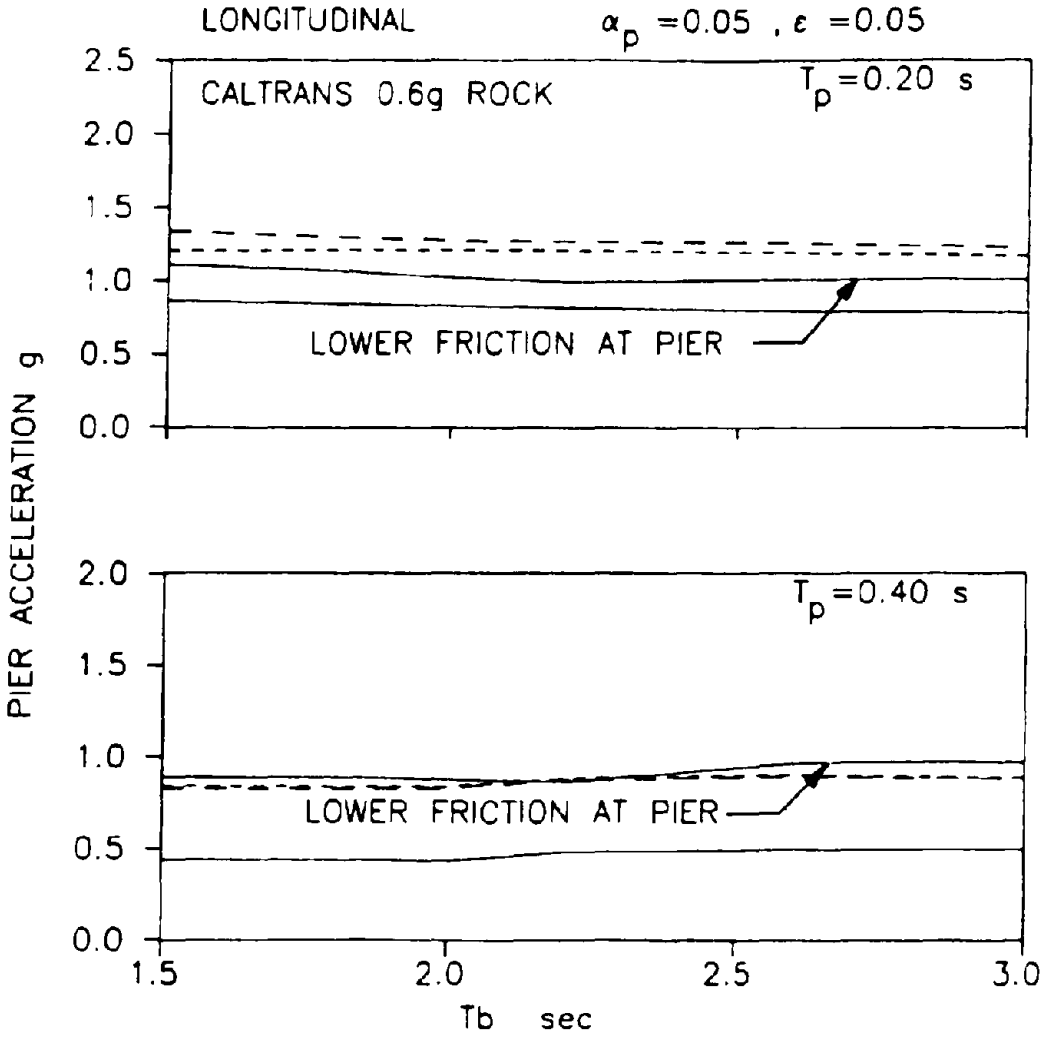

Fig. 9-4 - Pier Acceleration of Isolated Bridge for Caltrans 0.6g Rock Motion Applied in Longitudinal Direction.

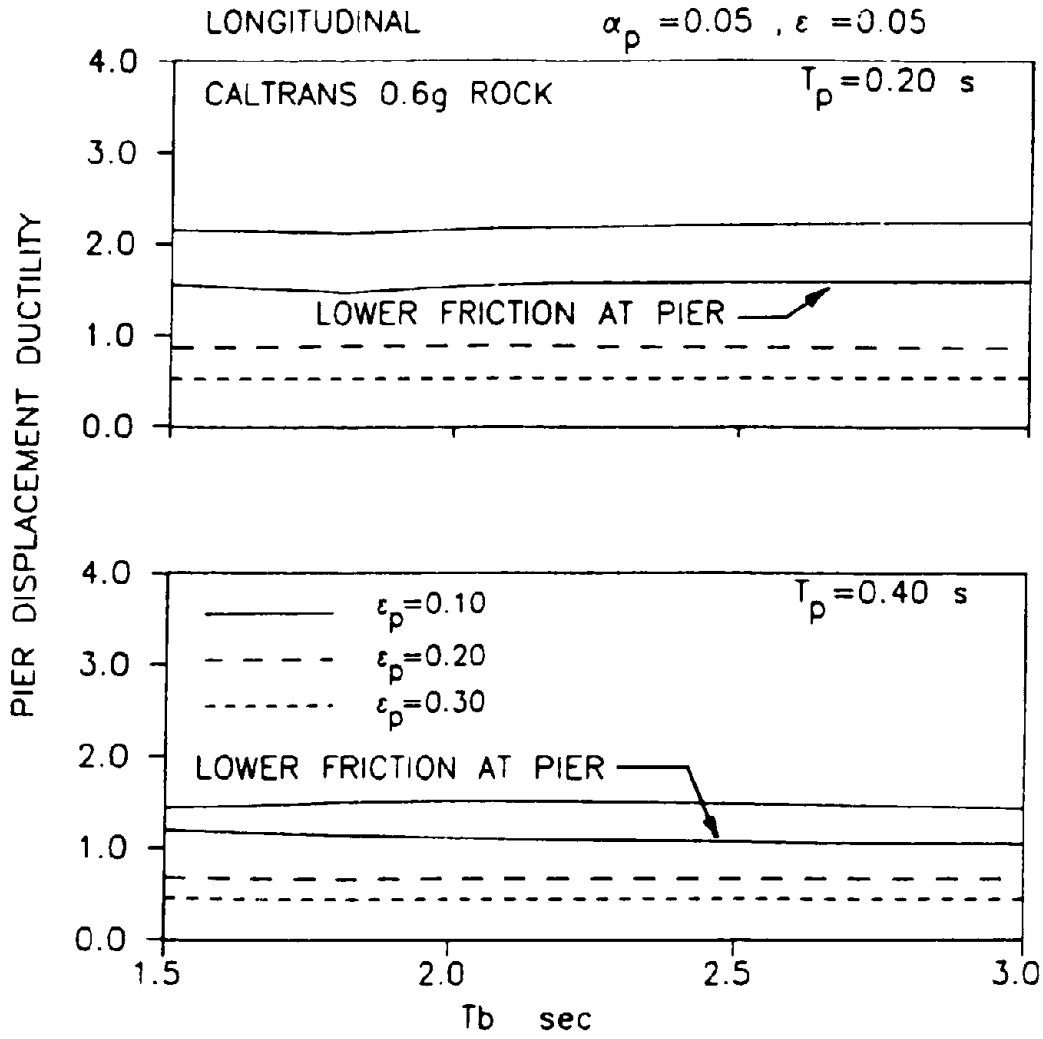

Fig. 9-5 · Pier Displacement Ductility of Isolated Bridge for Caltrans 0.6g Rock Motion Applied in Longitudinal Direction.

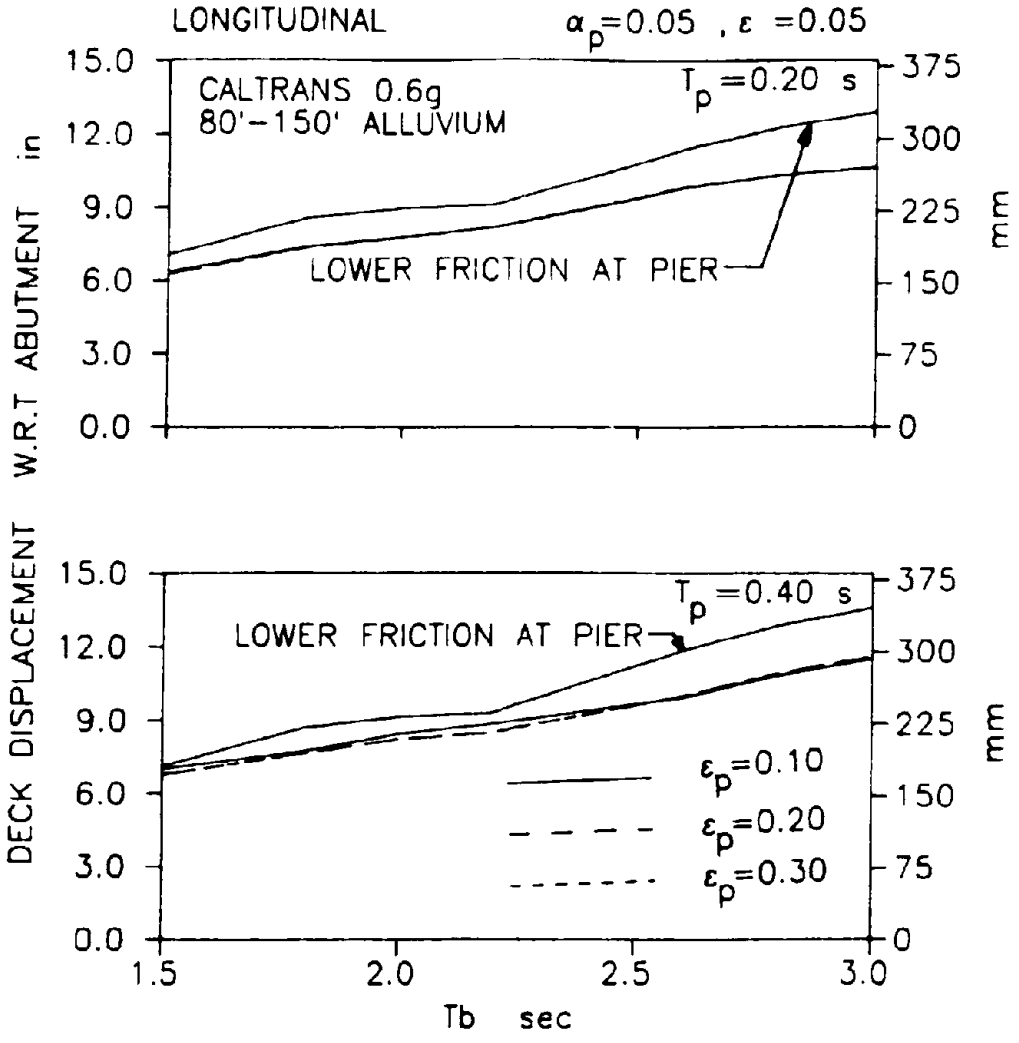

Fig. 9-6 - Deck (Bearing) Displacement at Abutment of Isolated Bridge for Caltrans 0.6g Deep Alluvium Motion Applied in Longitudinal Direction.

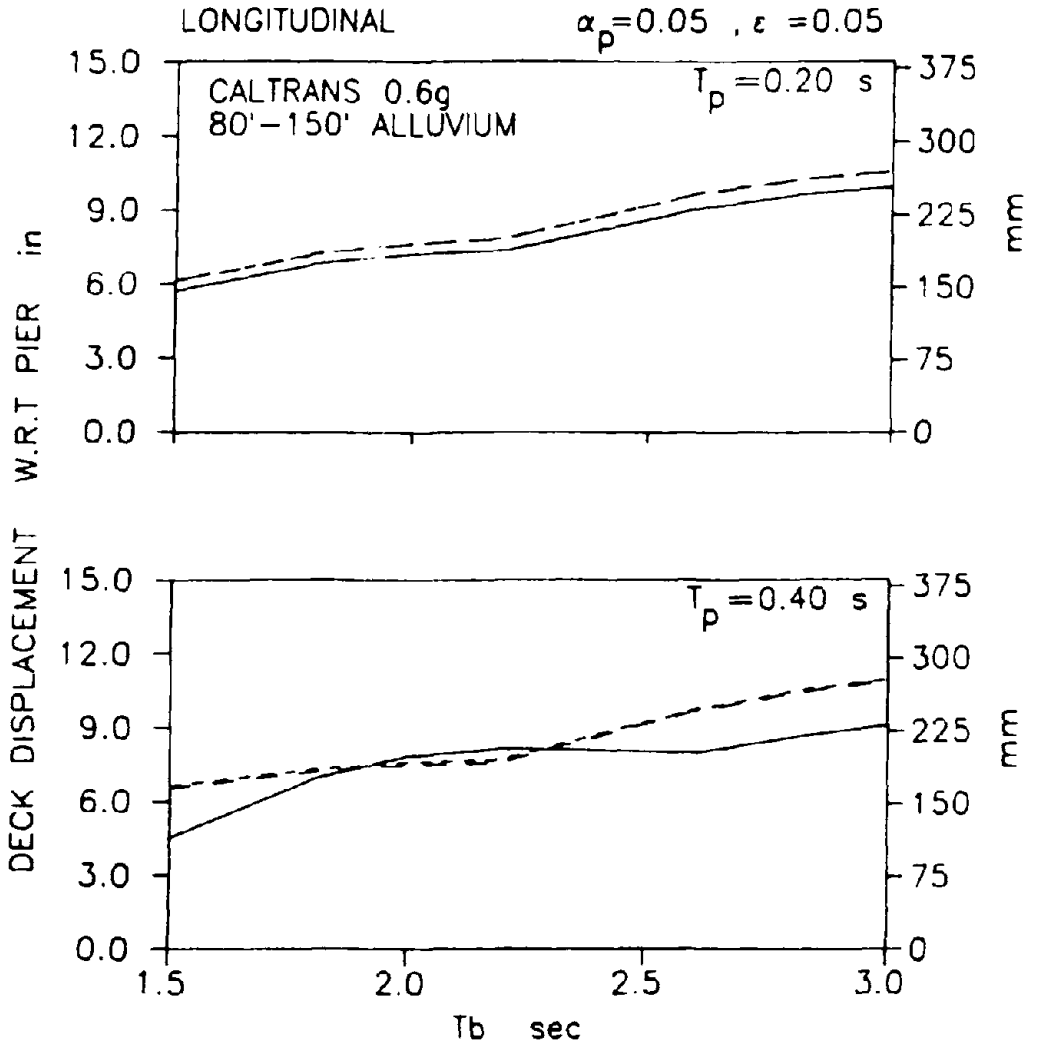

Fig. 9-7 - Deck (Bearing) Displacement at Pier of Isolated Bridge for Caltrans 0.6g Deep Alluvium Motion Applied in Longitudinal Direction.

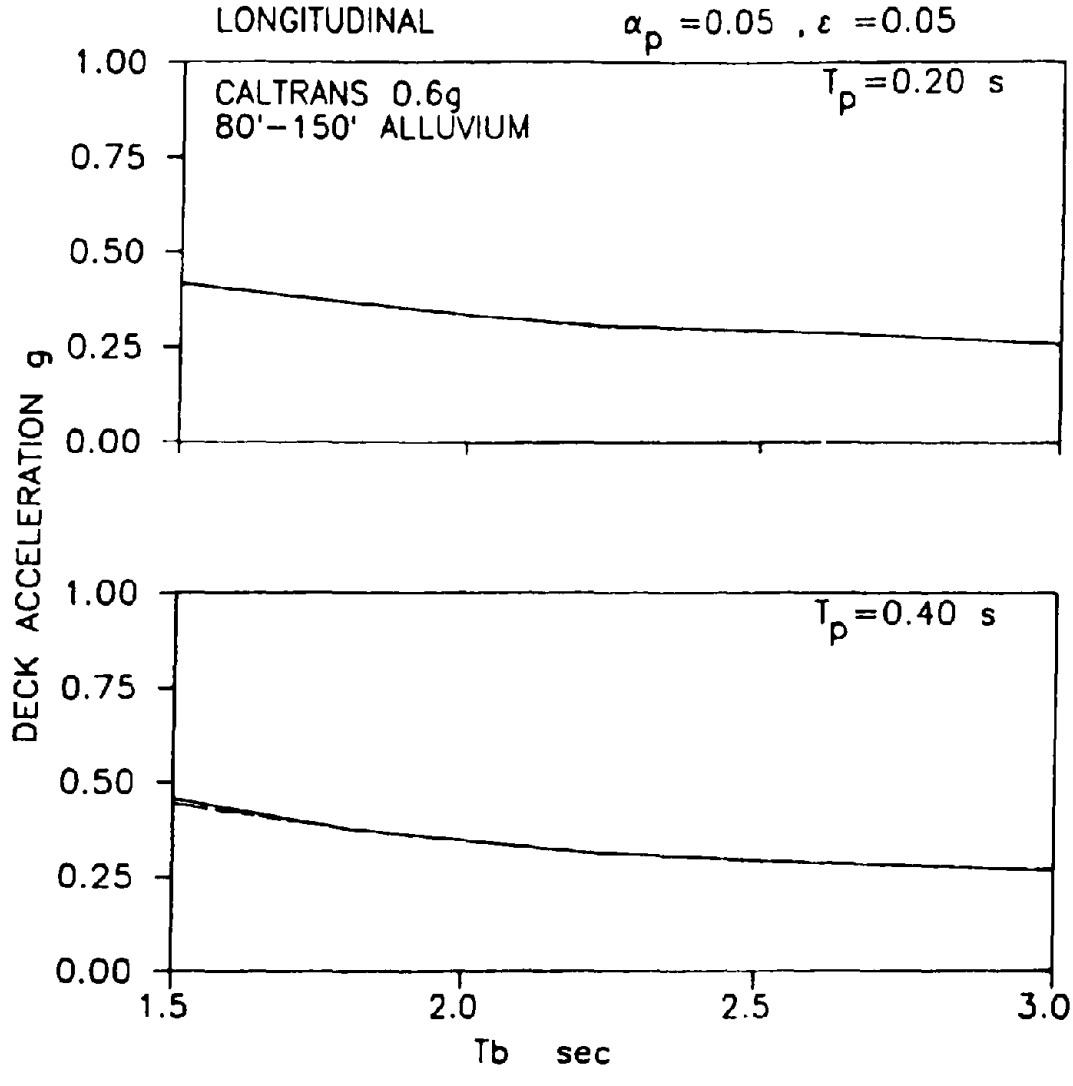

Fig. 9-8 - Deck Acceleration of Isolated Bridge for Caltrans 0.6g Deep Alluvium Motion Applied in Longitudinal Direction.

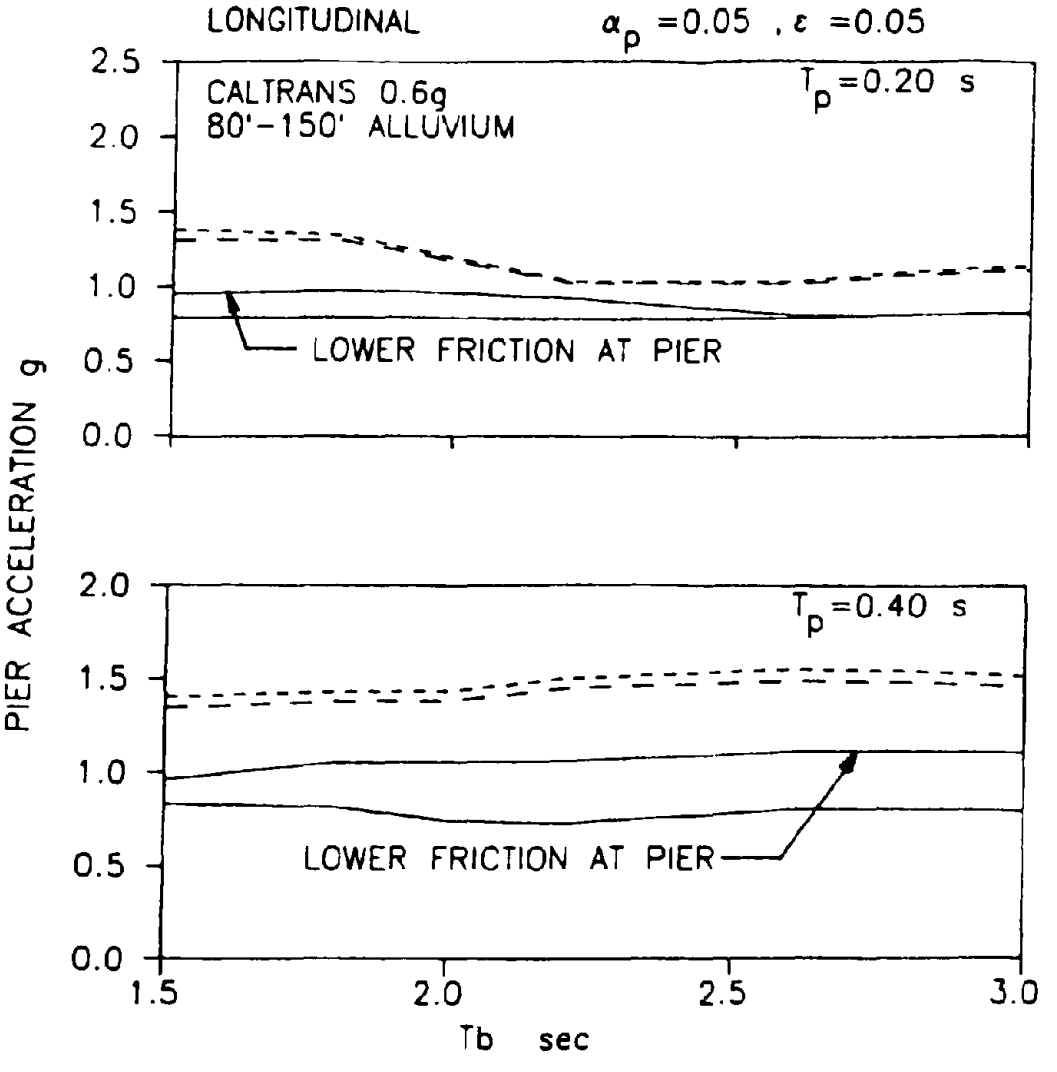

Fig. 9-9 - Pier Acceleration of Isolated Bridge for Caltrans 0.6g Deep Alluvium Motion Applied in Longitudinal Direction.

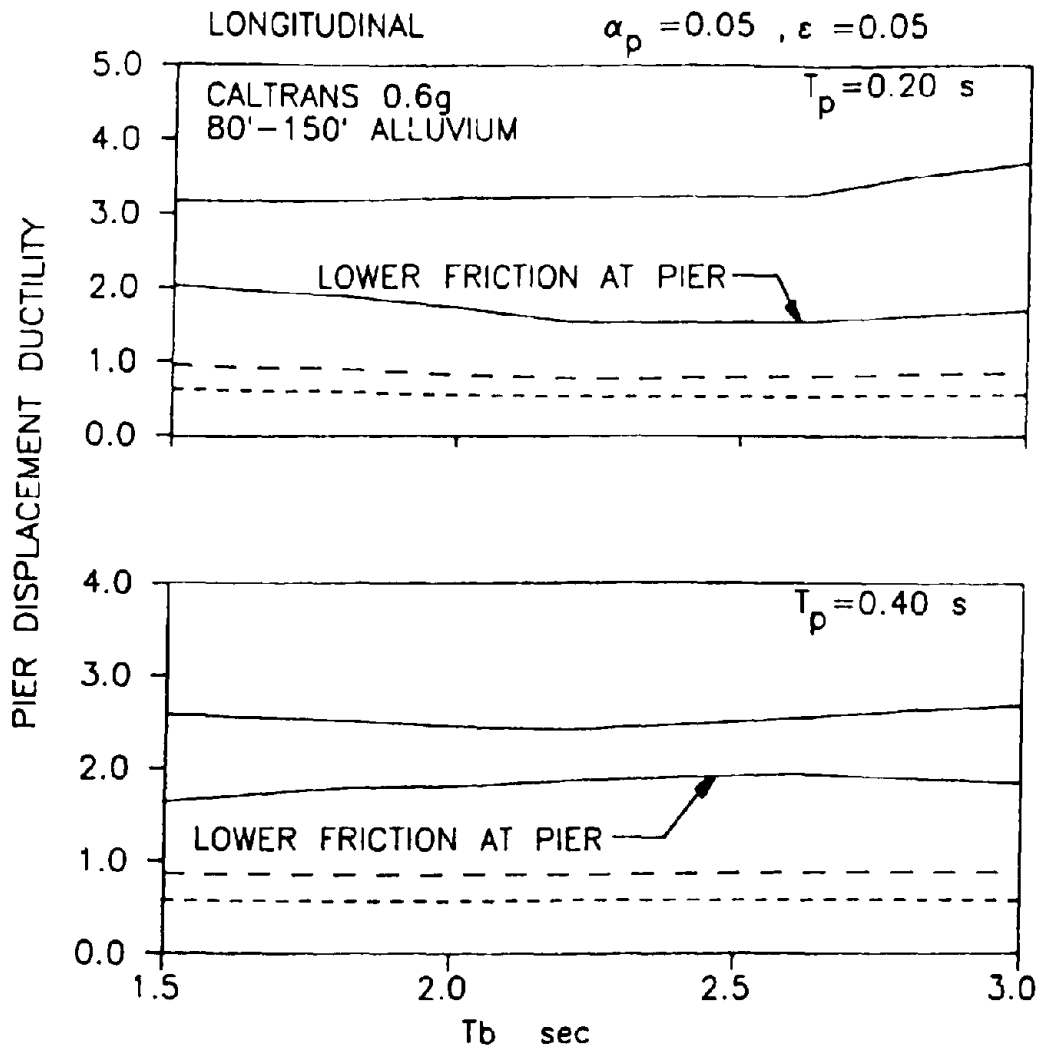

Fig. 9-10 - Pier Displacement Ductility of Isolated Bridge for Caltrans 0.6g Deep Alluvium Motion Applied in Longitudinal Direction.

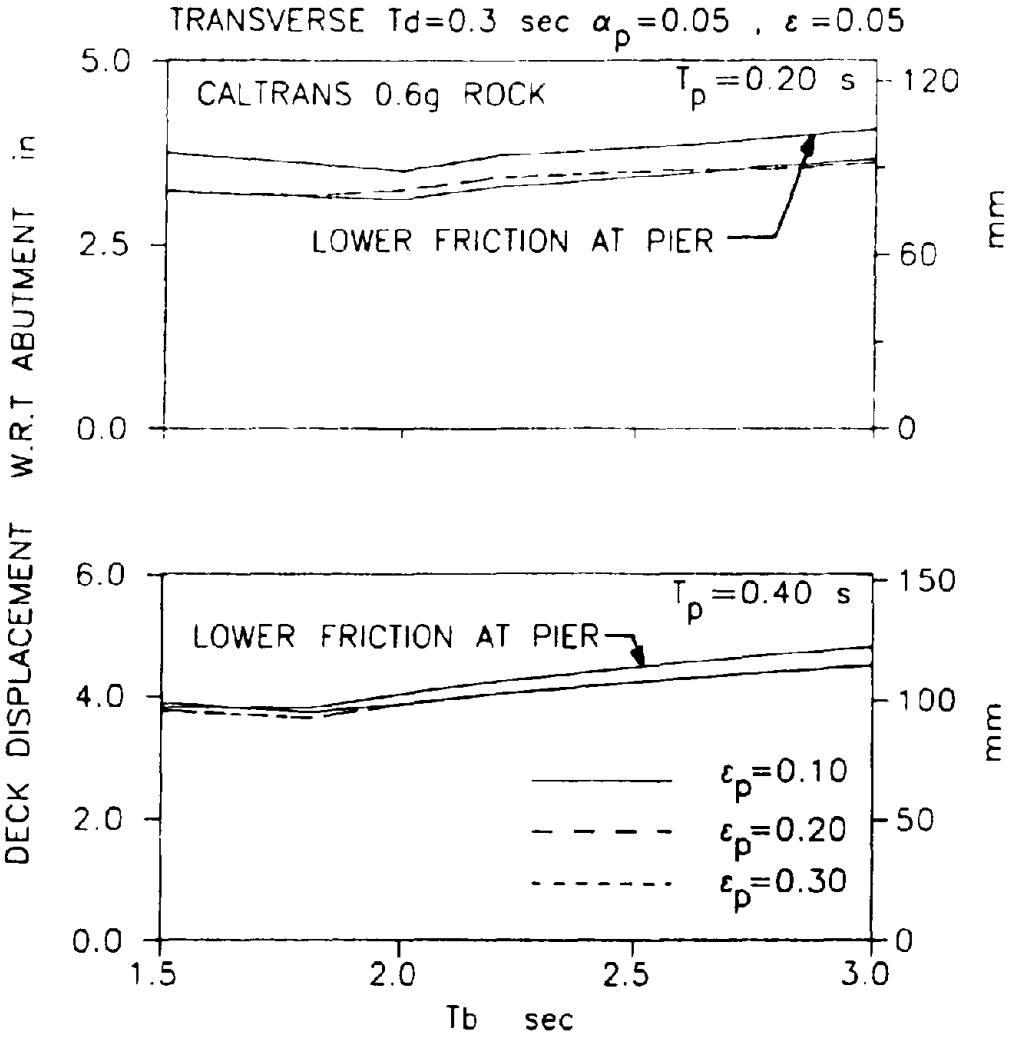

Fig. 9-11 - Deck (Bearing) Displacement at Abutment of Isolated Bridge with Td = 0.3 secs for Caltrans 0.6g Rock Motion Applied in Transverse Direction.

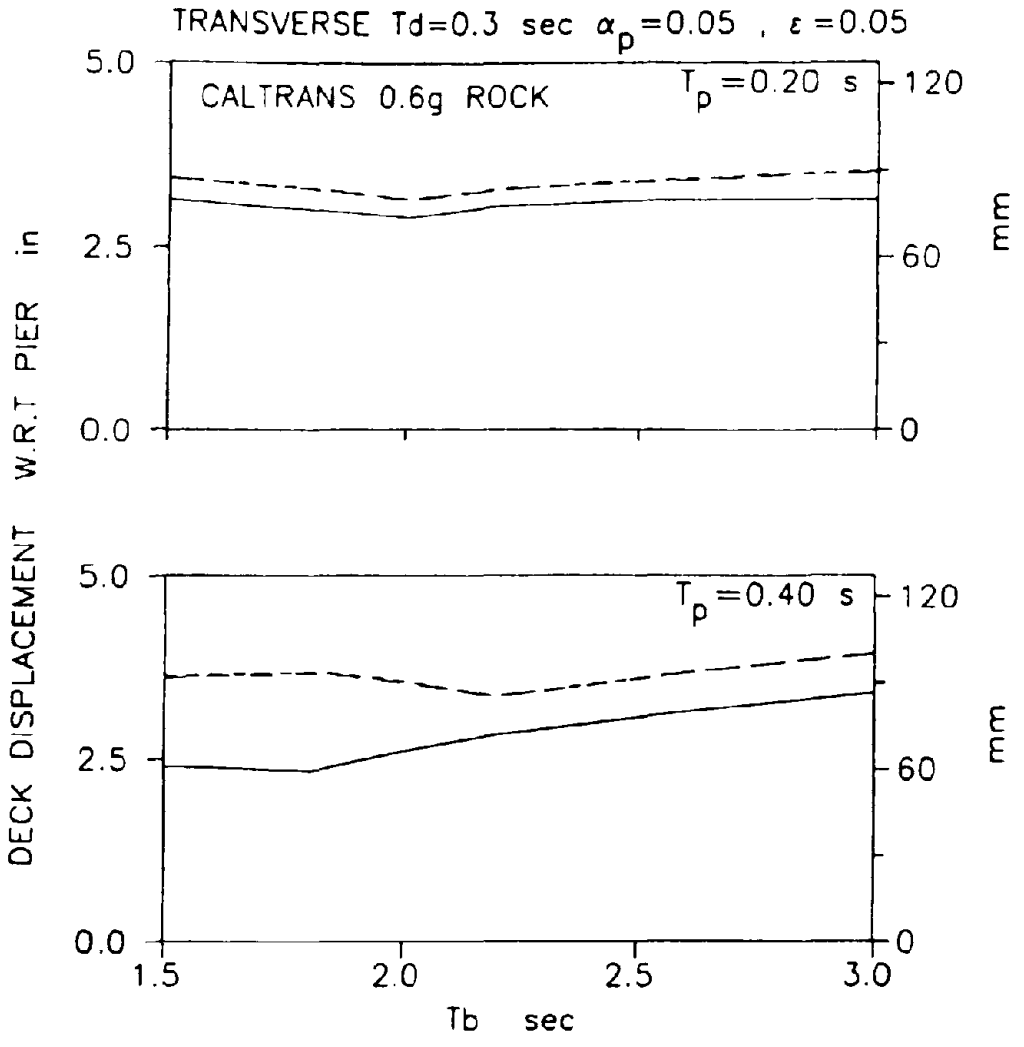

Fig. 9-12 - Deck (Bearing) Displacement at Pier of Isolated Bridge with Td = 0.3 secs for Caltrans 0.6g Rock Motion Applied in Transverse Direction.

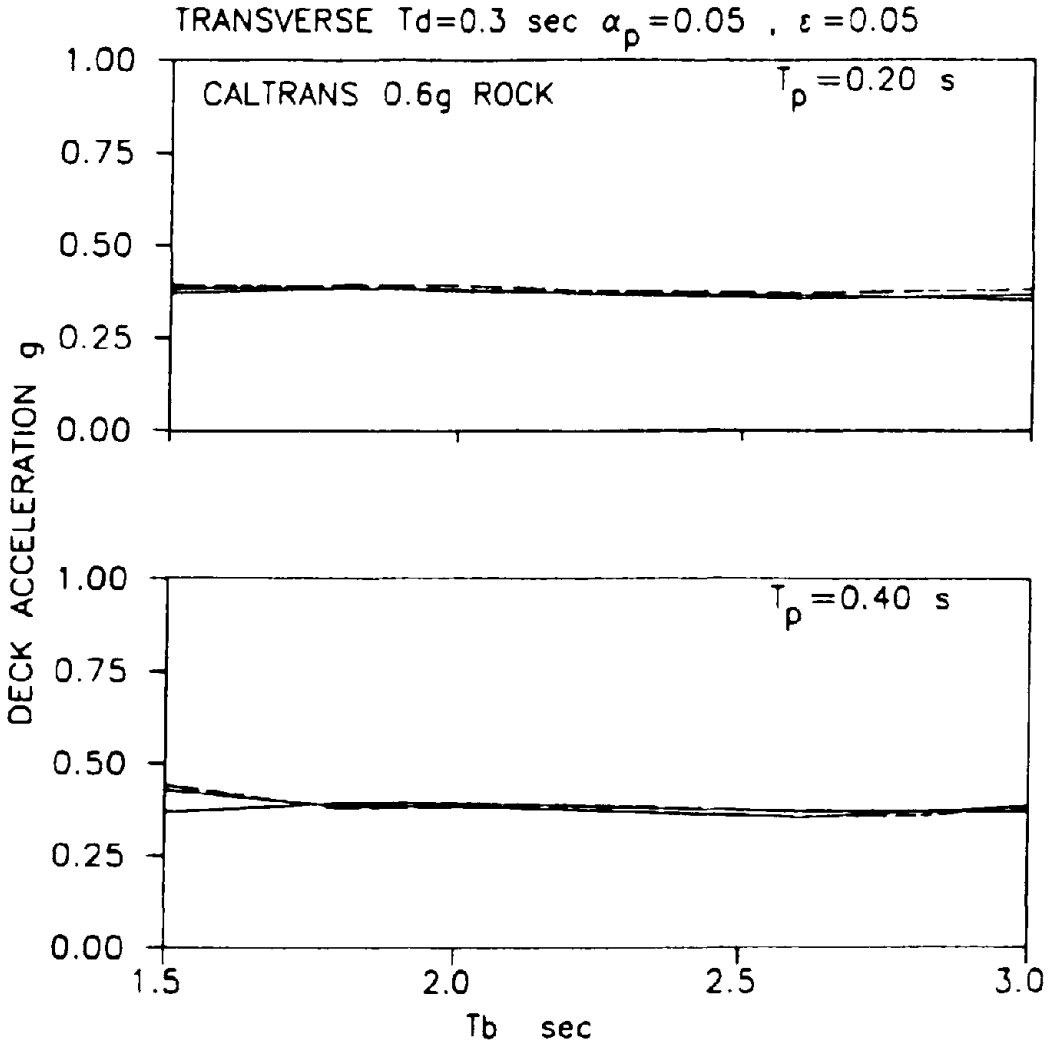

Fig. 9-13 - Deck Acceleration of Isolated Bridge with Td = 0.3 secs for Caltrans 0.6g Rock Motion Applied in Transverse Direction.

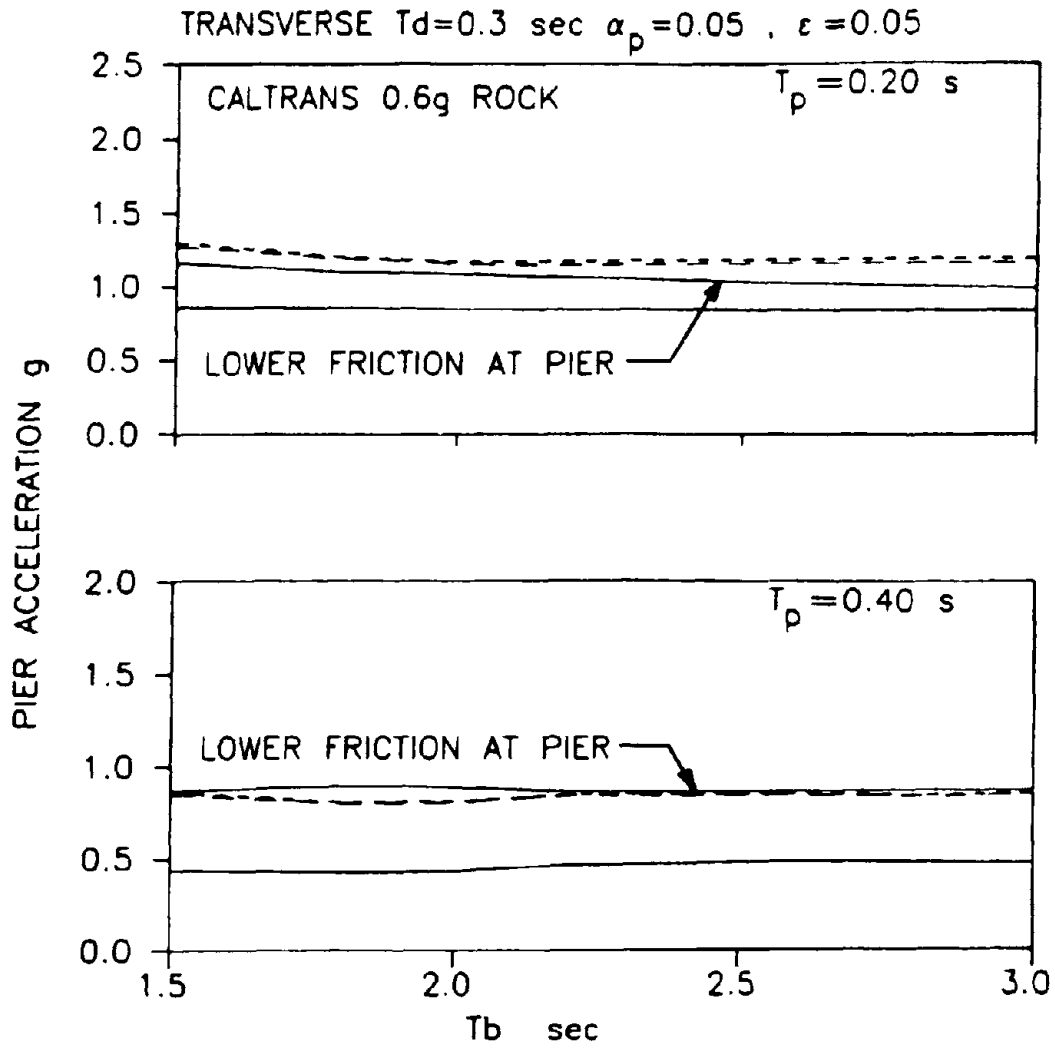

Fig. 9-14 - Pier Acceleration of Isolated Bridge with Td = 0.3 secs for Caltrans 0.6g Rock Motion Applied in Transverse Direction.

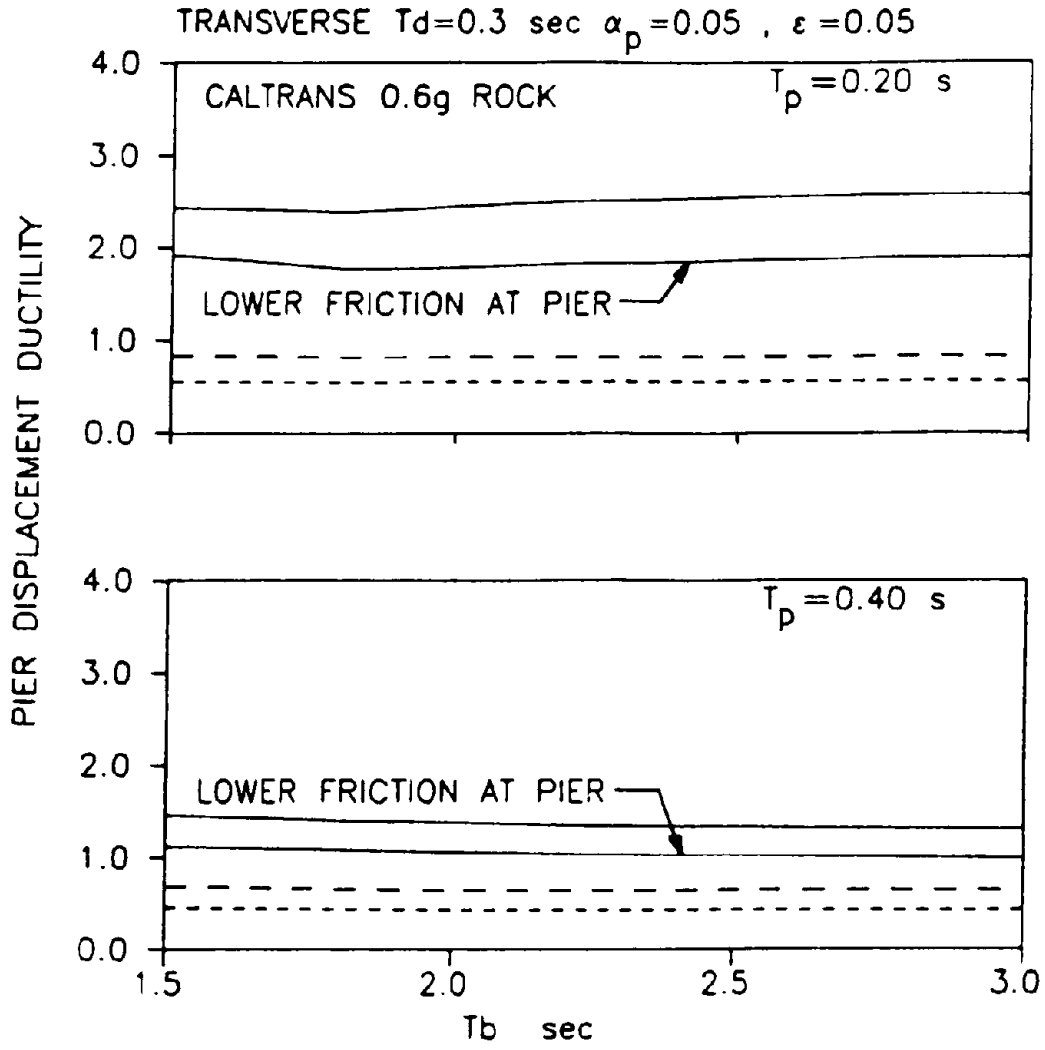

Fig. 9-15 - Pier Displacement Ductility of Isolated Bridge with Td = 0.3 secs for Caltrans 0.6g Rock Motion Applied in Transverse Direction.

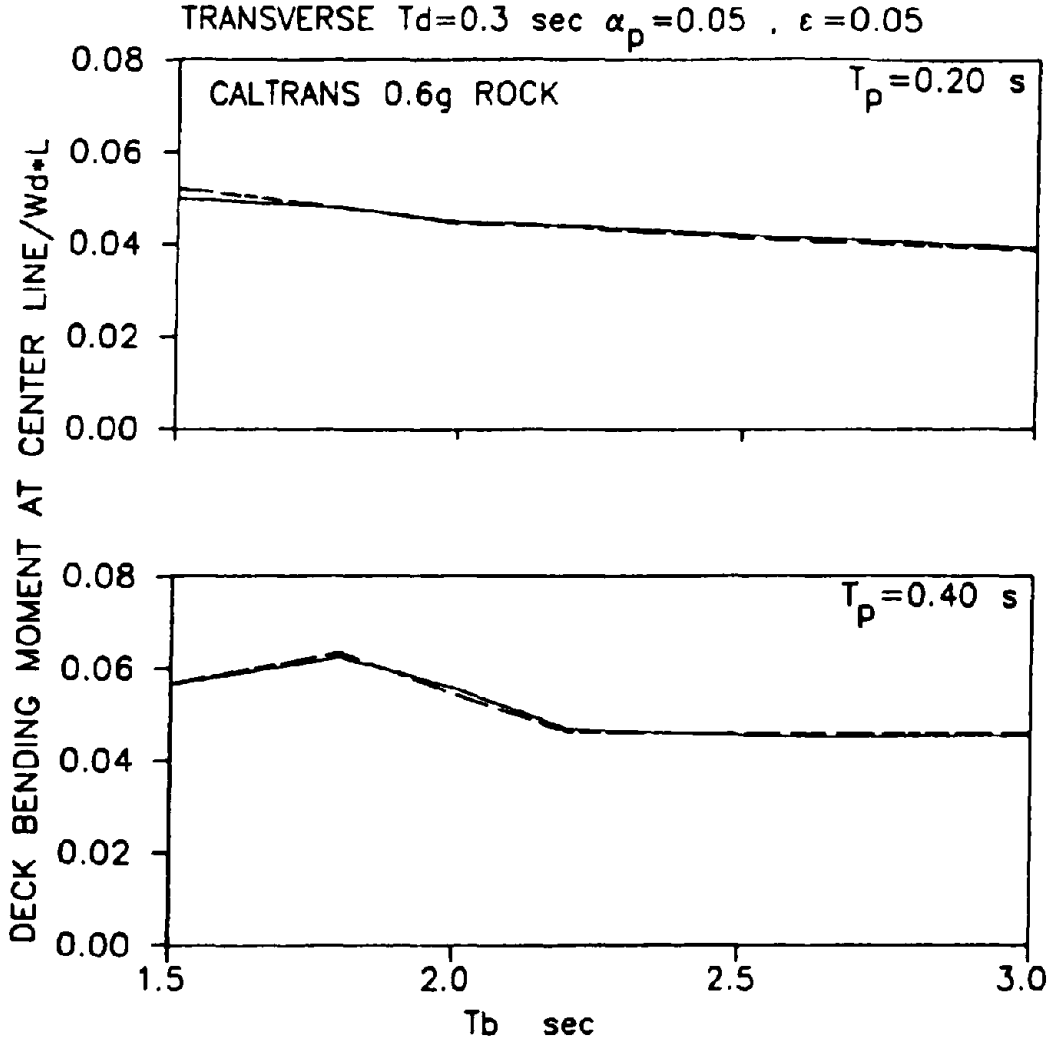

Fig. 9-16 - Deck Bending Moment of Isolated Bridge with Td = 0.3 secs for Caltrans 0.6g Rock Motion Applied in Transverse Direction.

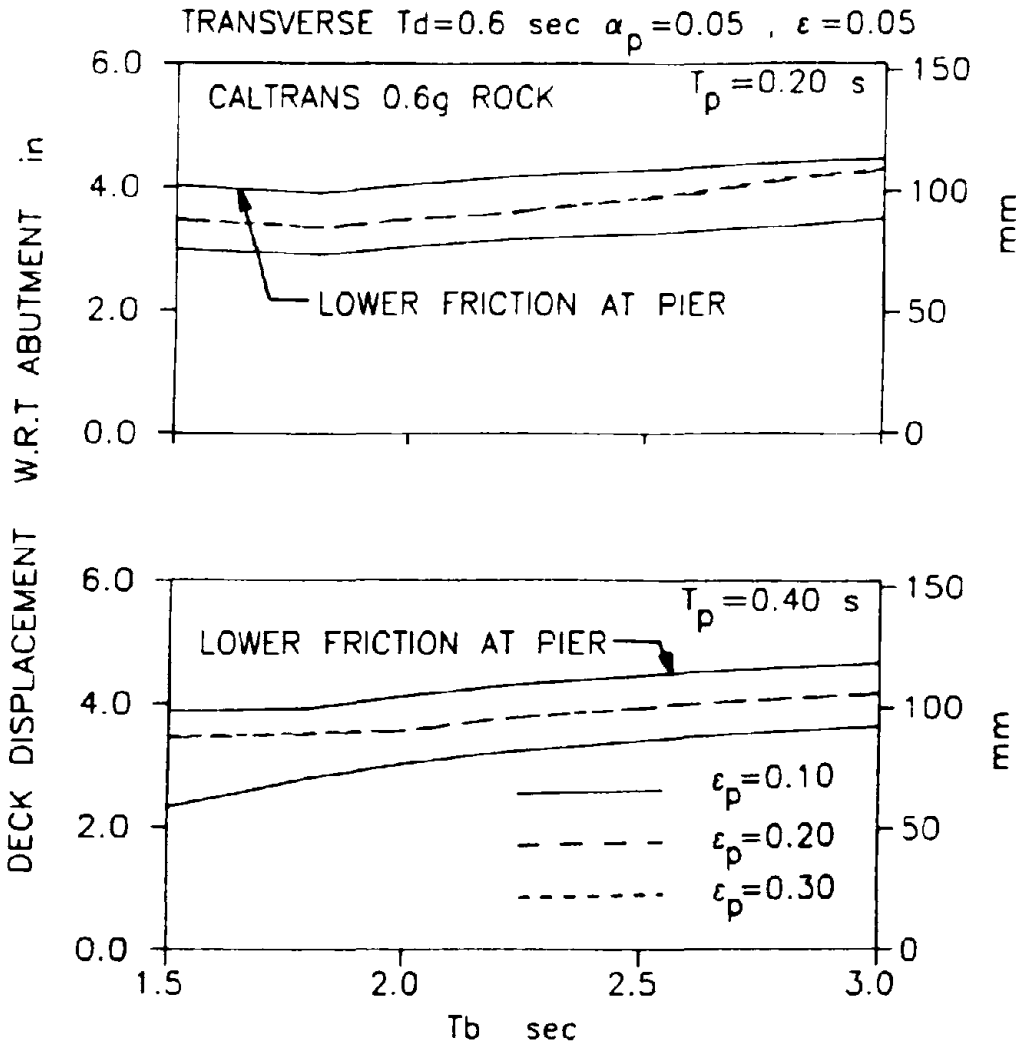

Fig. 9-17 - Deck (Bearing) Displacement at Abutment of Isolated Bridge with Td = 0.6 secs for Caltrans 0.6g Rock Motion Applied in Transverse Direction.

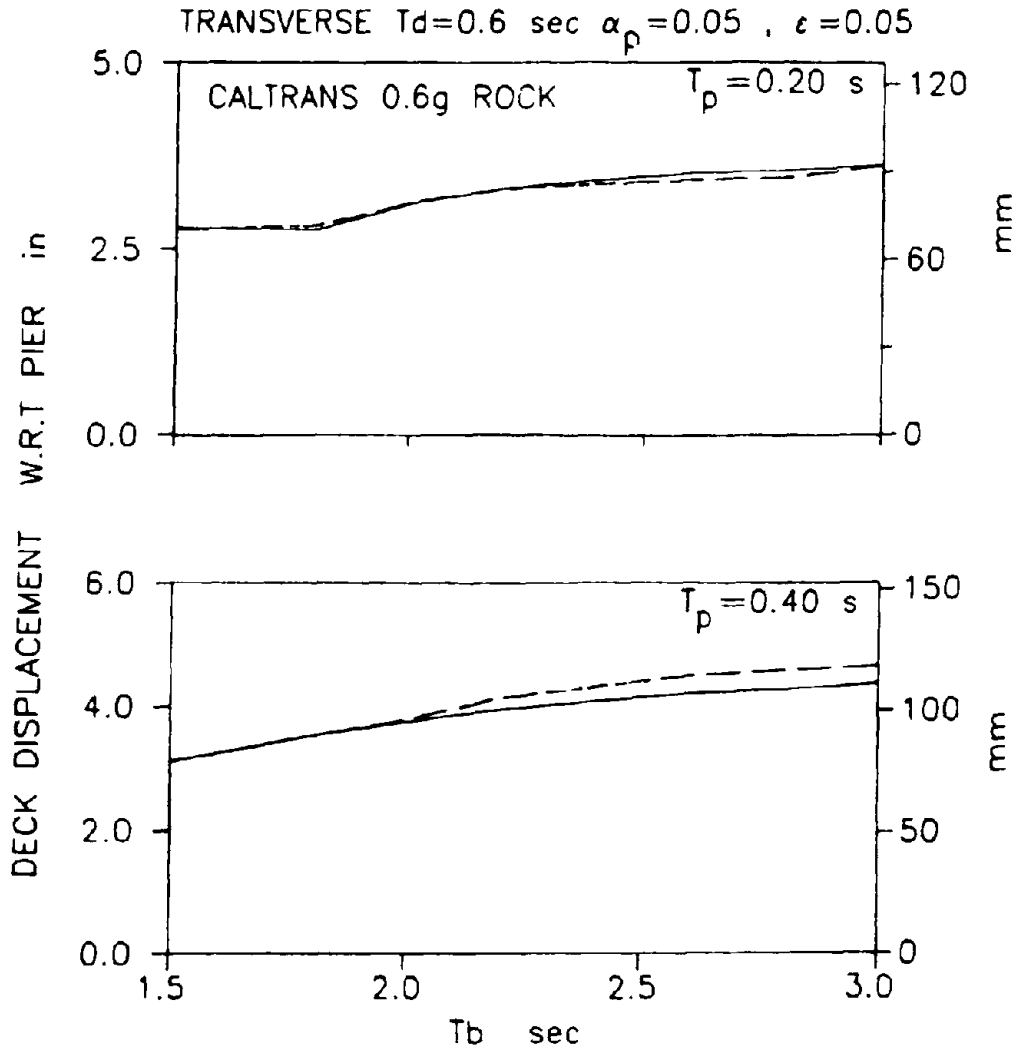

Fig. 9-18 - Deck (Bearing) Displacement at Pier of Isolated Bridge with Td = 0.6 secs for Caltrans 0.6g Rock Motion Applied in Transverse Direction.

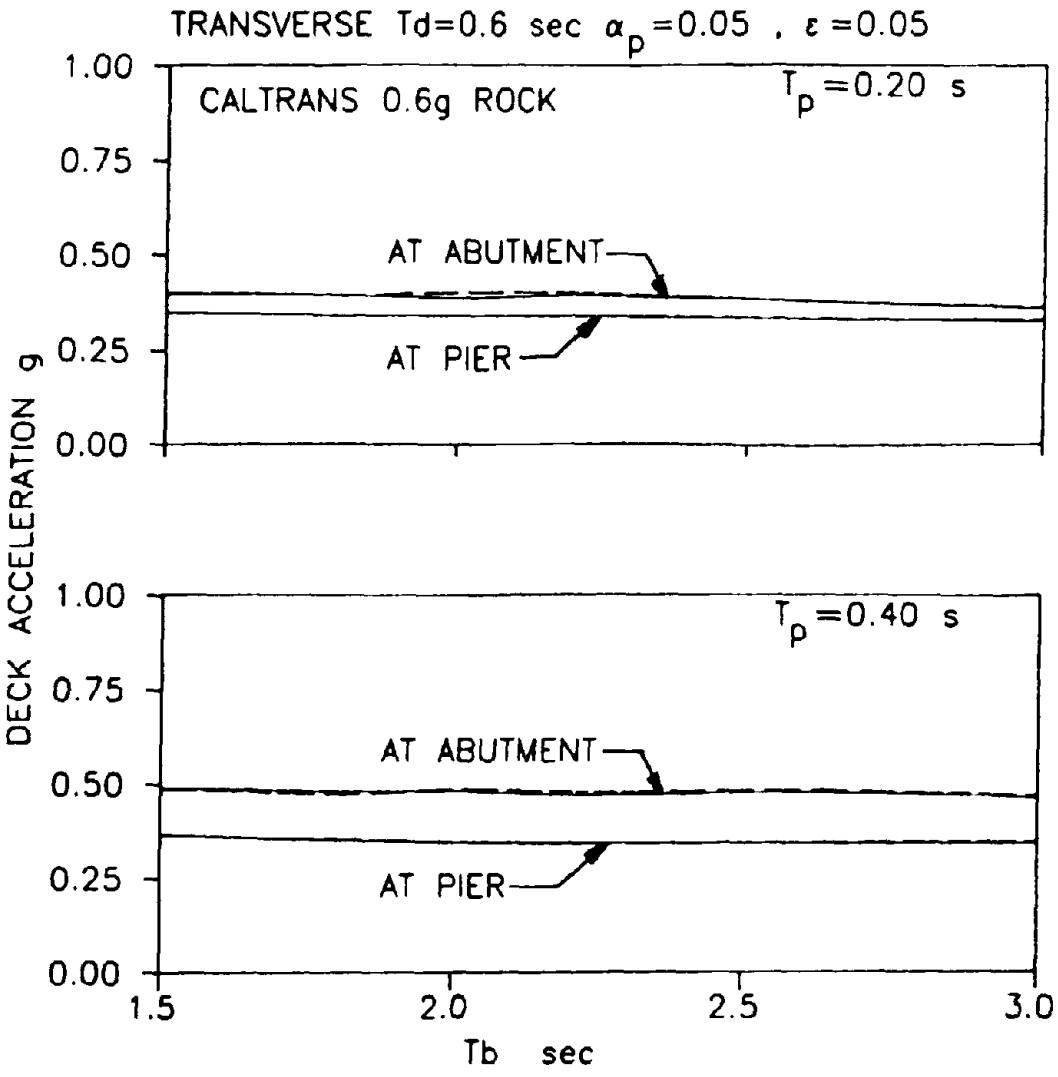

Fig. 9-19 - Deck Acceleration of Isolated Bridge with Td = 0.6 secs for Caltrans 0.6g Rock Motion Applied in Transverse Direction.

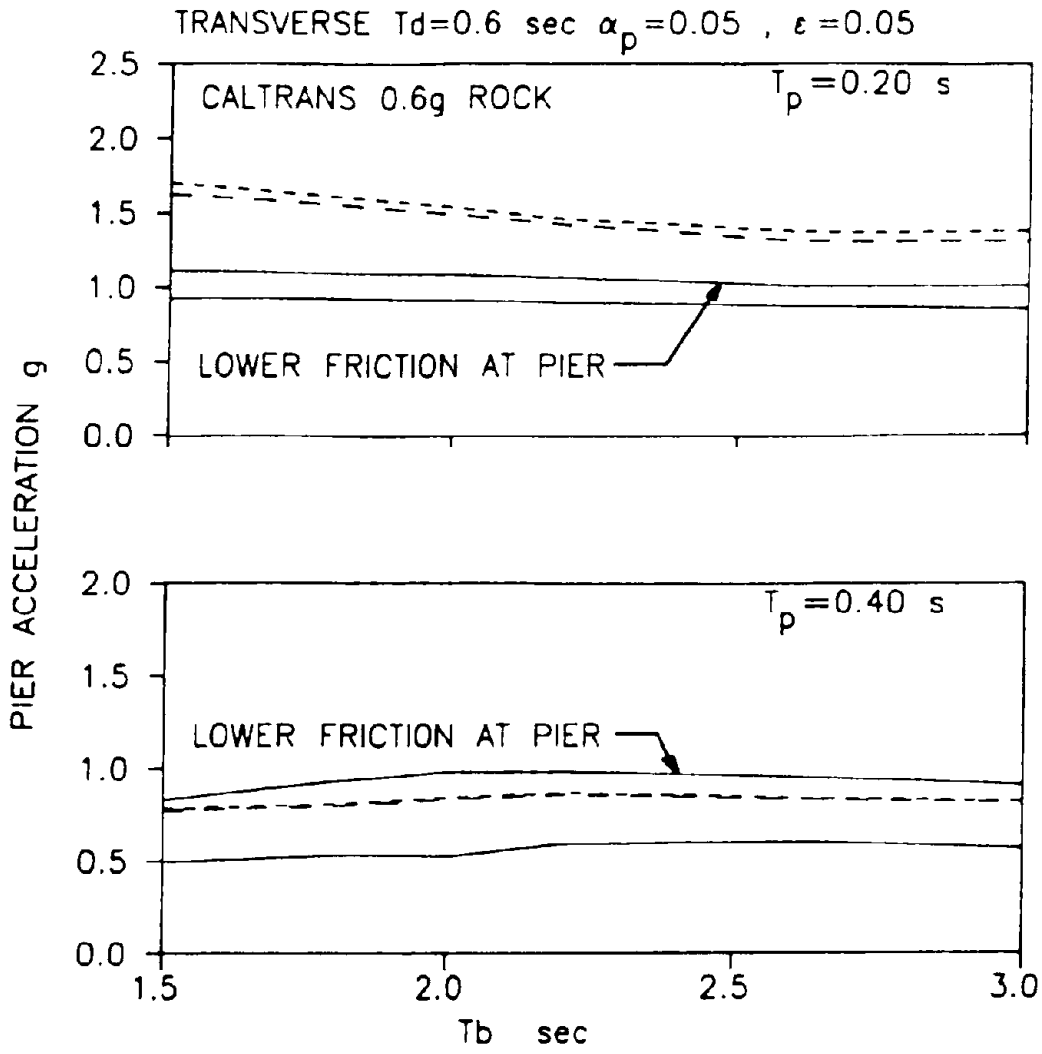

Fig. 9-20 - Pier Acceleration of Isolated Bridge with Td = 0.6 secs for Caltrans 0.6g Rock Motion Applied in Transverse Direction.

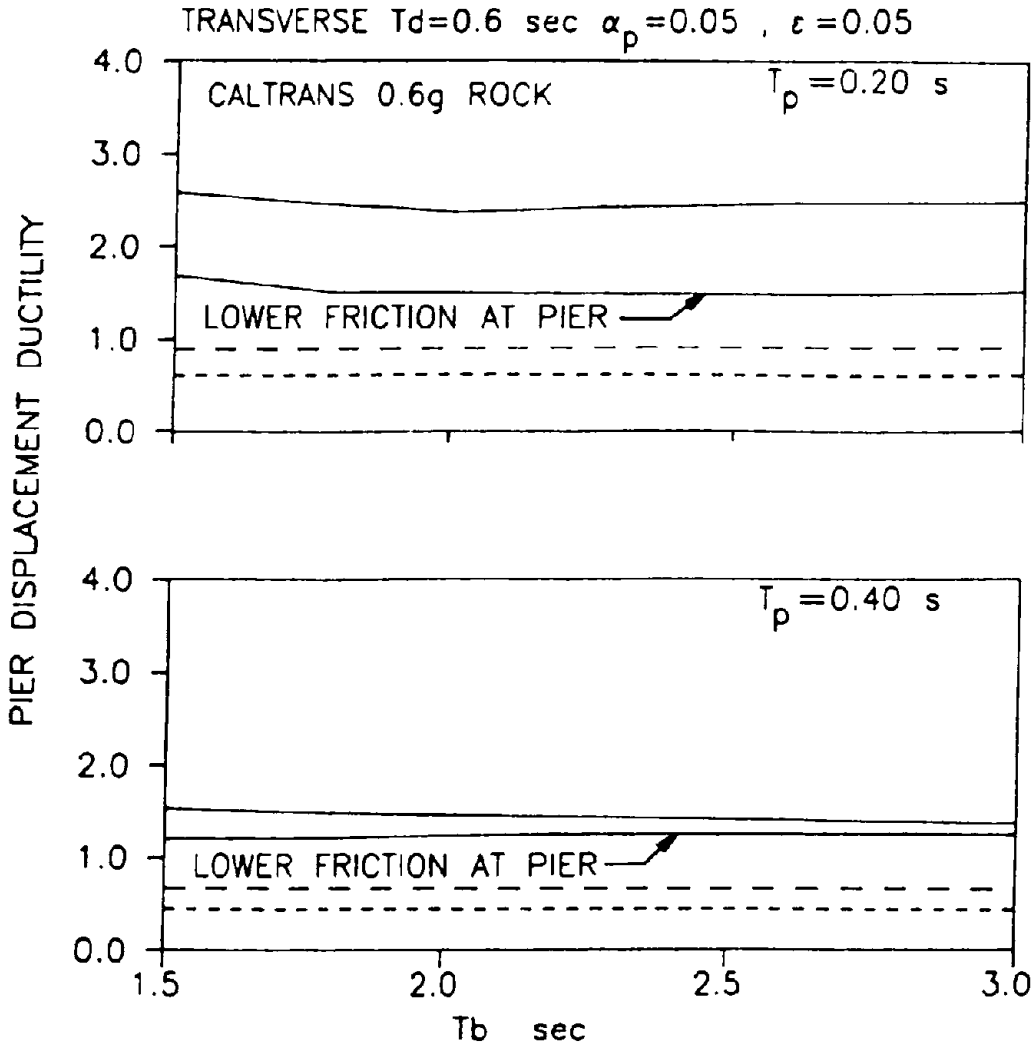

Fig. 9-21 - Pier Displacement Ductility of Isolated Bridge with Td = 0.6 secs for Caltrans 0.6g Rock Motion Applied in Transverse Direction.

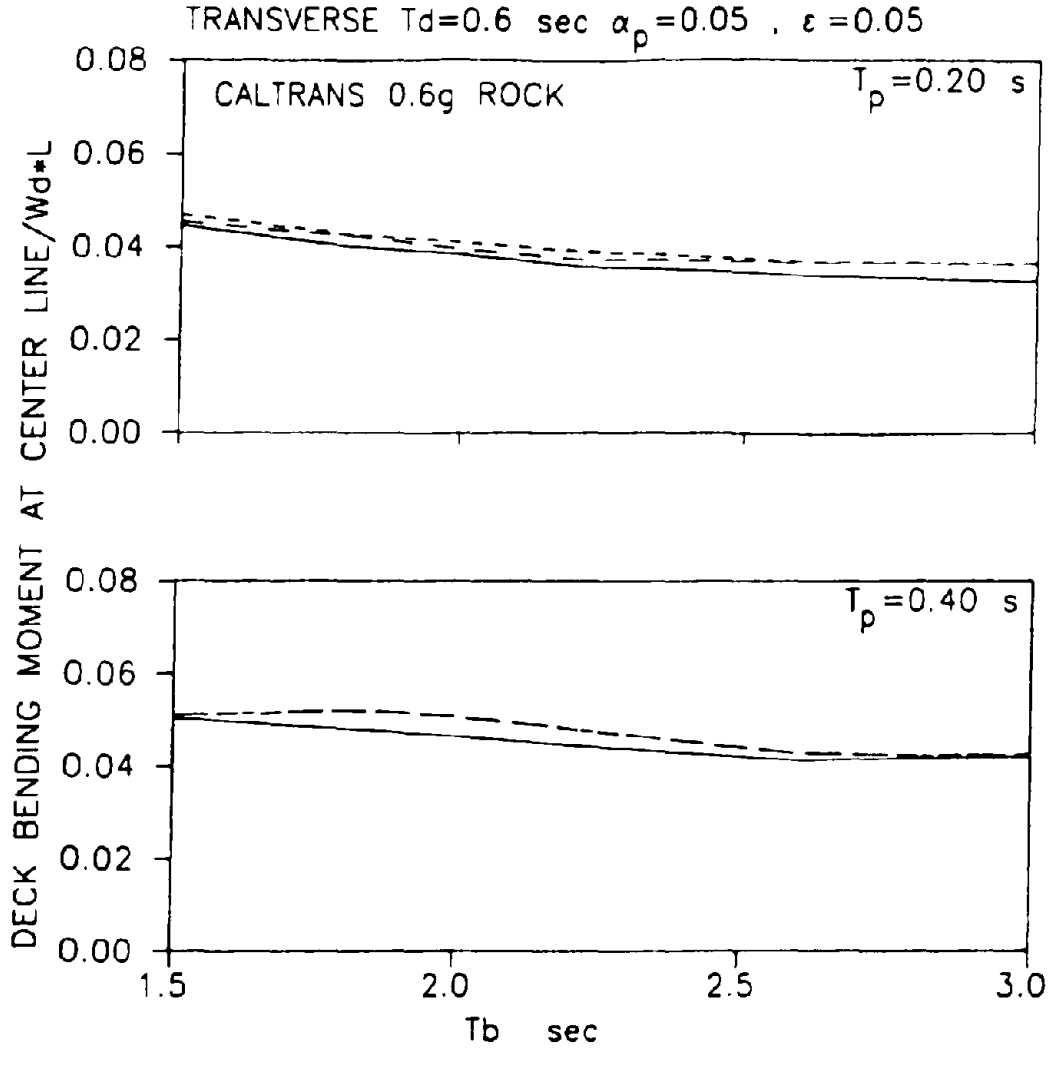

Fig. 9-22 - Deck Bending Moment of Isolated Bridge with Td = 0.6 secs for Caltrans 0.6g Rock Motion Applied in Transverse Direction.

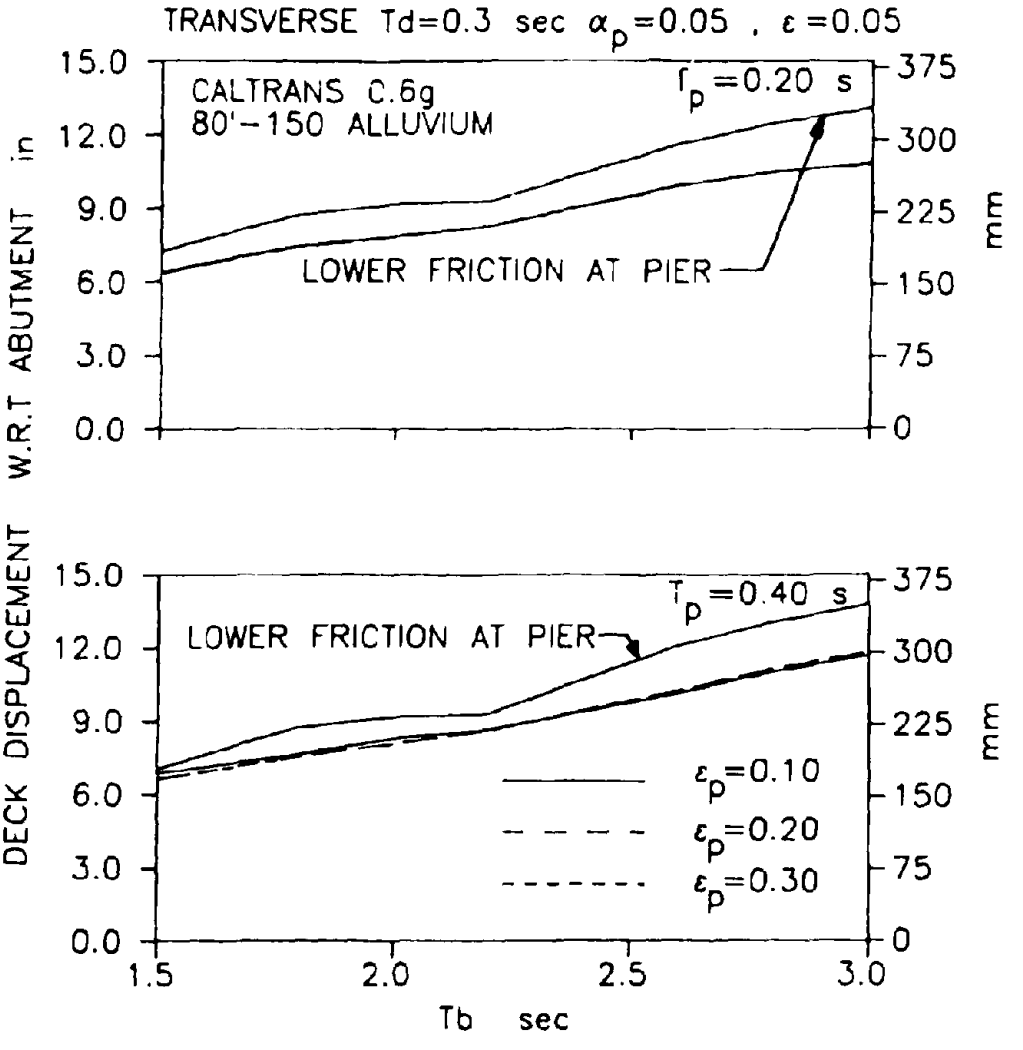

Fig. 9-23 - Deck (Bearing) Displacement at Abutment of Isolated Bridge with Td = 0.3 secs for Caltrans 0.6g Deep Alluvium Motion Applied in Transverse Direction.

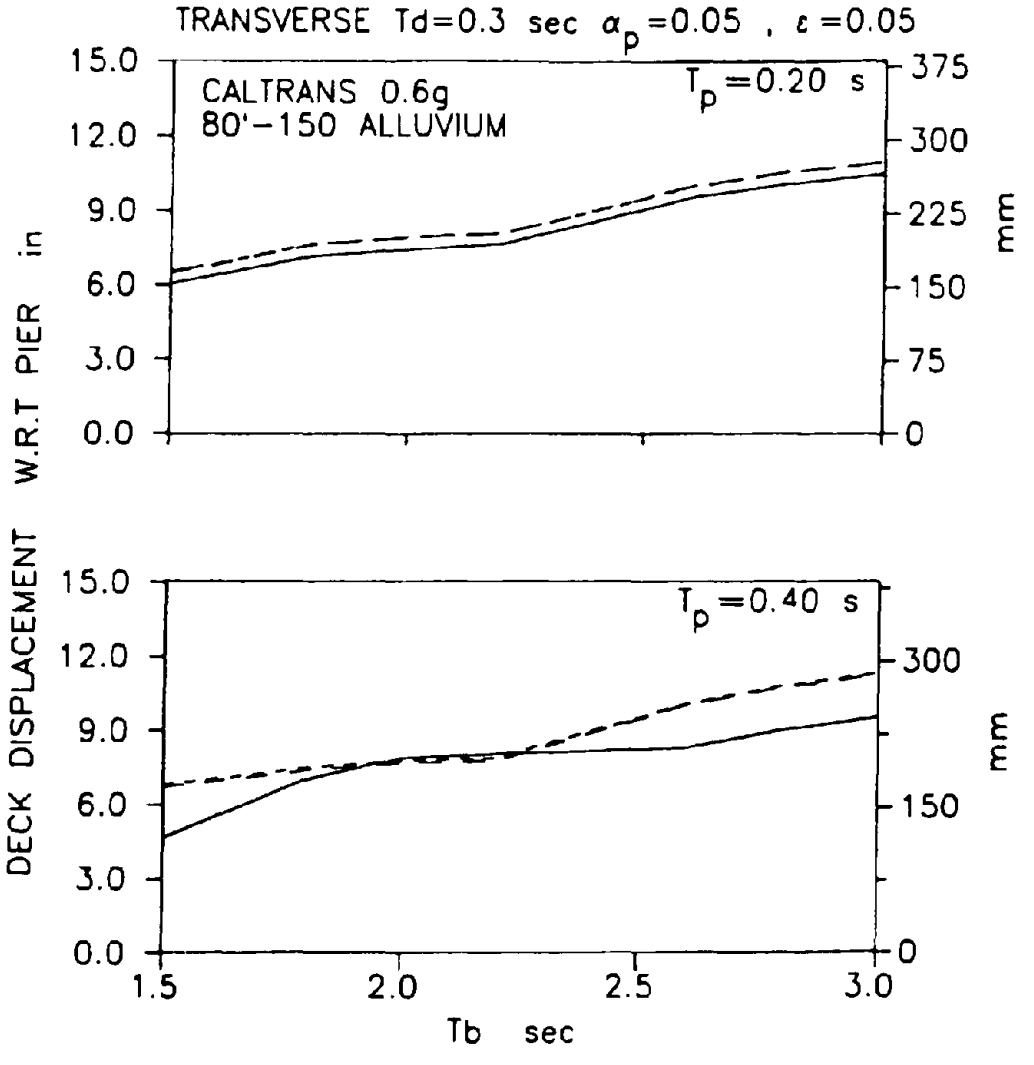

Fig. 9-24 - Deck (Bearing) Displacement at Pier of Isolated Bridge with Td = 0.3 secs for Caltrans 0.6g Deep Alluvium Motion Applied in Transverse Direction.

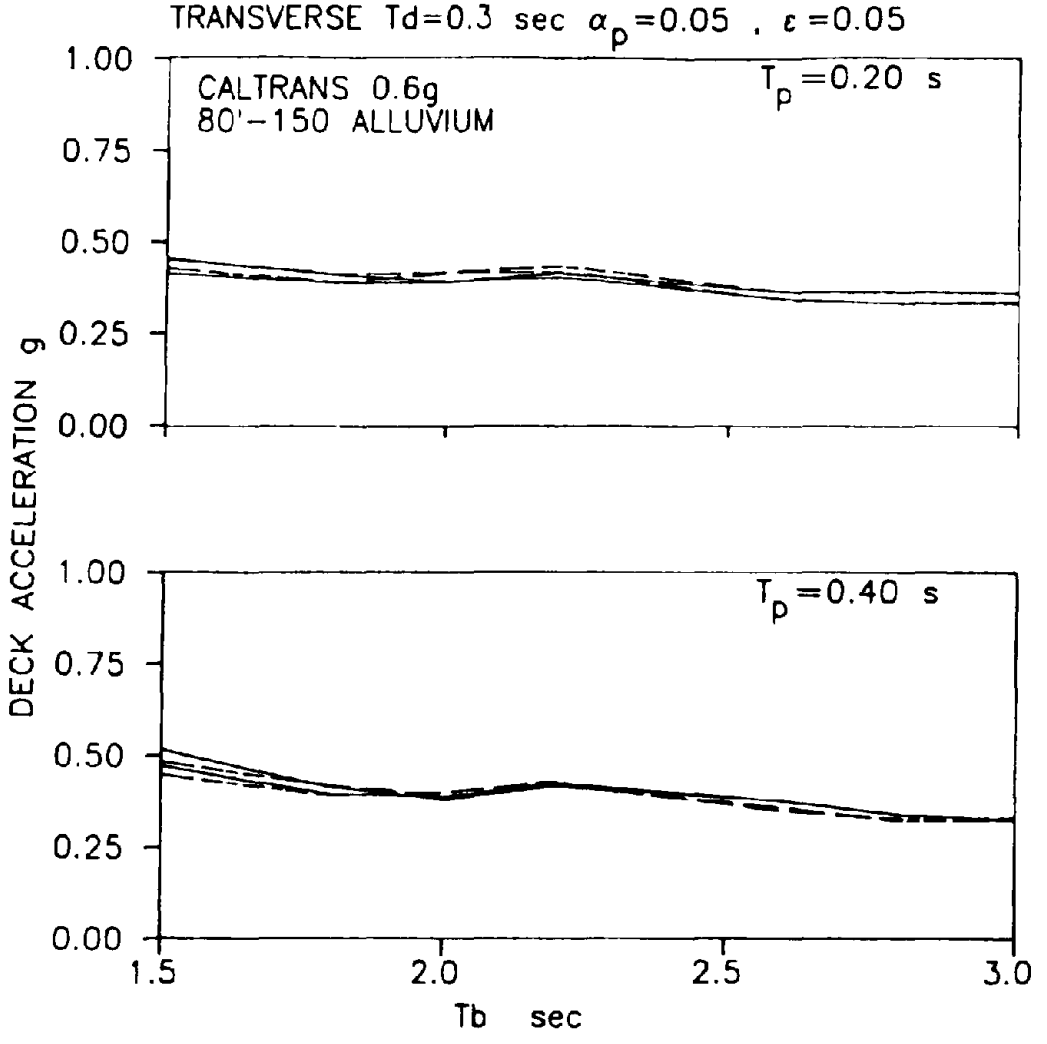

Fig. 9-25 - Deck Acceleration of Isolated Bridge with Td = 0.3 secs for Caltrans 0.6g Deep Alluvium Motion Applied in Transverse Direction.

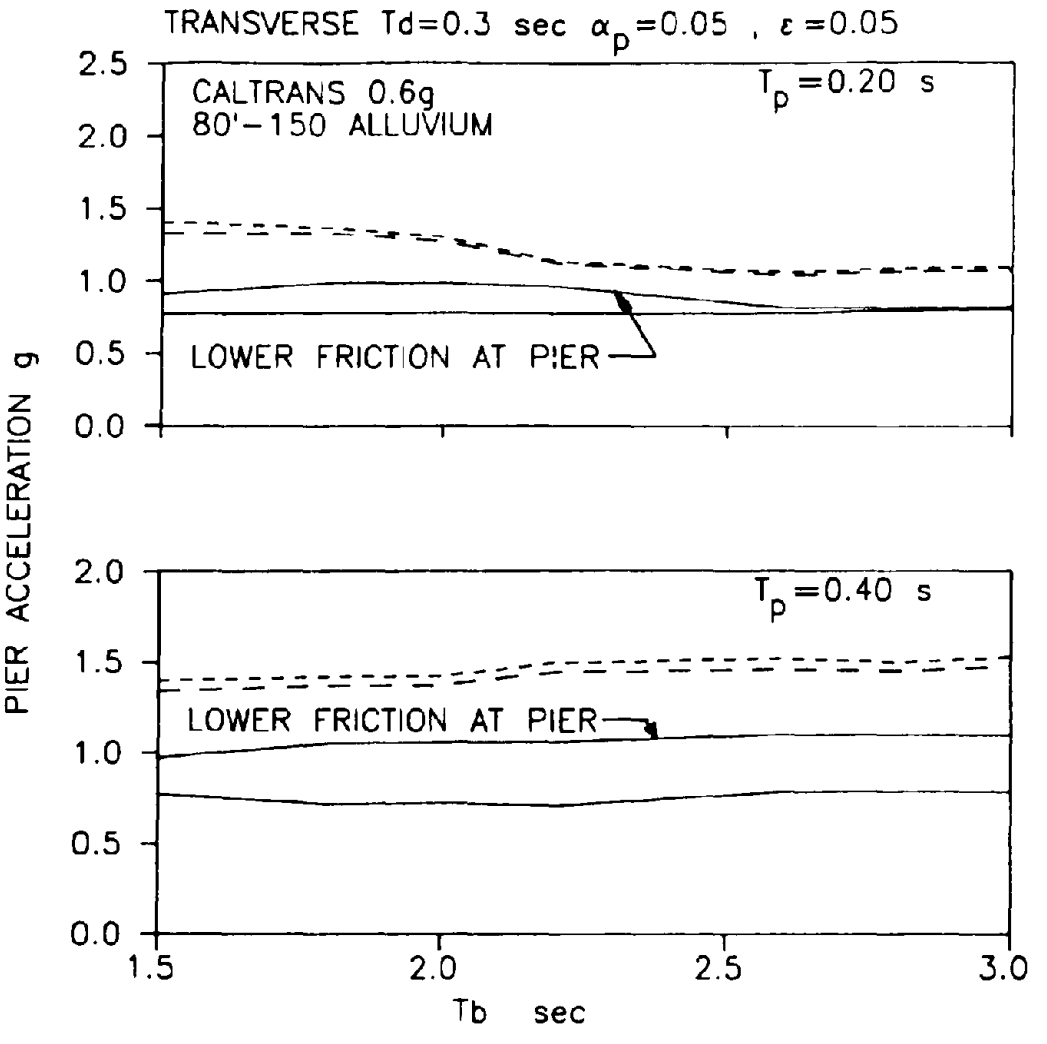

Fig. 9-26 - Pier Acceleration of Isolated Bridge with Td = 0.3 secs for Caltrans 0.6g Deep Alluvium Motion Applied in Transverse Direction.

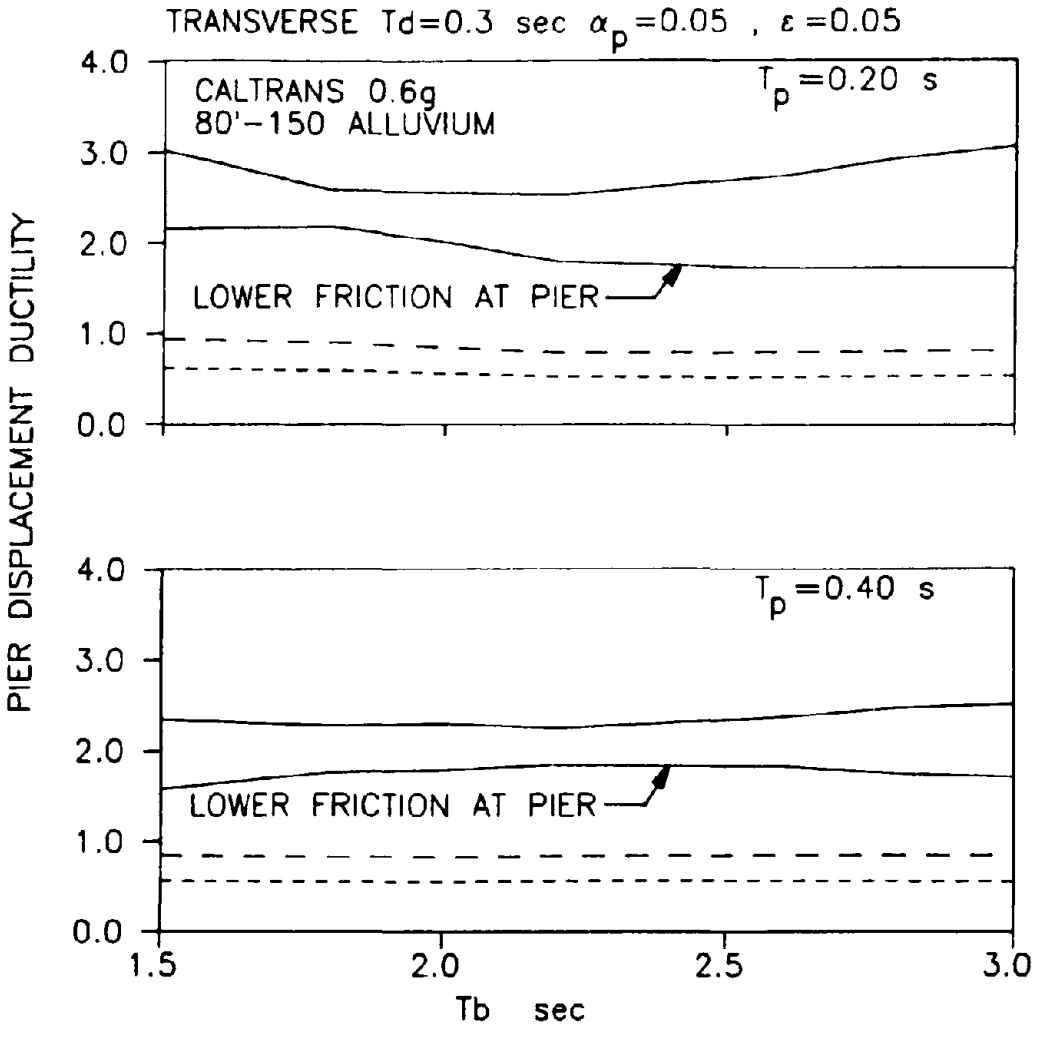

Fig. 9-27 - Pier Displacement Ductility of Isolated Bridge with Td = 0.3 secs for Caltrans 0.6g Deep Alluvium Motion Applied in Transverse Direction.

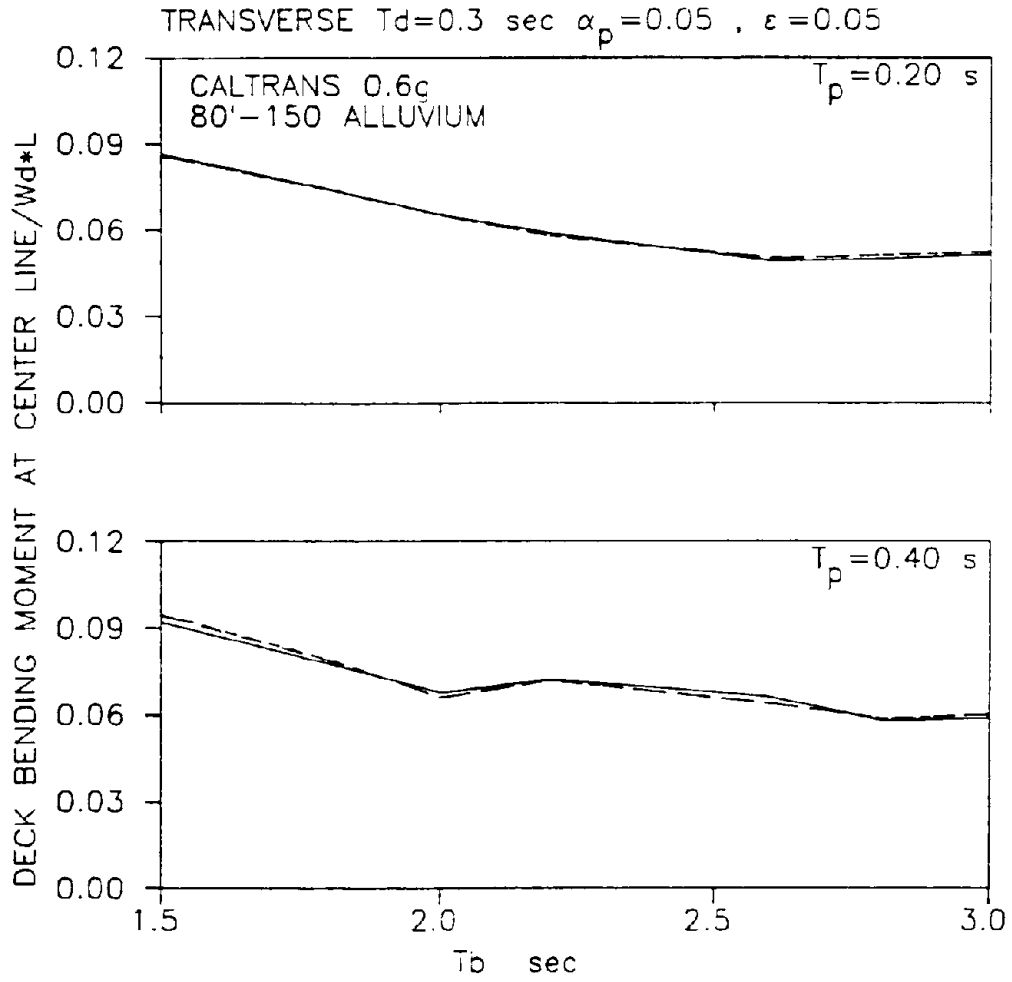

Fig. 9-28 - Deck Bending Moment of Isolated Bridge with Td = 0.3 secs for Caltrans 0.6g Deep Alluvium Motion Applied in Transverse Direction.

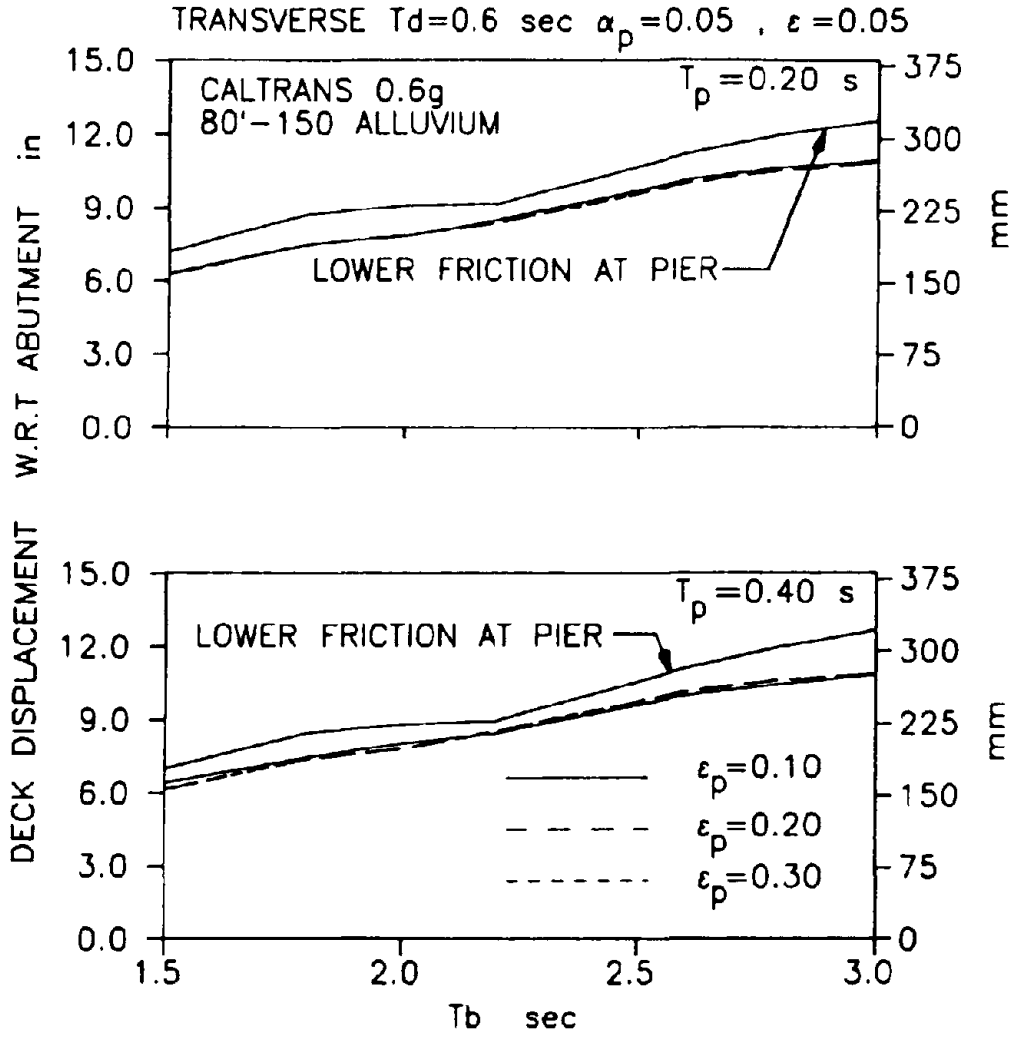

Fig. 9-29 - Deck (Bearing) Displacement at Abutment of Isolated Bridge with Td = 0.6 secs for Caltrans 0.6g Deep Alluvium Motion Applied in Transverse Direction.

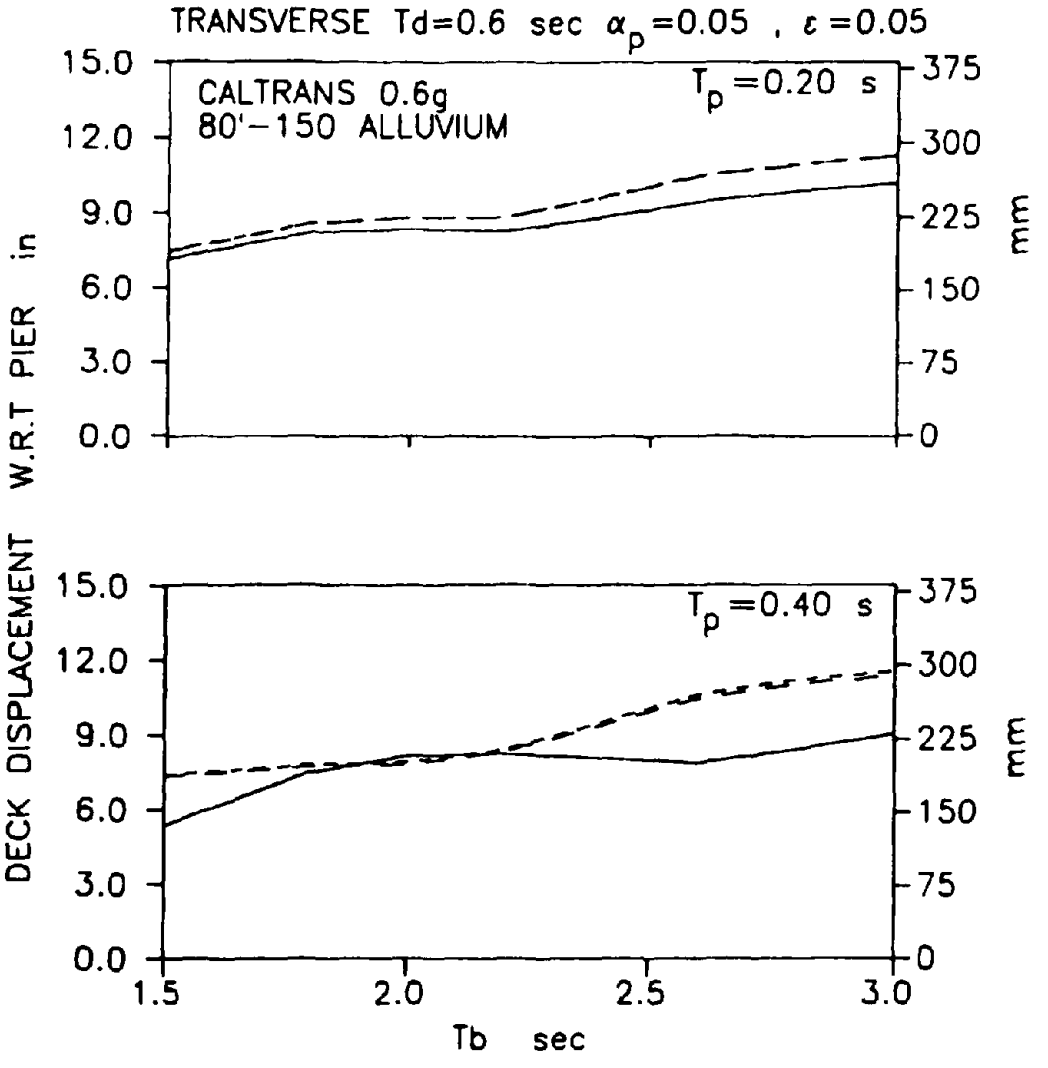

Fig. 9-30 - Deck (Bearing) Displacement at Pier of Isolated Bridge with Td = 0.6 secs for Caltrans 0.6g Deep Alluvium Motion Applied in Transverse Direction.

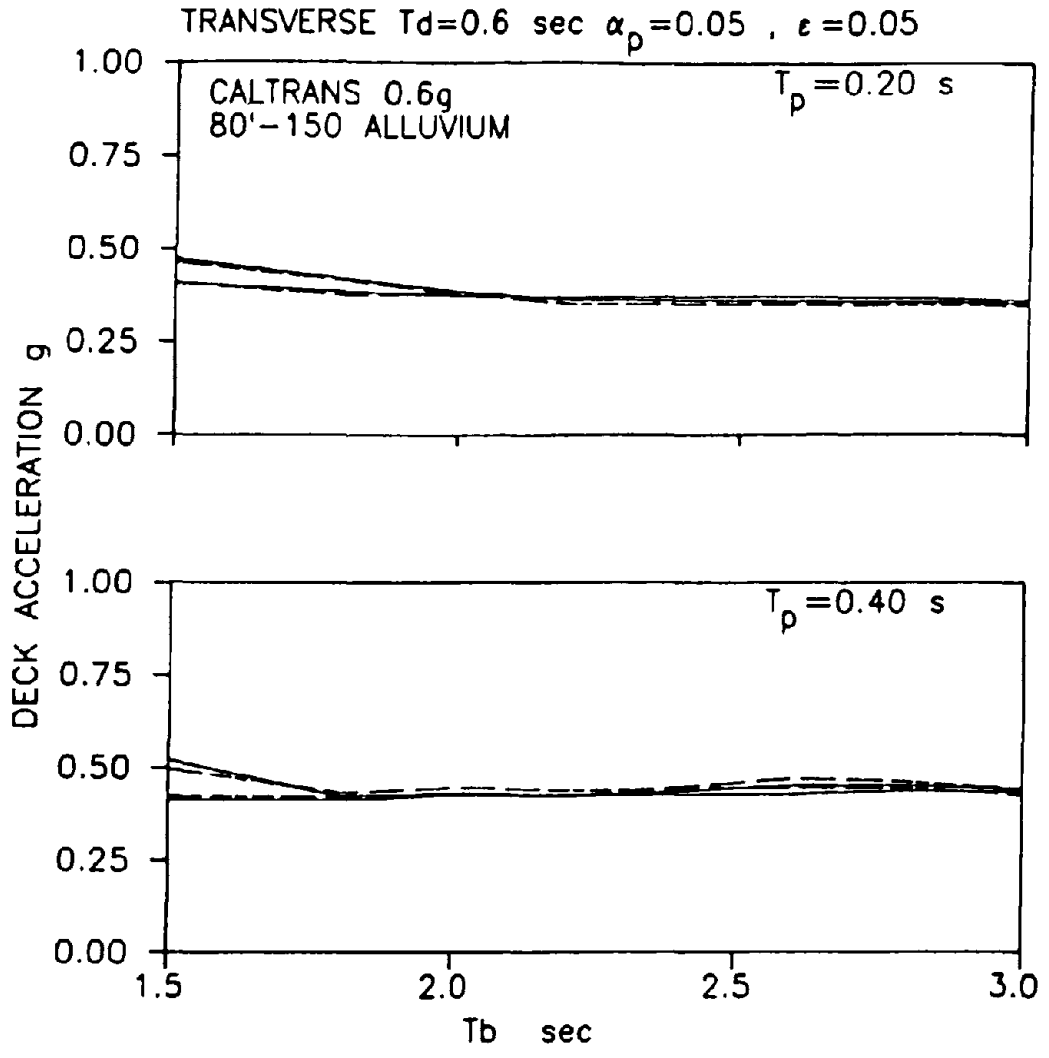

Fig. 9-31 - Deck Acceleration of Isolated Bridge with Td = 0.6 secs for Caltrans 0.6g Deep Alluvium Motion Applied in Transverse Direction.

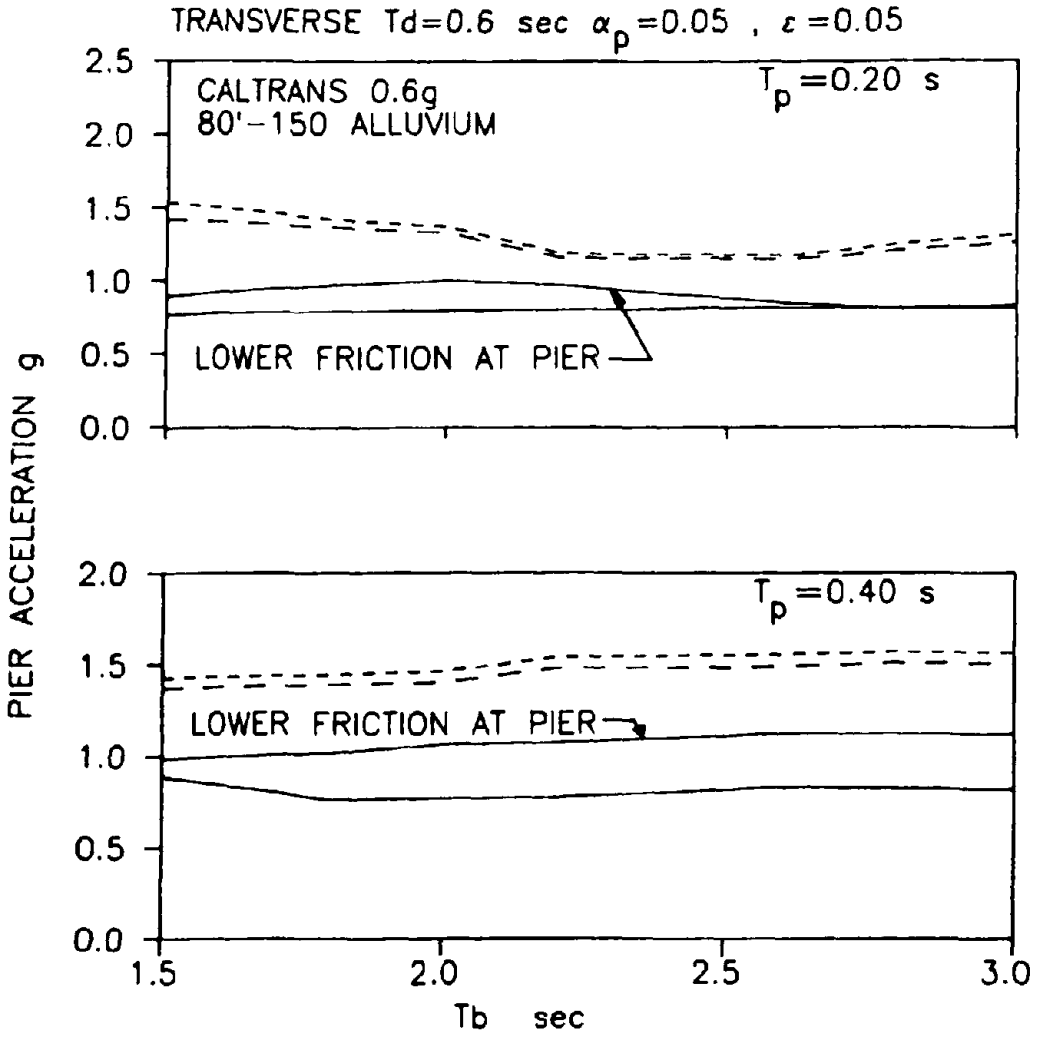

Fig. 9-32 - Pier Acceleration of Isolated Bridge with Td = 0.6 secs for Caltrans 0.6g Deep Alluvium Motion Applied in Transverse Direction.

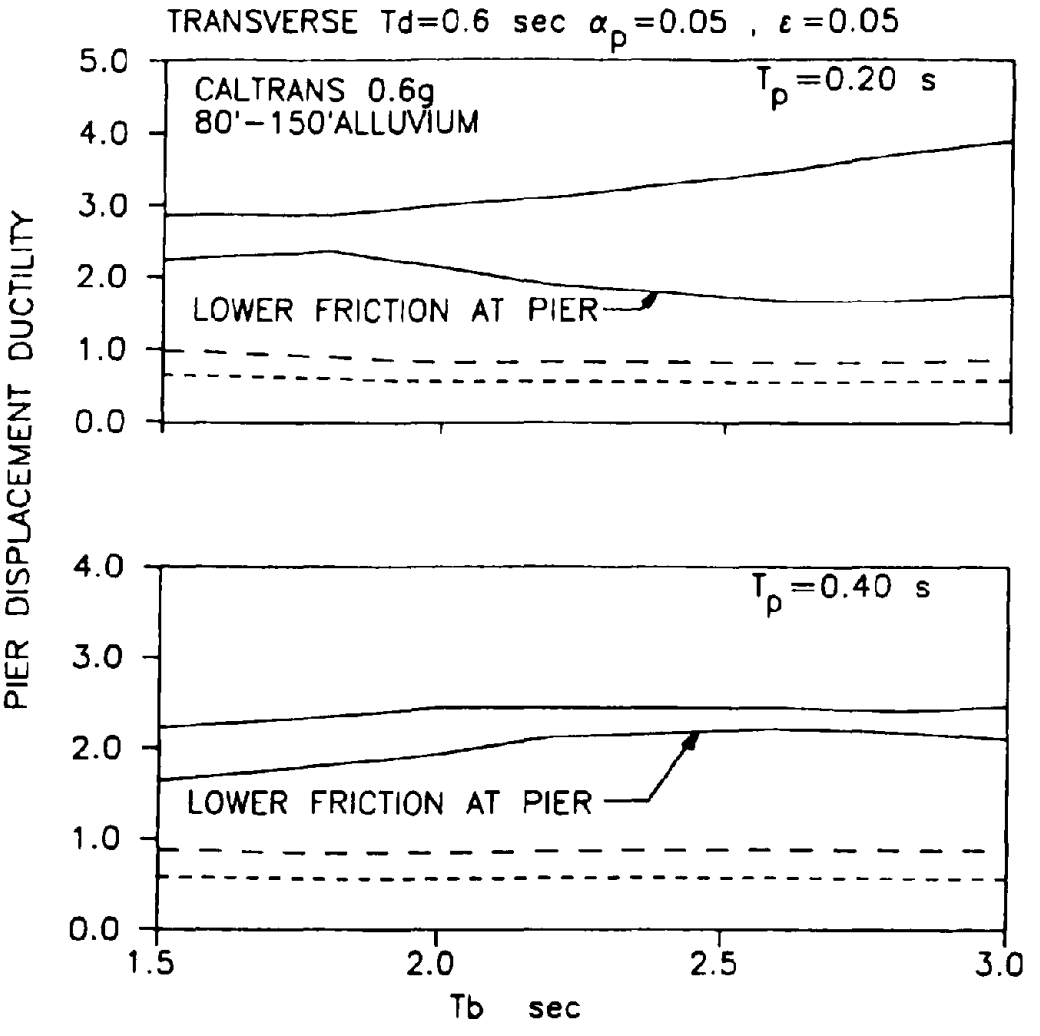

Fig. 9-33 - Pier Displacement Ductility of Isolated Bridge with Td = 0.6 secs for Caltrans 0.6g Deep Alluvium Motion Applied in Transverse Direction.

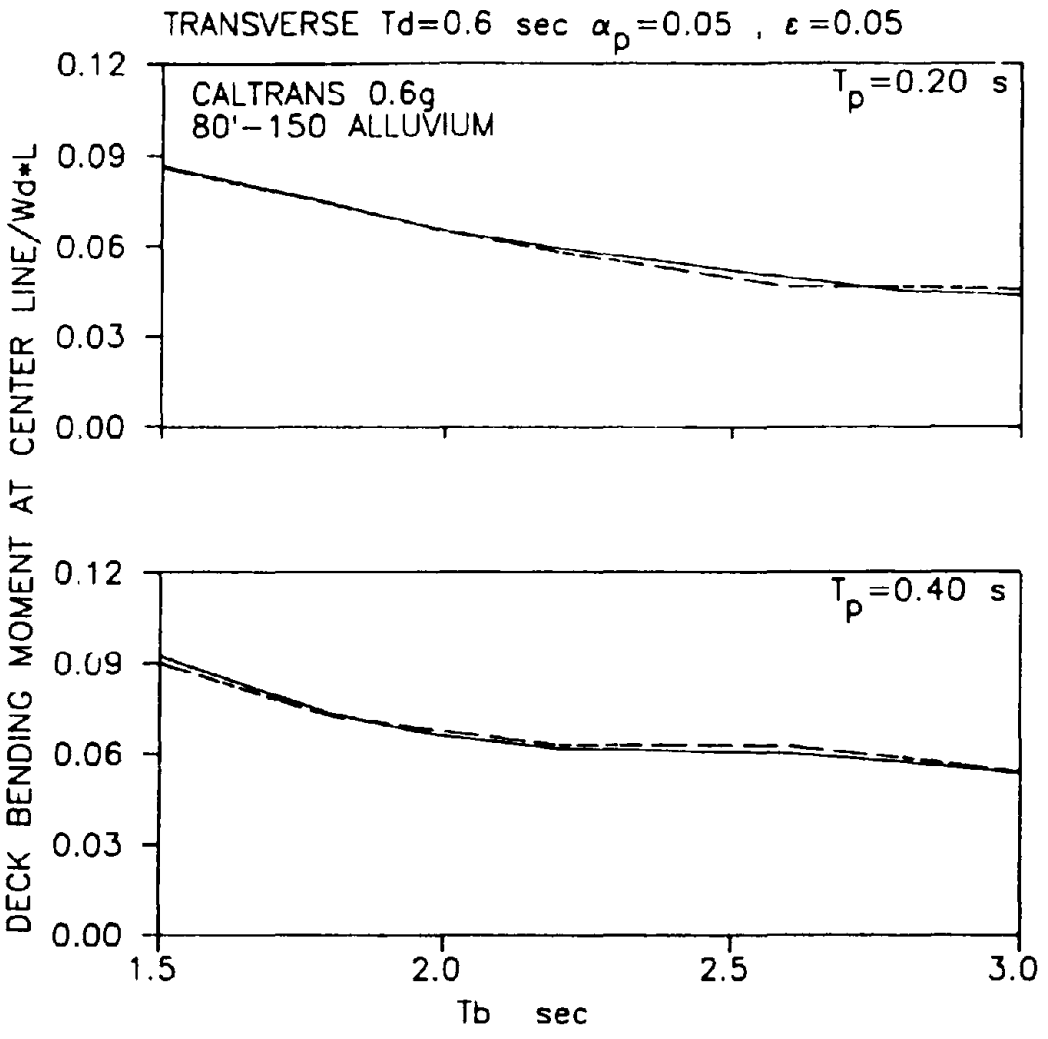

Fig. 9-34 - Deck Bending Moment of Isolated Bridge with Td = 0.6 secs for Caltrans 0.6g Deep Alluvium Motion Applied in Transverse Direction.

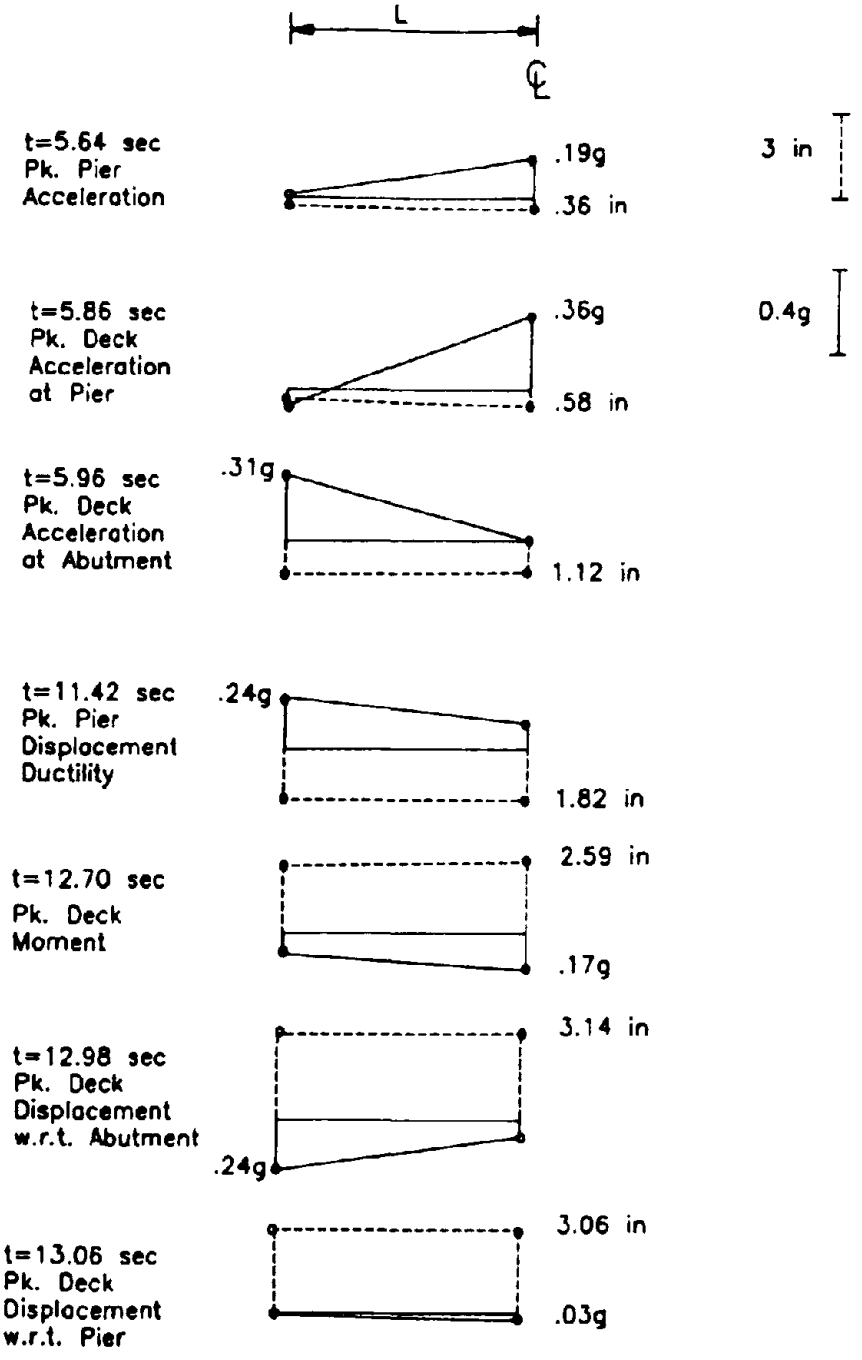

Fig. 9-35 - Profiles of Deck Acceleration (Solid Line) and Displacement (Dashed Line) of Two-span Continous Deck Isolated Bridge for Caltrans 0.6g Rock No. 1 Motion Applied in Transverse Direction.

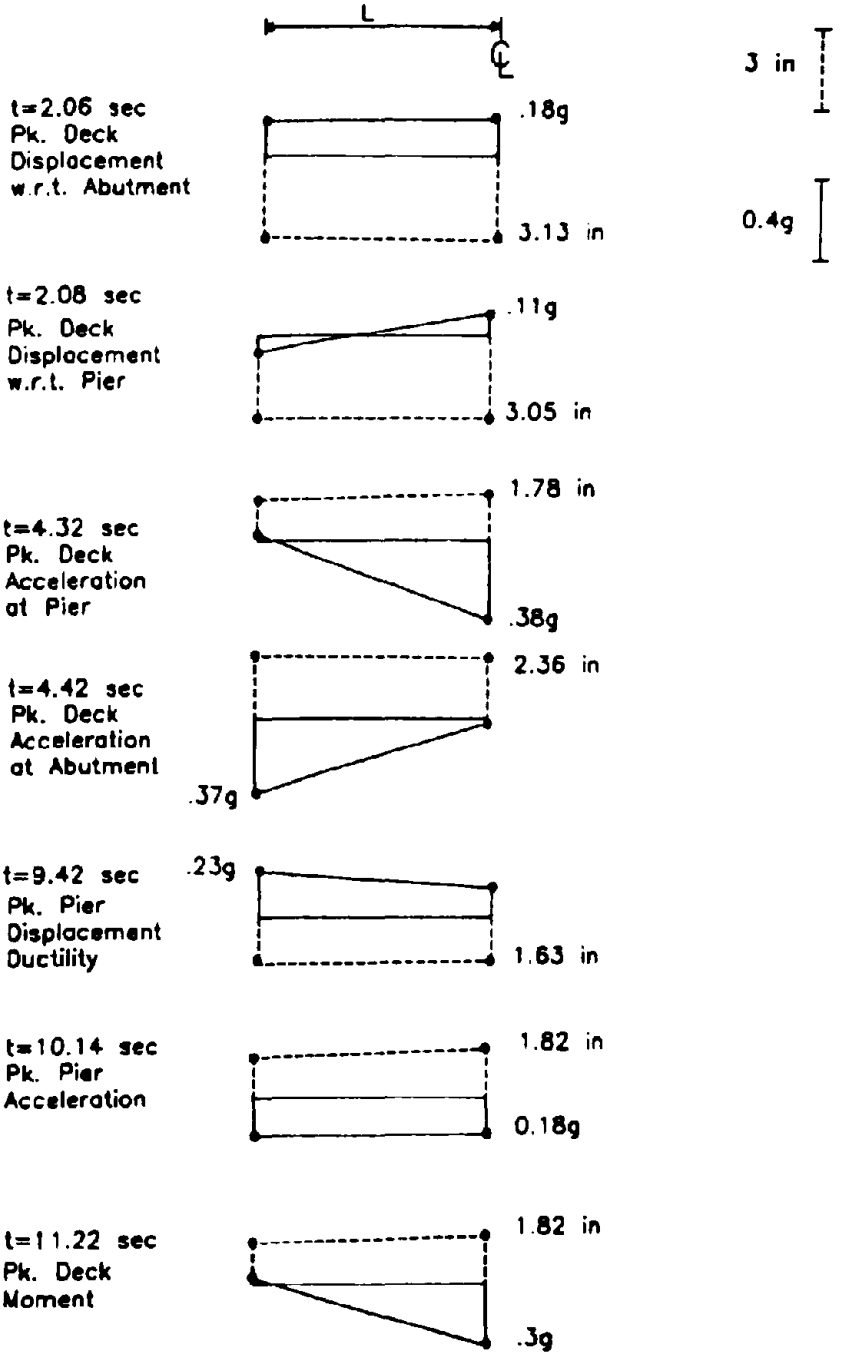

Fig. 9-36 - Profiles of Deck Acceleration (Solid Line) and Displacement (Dashed Line) of Two-span Continous Deck Isolated Bridge for Caltrans 0.6g Rock No. 3 Motion Applied in Transverse Direction.

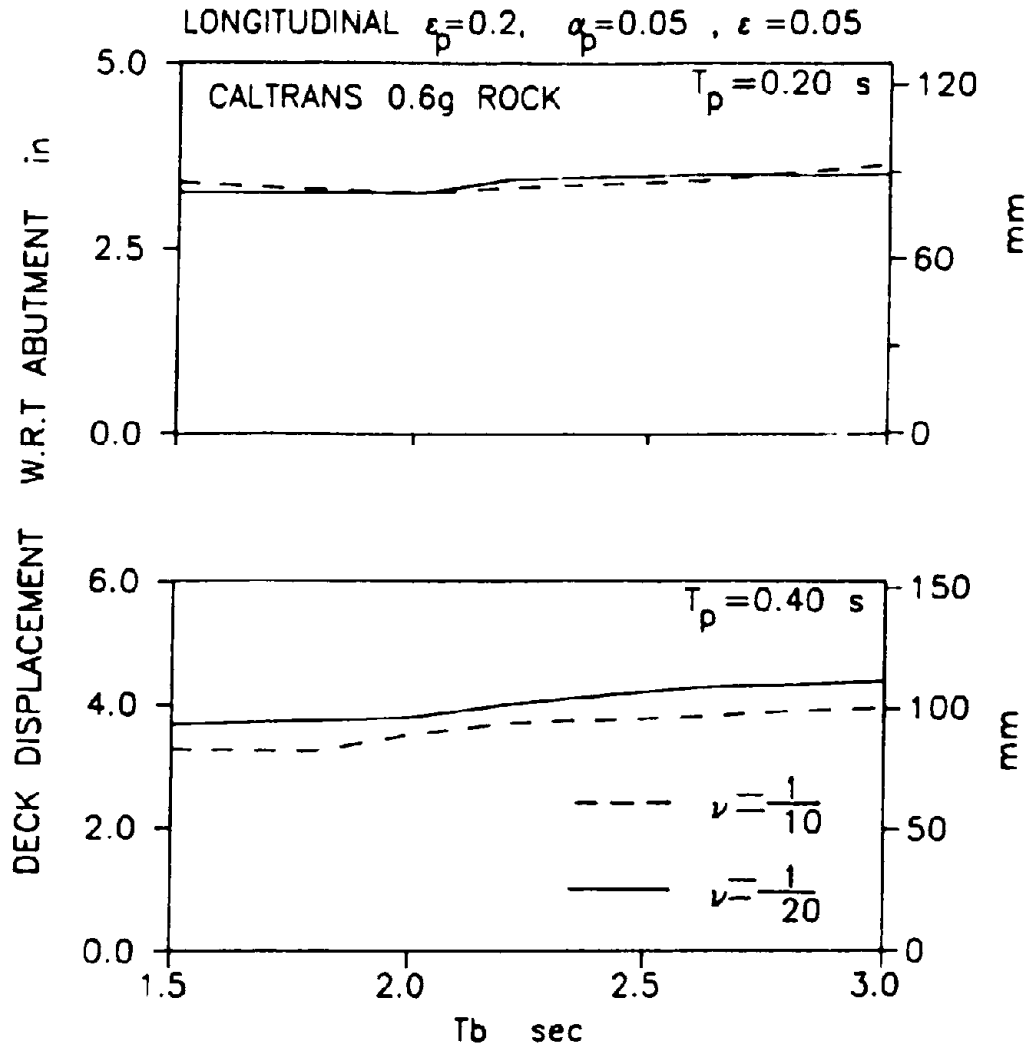

Fig. 9-37 - Deck (Bearing) Displacement at Abutment of Isolated Bridge for Caltrans 0.6g Rock Motion Applied in Longitudinal Direction,Effect of Mass Ratio.

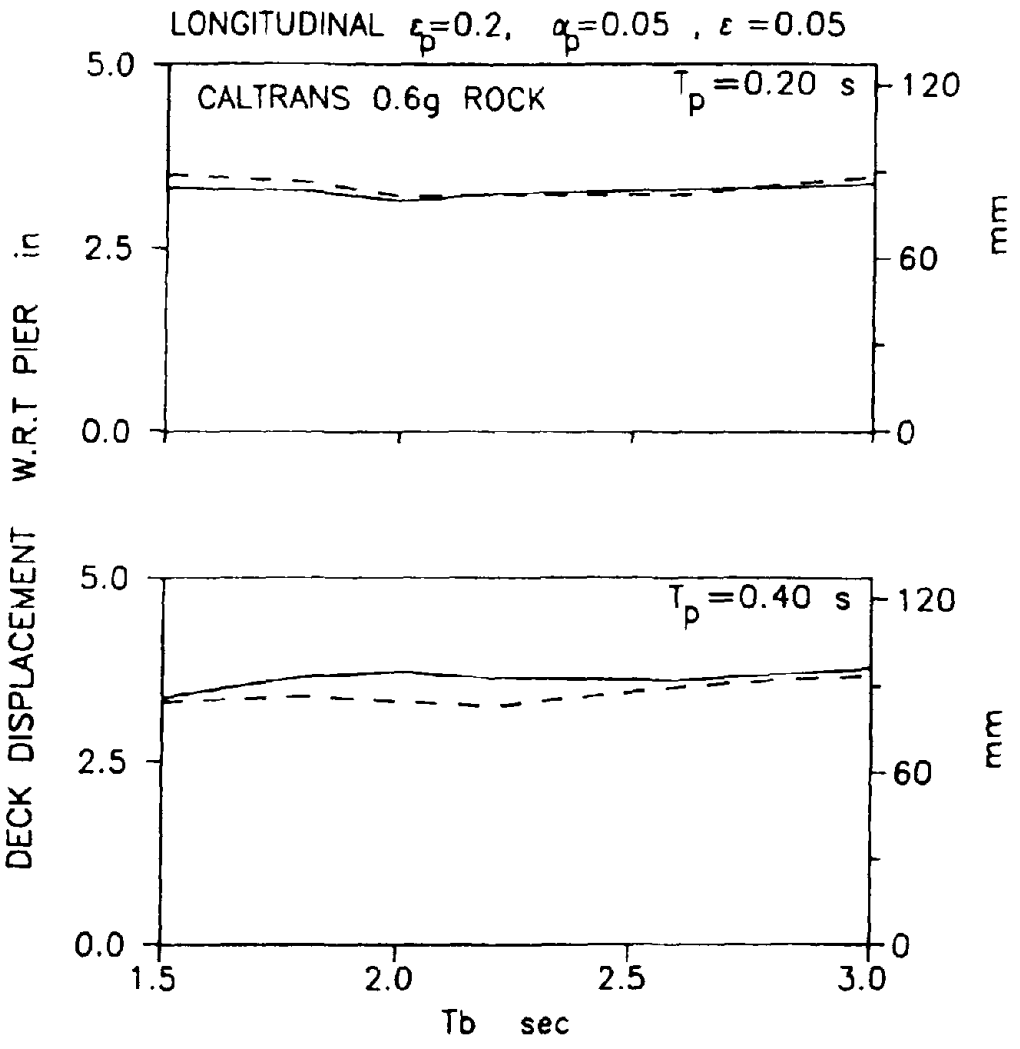

Fig. 9-38 - Deck (Bearing) Displacement at Pier of Isolated Bridge for Caltrans 0.6g Rock Motion Applied in Longitudinal Direction.Effect of Mass Ratio.

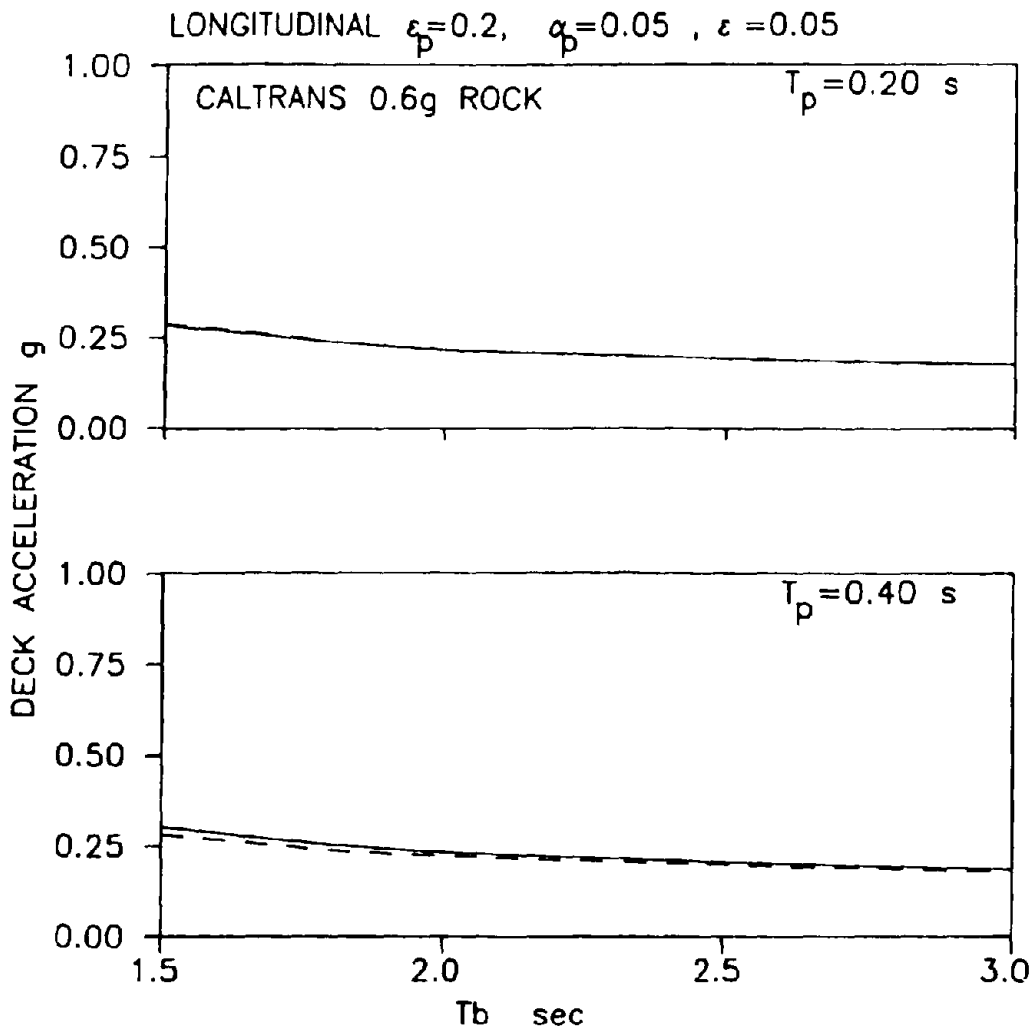

Fig. 9-39 - Deck Acceleration of Isolated Bridge for Caltrans 0.6g Rock Motion Applied in Longitudinal Direction,Effect of Mass Ratio.

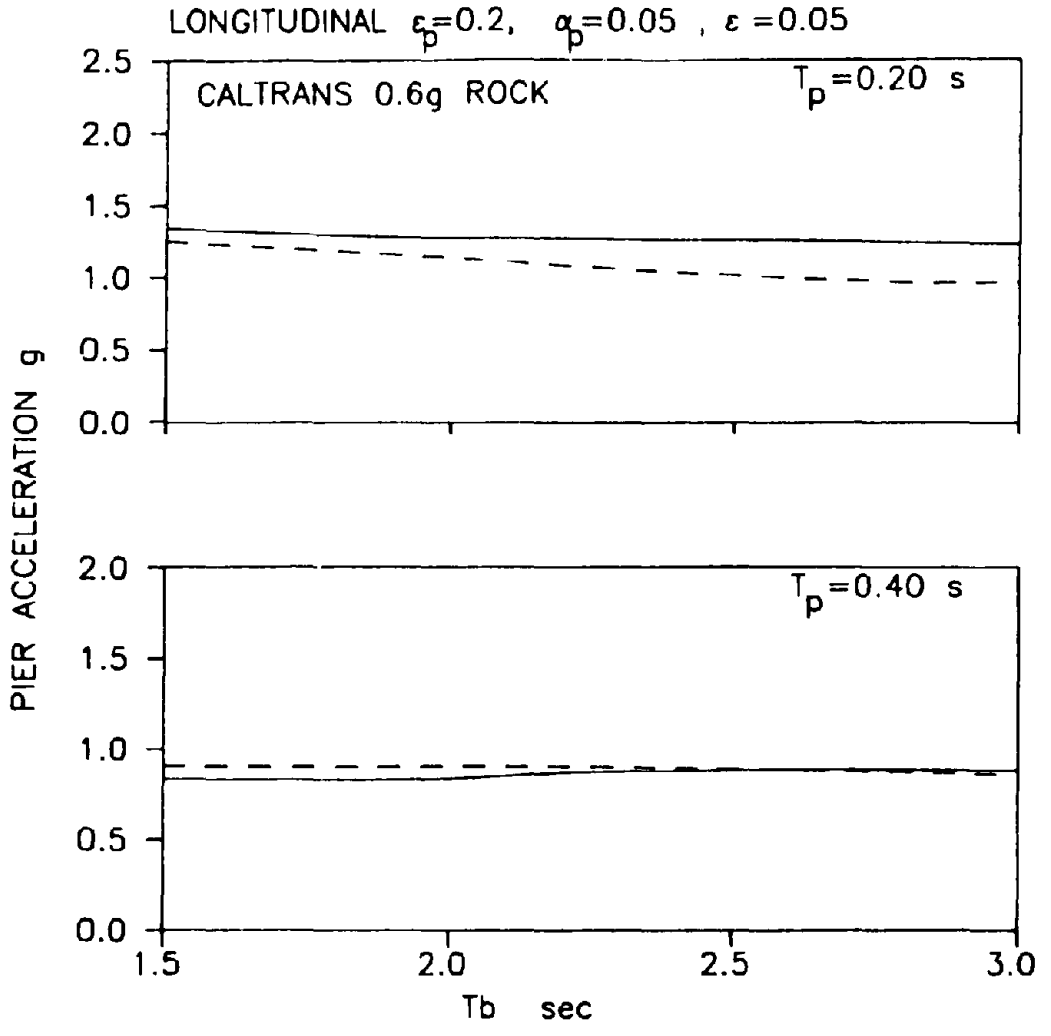

Fig. 9-40 - Pier Acceleration of Isolated Bridge for Caltrans 0.6g Rock Motion Applied in Longitudinal Direction.Effect of Mass Ratio.

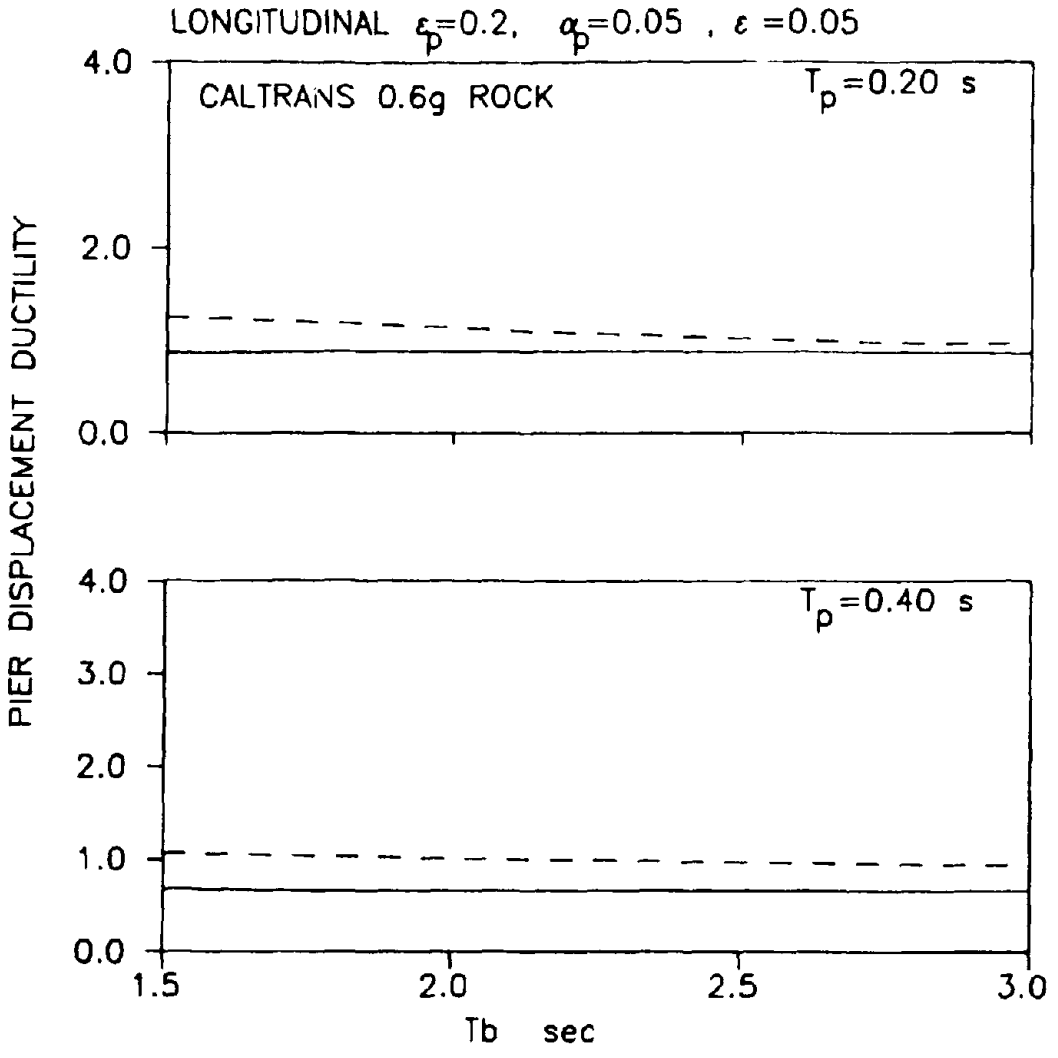

Fig. 9-41 - Pier Displacement Ductility of Isolated Bridge for Caltrans 0.6g Rock Motion Applied in Longitudinal Direction,Effect of Mass Ratio.

SECTION 10

SIMPLIFIED ANALYSIS METHODS

Two simplified analysis methods for predicting the bearing displacement and isolation system (or base) shear force are investigated. Both methods represent the seismic response of the bridge by a single-degree-of-freedom (SDOF) system with the deck and piers assumed to be infinitely rigid. The elastic and frictional properties of the sliding bearings and displacement control devices are lumped into a single inelastic element in which the force, F, is given by

$$F = \Sigma KU + f^{T}_{max} m_d g Z \qquad (10\text{-}1)$$

where U is the bearing displacement, ΣK is the total stiffness of spring assemblies of displacement control devices in the direction of excitation, $m_d g$ is the deck weight and Z, (7-5) takes values between ± 1. The quantity $f^{T}_{max} m_d g$ is the maximum value of the total frictional force (bearings and DCD). For example, in the studied equal length 2-span bridge

$$f^{T}_{max} m_d g = 2 f^{a}_{max} W_a + f^{p}_{max} W_p + e m_d g \qquad (10\text{-}2)$$

in which the superscripts a and p refer to the abutment and pier, respectively.

Equation (10-1) describes bilinear hysteretic behavior with very high initial stiffness, characteristic strength or yield force

equal to $f^T_{max} m_d g$ and stiffness after yielding equal to ΣK. The velocity dependence of frictional force is neglected.

10.1 Simplified Deck Model

The response of the isolated deck is determined directly from inelastic spectra which are produced by computing the maximum response of SDOF systems of different periods T_b, (8-6), and friction coefficients f^T_{max}. Such spectra are presented in Figure 10-1 and 10-2. This procedure is similar to those used for designing bridges with lead-rubber bearings in New Zealand (Ministry of Works and Development 1983) and California (Dynamic Isolation Systems 1984).

As may be seen in Figures 10-1 and 10-2, an advantage of this procedure is that it gives the designer a direct feel of the sensitivity of the parameters associated with the seismic response.

A comparison of the displacement predictions of the simplified deck model to those of the more complicated analytical model is presented in Figures 10-3 to 10-6. The displacement was obtained from the spectra of Figure 10-2 for $f^T_{max} = 0.139$ and using linear interpolation. The simplified deck model predicts well the bearing displacement, though in some cases it underpredicts the response by as much as 20%. As discussed earlier this error is primarily a result of neglecting the pier flexibility.

The simplified deck model predicts very well the base shear force as demonstrated in Figures 10-7 and 10-8. This is true even

when the deck displacement is underpredicted because the restoring force contributes only a portion to the base shear force. While the isolation system seismic force can be accurately predicted and distributed to the substructure, the shear force and displacement ductility of the pier cannot be accurately predicted because the pier acceleration is not known.

10.2 AASHTO Procedure

The American Association of State Highway and Transportation Officials-AASHTO (1991) very recently published guide specifications for seismic isolation design of highway bridges. The specifications allow the use of a static analysis procedure provided that a) the isolation system has self-centering capability and b) the effective damping of the isolation system is less than or equal to 30 percent of critical. The procedure describes the displacement across the isolation bearings (in units of inches)

$$d_i = \frac{10 A S_i T_e}{B} \qquad (10\text{-}3)$$

in which AS_i is the product of acceleration and site coefficients, T_e is the period of vibration and B is the damping coefficient related to the effective viscous damping ratio, β. Both T_e and β are calculated based on the effective (or secant) stiffness of the isolation system. For sliding systems with force at the isolation system described by (10-1), T_e and β take the form (see also Theodossiou et al. 1991 for more details)

$$T_e = 2\pi\left(\frac{f_{max}^T g}{d_i} + \frac{4\pi^2}{T_b^2}\right)^{-1/2} \qquad (10\text{-}4)$$

$$\beta = \frac{2}{\pi}\left(\frac{f_{max}^T}{f_{max}^T + \frac{4\pi^2 d_i}{gT_b^2}}\right) \qquad (10\text{-}5)$$

Displacement d_i is calculated in iterative process using (10-3) - (10-5). The procedure is almost identical to the International Conference of Building Officials-UBC (1991) seismic isolation regulations.

In applying the AASHTO procedure for a site characterized by CALTRANS bridge design spectra, the value of AS_i must be established. As explained in the AASHTO (1991) Commentary, equation (10-3) with B=1 represents an analytic expression for the long period 5%-damped displacement spectra. Based on this interpretation, values of AS_i equal to 0.6 and 1.2 were determined for the CALTRANS 0.6g rock and deep alluvium spectra, respectively.

The displacement predictions of the AASHTO procedure are compared to the results of the more complicated analytical model in Figures 10-3 to 10-6. We note first that the analyzed systems satisfy the AASHTO requirements on the lateral restoring force. Furthermore, the value of effective viscous damping ratio, β (10-5), is more than 30 percent of critical in the rock input with $T_b \geq 2$ secs, but is less than 30 percent in all other cases. In the cases of $\beta > 0.30$ the AASHTO procedure was extended by using the

values of the damping coefficient B in the International Conference of Building Officials-UBC (1991). The results of Figures 10-3 and 10-5 demonstrate that the AASHTO procedure predicts well and with acceptable degree of conservatism the isolation system displacement in the rock input. However, the procedure substantially overpredicts (by 50 to 100 percent) the displacement in the deep alluvium input. This is attributed to the inability of equivalent linear and viscous models to predict the behavior of sliding systems in motions rich in long period components (Makris 1989 and 1991).

The base shear force predictions of the AASHTO procedure are compared to the results of nonlinear dynamic analysis in Figures 10-7 and 10-8. As expected the AASHTO procedure predicts well the base shear force in the case of rock type input but overpredicts the force in the case of deep alluvium input. This, of course, is a result of the displacement overprediction.

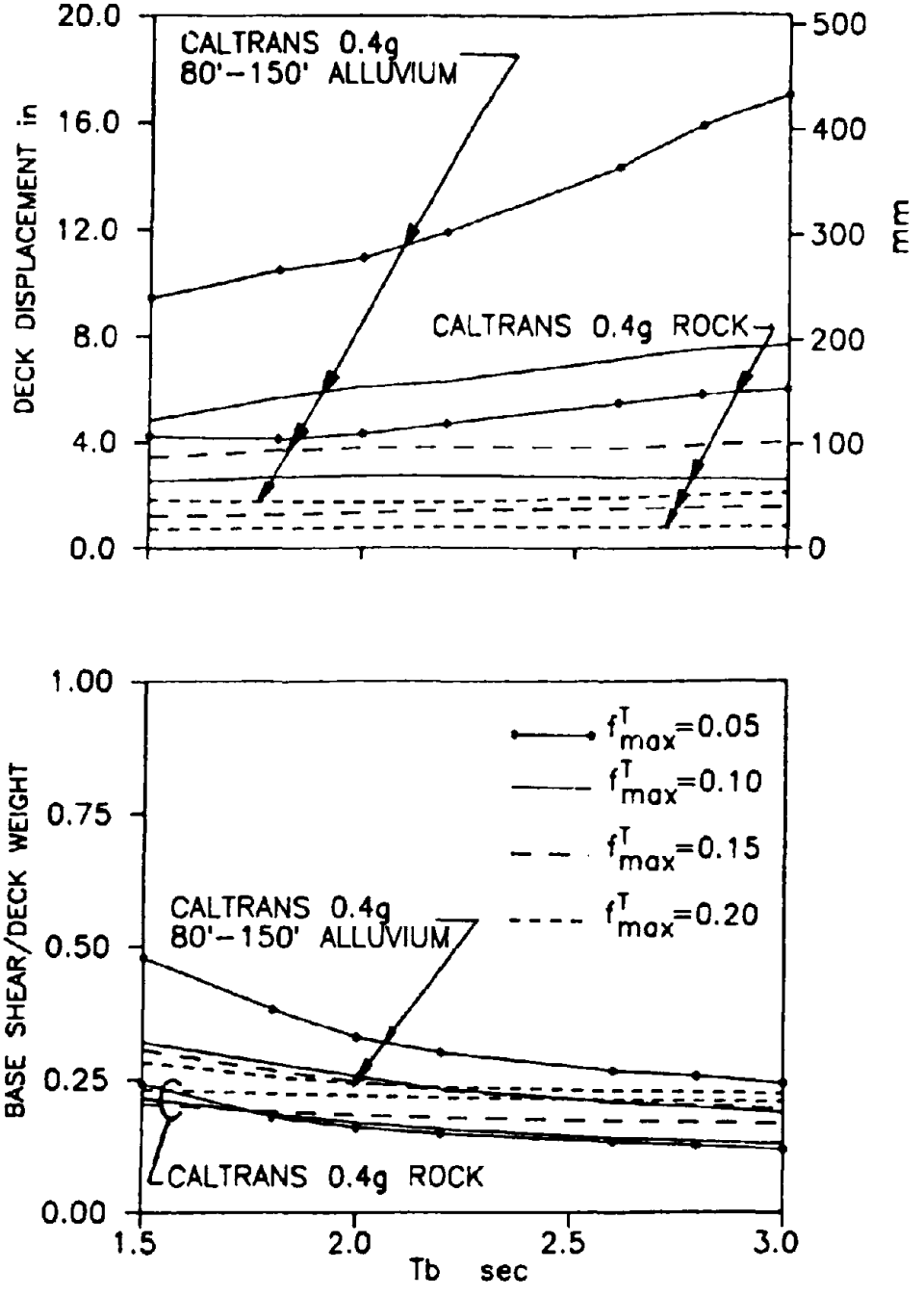

Fig. 10-1 - Inelastic Spectra for Design of Sliding Isolation Systems for Caltrans 0.4g Rock and Deep Alluvium Motions.

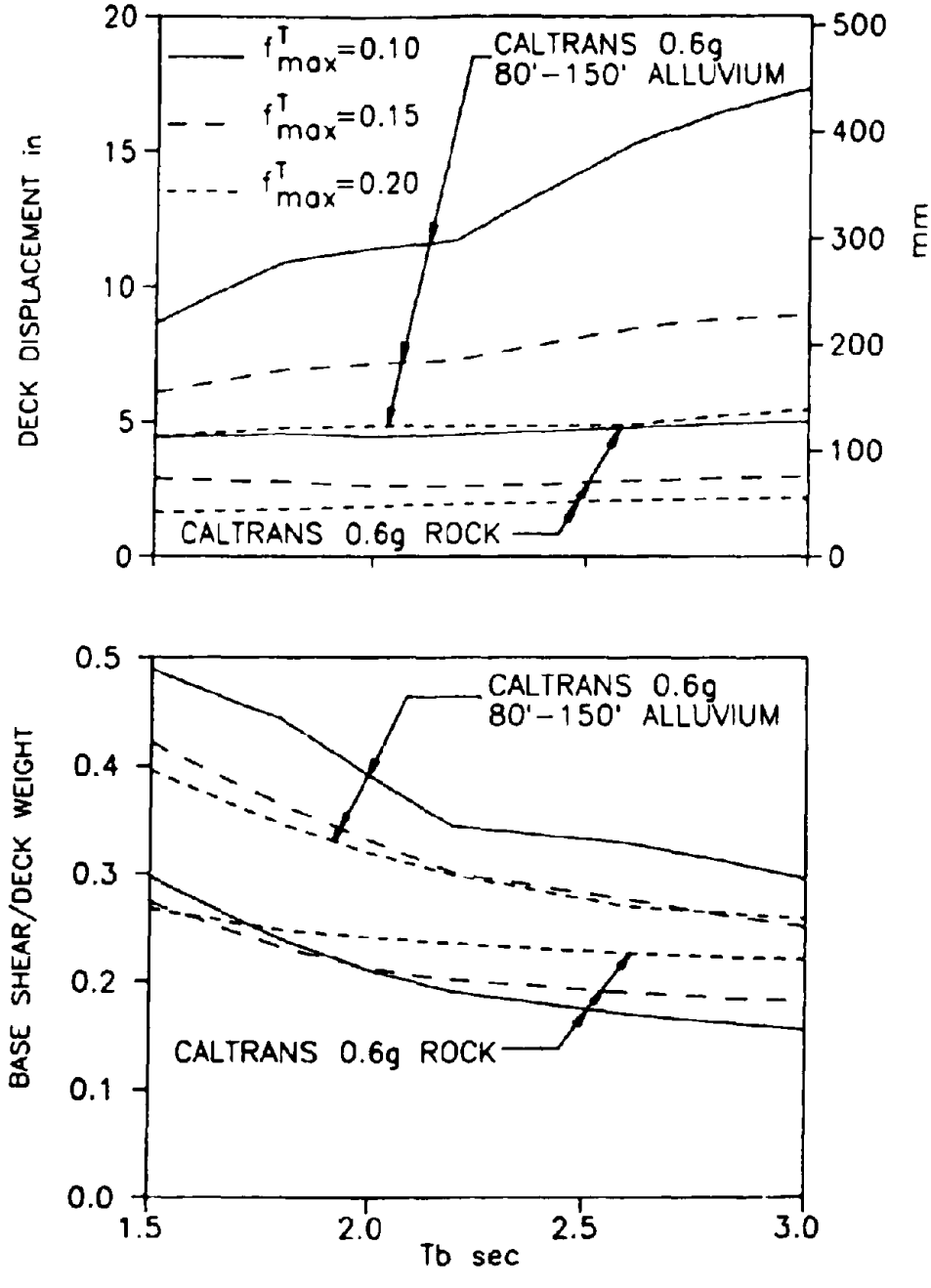

Fig. 10-2 - Inelastic Spectra for Design of Sliding Isolation Systems for Caltrans 0.6g Rock and Deep Alluvium Motions.

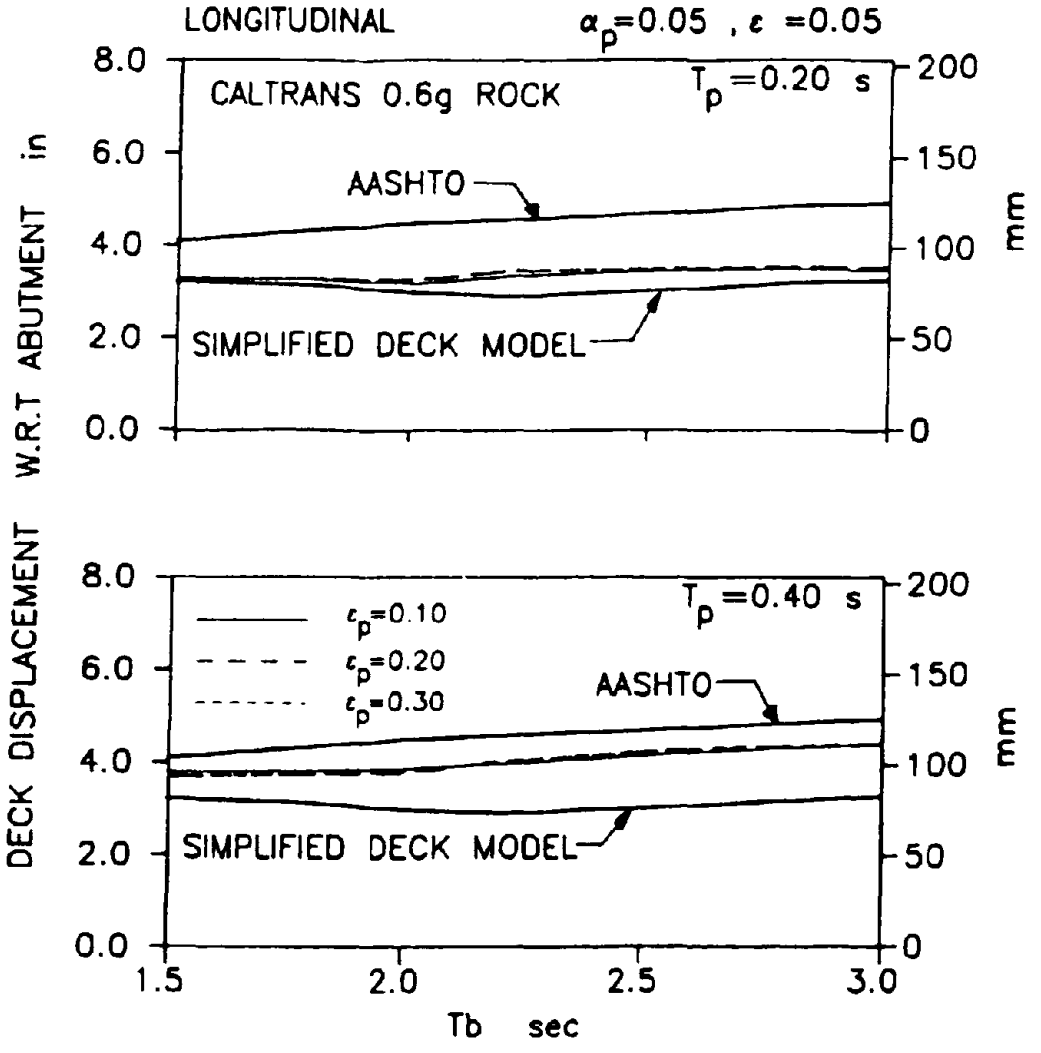

Fig. 10-3 - Prediction by Simplified Methods of Deck (Bearing) Displacement at Abutment of Isolated Bridge for Caltrans 0.6g Rock Motion Applied in Longitudinal Direction.

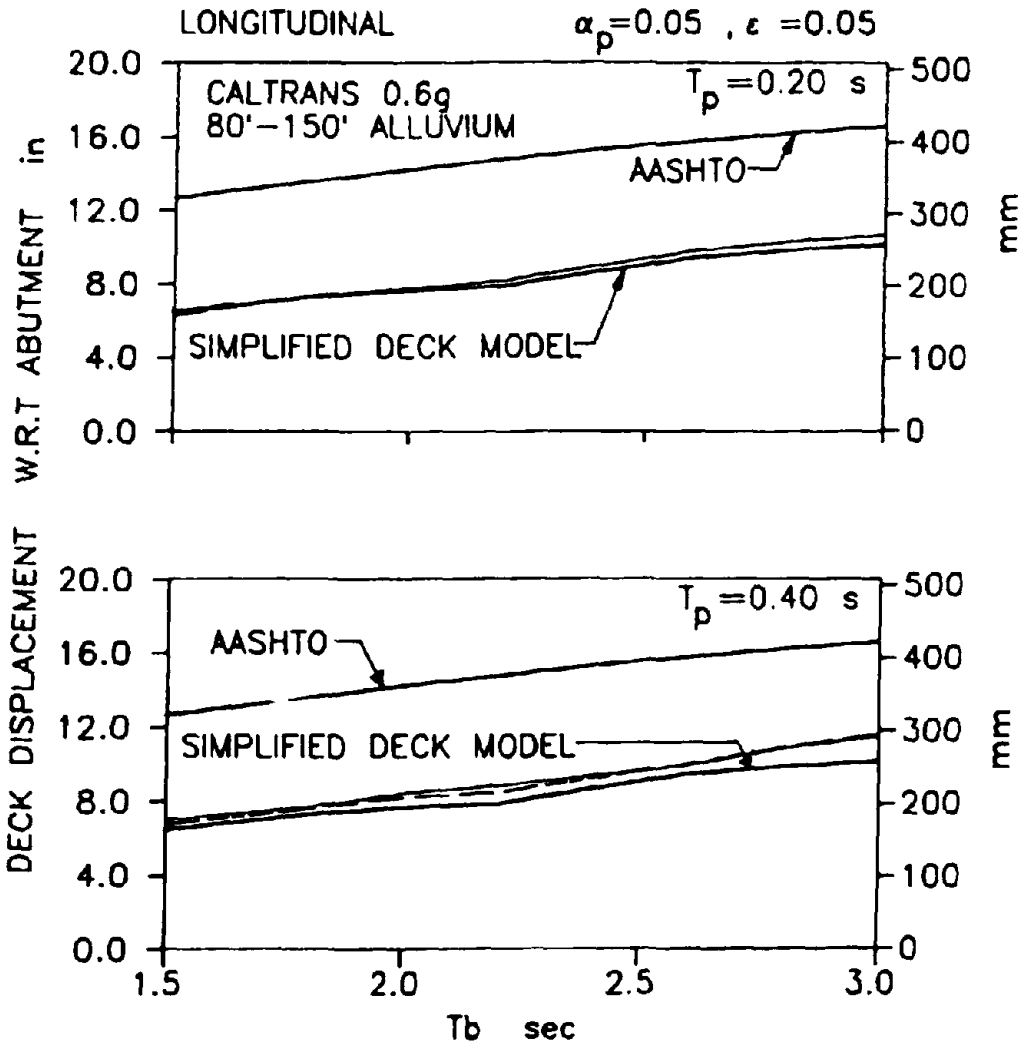

Fig. 10-4 - Prediction by Simplified Methods of Deck (Bearing) Displacement at Abutment of Isolated Bridge for Caltrans 0.6g Deep Alluvium Motion Applied in Longitudinal Direction.

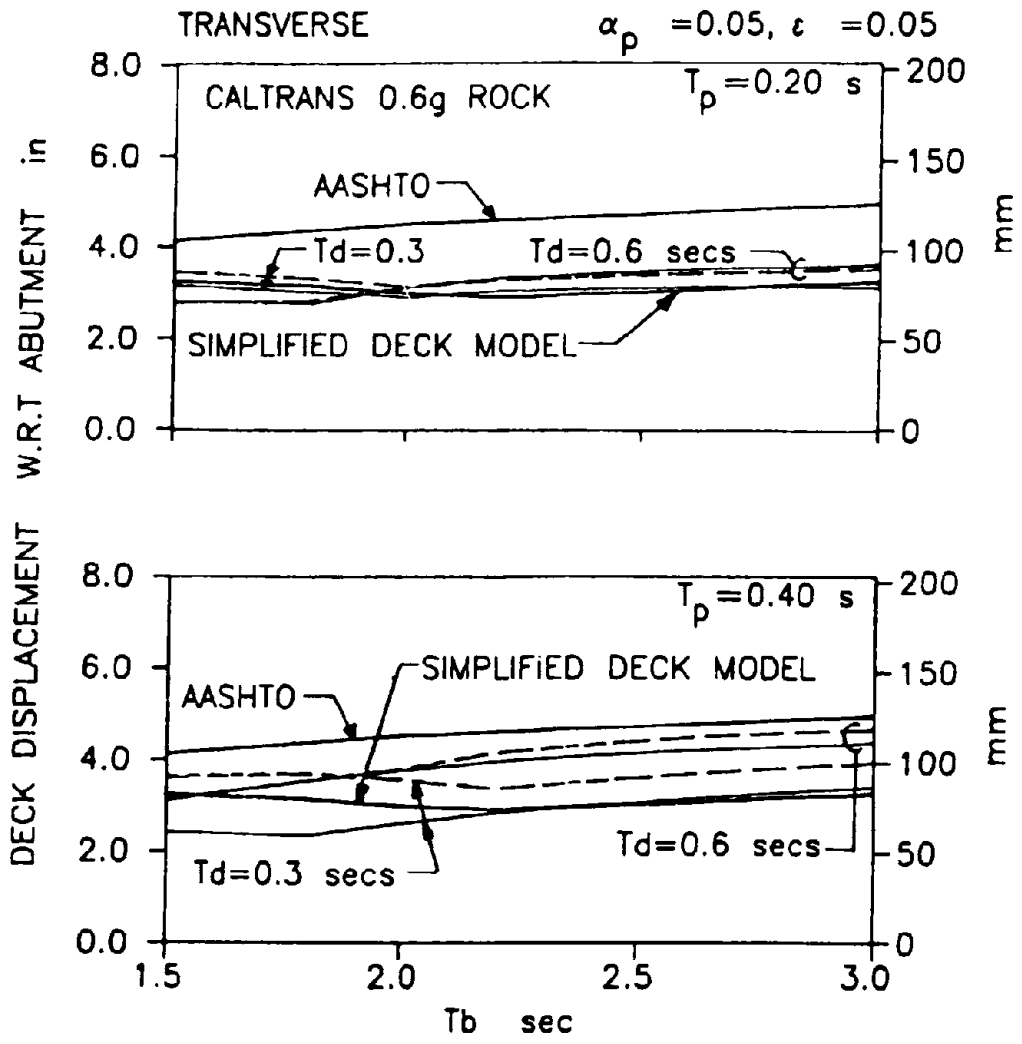

Fig. 10-5 - Prediction by Simplified Methods of Deck (Bearing) Displacement at Abutment of Isolated Bridge for Caltrans 0.6g Rock Motion Applied in Transverse Direction.

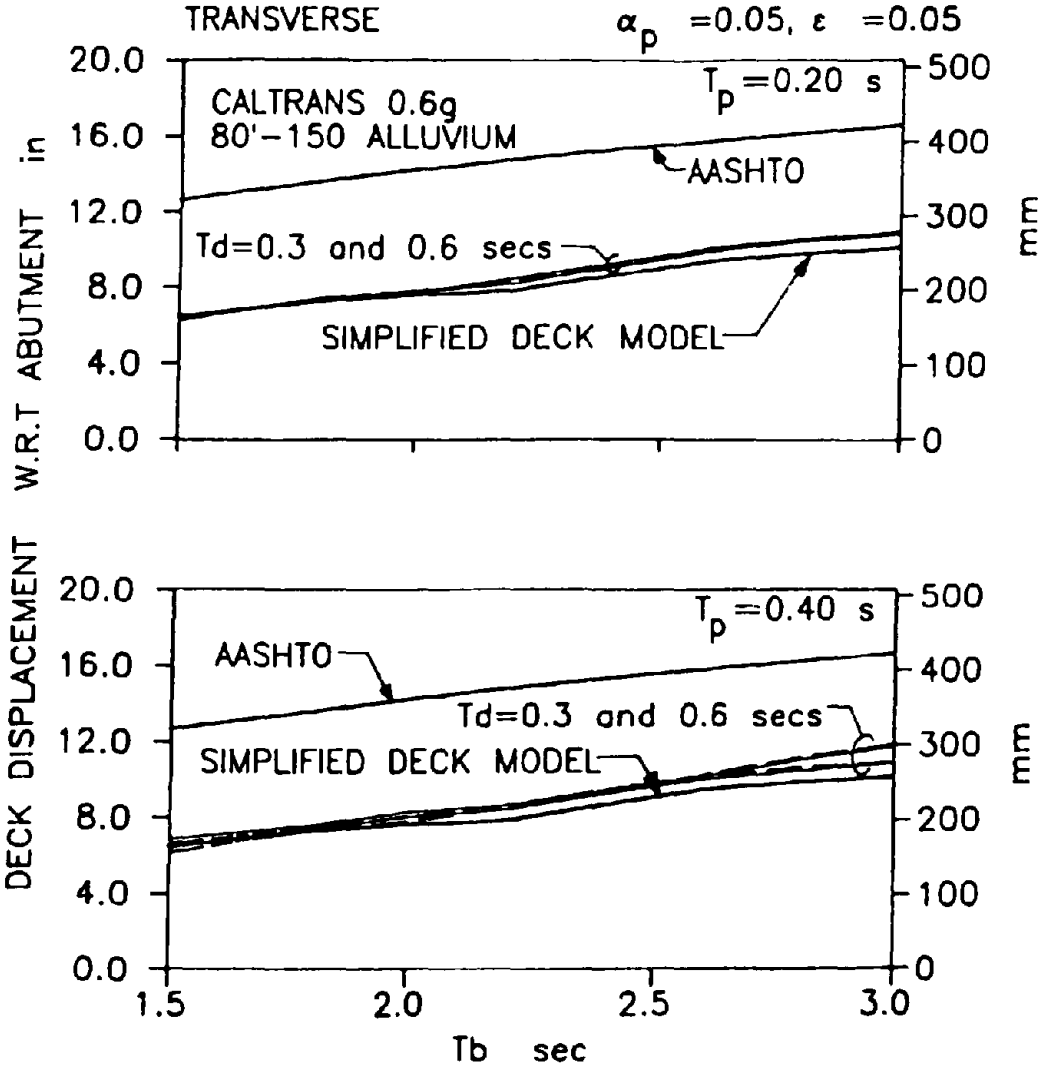

Fig. 10-6 - Prediction by Simplified Methods of Deck (Bearing) Displacement at Abutment of Isolated Bridge for Caltrans 0.6g Deep Alluvium Motion Applied in Transverse Direction.

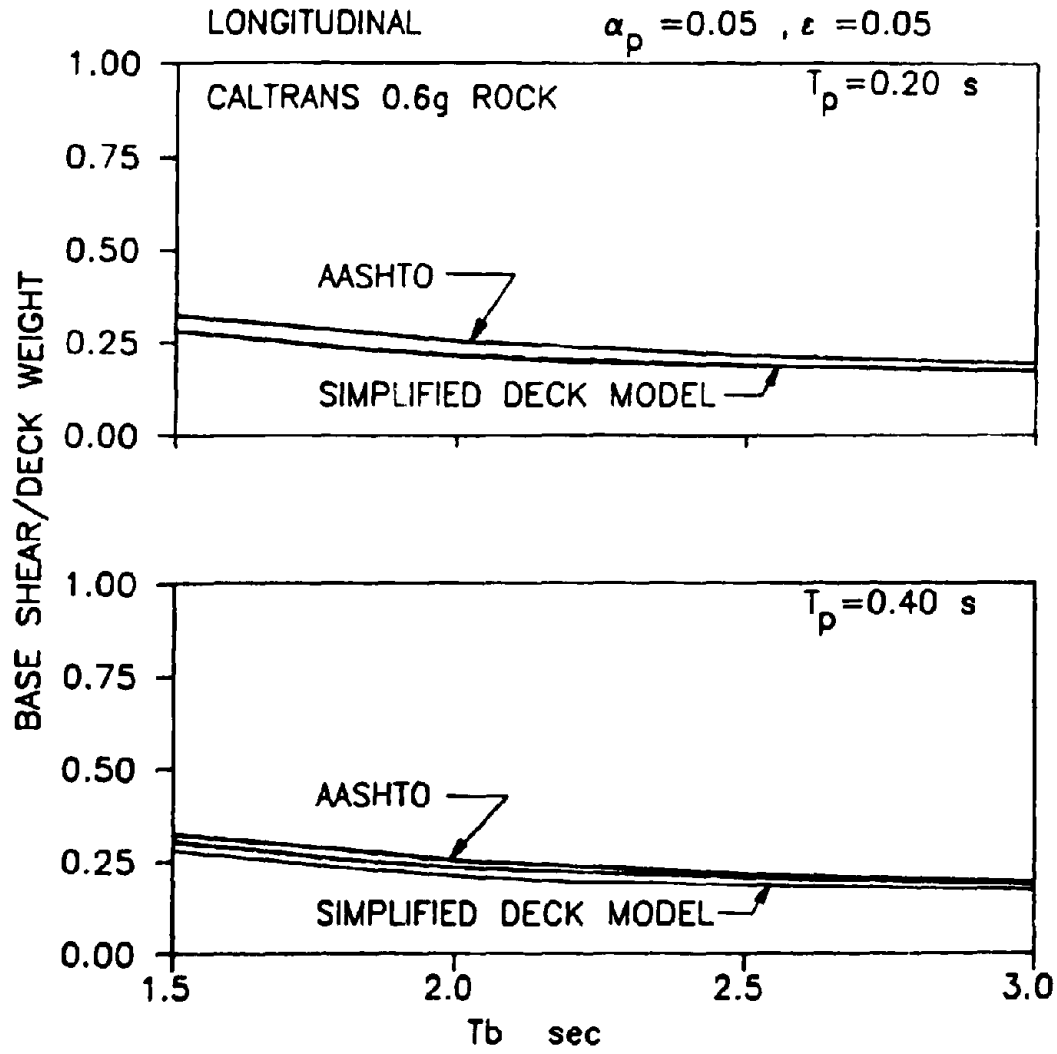

Fig. 10-7 - Prediction by Simplified Methods of Deck Base Shear of Isolated Bridge for Caltrans 0.6g Rock Motion Applied in Longitudinal Direction.

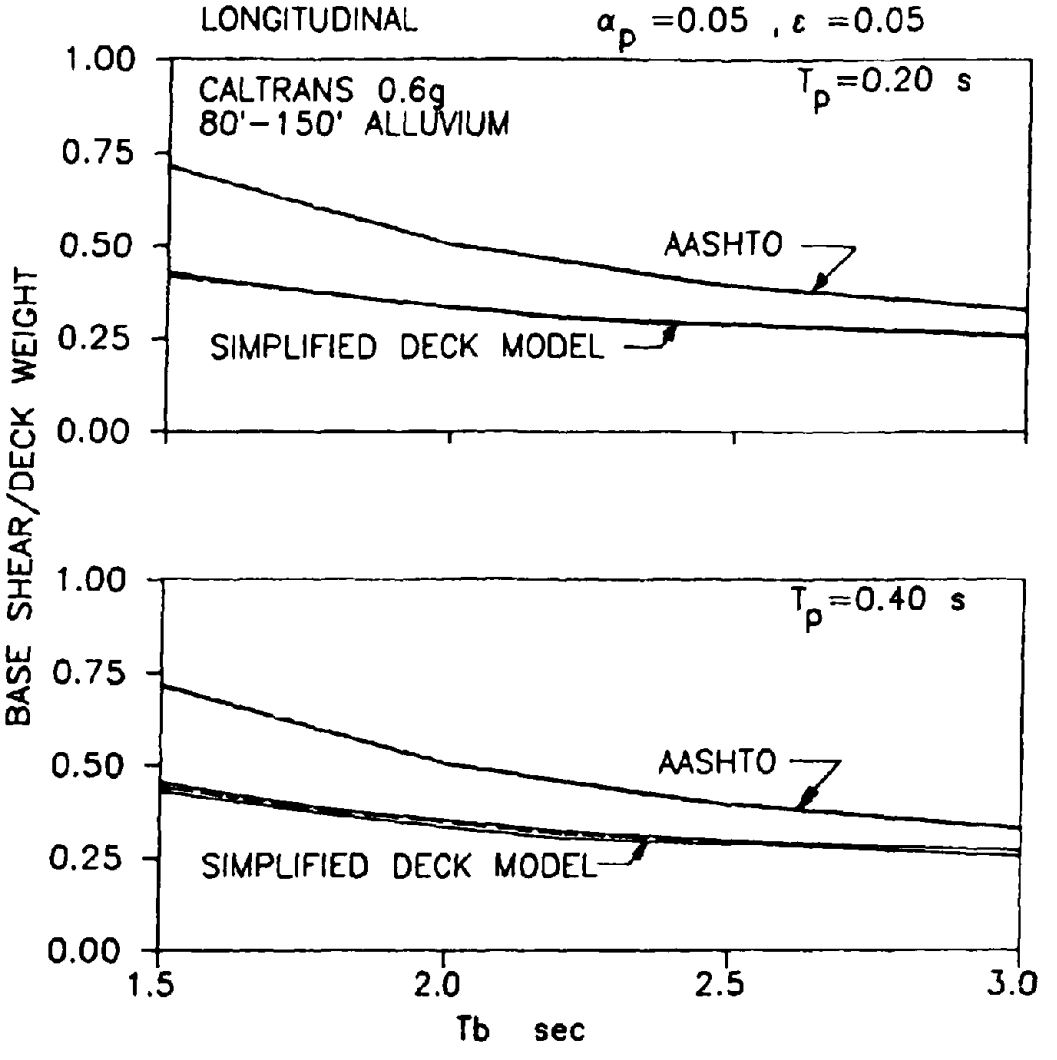

Fig. 10-8 - Prediction by Simplified Methods of Deck Base Shear of Isolated Bridge for Caltrans 0.6g Deep Alluvium Motion Applied in Longitudinal Direction.

SECTION 11

CONCLUSIONS

A sliding seismic isolation system for bridges consisting of Teflon disc bearings and displacement control devices has been tested on a shake table using a quarter scale, 51 kip (227.4 kN) model. In all tested configurations the conditions at the isolation interface could be described by a combination of strong frictional force and weak restoring force. The results show that:

1. The system performed well for strong earthquake motions having significantly different intensities and content of frequency. In all tests the deck acceleration was maintained at about 0.2 g while the bearing displacements did not exceed 4 in. (101.6 mm) in prototype scale.
2. The bearing displacements were less than the table displacements.
3. The displacement restraint mechanism of the displacement control device was successfully activated in one test and prevented the deck from undergoing excessive displacement.
4. The system has stable characteristics. This was demonstrated in a test in which the bearings were subjected to over 100 cycles of motion with 72 of these cycles at a displacement exceeding 0.5 in. (12.7 mm) or 45% of the system's displacement limit.
5. The behavior of the system at resonance may be qualitatively assessed by established principles of mechanics.

6. Permanent displacements in sliding isolation systems do not have adverse effects and are not cumulative.
7. The response of the system could be reliably predicted by analytical methods.

The effects of pier flexibility and strength, deck flexibility and distribution of isolation elements on the dynamic response of sliding isolated bridges could not be studied in the experimental program. Rather, these effects were studied analytically. The conclusions of the analytical study are:

1. Sliding isolation systems may produce a significant isolation effect as determined by the reduction in pier displacement ductility demand in comparison to that of non-isolated bridges.
2. Bearing displacements in sliding isolated bridges are in general less than the bearing displacements of comparable non-isolated bridges.
3. Deck flexibility has a minor effect on bearing displacements, pier displacement ductility and pier top acceleration.
4. Deck flexibility causes out-of-phase transverse response with high accelerations in flexible decks. As in the case of flexible buildings on sliding isolation systems, the high accelerations do not lead to increased bending moments in the deck because of the out-of-phase response.
5. Pier flexibility has an effect of bearing displacements. Bearing displacements in systems with flexible piers as much

as 20 percent larger than those in systems with stiff piers were noted.

6. Pier flexibility has a minor effect on the shear force across the isolation interface.
7. Sliding bearings of different frictional properties may be used to effectively direct loads away of elements of the substructure which are least capable of resisting them. In this way, low strength piers may remain essentially elastic in strong earthquake excitation.
8. A simplified analysis method which uses inelastic spectra could predict well the isolation system displacement and shear force. The method assumes rigid pier behavior, and therefore, could underpredict displacements by as much as 20 percent.
9. The AASHTO static analysis procedure predicts well and with acceptable conservatism the displacement and base shear force of sliding isolation systems in rock type motions but substantially overpredicts displacements and base shear forces in motions rich in long period components.

SECTION 12

REFERENCES

American Association of State Highway and Transportation Officials-AASHTO (1991). "Guide specifications for seismic isolation design." Washington, D.C.

Buckle, I.G. and Mayes, R.L. (1990). "Seismic isolation history, application, and performance - a world view." Earthquake Spectra, 6(2), 161-201.

Chalhoub, M.S. and Kelly, J.M. (1989). "Earthquake simulator evaluation of a combined sliding bearing and tension controlled rubber bearing isolation system." Proc. 1989 ASME Pressure Vessels and Piping Conf., American Society of Mechanical Engineers, vol. 181, 59-64.

Clough, R.W. and Penzien, J. (1975). Dynamics of Structures. McGraw-Hill, Inc., New York.

Constantinou, M.C., Mokha, A., and Reinhorn, A.M. (1990). "Teflon bearings in base isolation II: Modeling." J. Struct. Engrg., ASCE, 116(2), 455-474.

Constantinou, M.C., Mokha, A., and Reinhorn, A.M. (1991a). "Study of sliding bearing and helical-steel-spring isolation system." J. Struct. Engrg., ASCE, 117 (4), 1257-1275.

Constantinou, M.C., Reinhorn, A.M., Mokha, A., and Watson, R. (1991b). "Displacement control device for base-isolated bridges." Earthquake Spectra, 7(2), 179-200.

Den Hartog, J.P. (1931). "Forced vibrations with combined Coulomb and viscous friction." Trans. ASME 53 (APM-53-9), 107-115.

Dynamic Isolation Systems (1984). "Seismic base isolation using lead-rubber bearings - Design procedures for bridges." Berkeley, CA.

Eisenberg, Y. (1990). Personal communication of M.C. Constantinou with Professor Y. Eisenberg, Academy of Sciences of U.S.S.R., April.

Gasparini, D.A., and Vanmarke, E.H. (1976). "Simulated earthquake motions compatible with prescribed response spectra." Report No. R76-4, Dept. of Civil Engineering, Massachusetts Institute of Technology, Cambridge, Mass., Jan.

Gates, J.H. (1979). "Factors considered in the development of the California seismic design criteria for bridges." Proc. Workshop on Earthquake Resistance of Highway Bridges, Applied Technology Council, Palo Alto, Calif., 141-162.

Ghobarah, A. and Ali, H.M. (1988). "Seismic performance of highway bridges." Eng. Struct., 10, 157-166.

Griffith, M.C., Aiken, I.D. and Kelly, J.M (1988). "Experimental evaluation of seismic isolation of a 9-story braced steel frame subject to uplift." Report No. UCB/EERC-88/05, Earthquake Engrg. Res. Ctr., Univ. of California, Berkeley, Calif., May.

Gueraud, R., Noel-Leroux J.P., Livolant, M. and Michalopoulos, A.P. (1985)." Seismic isolation using sliding-elastomer bearing pads." Nuclear Engrg. and Design, Vol. 84, 363-377.

International Conference of Building Officials (1991). "Uniform building code, earthquake regulations for seismic-isolated structures." Whittier, Calif.

Kawamura, S., Kitazawa, K., Hisano, M. and Nagashima, I. (1988). "Study of a sliding-type base isolation system. System composition and element properties." Proceedings of 9th World Conference on Earthquake Engineering, Tokyo-Kyoto, Japan, Vol. V, 735-740.

Kelly, J.M. (1991). "Base isolation: origins and development." News-Earthquake Engrg. Res. Ctr., Univ. of California, Berkeley, Calif., 12(1), 1-3.

Kelly, J.M. (1986a). "Aseismic base isolation: review and bibliography." Soil Dyn. Earthquake Engrg., Vol. 5(3), 202-216.

Kelly, J.M., Buckle, I.G., and Tsai, H-C. (1986b). "Earthquake simulator testing of a base-isolated bridge deck." Report No. UCB/EERC-85/09, Earthquake Engrg. Res. Ctr., Univ. of California, Berkeley, Calif., Jan.

Lam, I.P. and Martin, G.R. (1986). "Seismic design of highway bridge foundations, Vol. III. Example problems and sensitivity studies." Report No. FHWA/RD-86/103, Federal Highway Administration, Virginia.

Makris, N. (1989). "Analysis of motion of harmonically excited sliding isolation systems." M.S. Thesis, Dept. of Civil Engrg., State Univ. of New York, Buffalo, NY.

Makris, N. and Constantinou, M.C. (1991). "Analysis of motion resisted by friction II: velocity dependent friction." Mech. Struct. & Mach., 19(4), 511-536.

Marioni, A. (1991). "Antiseismic devices on the Mortaiolo viaduct." 3rd World Congress on Joint Sealing and Bearing Systems for Concrete Structures. Vol. 2 of Preprints, 1263-1280, Toronto, Canada.

Mayes, R.L., Buckle, I.G., Kelly, T.E. and Jones, L.R. (1991). "AASHTO seismic isolation design requirements for highway bridges." Proc. 9th Structures Congress, ASCE, 656-659.

Medeot, R. (1991). "The evolution of aseismic devices for bridges in Italy." 3rd World Congress on Joint Sealing and Bearing Systems for Concrete Structures, Vol. 2 of Preprints, 1295-1320, Toronto, Canada.

Mokha, A., Constantinou, M.C., and Reinhorn, A.M. (1988). "Teflon bearings in aseismic base isolation. Experimental studies and mathematical modeling." Report No. NCEER-88-0038, Nat. Ctr. for Earthquake Engrg. Res., State Univ. of New York, Buffalo, NY.

Mokha, A., Constantinou, M.C. and Reinhorn, A.M. (1990). "Teflon bearings in base isolation. I: Testing." J. Struct. Engrg., ASCE, 116(2), 438-454.

Mokha, A., Constantinou, M.C. and Reinhorn, A.M. (1991a). "Further results on frictional properties of Teflon bearings." J. Struct. Engrg., ASCE, 117(2), 622-626.

Mokha, A., Constantinou, M.C., Reinhorn, A.M., and Zayas, V. (1991b). "Experimental study of friction pendulum isolation system." J. Struct. Engrg., ASCE, 117(4), 1201-1217.

Mostaghel, N., and Khodaverdian, M., (1991). "R-FBI analyses and experiments." Proc. 1991 ASME Pressure Vessels and Piping Conf., American Society of Mechanical Engineers, Vol. 222, 7-14.

New Zealand Ministry of Works and Development (1983). "Design of lead-rubber bridge bearings." Civil Division Publication 818/A, Wellington, New Zealand.

Theodossiou, D. and Constantinou, M.C. (1991). "Evaluation of SEAOC design requirements for sliding isolated structures." Report No. NCEER-91-0015, Nat. Center for Earthquake Engrg. Res., State Univ. of New York, Buffalo, NY, June.

Turkington, D.H., Carr, A.J., Cooke, N. and Moss, P.J. (1989a). "Seismic design of bridges on lead-rubber bearings." J. Struct. Engrg., ASCE, 115(2), 3000-3016.

Turkington, D.H., Carr, A.J., Cooke, N. and Moss, P.J. (1989b). "Design method for bridges on lead-rubber bearings." J. Struct. Engrg., ASCE, 115(2), 3017-3030.

Zayas, V., Low, S.S. and Mahin, S.A. (1987). "The FPS earthquake resisting system, experimental report." Report No. UCB/EERC-87/01, Earthquake Engineering Research Center, University of California, Berkeley, Calif., June.

APPENDIX A

EXPERIMENTAL RESULTS

The recorded time histories of deck (bearing) displacement and acceleration and loops of force in displacement control device and base shear force versus deck displacement are presented in this appendix. One set of four figures is presented for each test. Each test is identified by a test code. The first two letters or numbers in the test code identify the sliding interface: T2 for unfilled Teflon at 2000 psi (13.8 MPa), TB for material Techmet-B. The next three letters or numbers identify the force in the displacement control device: F25 for force approximately equal to 2.5 kips (11.15 kN). The remaining letter and numbers identify the excitation. The test results are presented in the order they were conducted (see also Table 6-I).

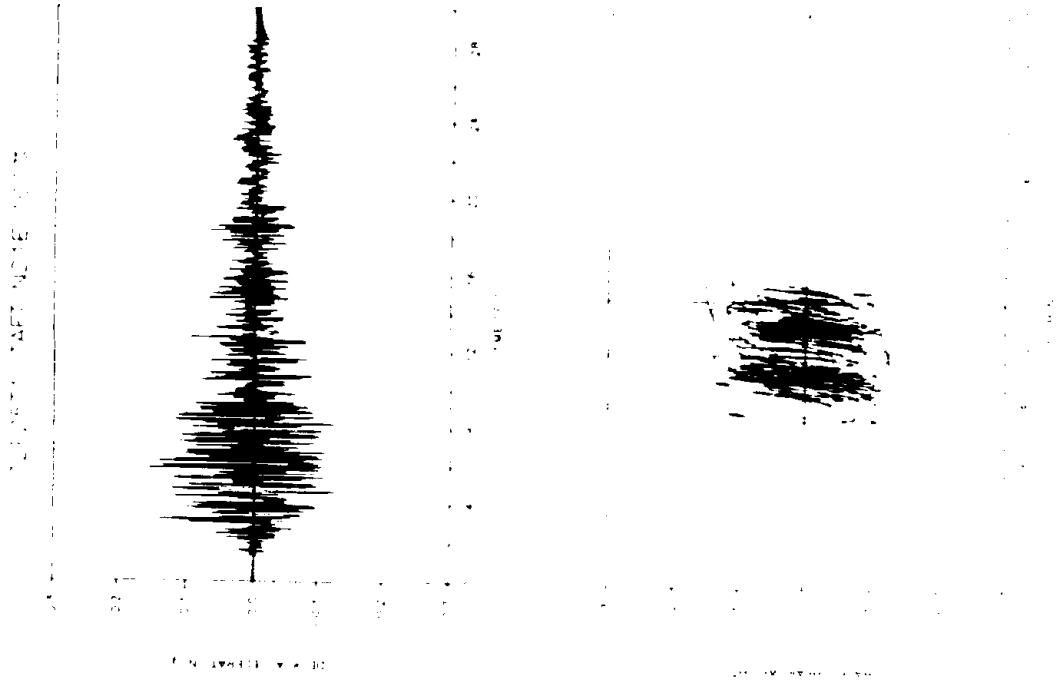

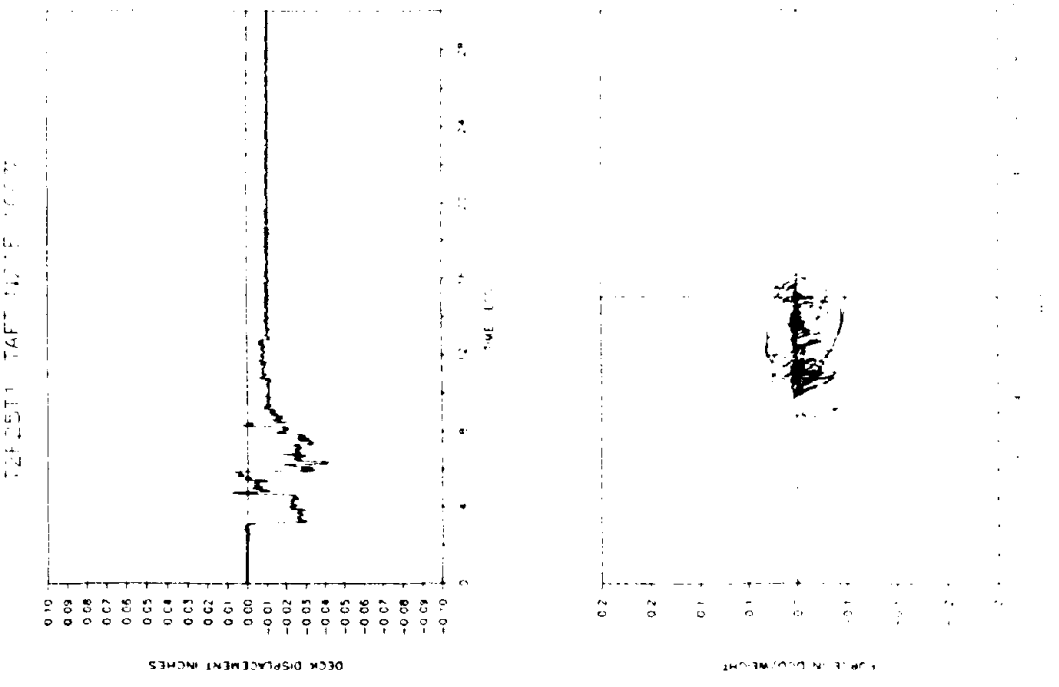

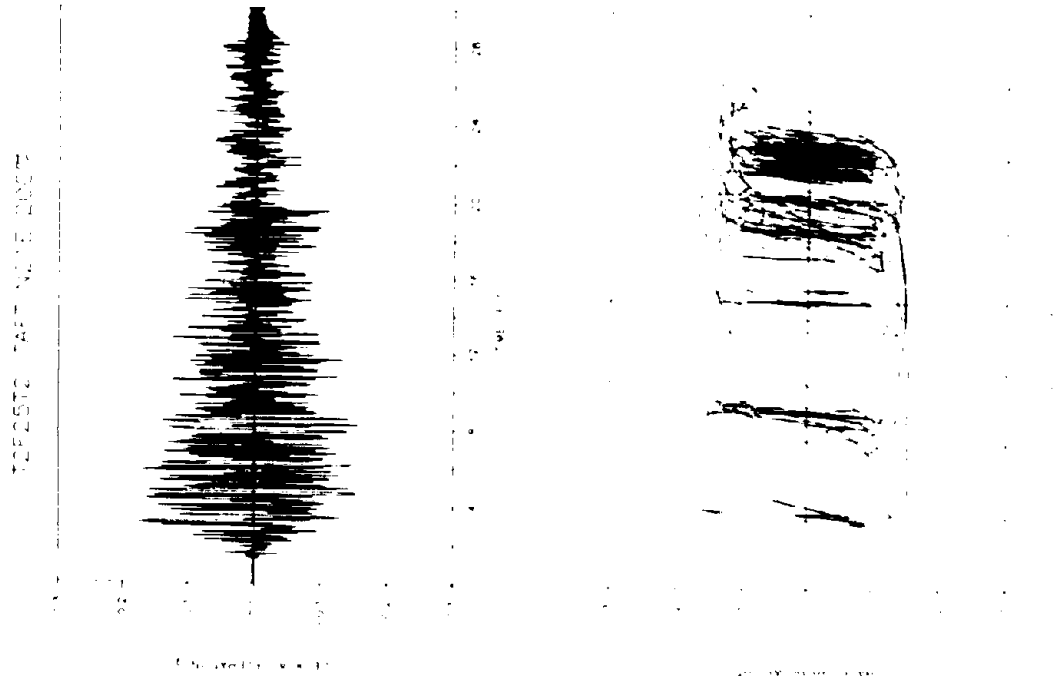

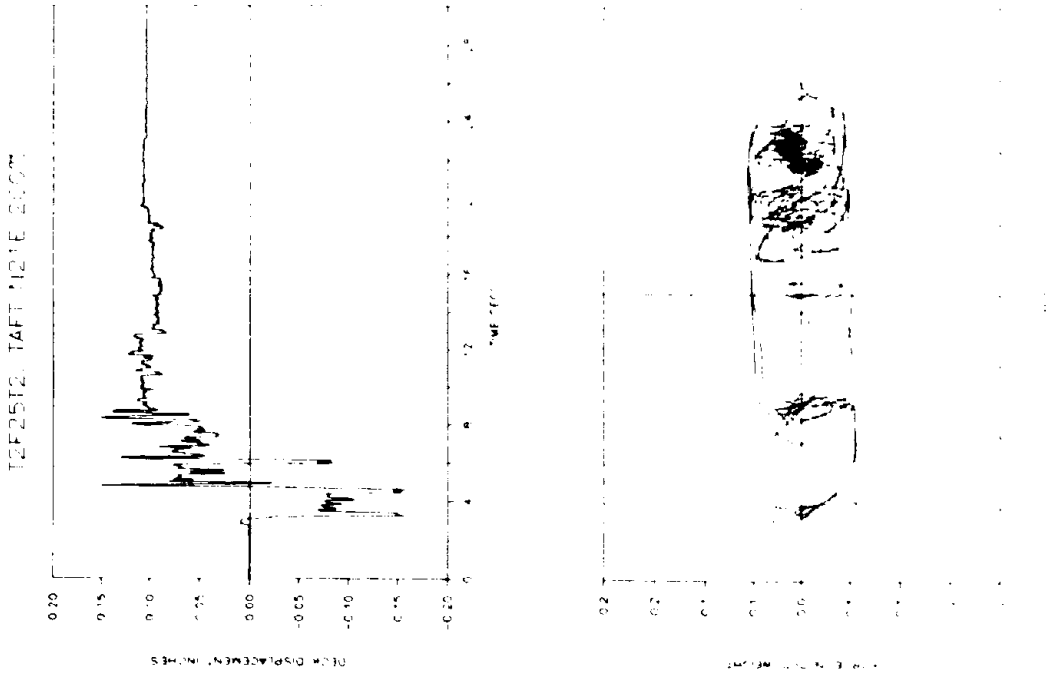

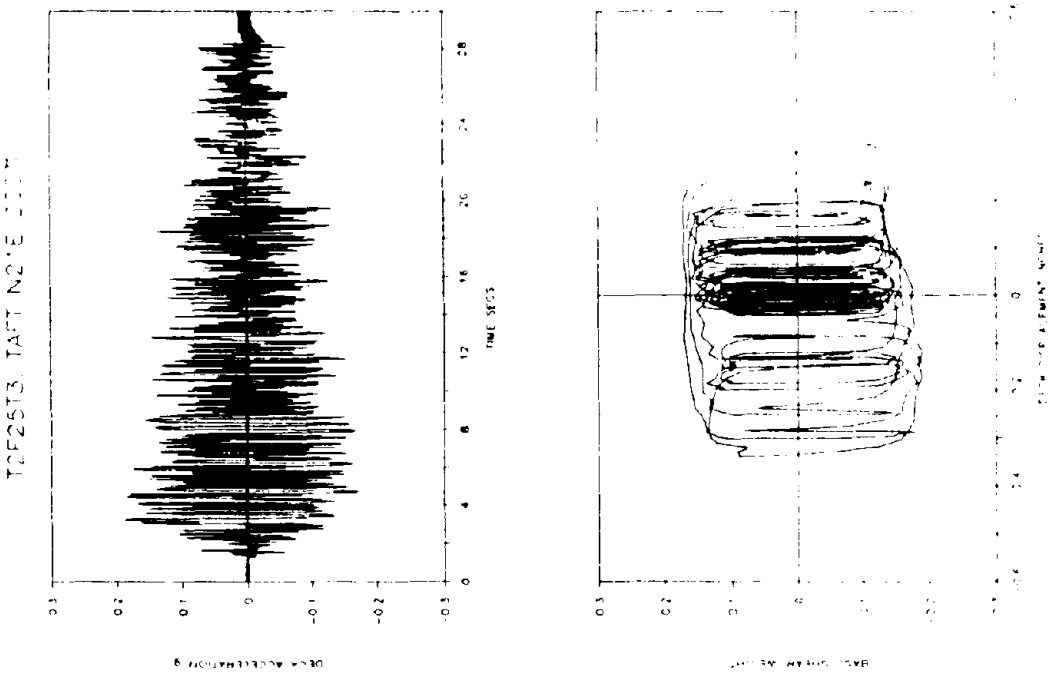

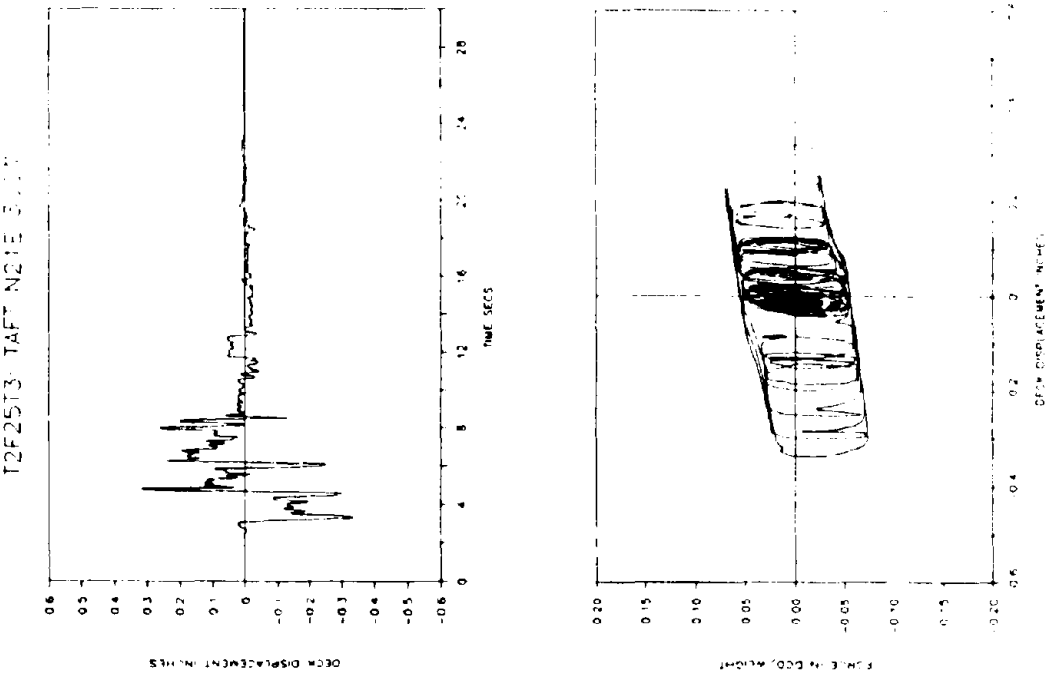

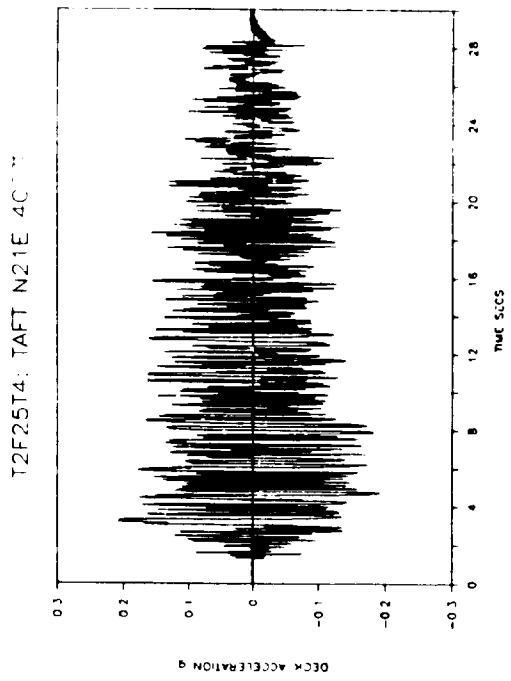

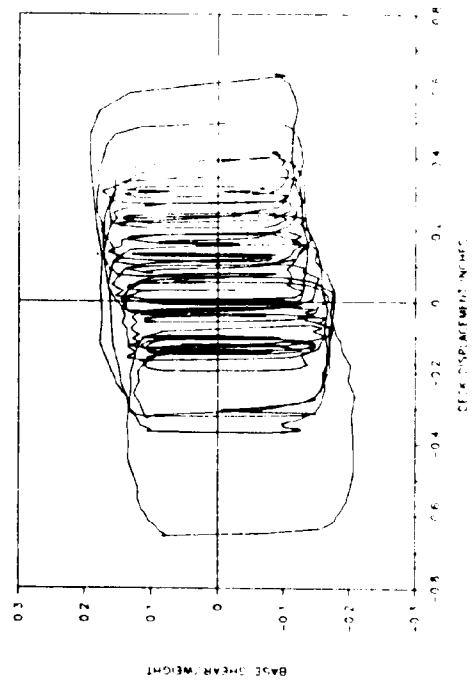

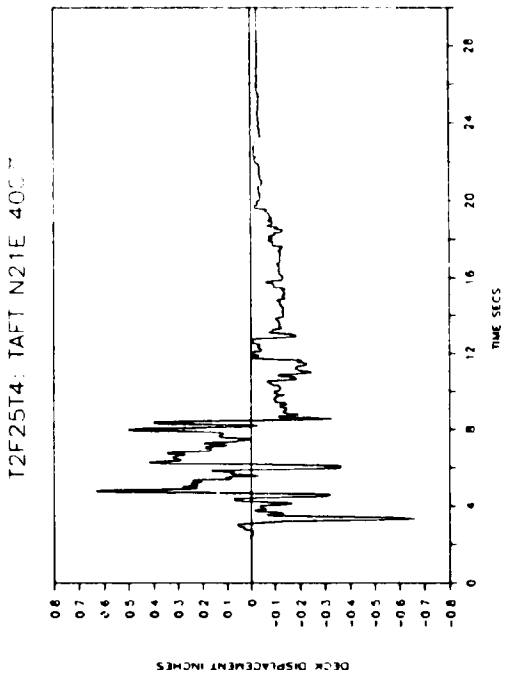

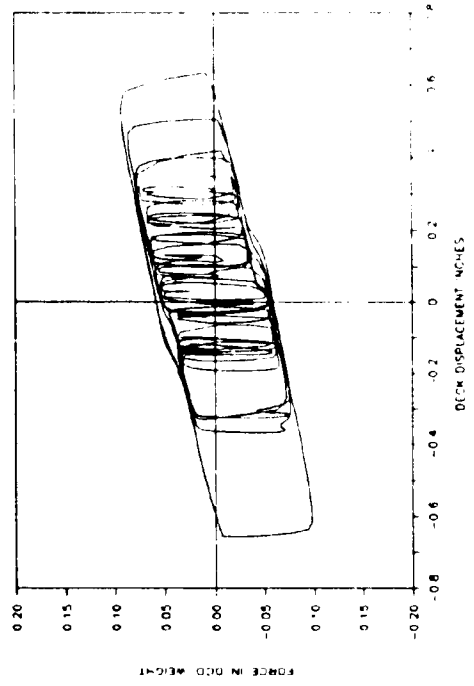

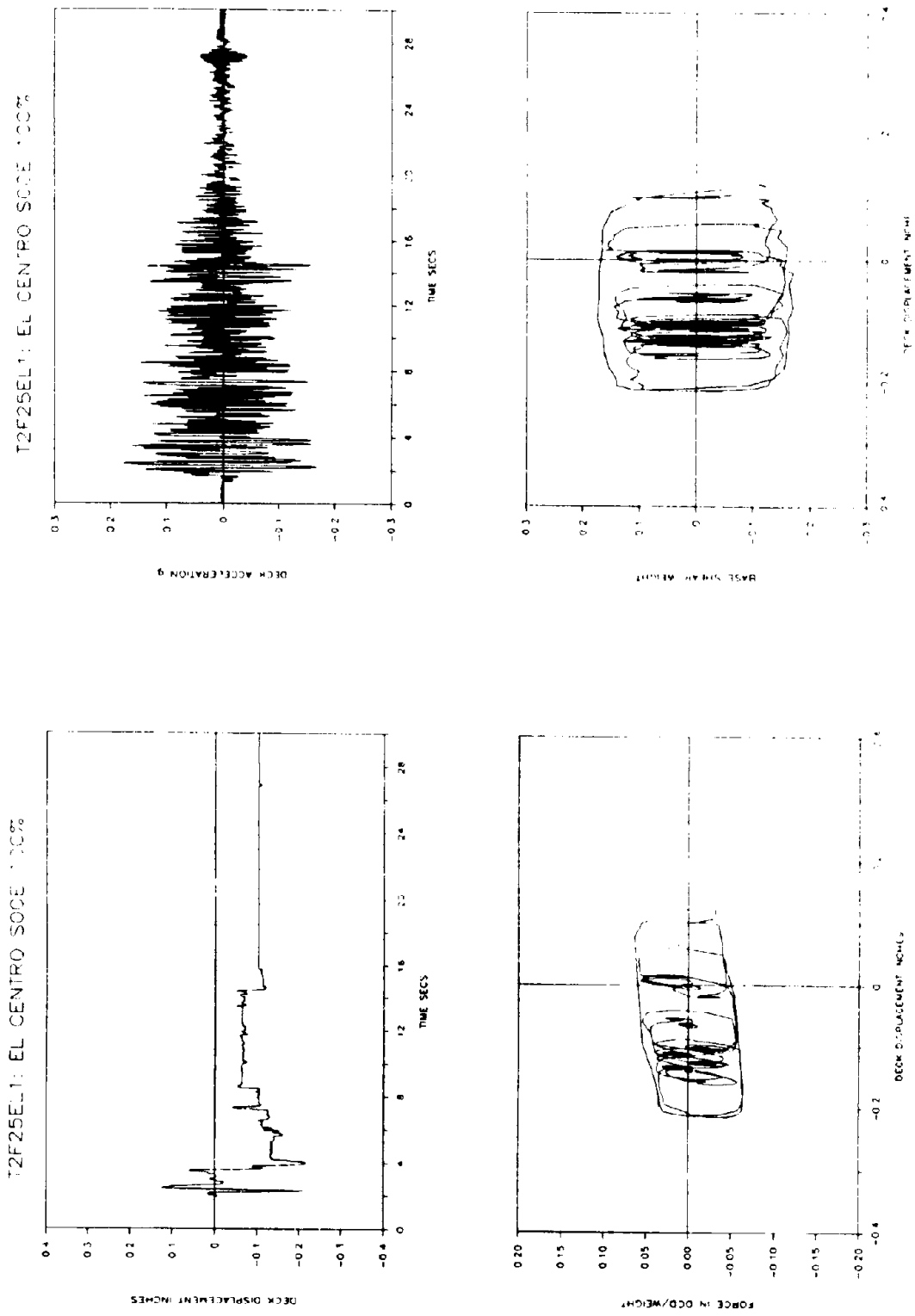

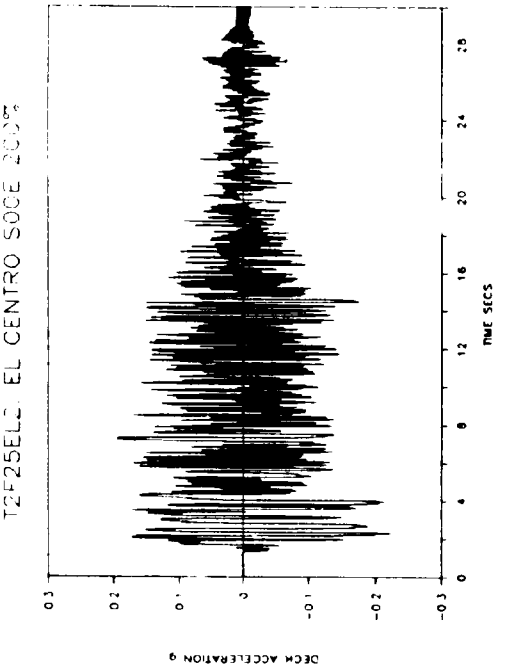

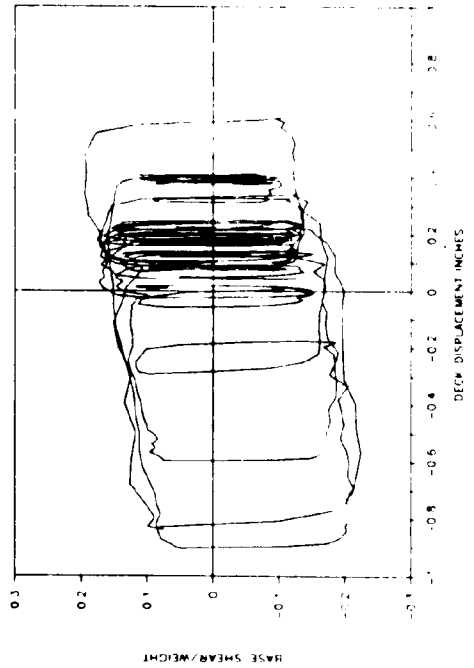

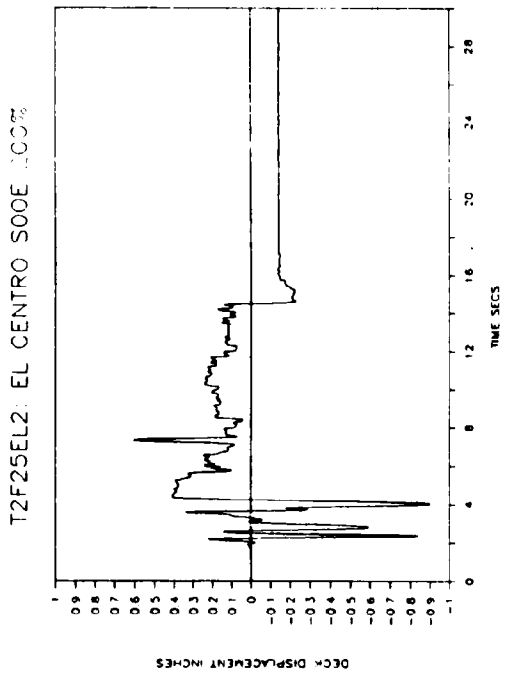

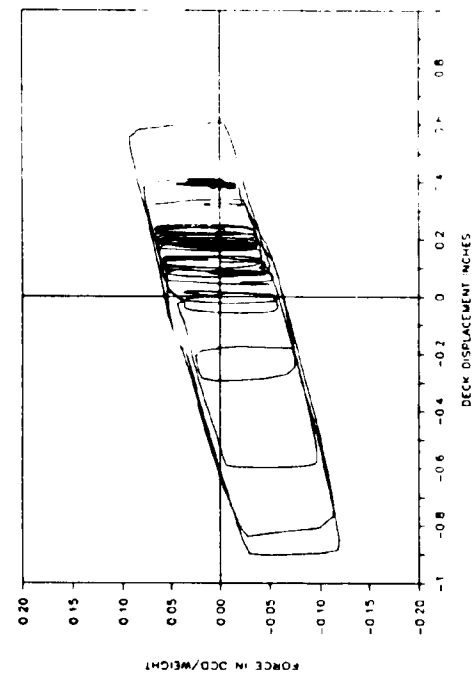

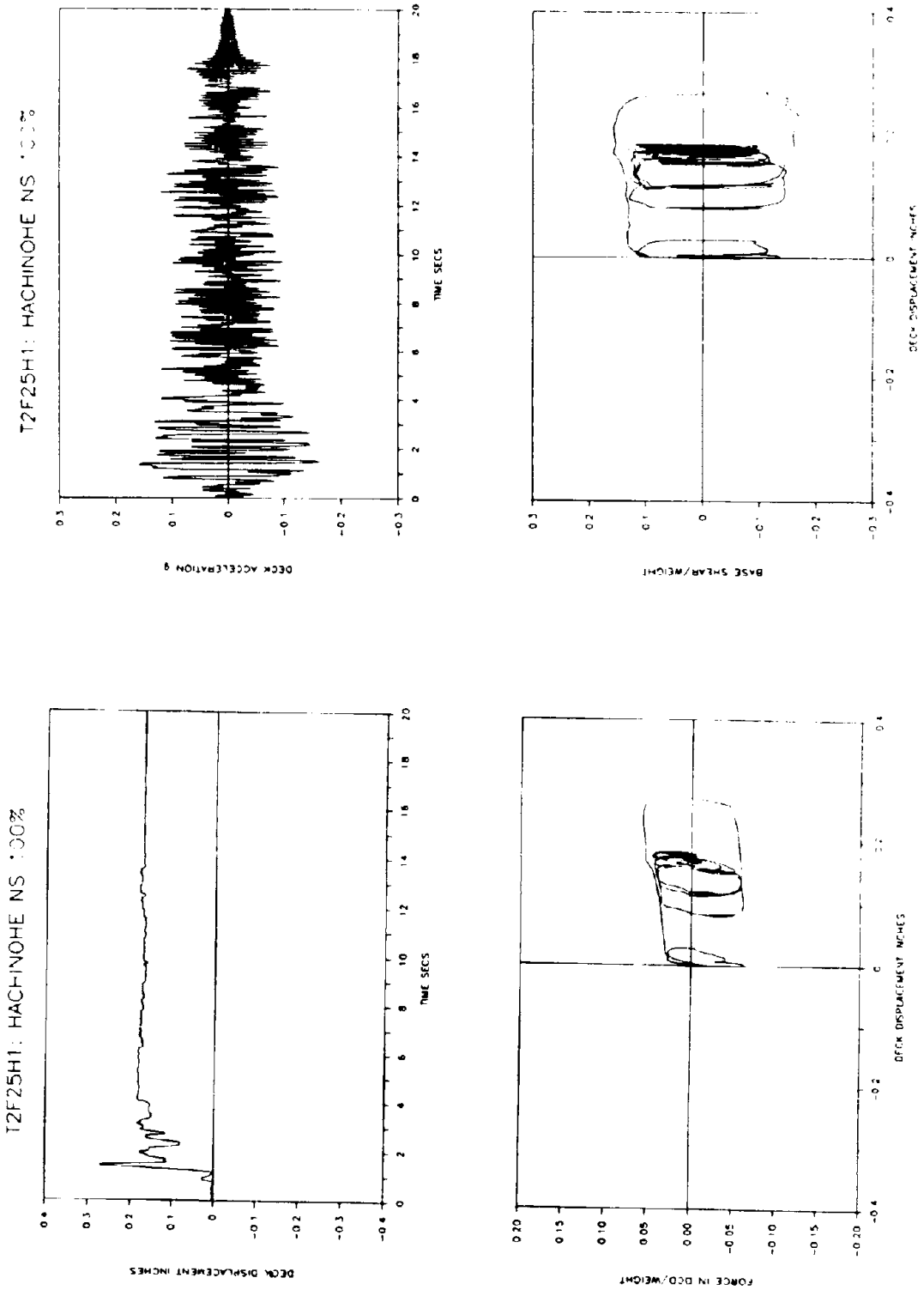

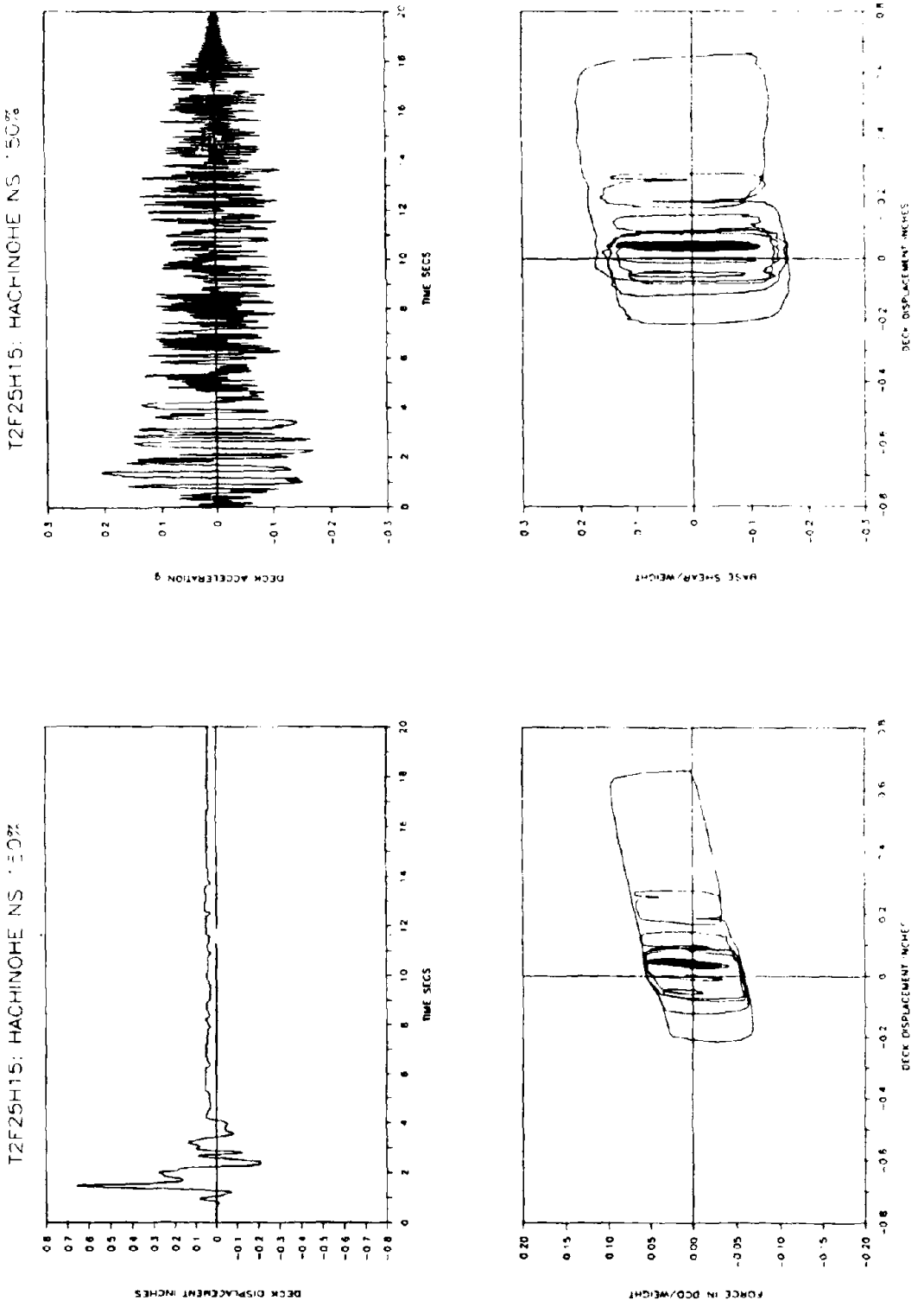

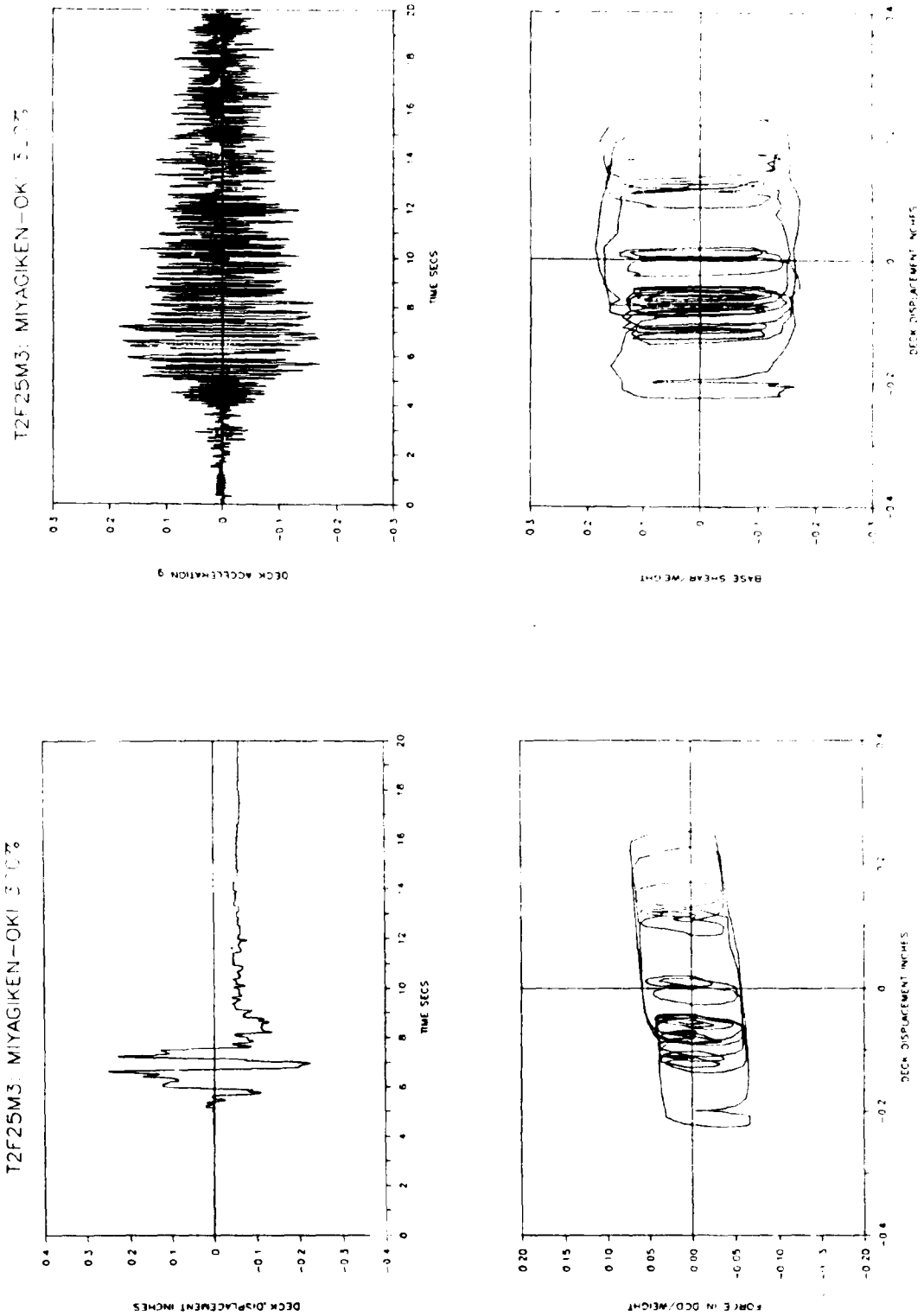

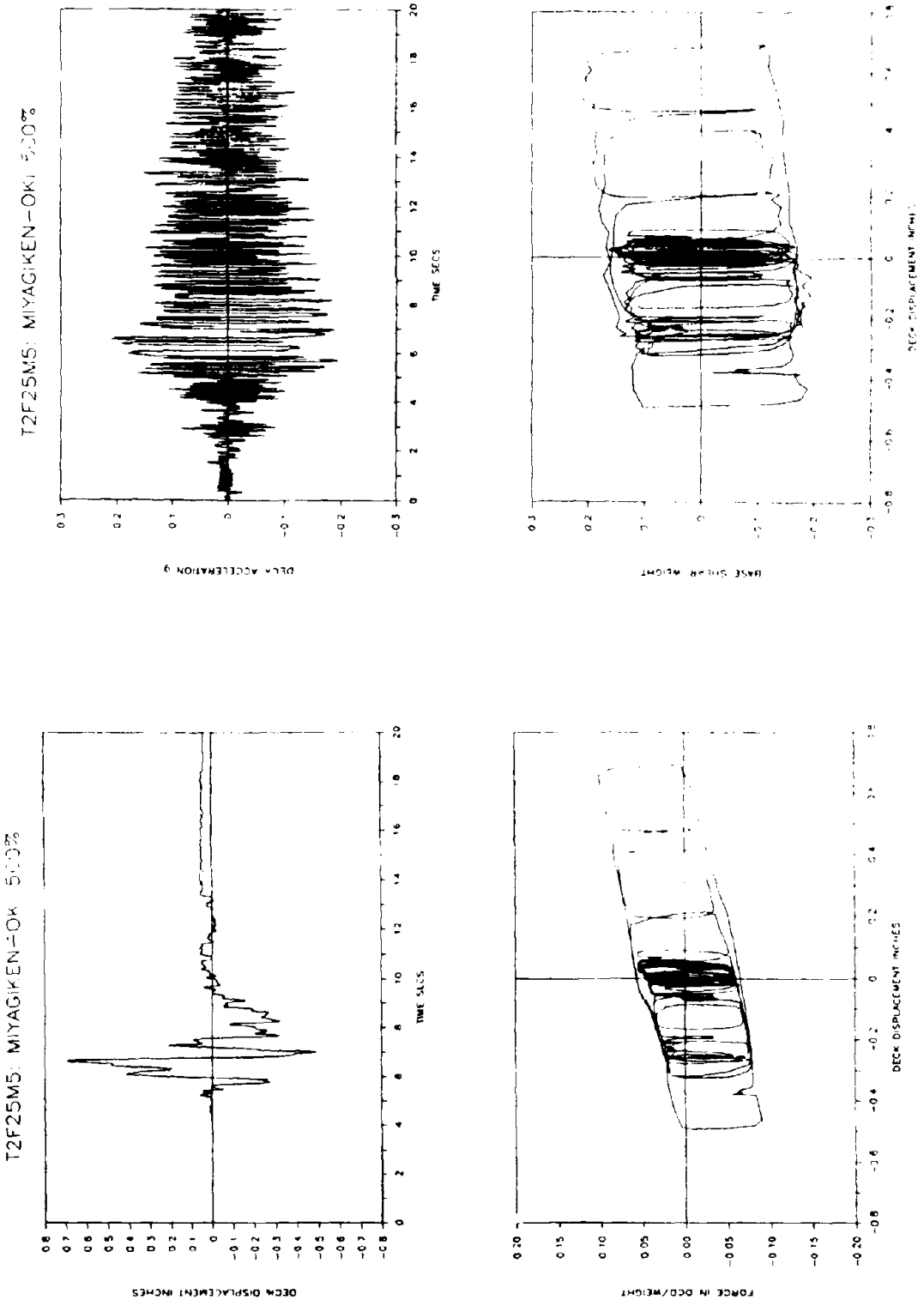

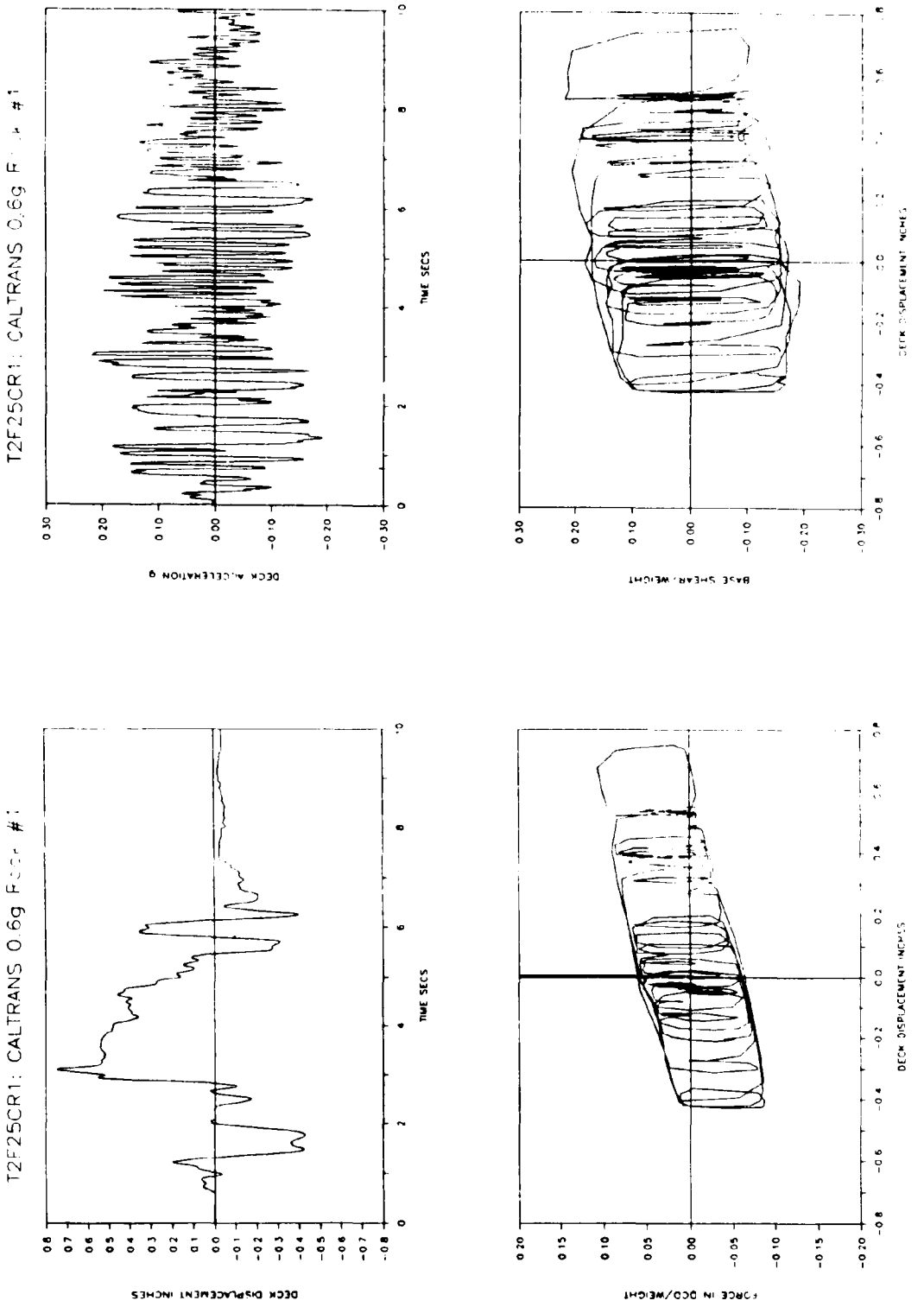

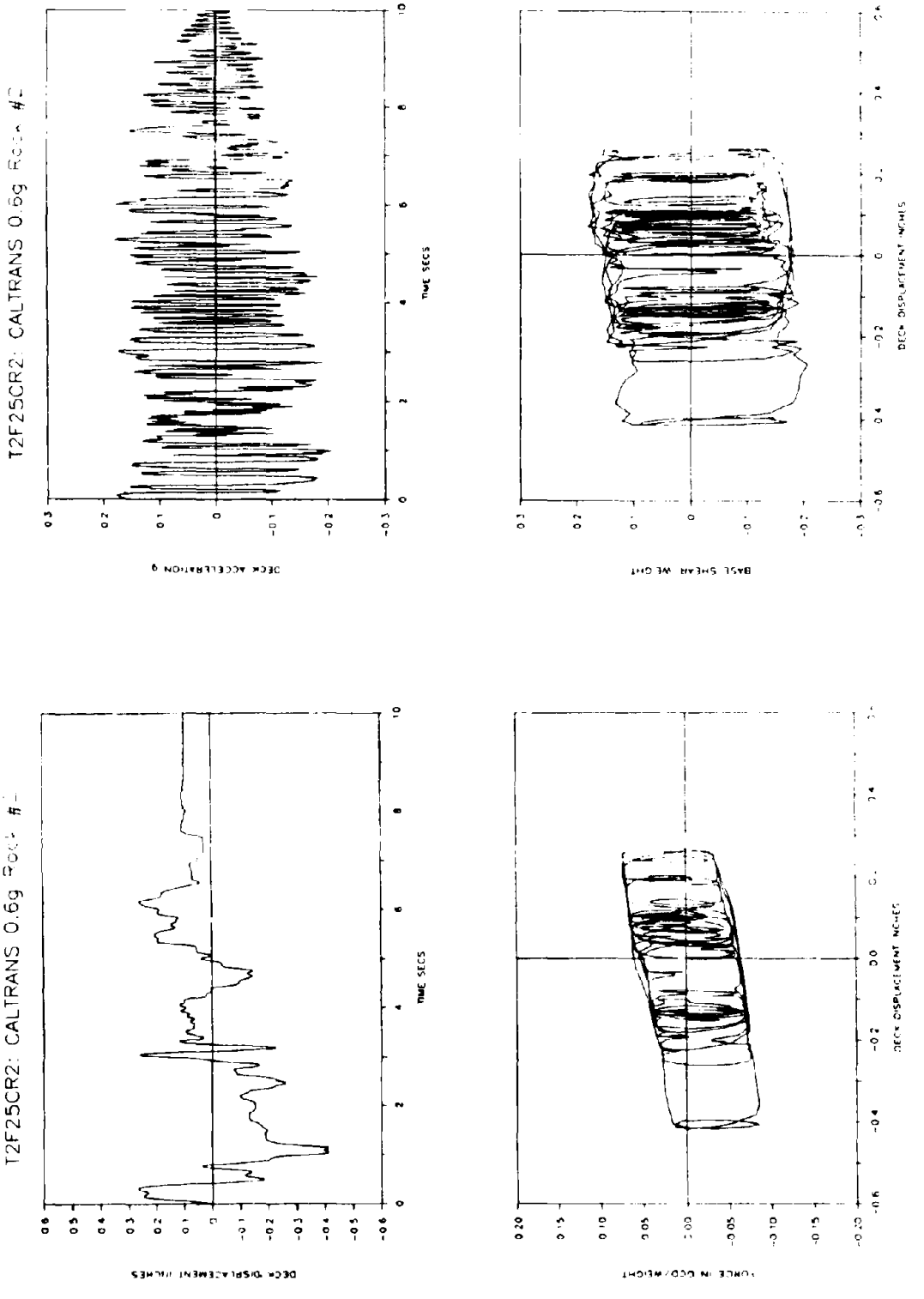

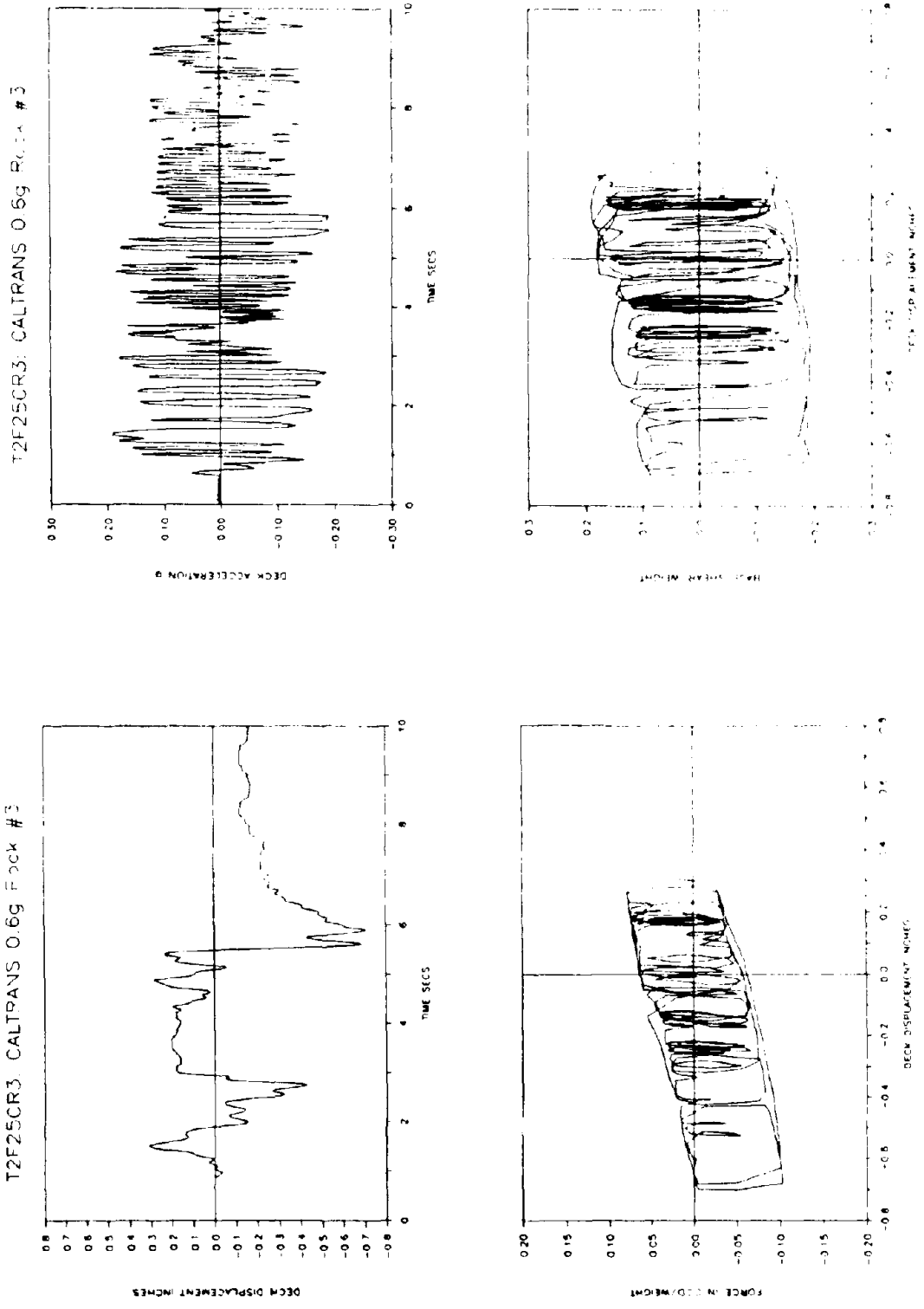

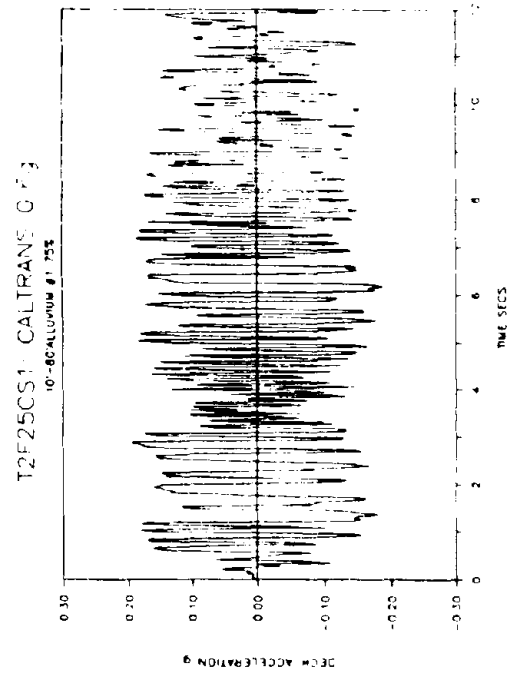

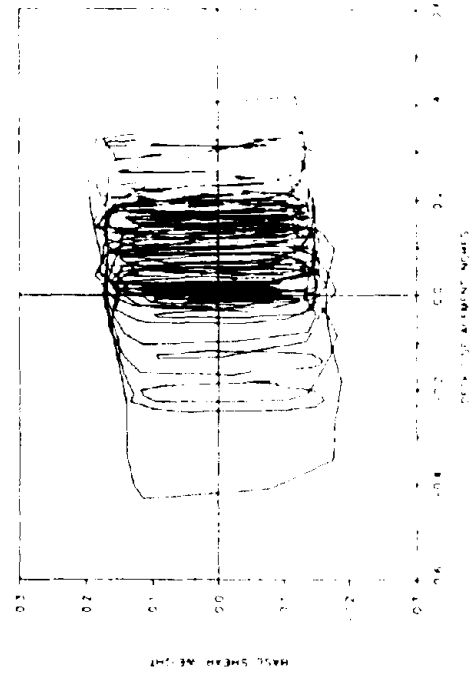

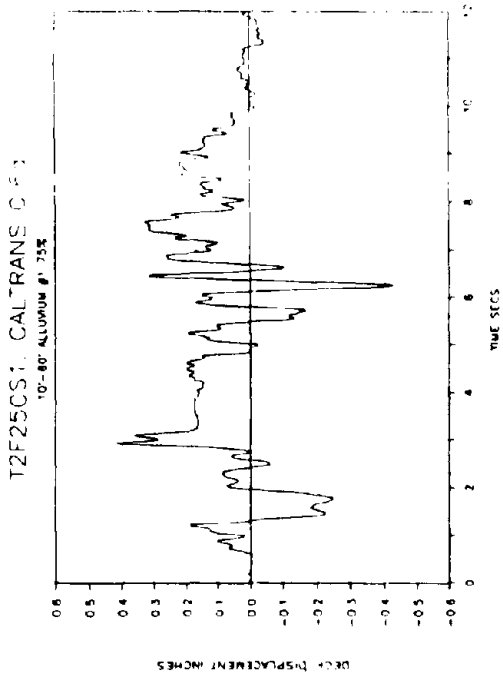

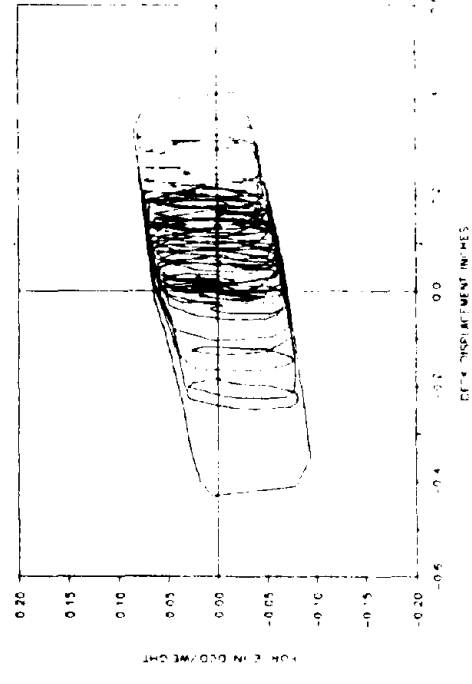

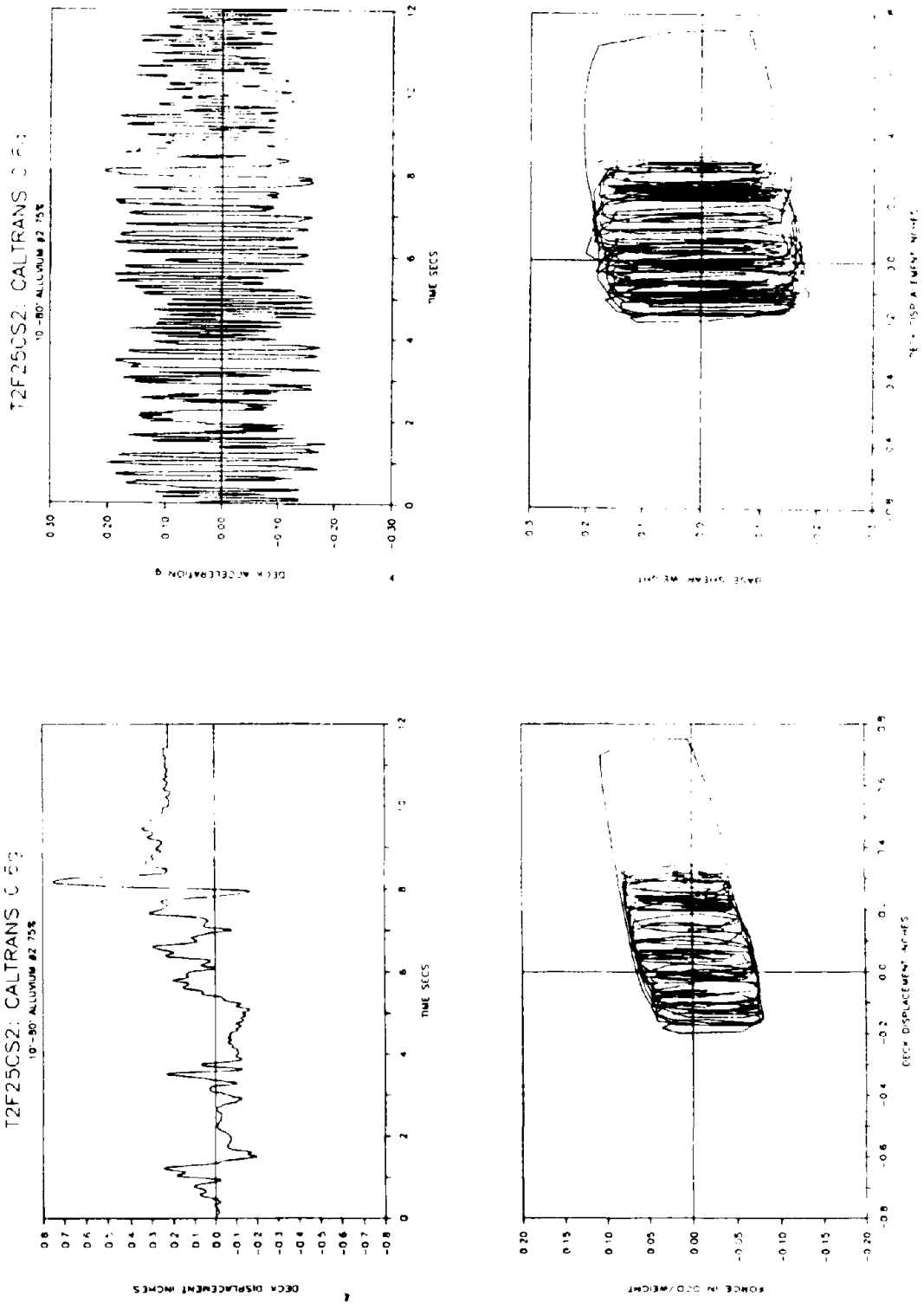

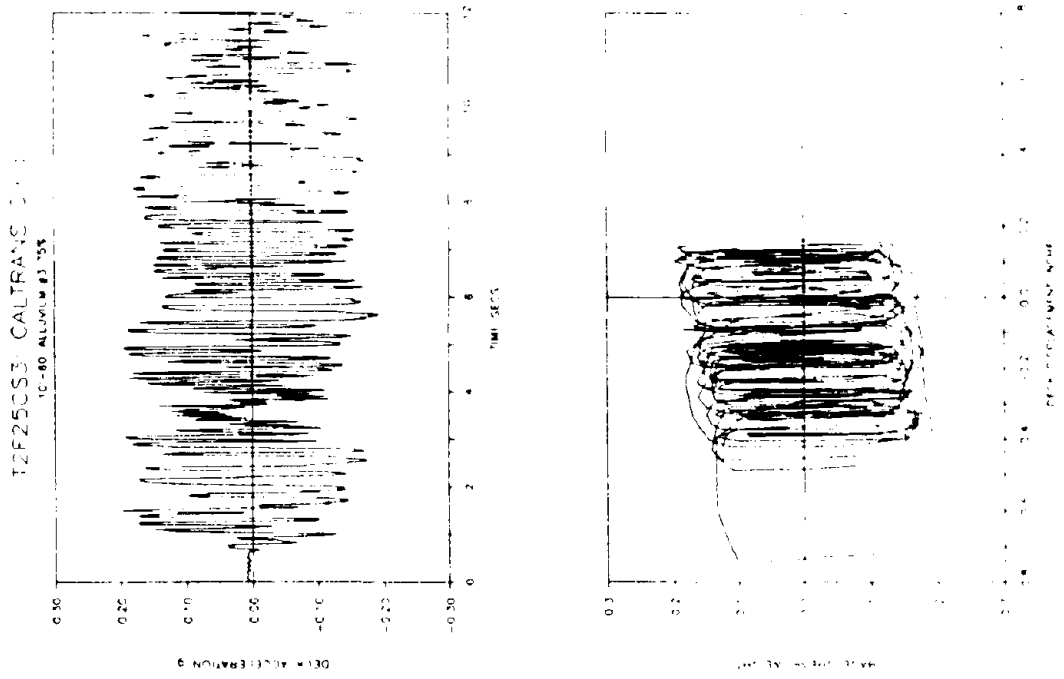

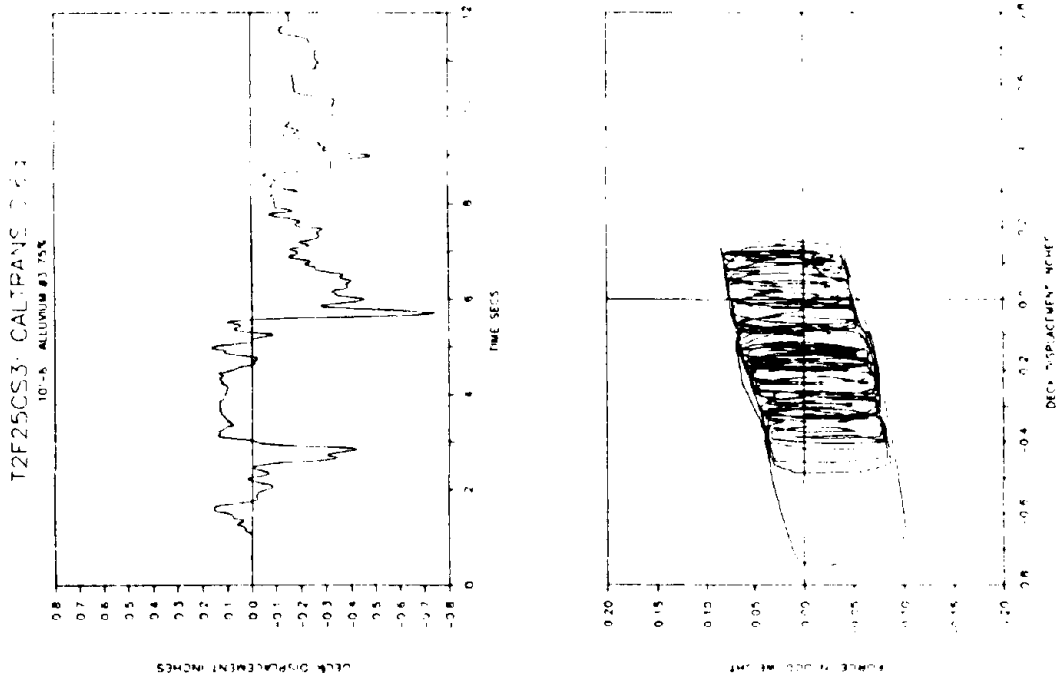

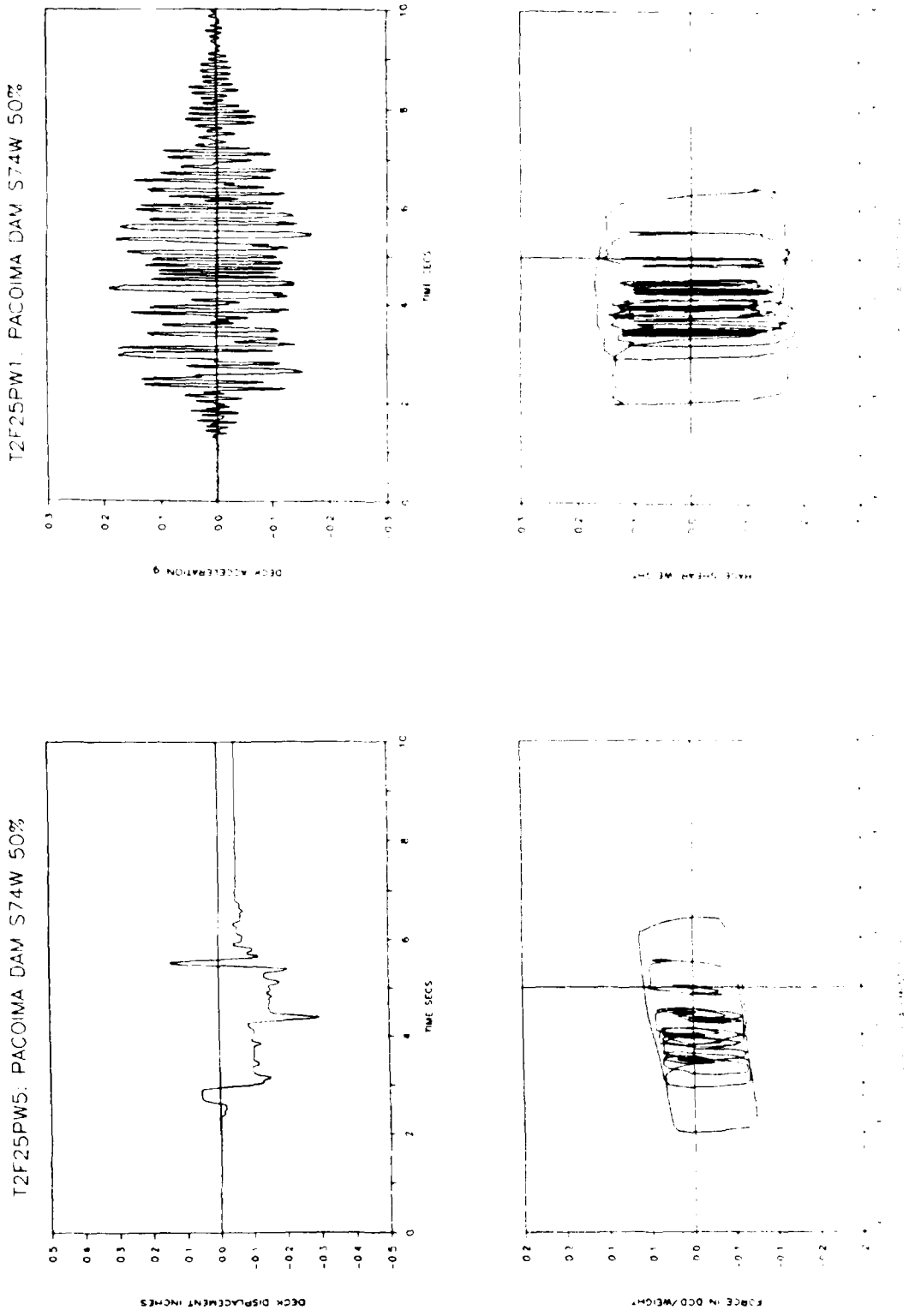
T2F25PW1: PACOIMA DAM S74W 50%
T2F25PW5: PACOIMA DAM S74W 50%

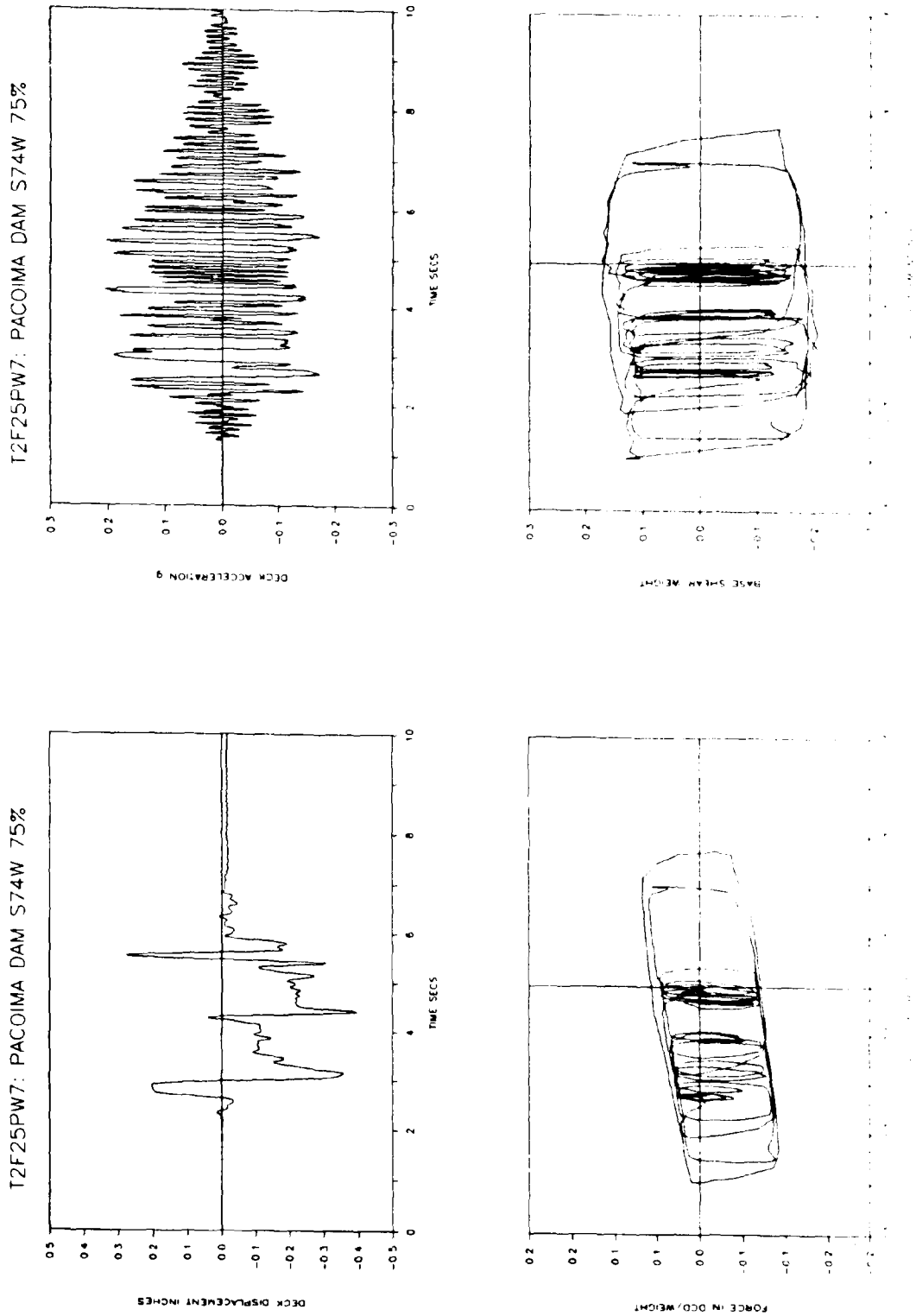

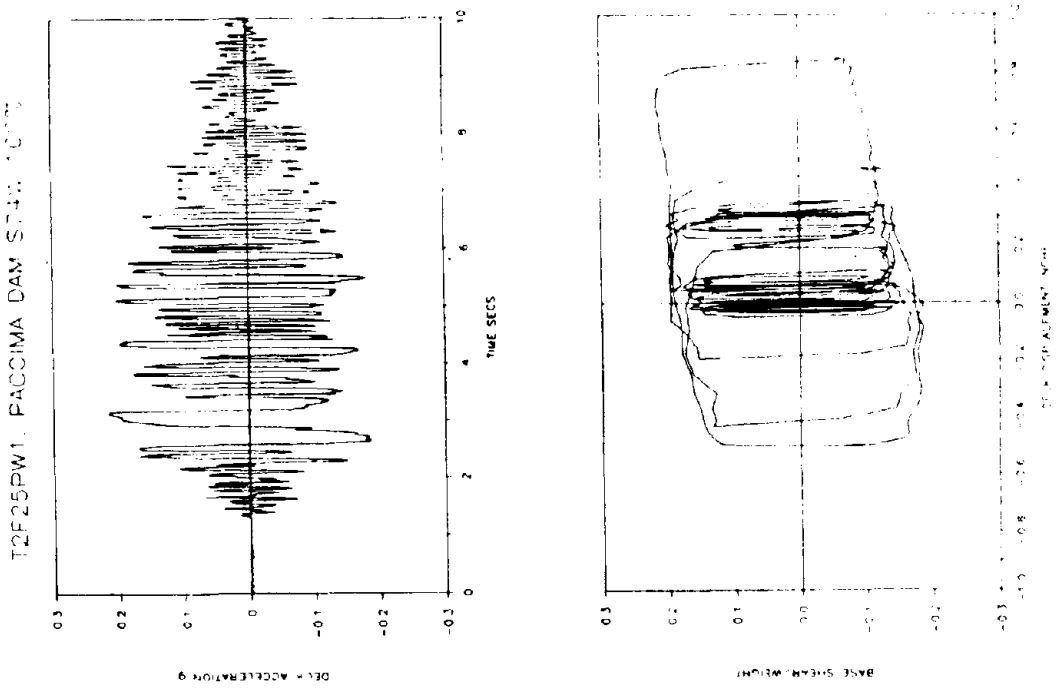

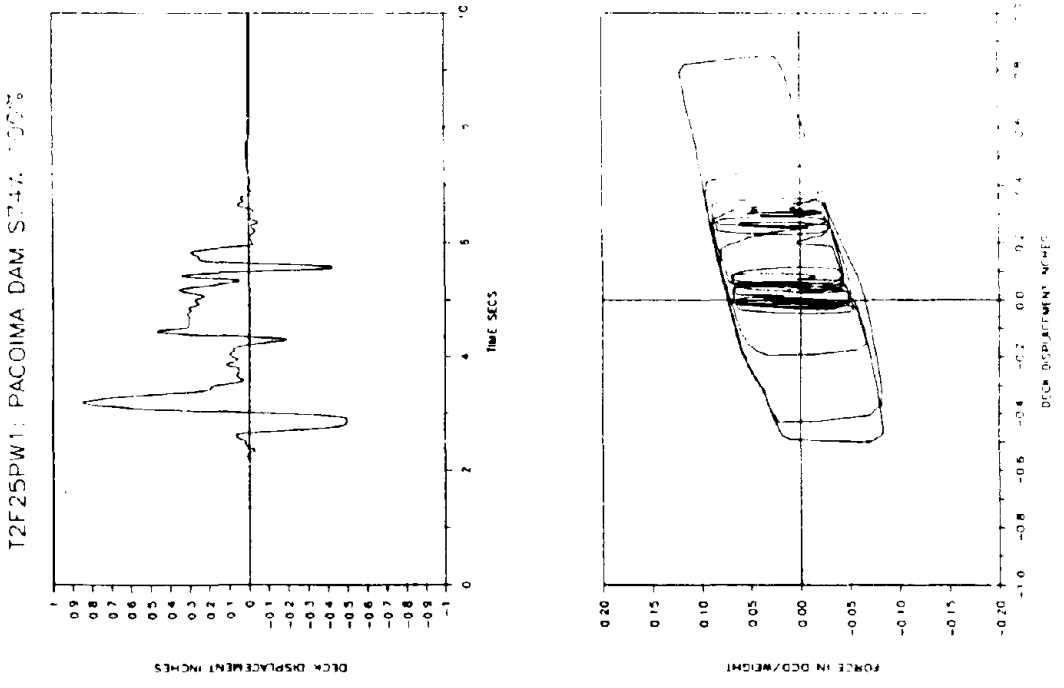

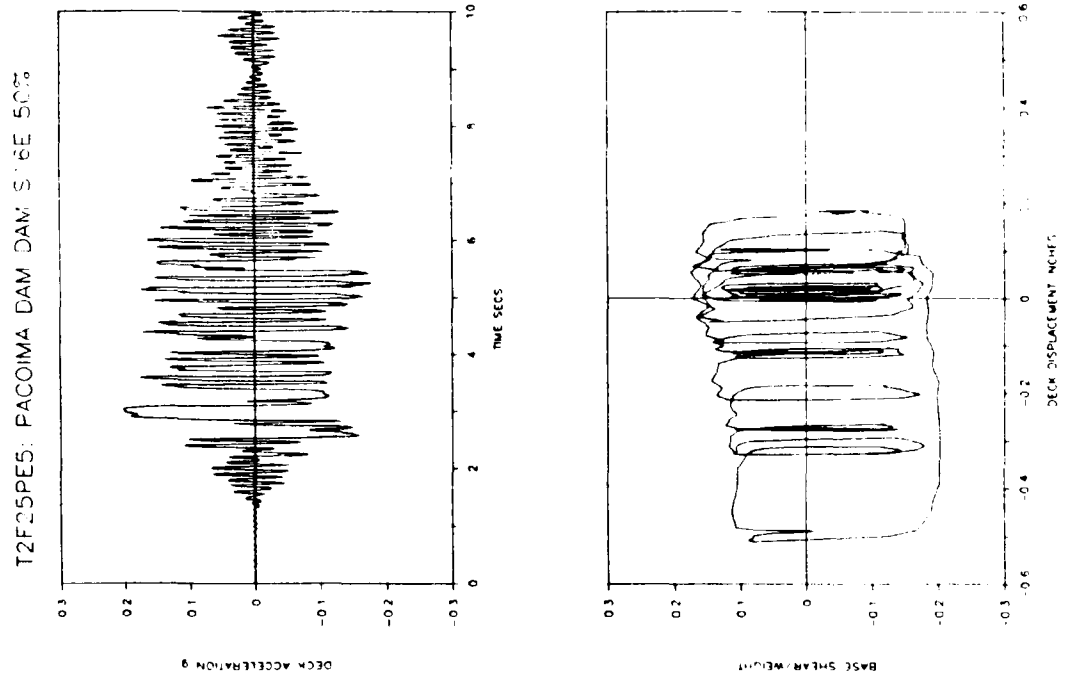

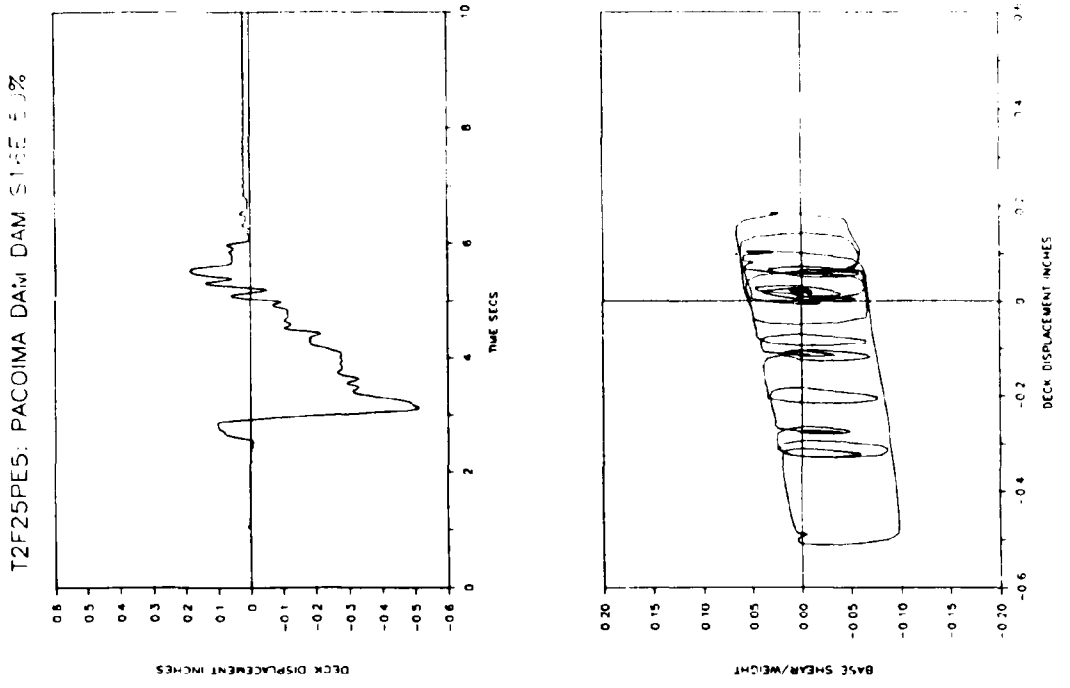

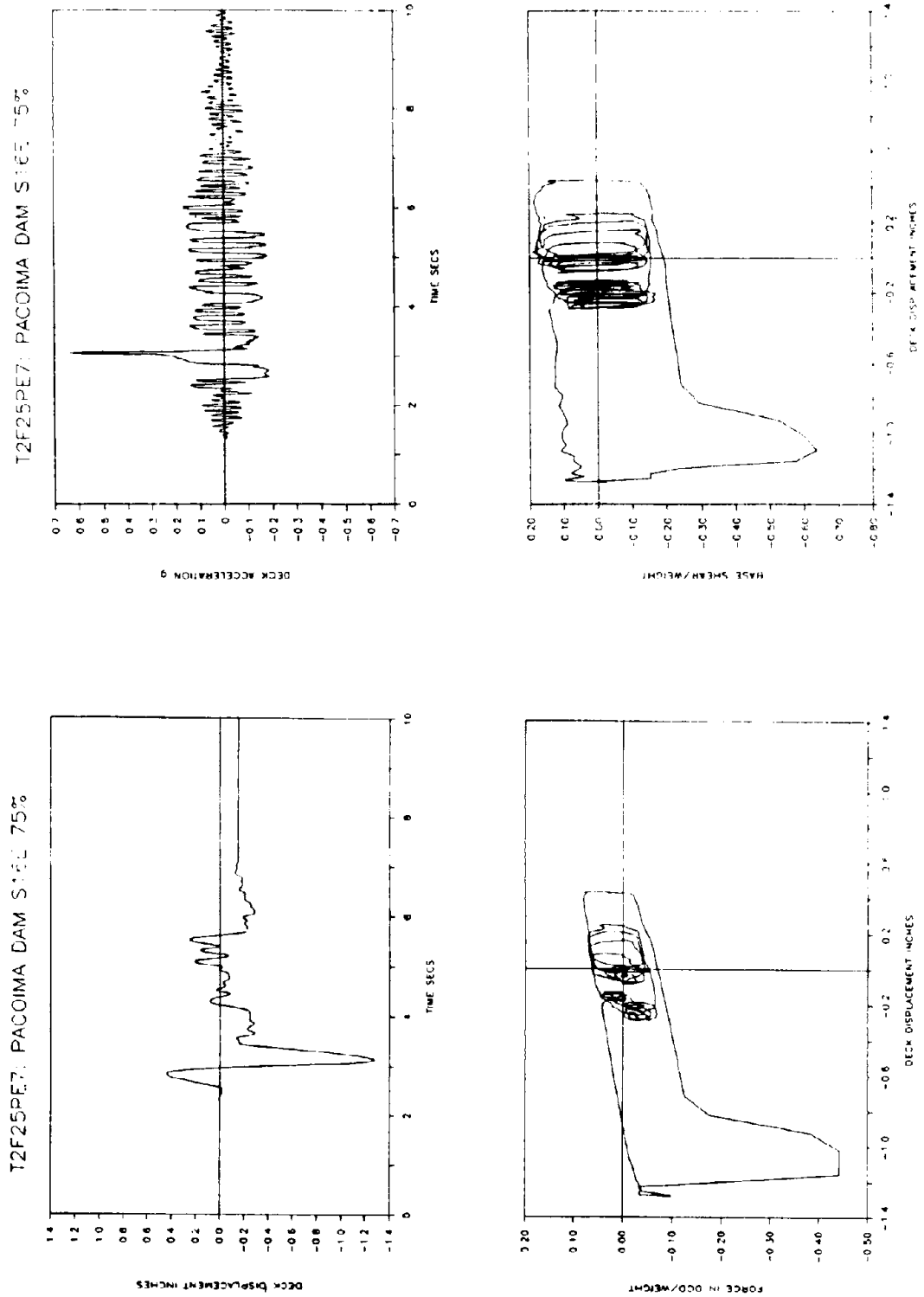

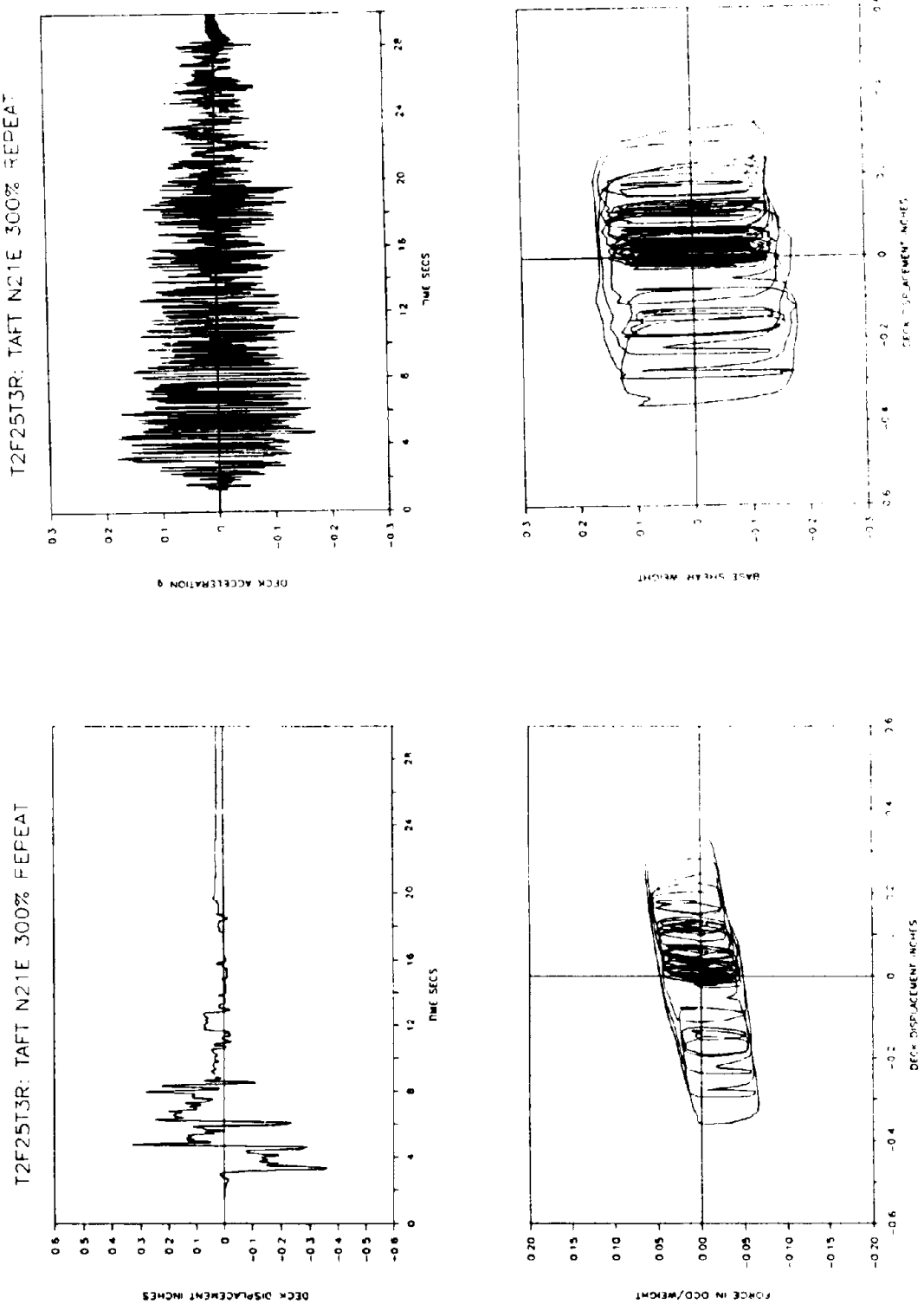

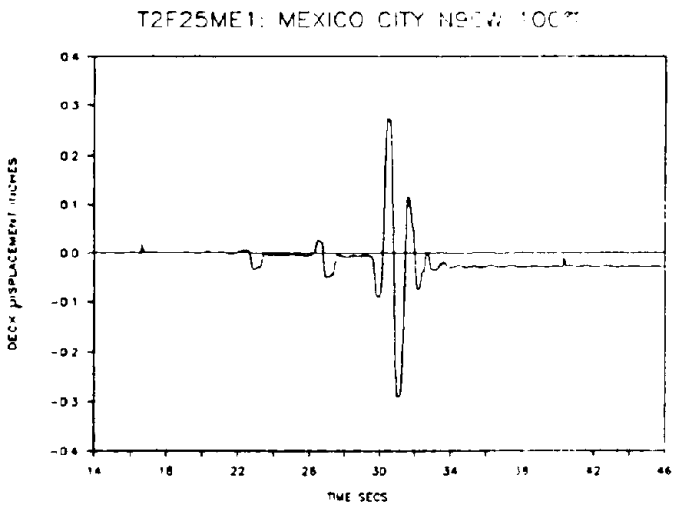
T2F25ME1: MEXICO CITY N90W 100%
DECK DISPLACEMENT INCHES
TIME SECS

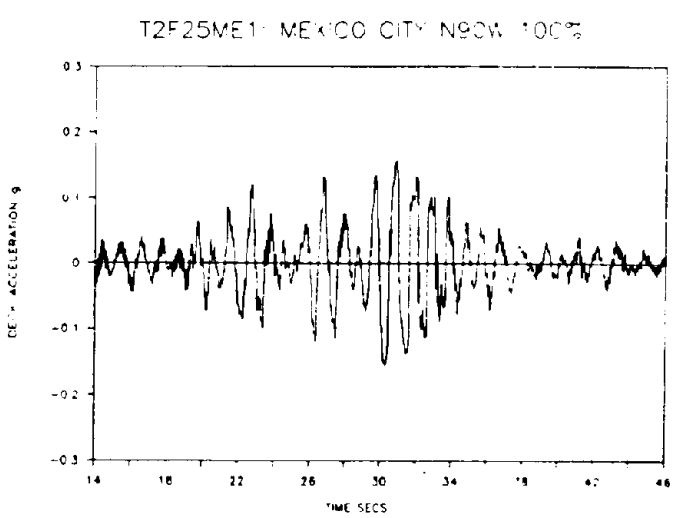
T2F25ME1: MEXICO CITY N90W 100%
TIME SECS

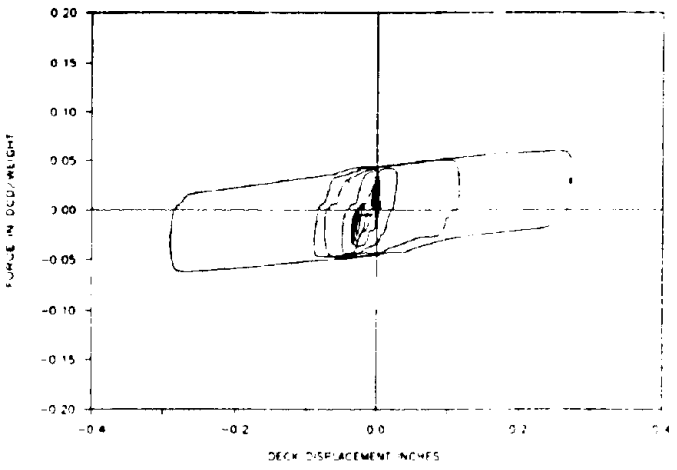
FORCE IN DECK/WEIGHT
DECK DISPLACEMENT INCHES

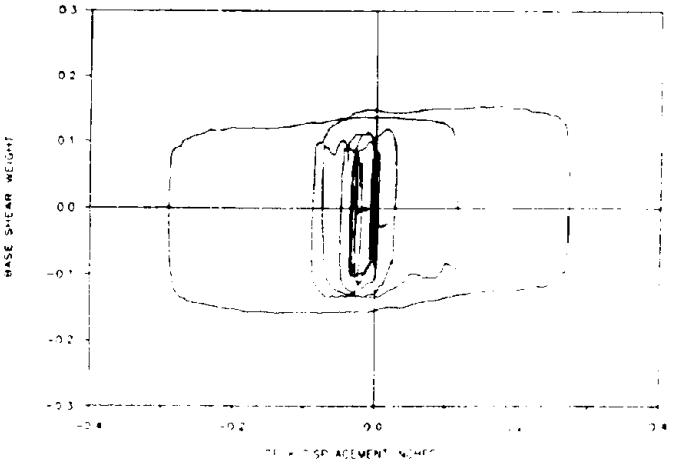
BASE SHEAR WEIGHT

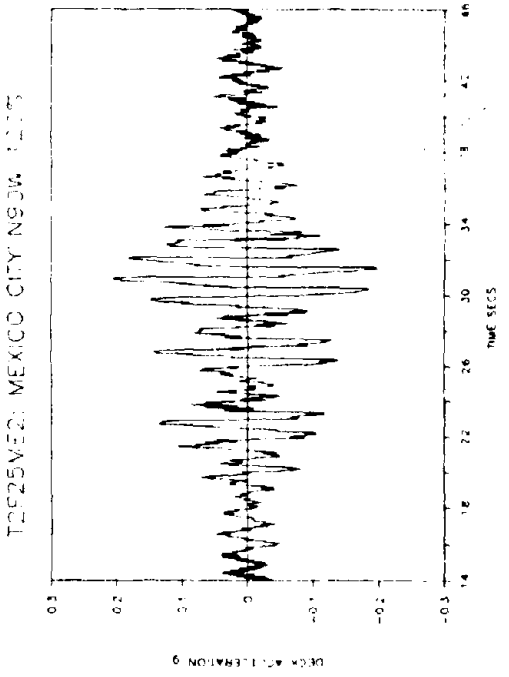

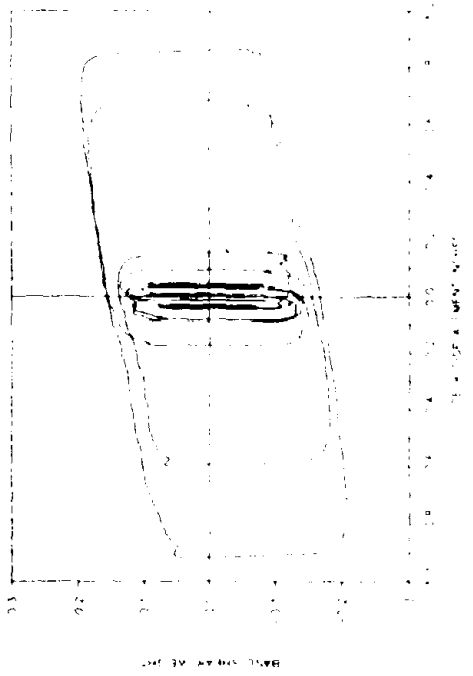

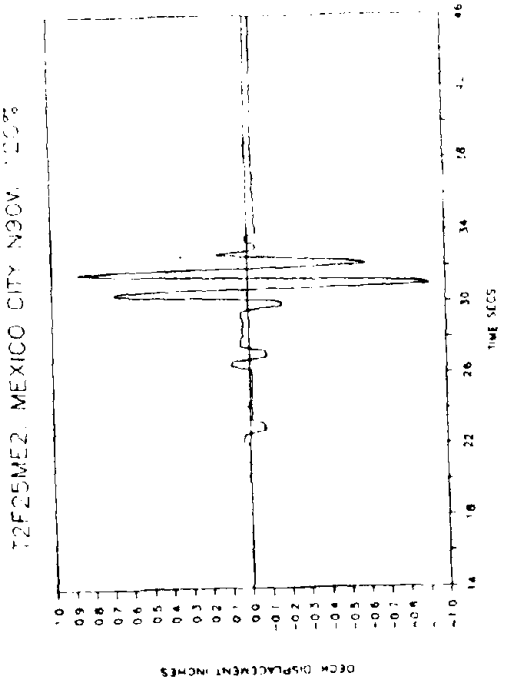

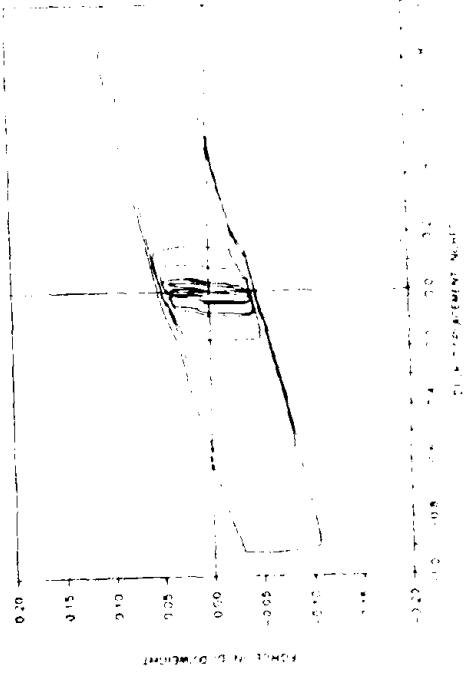

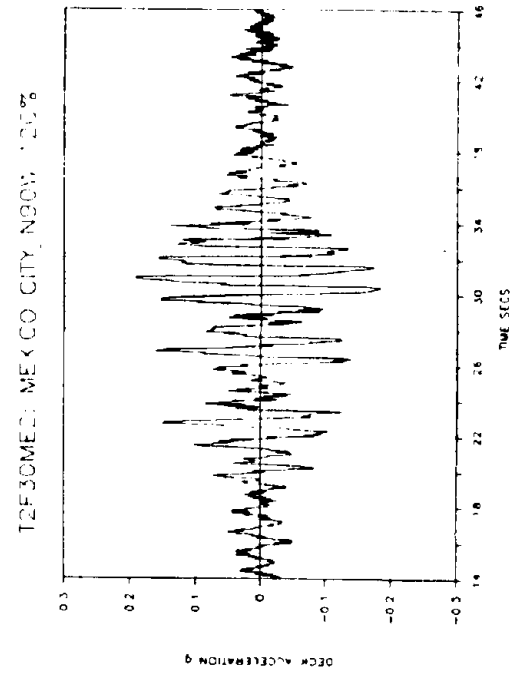

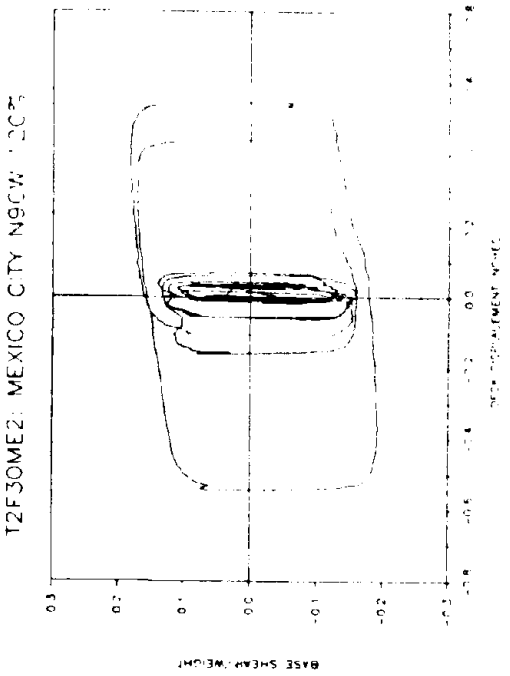

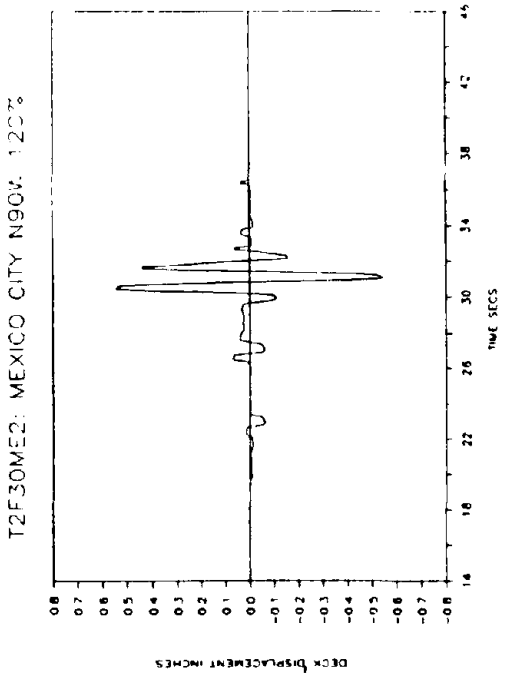

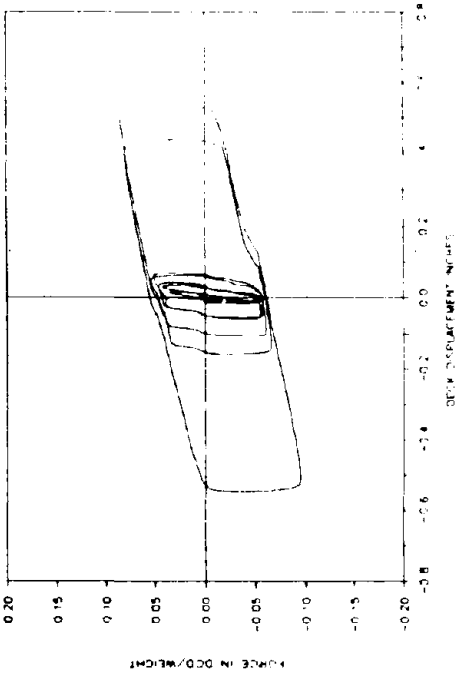

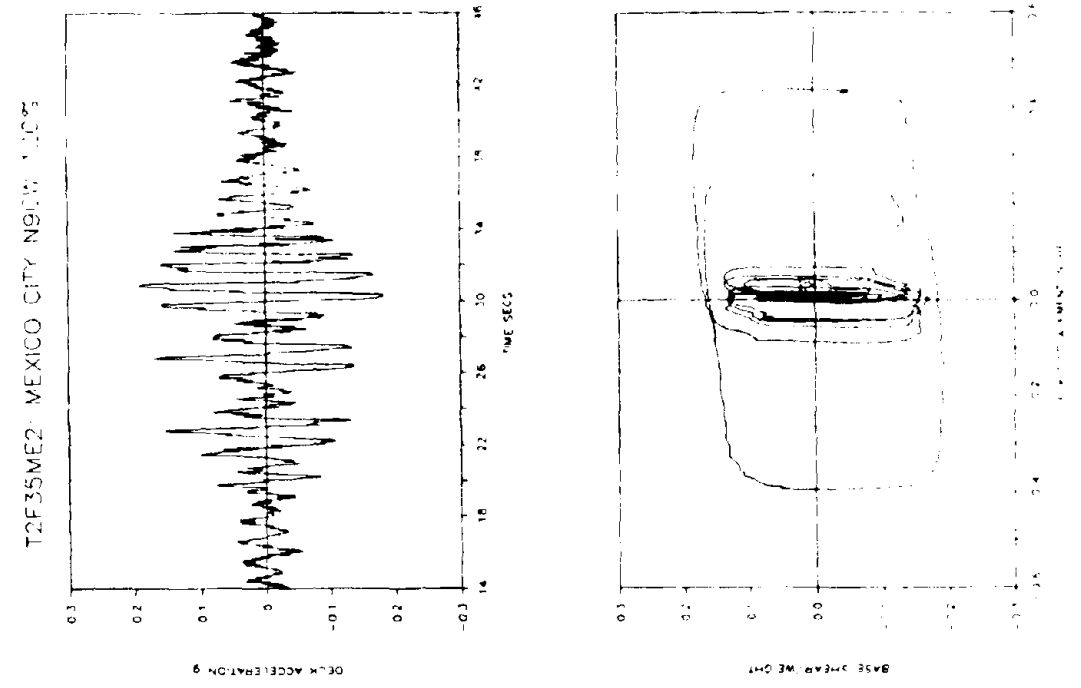

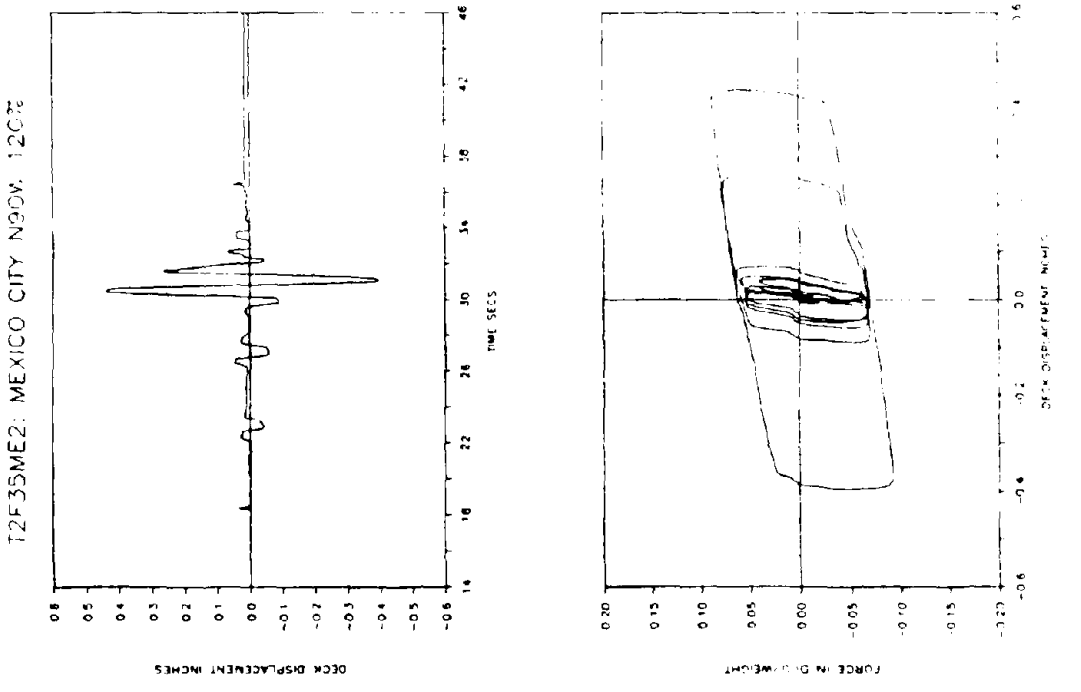

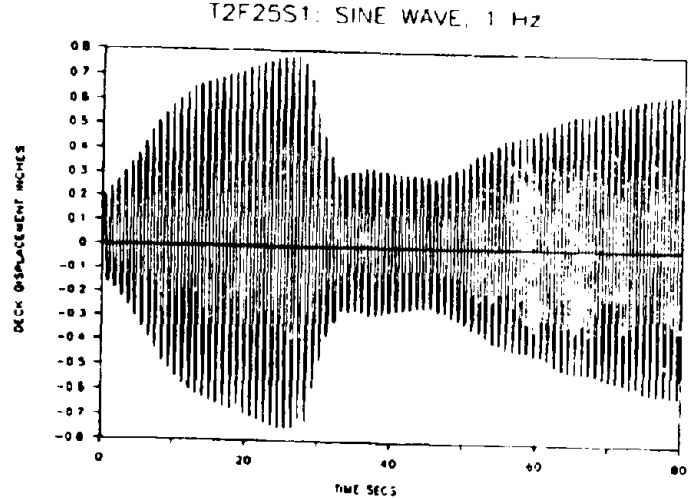
T2F25S1: SINE WAVE, 1 Hz
DECK DISPLACEMENT INCHES
TIME SECS

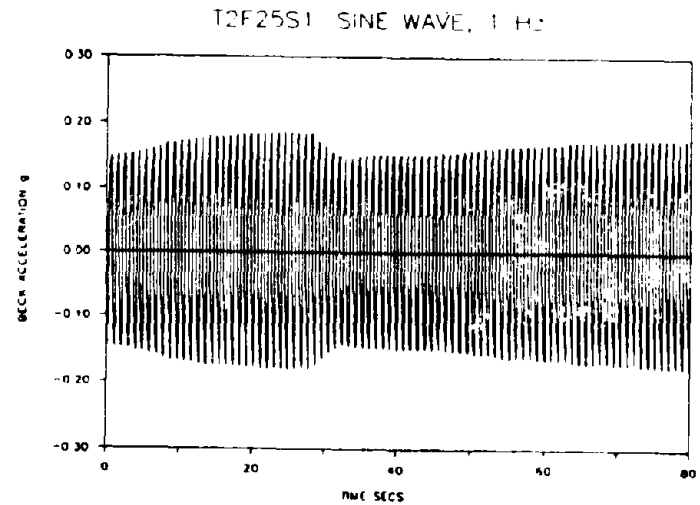
T2F25S1 SINE WAVE, 1 Hz
DECK ACCELERATION g
TIME SECS

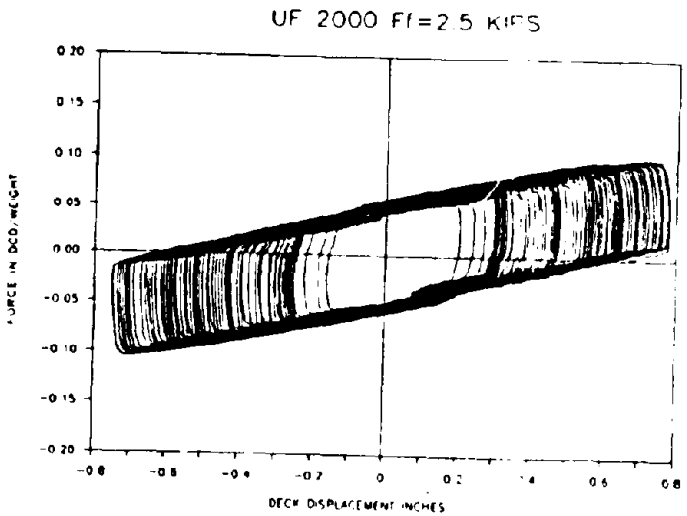
UF 2000 Ff=2.5 KIPS
FORCE IN DCD, WEIGHT
DECK DISPLACEMENT INCHES

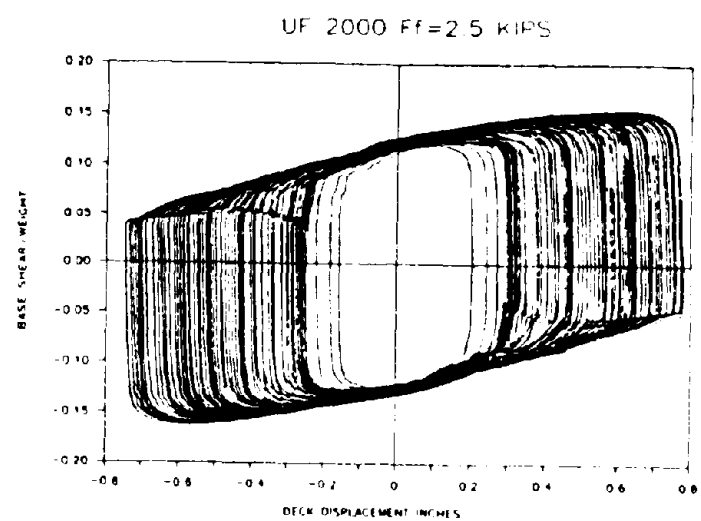
UF 2000 Ff=2.5 KIPS
BASE SHEAR, WEIGHT
DECK DISPLACEMENT INCHES

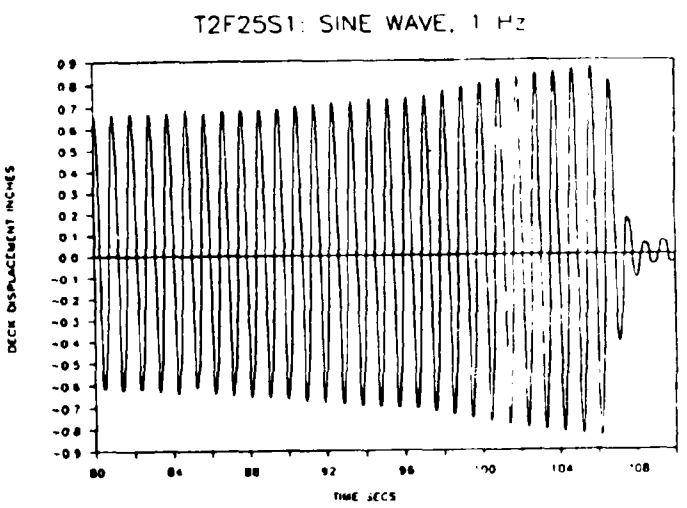
T2F25S1: SINE WAVE, 1 Hz
DECK DISPLACEMENT INCHES
TIME SECS

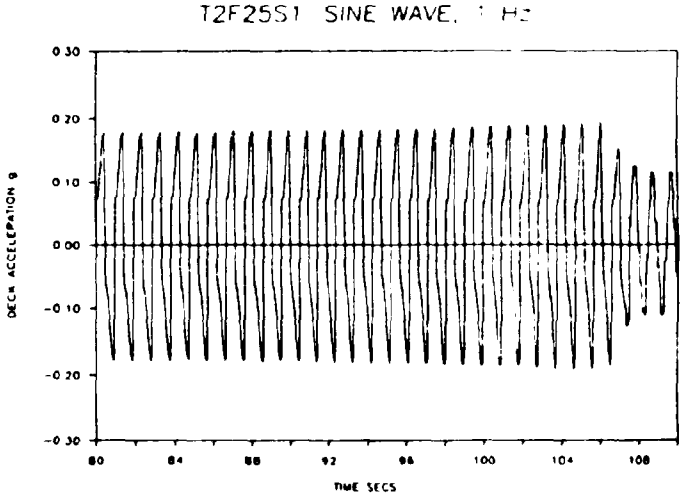
T2F25S1 SINE WAVE, 1 Hz
DECK ACCELERATION g
TIME SECS

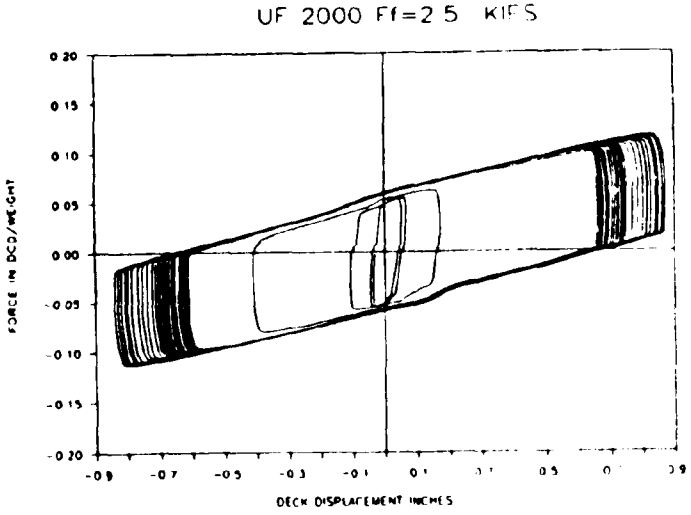
UF 2000 Ff=2.5 KIPS
FORCE IN DCD/WEIGHT
DECK DISPLACEMENT INCHES

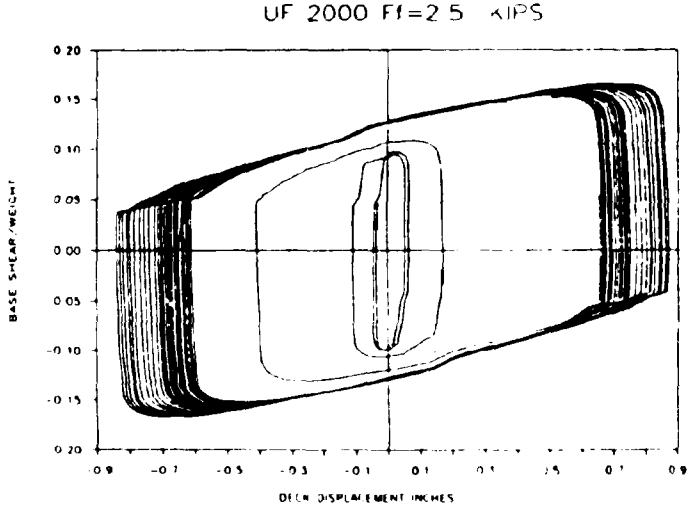
UF 2000 Ff=2.5 KIPS
BASE SHEAR/WEIGHT
DECK DISPLACEMENT INCHES

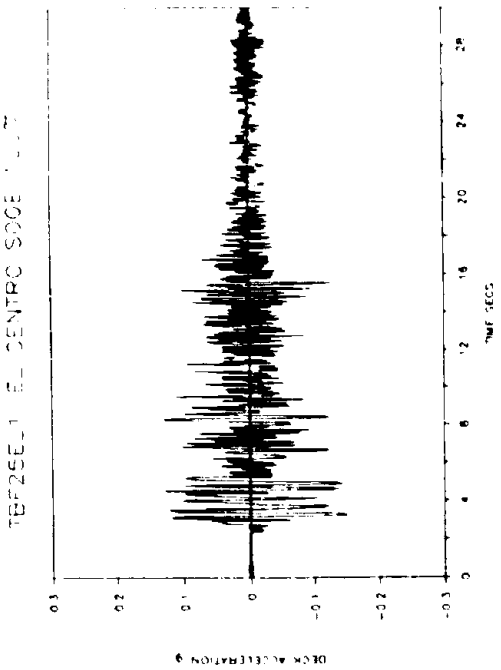

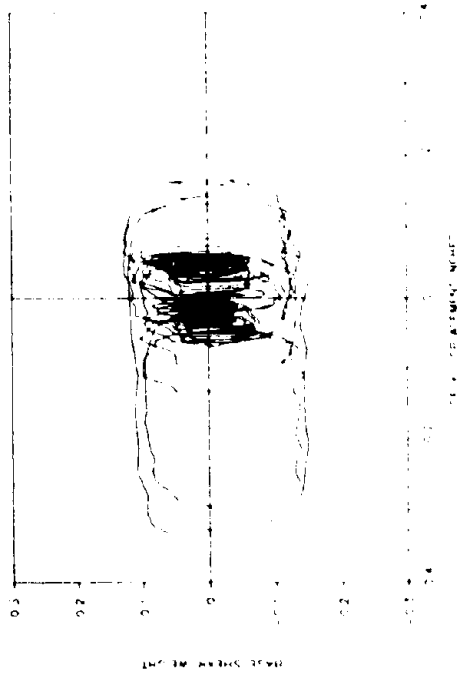

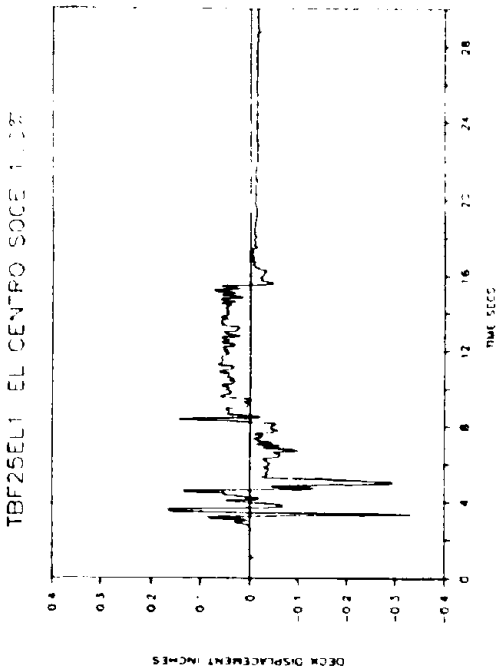

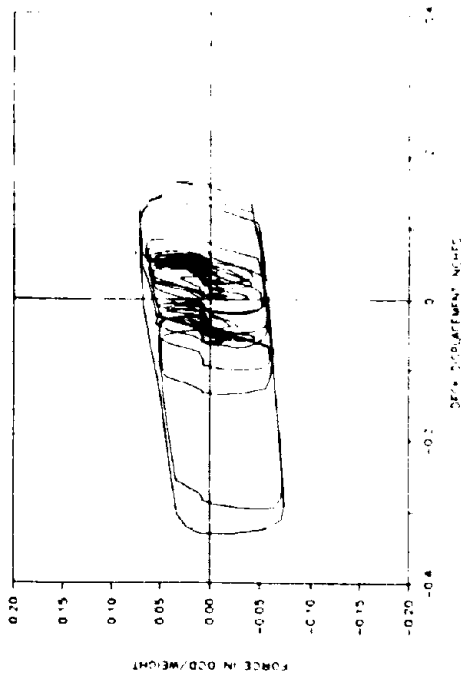

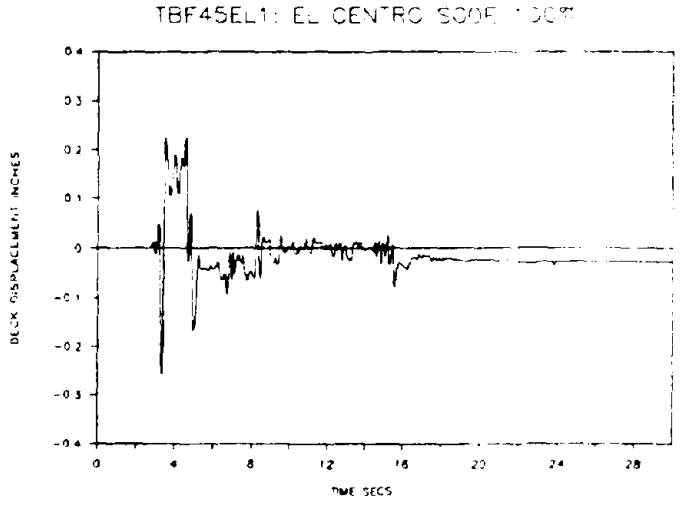
TBF45EL1: EL CENTRO SCOE
TIME SECS

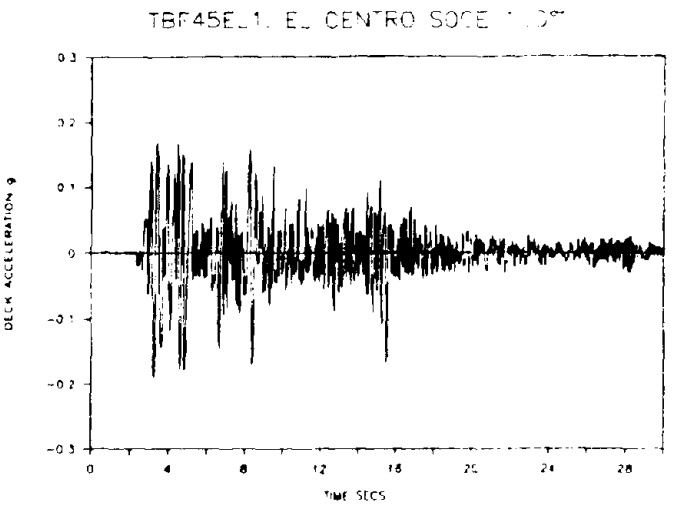
TBF45EL1: EL CENTRO SCOE
DECK ACCELERATION g
TIME SECS

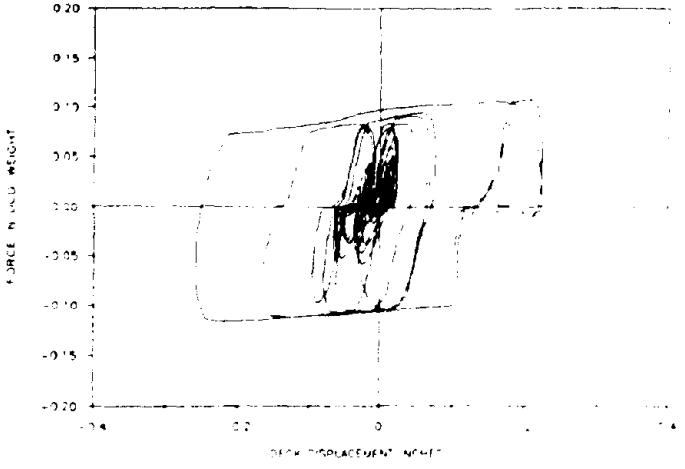

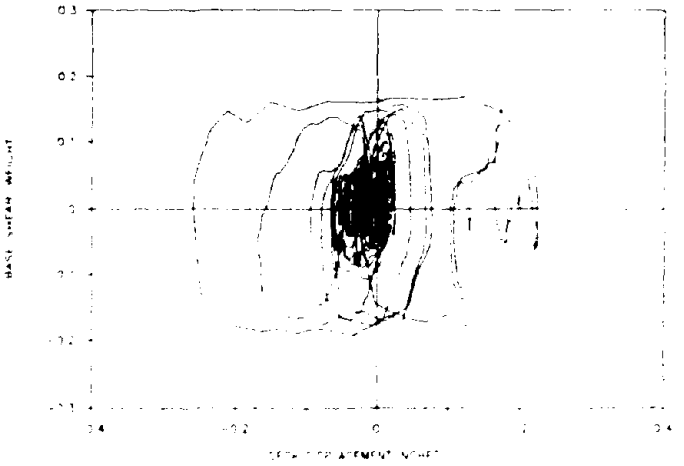

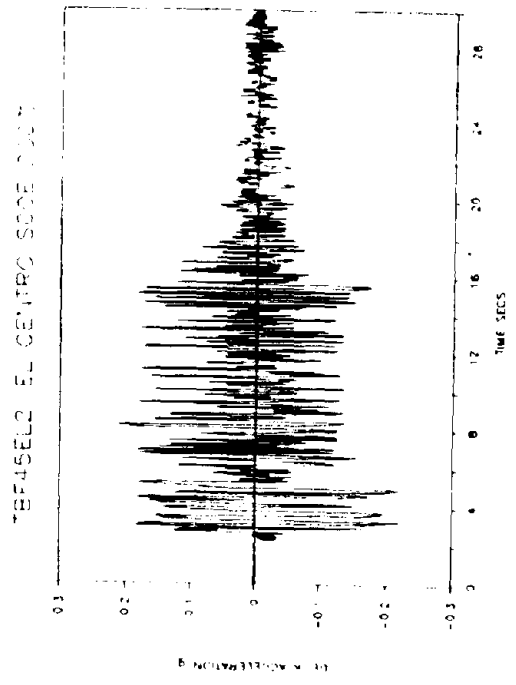

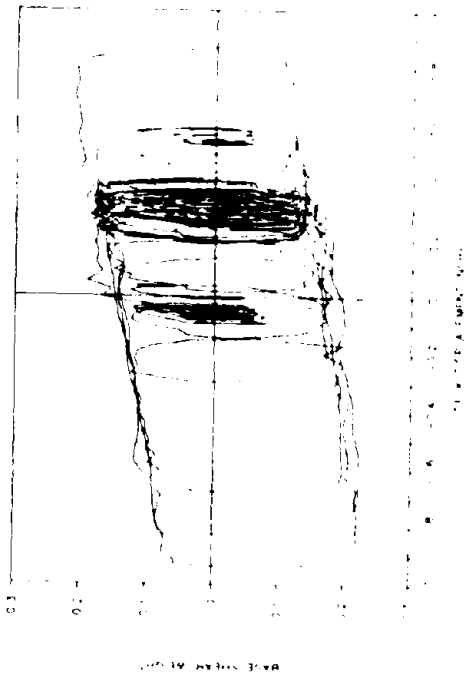

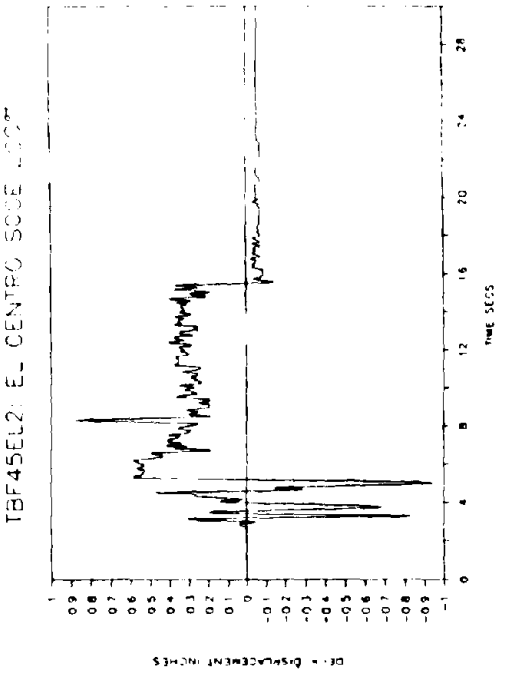

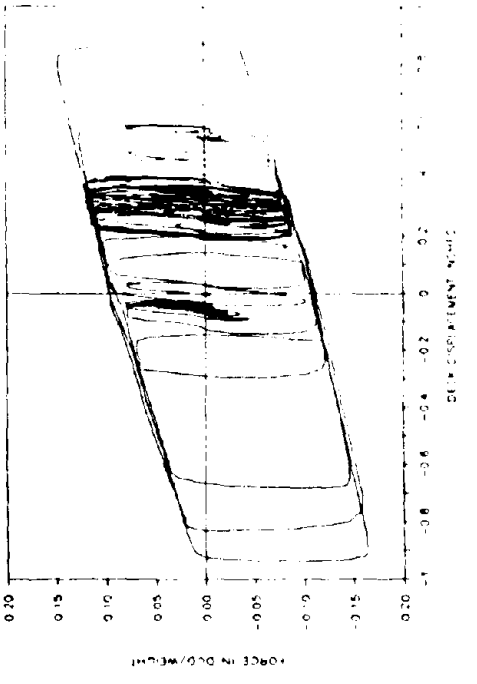

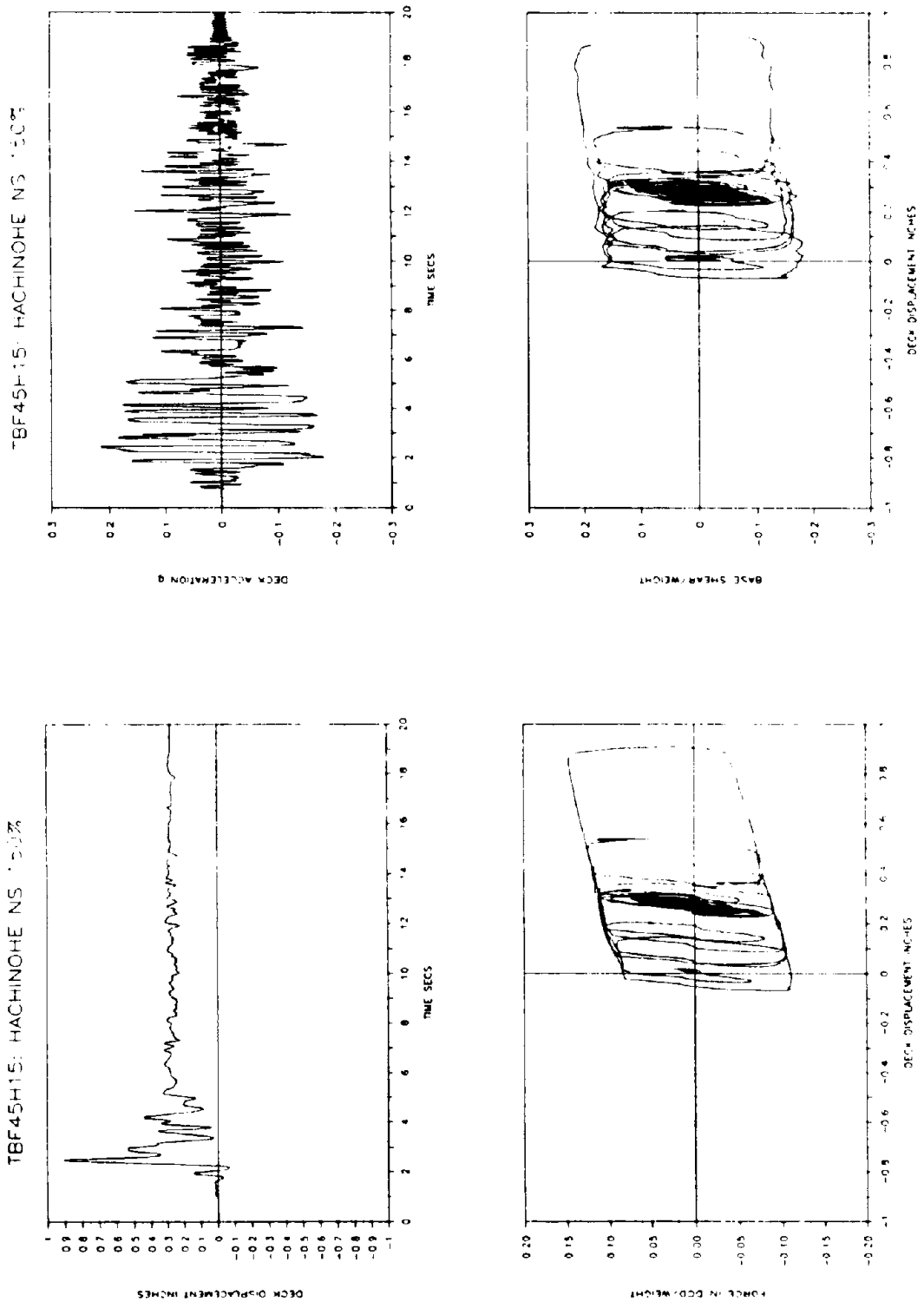

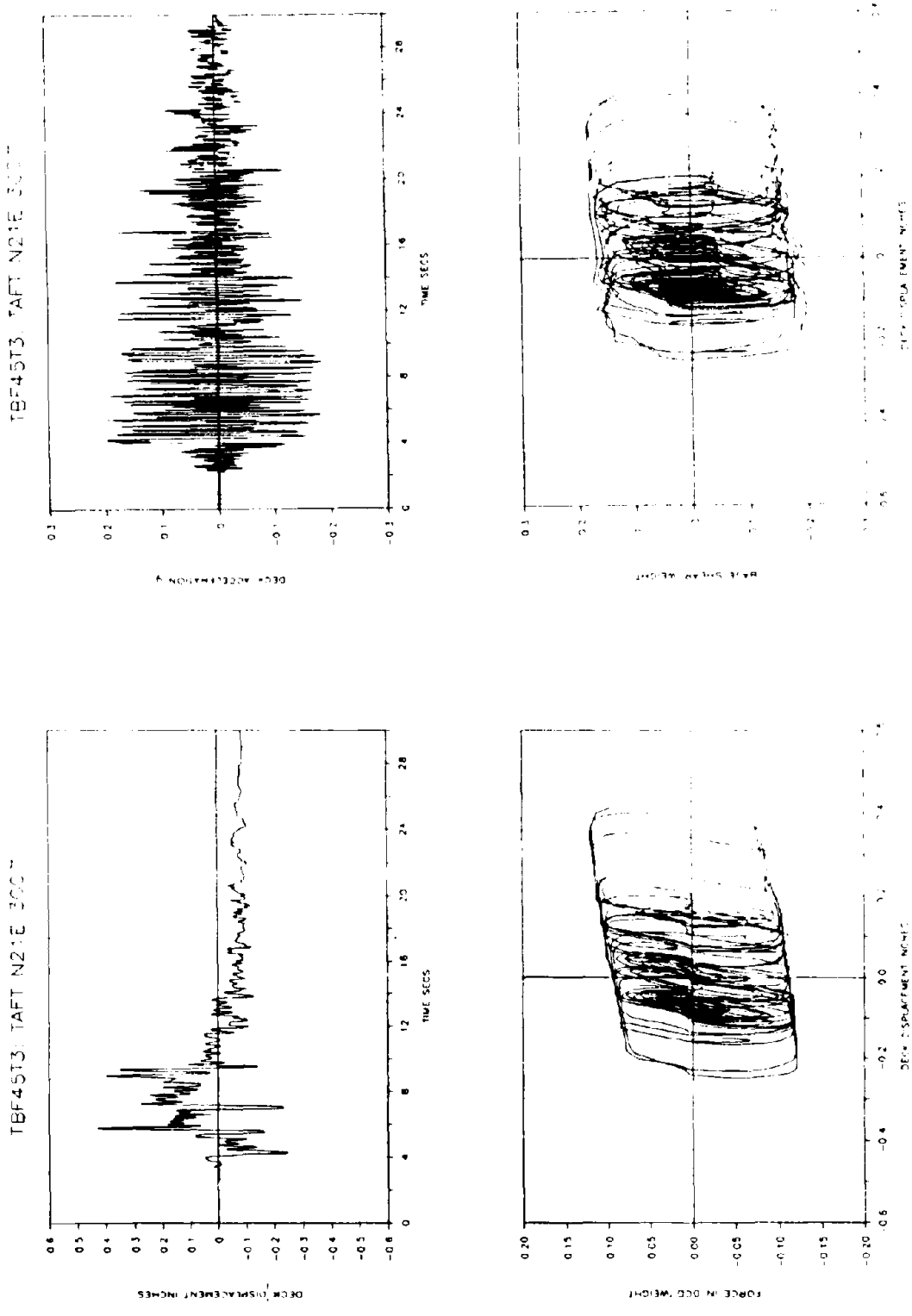

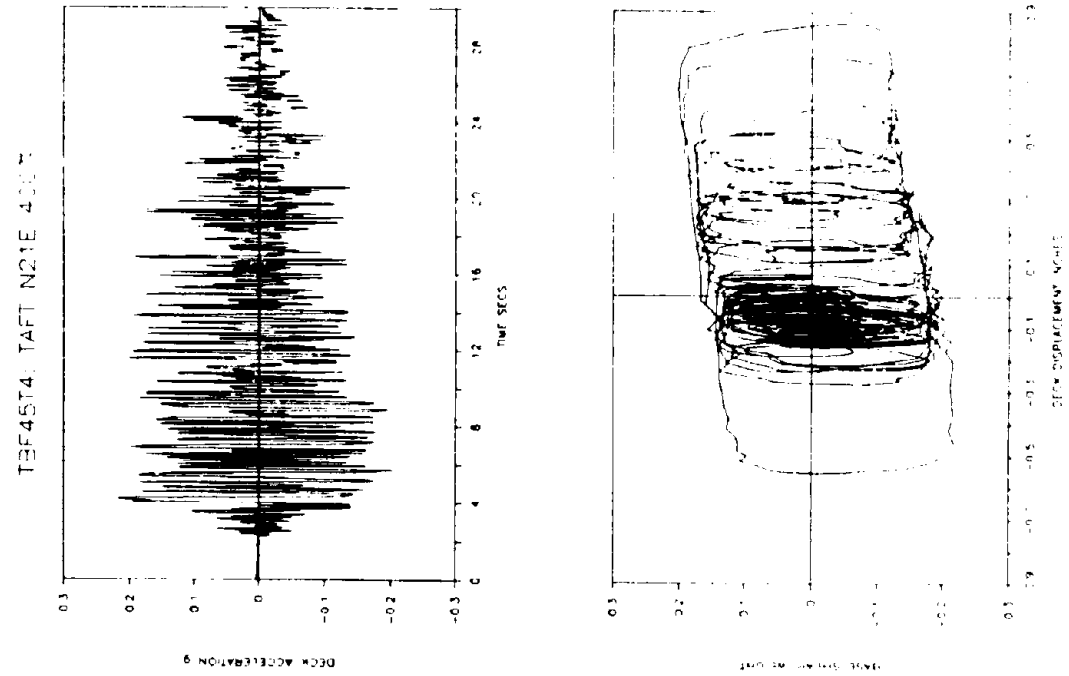

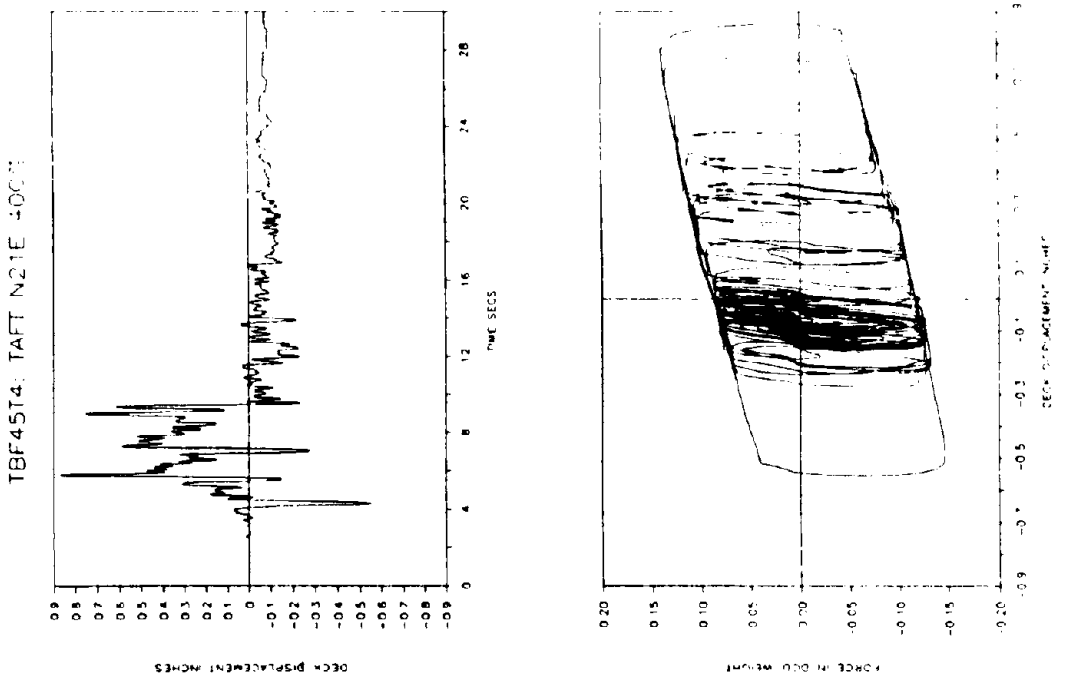

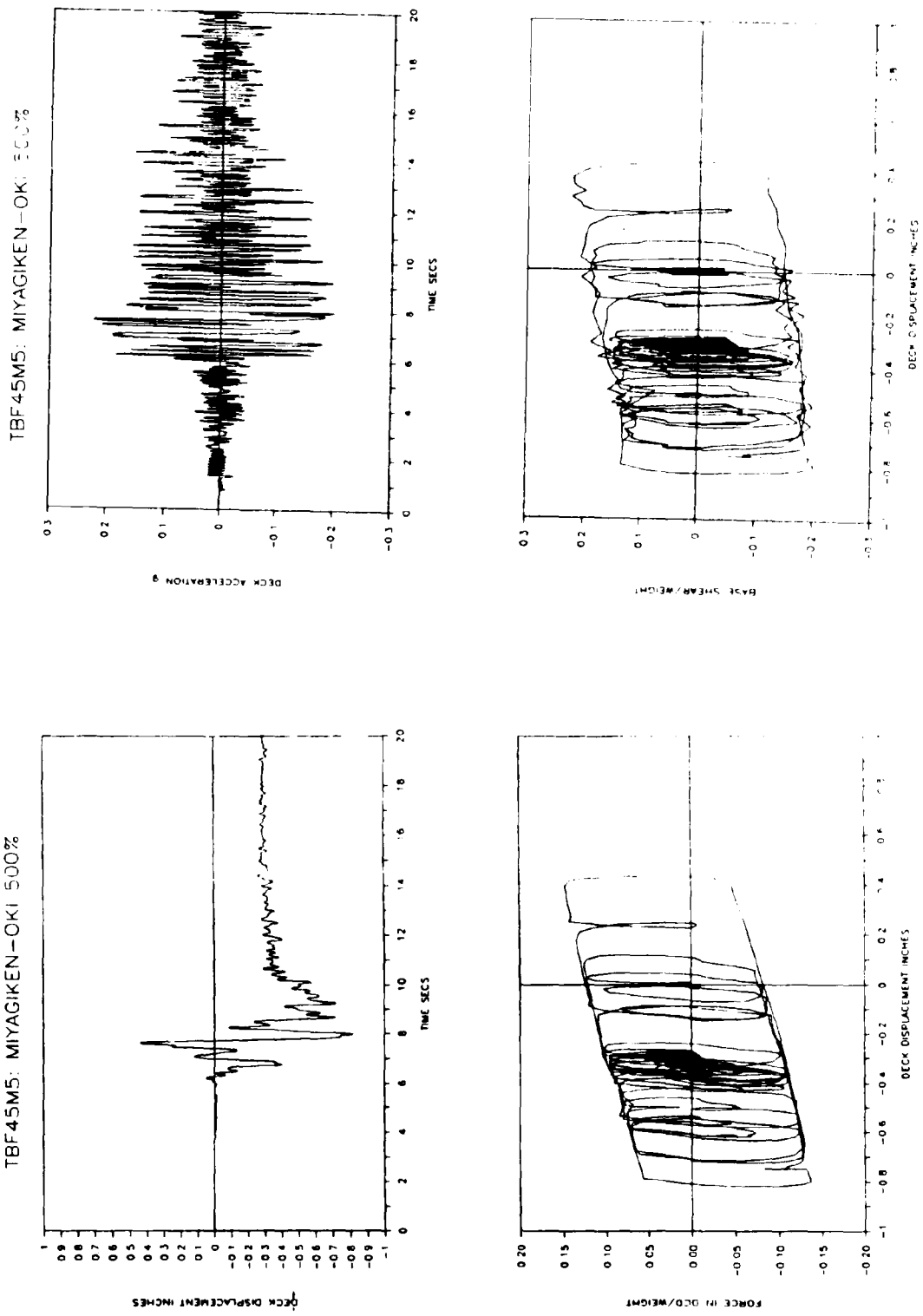

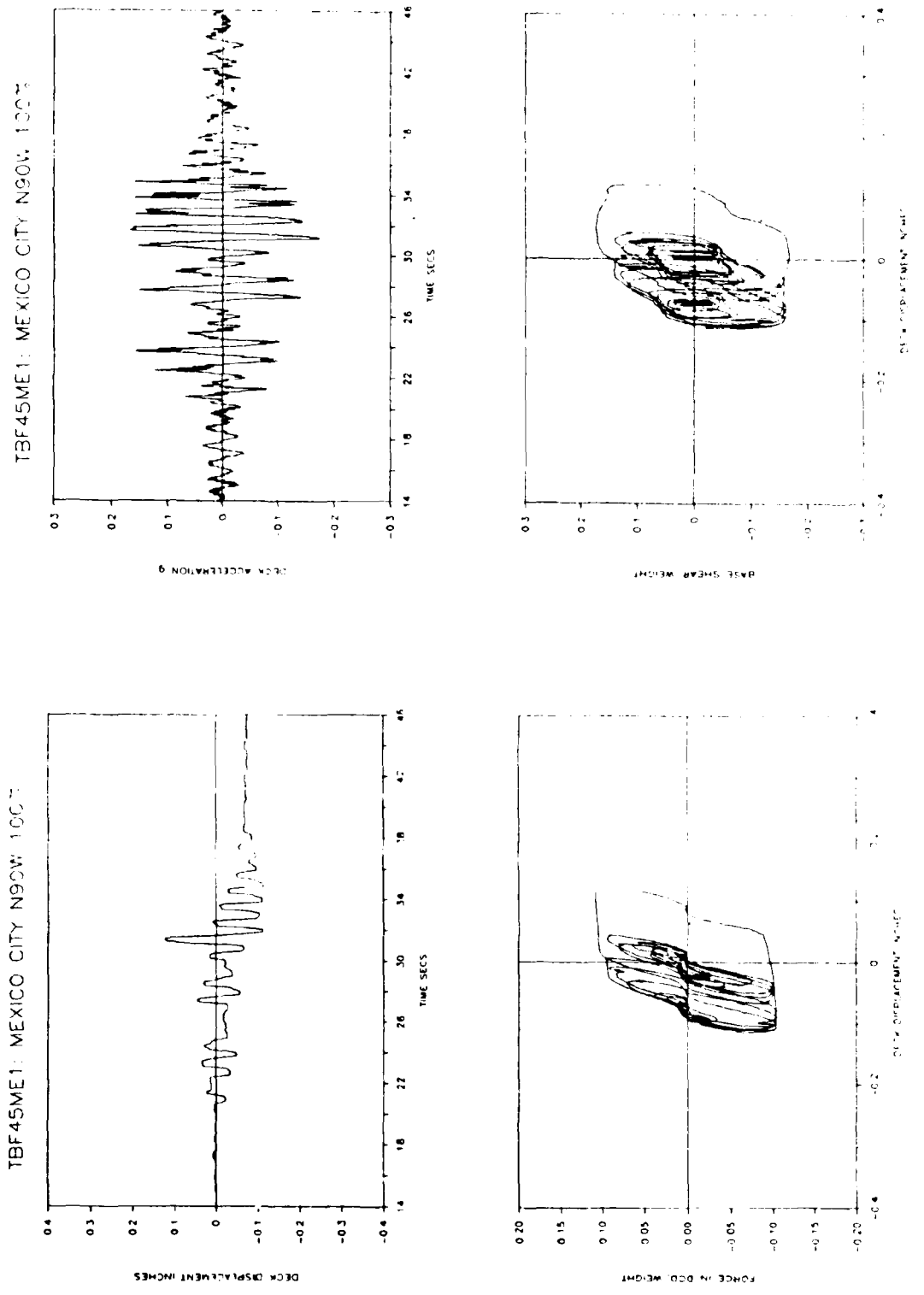

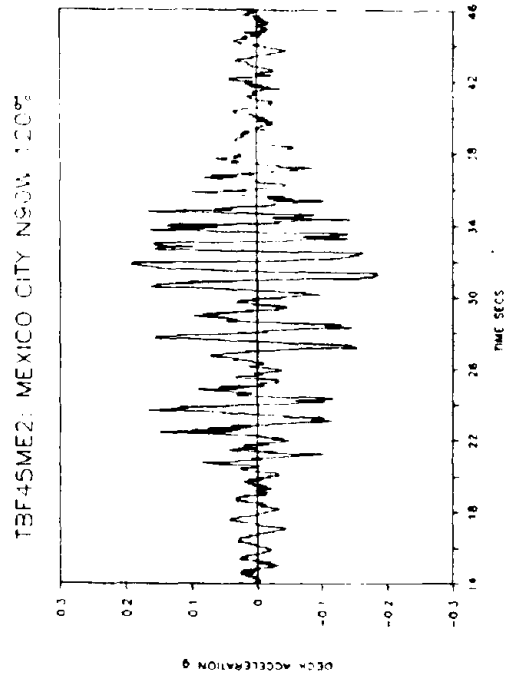

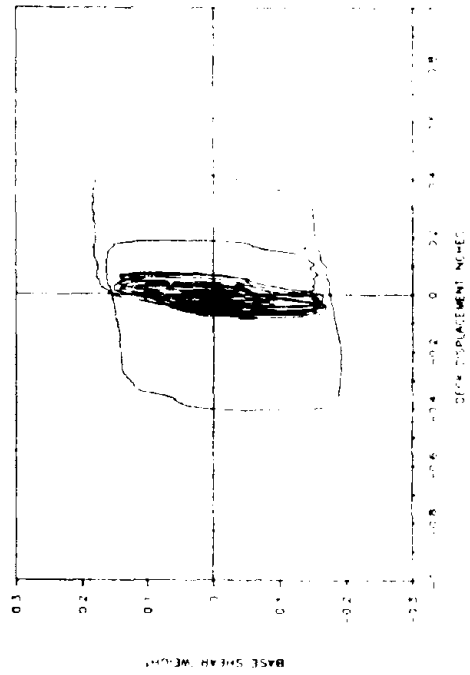

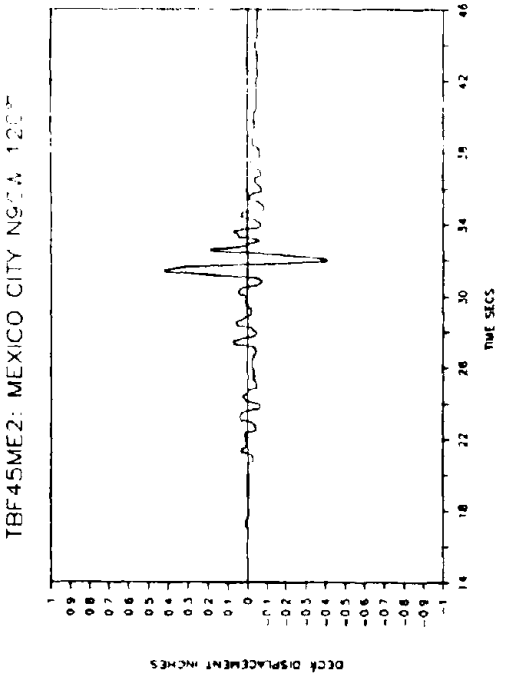

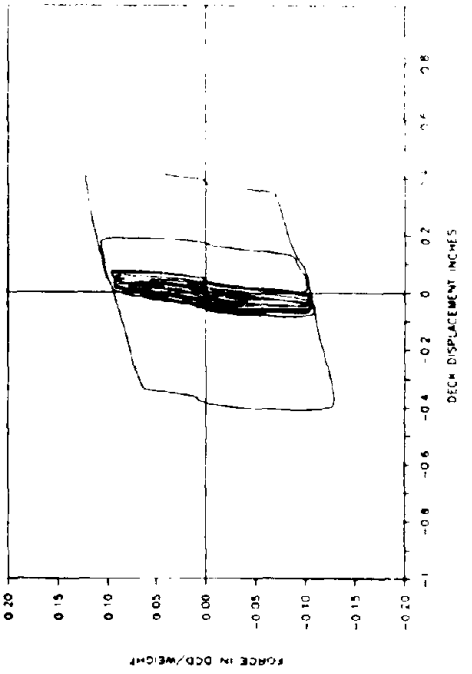

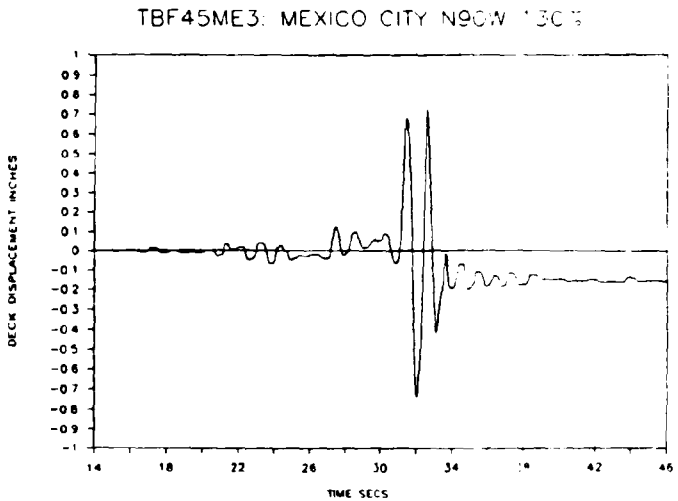
TBF45ME3: MEXICO CITY N90W 130%
DECK DISPLACEMENT INCHES
TIME SECS

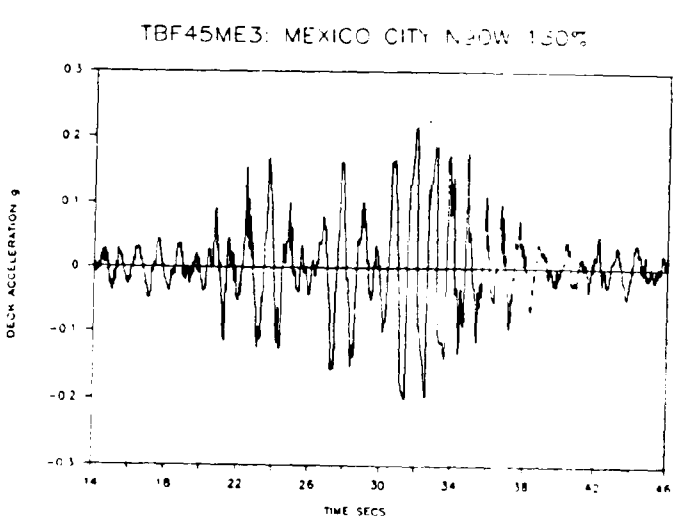
TBF45ME3: MEXICO CITY N90W 130%
DECK ACCELERATION g
TIME SECS

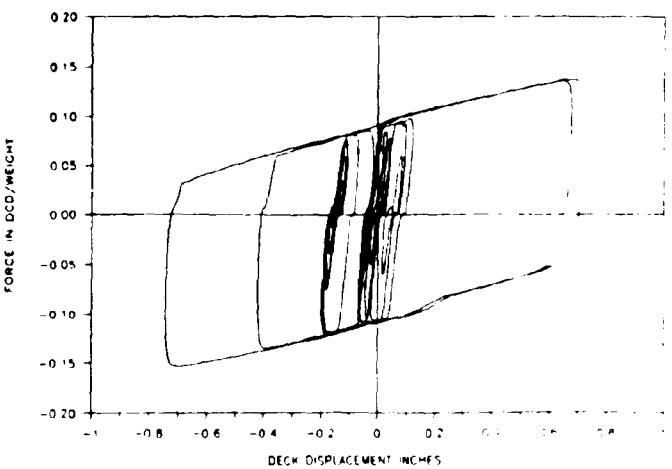
FORCE IN DCD/WEIGHT
DECK DISPLACEMENT INCHES

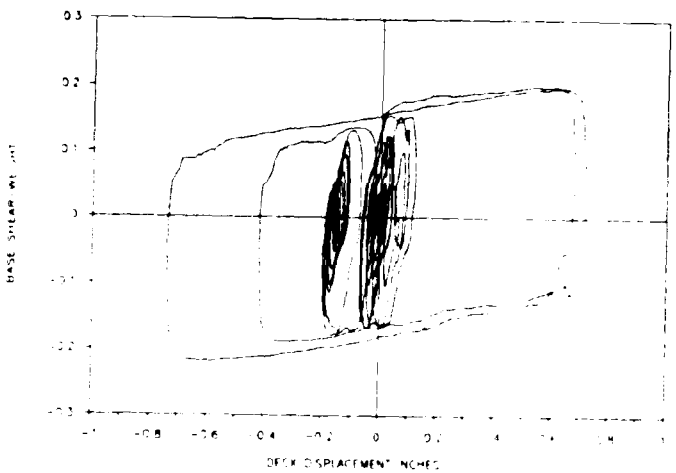
DECK DISPLACEMENT INCHES

NATIONAL CENTER FOR EARTHQUAKE ENGINEERING RESEARCH
LIST OF TECHNICAL REPORTS

The National Center for Earthquake Engineering Research (NCEER) publishes technical reports on a variety of subjects related to earthquake engineering written by authors funded through NCEER. These reports are available from both NCEER's Publications Department and the National Technical Information Service (NTIS). Requests for reports should be directed to the Publications Department, National Center for Earthquake Engineering Research, State University of New York at Buffalo, Red Jacket Quadrangle, Buffalo, New York 14261. Reports can also be requested through NTIS, 5285 Port Royal Road, Springfield, Virginia 22161. NTIS accession numbers are shown in parenthesis, if available.

NCEER-87-0001 "First-Year Program in Research, Education and Technology Transfer," 3/5/87, (PB88-134275/AS).

NCEER-87-0002 "Experimental Evaluation of Instantaneous Optimal Algorithms for Structural Control," by R.C. Lin, T.T. Soong and A.M. Reinhorn, 4/20/87, (PB88-134341/AS).

NCEER-87-0003 "Experimentation Using the Earthquake Simulation Facilities at University at Buffalo," by A.M. Reinhorn and R.L. Ketter, to be published.

NCEER-87-0004 "The System Characteristics and Performance of a Shaking Table," by J.S. Hwang, K.C. Chang and G.C. Lee, 6/1/87, (PB88-134259/AS). This report is available only through NTIS (see address given above).

NCEER-87-0005 "A Finite Element Formulation for Nonlinear Viscoplastic Material Using a Q Model," by O. Gyebi and G. Dasgupta, 11/2/87, (PB88-213764/AS).

NCEER-87-0006 "Symbolic Manipulation Program (SMP) - Algebraic Codes for Two and Three Dimensional Finite Element Formulations," by X. Lee and G. Dasgupta, 11/9/87, (PB88-219522/AS).

NCEER-87-0007 "Instantaneous Optimal Control Laws for Tall Buildings Under Seismic Excitations," by J.N. Yang, A. Akbarpour and P. Ghaemmaghami, 6/10/87, (PB88-134333/AS).

NCEER-87-0008 "IDARC: Inelastic Damage Analysis of Reinforced Concrete Frame - Shear-Wall Structures," by Y.J. Park, A.M. Reinhorn and S.K. Kunnath, 7/20/87, (PB88-134325/AS).

NCEER-87-0009 "Liquefaction Potential for New York State: A Preliminary Report on Sites in Manhattan and Buffalo," by M. Budhu, V. Vijayakumar, R.F. Giese and L. Baumgras, 8/31/87, (PB88-163704/AS). This report is available only through NTIS (see address given above).

NCEER-87-0010 "Vertical and Torsional Vibration of Foundations in Inhomogeneous Media," by A.S. Veletsos and K.W. Dotson, 6/1/87, (PB88-134291/AS).

NCEER-87-0011 "Seismic Probabilistic Risk Assessment and Seismic Margins Studies for Nuclear Power Plants," by Howard H.M. Hwang, 6/15/87, (PB88-134267/AS).

NCEER-87-0012 "Parametric Studies of Frequency Response of Secondary Systems Under Ground-Acceleration Excitations," by Y. Yong and Y.K. Lin, 6/10/87, (PB88-134309/AS).

NCEER-87-0013 "Frequency Response of Secondary Systems Under Seismic Excitation," by J.A. HoLung, J. Cai and Y.K. Lin, 7/31/87, (PB88-134317/AS).

NCEER-87-0014 "Modelling Earthquake Ground Motions in Seismically Active Regions Using Parametric Time Series Methods," by G.W. Ellis and A.S. Cakmak, 8/25/87, (PB88-134283/AS).

NCEER-87-0015 "Detection and Assessment of Seismic Structural Damage," by E. DiPasquale and A.S. Cakmak, 8/25/87, (PB88-163712/AS).

NCEER-87-0016 "Pipeline Experiment at Parkfield, California," by J. Isenberg and E. Richardson, 9/15/87, (PB88-163720/AS). This report is available only through NTIS (see address given above).

NCEER-87-0017 "Digital Simulation of Seismic Ground Motion," by M. Shinozuka, G. Deodatis and T. Harada, 8/31/87, (PB88-155197/AS). This report is available only through NTIS (see address given above).

NCEER-87-0018 "Practical Considerations for Structural Control: System Uncertainty, System Time Delay and Truncation of Small Control Forces," J.N. Yang and A. Akbarpour, 8/10/87, (PB88-163738/AS).

NCEER-87-0019 "Modal Analysis of Nonclassically Damped Structural Systems Using Canonical Transformation," by J.N. Yang, S. Sarkani and F.X. Long, 9/27/87, (PB88-187851/AS).

NCEER-87-0020 "A Nonstationary Solution in Random Vibration Theory," by J.R. Red-Horse and P.D. Spanos, 11/3/87, (PB88-163746/AS).

NCEER-87-0021 "Horizontal Impedances for Radially Inhomogeneous Viscoelastic Soil Layers," by A.S. Veletsos and K.W. Dotson, 10/15/87, (PB88-150859/AS).

NCEER-87-0022 "Seismic Damage Assessment of Reinforced Concrete Members," by Y.S. Chung, C. Meyer and M. Shinozuka, 10/9/87, (PB88-150867/AS). This report is available only through NTIS (see address given above).

NCEER-87-0023 "Active Structural Control in Civil Engineering," by T.T. Soong, 11/11/87, (PB88-187778/AS).

NCEER-87-0024 Vertical and Torsional Impedances for Radially Inhomogeneous Viscoelastic Soil Layers," by K.W. Dotson and A.S. Veletsos, 12/87, (PB88-187786/AS).

NCEER-87-0025 "Proceedings from the Symposium on Seismic Hazards, Ground Motions, Soil-Liquefaction and Engineering Practice in Eastern North America," October 20-22, 1987, edited by K.H. Jacob, 12/87, (PB88-188115/AS).

NCEER-87-0026 "Report on the Whittier-Narrows, California, Earthquake of October 1, 1987," by J. Pantelic and A. Reinhorn, 11/87, (PB88-187752/AS). This report is available only through NTIS (see address given above).

NCEER-87-0027 "Design of a Modular Program for Transient Nonlinear Analysis of Large 3-D Building Structures," by S. Srivastav and J.F. Abel, 12/30/87, (PB88-187950/AS).

NCEER-87-0028 "Second-Year Program in Research, Education and Technology Transfer," 3/8/88, (PB88-219480/AS).

NCEER-88-0001 "Workshop on Seismic Computer Analysis and Design of Buildings With Interactive Graphics," by W. McGuire, J.F. Abel and C.H. Conley, 1/18/88, (PB88-187760/AS).

NCEER-88-0002 "Optimal Control of Nonlinear Flexible Structures," by J.N. Yang, F.X. Long and D. Wong, 1/22/88, (PB88-213772/AS).

NCEER-88-0003 "Substructuring Techniques in the Time Domain for Primary-Secondary Structural Systems," by G.D. Manolis and G. Juhn, 2/10/88, (PB88-213780/AS).

NCEER-88-0004 "Iterative Seismic Analysis of Primary-Secondary Systems," by A. Singhal, L.D. Lutes and P.D. Spanos, 2/23/88, (PB88-213798/AS).

NCEER-88-0005 "Stochastic Finite Element Expansion for Random Media," by P.D. Spanos and R. Ghanem, 3/14/88, (PB88-213806/AS).

NCEER-88-0006 "Combining Structural Optimization and Structural Control," by F.Y. Cheng and C.P. Pantelides, 1/10/88, (PB88-213814/AS).

NCEER-88-0007 "Seismic Performance Assessment of Code-Designed Structures," by H.H-M. Hwang, J-W. Jaw and H-J. Shau, 3/20/88, (PB88-219423/AS).

NCEER-88-0008 "Reliability Analysis of Code-Designed Structures Under Natural Hazards," by H.H-M. Hwang, H. Ushiba and M. Shinozuka, 2/29/88, (PB88-229471/AS).

NCEER-88-0009 "Seismic Fragility Analysis of Shear Wall Structures," by J-W Jaw and H.H-M. Hwang, 4/30/88, (PB89-102867/AS).

NCEER-88-0010 "Base Isolation of a Multi-Story Building Under a Harmonic Ground Motion - A Comparison of Performances of Various Systems," by F-G Fan, G. Ahmadi and I.G. Tadjbakhsh, 5/18/88, (PB89-122238/AS).

NCEER-88-0011 "Seismic Floor Response Spectra for a Combined System by Green's Functions," by F.M. Lavelle, L.A. Bergman and P.D. Spanos, 5/1/88, (PB89-102875/AS).

NCEER-88-0012 "A New Solution Technique for Randomly Excited Hysteretic Structures," by G.Q. Cai and Y.K. Lin, 5/16/88, (PB89-102883/AS).

NCEER-88-0013 "A Study of Radiation Damping and Soil-Structure Interaction Effects in the Centrifuge," by K. Weissman, supervised by J.H. Prevost, 5/24/88, (PB89-144703/AS).

NCEER-88-0014 "Parameter Identification and Implementation of a Kinematic Plasticity Model for Frictional Soils," by J.H. Prevost and D.V. Griffiths, to be published.

NCEER-88-0015 "Two- and Three- Dimensional Dynamic Finite Element Analyses of the Long Valley Dam," by D.V. Griffiths and J.H. Prevost, 6/17/88, (PB89-144711/AS).

NCEER-88-0016 "Damage Assessment of Reinforced Concrete Structures in Eastern United States," by A.M. Reinhorn, M.J. Seidel, S.K. Kunnath and Y.J. Park, 6/15/88, (PB89-122220/AS).

NCEER-88-0017 "Dynamic Compliance of Vertically Loaded Strip Foundations in Multilayered Viscoelastic Soils," by S. Ahmad and A.S.M. Israil, 6/17/88, (PB89-102891/AS).

NCEER-88-0018 "An Experimental Study of Seismic Structural Response With Added Viscoelastic Dampers," by R.C. Lin, Z. Liang, T.T. Soong and R.H. Zhang, 6/30/88, (PB89-122212/AS).

NCEER-88-0019 "Experimental Investigation of Primary - Secondary System Interaction," by G.D. Manolis, G. Juhn and A.M. Reinhorn, 5/27/88, (PB89-122204/AS).

NCEER-88-0020 "A Response Spectrum Approach For Analysis of Nonclassically Damped Structures," by J.N. Yang, S. Sarkani and F.X. Long, 4/22/88, (PB89-102909/AS).

NCEER-88-0021 "Seismic Interaction of Structures and Soils: Stochastic Approach," by A.S. Veletsos and A.M. Prasad, 7/21/88, (PB89-122196/AS).

NCEER-88-0022 "Identification of the Serviceability Limit State and Detection of Seismic Structural Damage," by E. DiPasquale and A.S. Cakmak, 6/15/88, (PB89-122188/AS).

NCEER-88-0023 "Multi-Hazard Risk Analysis: Case of a Simple Offshore Structure," by B.K. Bhartia and E.H. Vanmarcke, 7/21/88, (PB89-145213/AS).

NCEER-88-0024 "Automated Seismic Design of Reinforced Concrete Buildings," by Y.S. Chung, C. Meyer and M. Shinozuka, 7/5/88, (PB89-122170/AS).

NCEER-88-0025 "Experimental Study of Active Control of MDOF Structures Under Seismic Excitations," by L.L. Chung, R.C. Lin, T.T. Soong and A.M. Reinhorn, 7/10/88, (PB89-122600/AS).

NCEER-88-0026 "Earthquake Simulation Tests of a Low-Rise Metal Structure," by J.S. Hwang, K.C. Chang, G.C. Lee and R.L. Ketter, 8/1/88, (PB89-102917/AS).

NCEER-88-0027 "Systems Study of Urban Response and Reconstruction Due to Catastrophic Earthquakes," by F. Kozin and H.K. Zhou, 9/22/88, (PB90-162348/AS).

NCEER-88-0028 "Seismic Fragility Analysis of Plane Frame Structures," by H.H-M. Hwang and Y.K. Low, 7/31/88, (PB89-131445/AS).

NCEER-88-0029 "Response Analysis of Stochastic Structures," by A. Kardara, C. Bucher and M. Shinozuka, 9/22/88, (PB89-174429/AS).

NCEER-88-0030 "Nonnormal Accelerations Due to Yielding in a Primary Structure," by D.C.K. Chen and L.D. Lutes, 9/19/88, (PB89-131437/AS).

NCEER-88-0031 "Design Approaches for Soil-Structure Interaction," by A.S. Veletsos, A.M. Prasad and Y. Tang, 12/30/88, (PB89-174437/AS).

NCEER-88-0032 "A Re-evaluation of Design Spectra for Seismic Damage Control," by C.J. Turkstra and A.G. Tallin, 11/7/88, (PB89-145221/AS).

NCEER-88-0033 "The Behavior and Design of Noncontact Lap Splices Subjected to Repeated Inelastic Tensile Loading," by V.E. Sagan, P. Gergely and R.N. White, 12/8/88, (PB89-163737/AS).

NCEER-88-0034 "Seismic Response of Pile Foundations," by S.M. Mamoon, P.K. Banerjee and S. Ahmad, 11/1/88, (PB89-145239/AS).

NCEER-88-0035 "Modeling of R/C Building Structures With Flexible Floor Diaphragms (IDARC2)," by A.M. Reinhorn, S.K. Kunnath and N. Panahshahi, 9/7/88, (PB89-207153/AS).

NCEER-88-0036 "Solution of the Dam-Reservoir Interaction Problem Using a Combination of FEM, BEM with Particular Integrals, Modal Analysis, and Substructuring," by C-S. Tsai, G.C. Lee and R.L. Ketter, 12/31/88, (PB89-207146/AS).

NCEER-88-0037 "Optimal Placement of Actuators for Structural Control," by F.Y. Cheng and C.P. Pantelides, 8/15/88, (PB89-162846/AS).

NCEER-88-0038 "Teflon Bearings in Aseismic Base Isolation: Experimental Studies and Mathematical Modeling," by A. Mokha, M.C. Constantinou and A.M. Reinhorn, 12/5/88, (PB89-218457/AS).

NCEER-88-0039 "Seismic Behavior of Flat Slab High-Rise Buildings in the New York City Area," by P. Weidlinger and M. Ettouney, 10/15/88, (PB90-145681/AS).

NCEER-88-0040 "Evaluation of the Earthquake Resistance of Existing Buildings in New York City," by P. Weidlinger and M. Ettouney, 10/15/88, to be published.

NCEER-88-0041 "Small-Scale Modeling Techniques for Reinforced Concrete Structures Subjected to Seismic Loads," by W. Kim, A. El-Attar and R.N. White, 11/22/88, (PB89-189625/AS).

NCEER-88-0042 "Modeling Strong Ground Motion from Multiple Event Earthquakes," by G.W. Ellis and A.S. Cakmak, 10/15/88, (PB89-174445/AS).

NCEER-88-0043 "Nonstationary Models of Seismic Ground Acceleration," by M. Grigoriu, S.E. Ruiz and E. Rosenblueth, 7/15/88, (PB89-189617/AS).

NCEER-88-0044 "SARCF User's Guide: Seismic Analysis of Reinforced Concrete Frames," by Y.S. Chung, C. Meyer and M. Shinozuka, 11/9/88, (PB89-174452/AS).

NCEER-88-0045 "First Expert Panel Meeting on Disaster Research and Planning," edited by J. Pantelic and J. Stoyle, 9/15/88, (PB89-174460/AS).

NCEER-88-0046 "Preliminary Studies of the Effect of Degrading Infill Walls on the Nonlinear Seismic Response of Steel Frames," by C.Z. Chrysostomou, P. Gergely and J.F. Abel, 12/19/88, (PB89-208383/AS).

NCEER-88-0047 "Reinforced Concrete Frame Component Testing Facility - Design, Construction, Instrumentation and Operation," by S.P. Pessiki, C. Conley, T. Bond, P. Gergely and R.N. White, 12/16/88, (PB89-174478/AS).

NCEER-89-0001 "Effects of Protective Cushion and Soil Compliancy on the Response of Equipment Within a Seismically Excited Building," by J.A. HoLung, 2/16/89, (PB89-207179/AS).

NCEER-89-0002 "Statistical Evaluation of Response Modification Factors for Reinforced Concrete Structures," by H.H-M. Hwang and J-W. Jaw, 2/17/89, (PB89-207187/AS).

NCEER-89-0003 "Hysteretic Columns Under Random Excitation," by G-Q. Cai and Y.K. Lin, 1/9/89, (PB89-196513/AS).

NCEER-89-0004 "Experimental Study of 'Elephant Foot Bulge' Instability of Thin-Walled Metal Tanks," by Z-H. Jia and R.L. Ketter, 2/22/89, (PB89-207195/AS).

NCEER-89-0005 "Experiment on Performance of Buried Pipelines Across San Andreas Fault," by J. Isenberg, E. Richardson and T.D. O'Rourke, 3/10/89, (PB89-218440/AS).

NCEER-89-0006 "A Knowledge-Based Approach to Structural Design of Earthquake-Resistant Buildings," by M. Subramani, P. Gergely, C.H. Conley, J.F. Abel and A.H. Zaghw, 1/15/89, (PB89-218465/AS).

NCEER-89-0007 "Liquefaction Hazards and Their Effects on Buried Pipelines," by T.D. O'Rourke and P.A. Lane, 2/1/89, (PB89-218481).

NCEER-89-0008 "Fundamentals of System Identification in Structural Dynamics," by H. Imai, C-B. Yun, O. Maruyama and M. Shinozuka, 1/26/89, (PB89-207211/AS).

NCEER-89-0009 "Effects of the 1985 Michoacan Earthquake on Water Systems and Other Buried Lifelines in Mexico," by A.G. Ayala and M.J. O'Rourke, 3/8/89, (PB89-207229/AS).

NCEER-89-R010 "NCEER Bibliography of Earthquake Education Materials," by K.E.K. Ross, Second Revision, 9/1/89, (PB90-125352/AS).

NCEER-89-0011 "Inelastic Three-Dimensional Response Analysis of Reinforced Concrete Building Structures (IDARC-3D), Part I - Modeling," by S.K. Kunnath and A.M. Reinhorn, 4/17/89, (PB90-114612/AS).

NCEER-89-0012 "Recommended Modifications to ATC-14," by C.D. Poland and J.O. Malley, 4/12/89, (PB90-108648/AS).

NCEER-89-0013 "Repair and Strengthening of Beam-to-Column Connections Subjected to Earthquake Loading," by M. Corazao and A.J. Durrani, 2/28/89, (PB90-109885/AS).

NCEER-89-0014 "Program EXKAL2 for Identification of Structural Dynamic Systems," by O. Maruyama, C-B. Yun, M. Hoshiya and M. Shinozuka, 5/19/89, (PB90-109877/AS).

NCEER-89-0015 "Response of Frames With Bolted Semi-Rigid Connections, Part I - Experimental Study and Analytical Predictions," by P.J. DiCorso, A.M. Reinhorn, J.R. Dickerson, J.B. Radziminski and W.L. Harper, 6/1/89, to be published.

NCEER-89-0016 "ARMA Monte Carlo Simulation in Probabilistic Structural Analysis," by P.D. Spanos and M.P. Mignolet, 7/10/89, (PB90-109893/AS).

NCEER-89-P017 "Preliminary Proceedings from the Conference on Disaster Preparedness - The Place of Earthquake Education in Our Schools," Edited by K.E.K. Ross, 6/23/89.

NCEER-89-0017 "Proceedings from the Conference on Disaster Preparedness - The Place of Earthquake Education in Our Schools," Edited by K.E.K. Ross, 12/31/89, (PB90-207895).

NCEER 89-0018 "Multidimensional Models of Hysteretic Material Behavior for Vibration Analysis of Shape Memory Energy Absorbing Devices, by E.J. Graesser and F.A. Cozzarelli, 6/7/89, (PB90-164146/AS).

NCEER-89-0019 "Nonlinear Dynamic Analysis of Three-Dimensional Base Isolated Structures (3D-BASIS)," by S. Nagarajaiah, A.M. Reinhorn and M.C. Constantinou, 8/3/89, (PB90-161936/AS).

NCEER-89-0020 "Structural Control Considering Time-Rate of Control Forces and Control Rate Constraints," by F.Y. Cheng and C.P. Pantelides, 8/3/89, (PB90-120445/AS).

NCEER-89-0021 "Subsurface Conditions of Memphis and Shelby County," by K.W. Ng, T-S. Chang and H-H.M. Hwang, 7/26/89, (PB90-120437/AS).

NCEER-89-0022 "Seismic Wave Propagation Effects on Straight Jointed Buried Pipelines," by K. Elhmadi and M.J. O'Rourke, 8/24/89, (PB90-162322/AS).

NCEER-89-0023 "Workshop on Serviceability Analysis of Water Delivery Systems," edited by M. Grigoriu, 3/6/89, (PB90-127424/AS).

NCEER-89-0024 "Shaking Table Study of a 1/5 Scale Steel Frame Composed of Tapered Members," by K.C. Chang, J.S. Hwang and G.C. Lee, 9/18/89, (PB90-160169/AS).

NCEER-89-0025 "DYNA1D: A Computer Program for Nonlinear Seismic Site Response Analysis - Technical Documentation," by Jean H. Prevost, 9/14/89, (PB90-161944/AS).

NCEER-89-0026 "1:4 Scale Model Studies of Active Tendon Systems and Active Mass Dampers for Aseismic Protection," by A.M. Reinhorn, T.T. Soong, R.C. Lin, Y.P. Yang, Y. Fukao, H. Abe and M. Nakai, 9/15/89, (PB90-173246/AS).

NCEER-89-0027 "Scattering of Waves by Inclusions in a Nonhomogeneous Elastic Half Space Solved by Boundary Element Methods," by P.K. Hadley, A. Askar and A.S. Cakmak, 6/15/89, (PB90-145699/AS).

NCEER-89-0028 "Statistical Evaluation of Deflection Amplification Factors for Reinforced Concrete Structures," by H.H.M. Hwang, J-W. Jaw and A.L. Ch'ng, 8/31/89, (PB90-164633/AS).

NCEER-89-0029 "Bedrock Accelerations in Memphis Area Due to Large New Madrid Earthquakes," by H.H.M. Hwang, C.H.S. Chen and G. Yu, 11/7/89, (PB90-162330/AS).

NCEER-89-0030 "Seismic Behavior and Response Sensitivity of Secondary Structural Systems," by Y.Q. Chen and T.T. Soong, 10/23/89, (PB90-164658/AS).

NCEER-89-0031 "Random Vibration and Reliability Analysis of Primary-Secondary Structural Systems," by Y. Ibrahim, M. Grigoriu and T.T. Soong, 11/10/89, (PB90-161951/AS).

NCEER-89-0032 "Proceedings from the Second U.S. - Japan Workshop on Liquefaction, Large Ground Deformation and Their Effects on Lifelines, September 26-29, 1989," Edited by T.D. O'Rourke and M. Hamada, 12/1/89, (PB90-209388/AS).

NCEER-89-0033 "Deterministic Model for Seismic Damage Evaluation of Reinforced Concrete Structures," by J.M. Bracci, A.M. Reinhorn, J.B. Mander and S.K. Kunnath, 9/27/89.

NCEER-89-0034 "On the Relation Between Local and Global Damage Indices," by E. DiPasquale and A.S. Cakmak, 8/15/89, (PB90-173865).

NCEER-89-0035 "Cyclic Undrained Behavior of Nonplastic and Low Plasticity Silts," by A.J. Walker and H.E. Stewart, 7/26/89, (PB90-183518/AS).

NCEER-89-0036 "Liquefaction Potential of Surficial Deposits in the City of Buffalo, New York," by M. Budhu, R. Giese and L. Baumgrass, 1/17/89, (PB90-208455/AS).

NCEER-89-0037 "A Determinstic Assessment of Effects of Ground Motion Incoherence," by A.S. Veletsos and Y. Tang, 7/15/89, (PB90-164294/AS).

NCEER-89-0038 "Workshop on Ground Motion Parameters for Seismic Hazard Mapping," July 17-18, 1989, edited by R.V. Whitman, 12/1/89, (PB90-173923/AS).

NCEER-89-0039 "Seismic Effects on Elevated Transit Lines of the New York City Transit Authority," by C.J. Costantino, C.A. Miller and E. Heymsfield, 12/26/89, (PB90-207887/AS).

NCEER-89-0040 "Centrifugal Modeling of Dynamic Soil-Structure Interaction," by K. Weissman, Supervised by J.H. Prevost, 5/10/89, (PB90-207879/AS).

NCEER-89-0041 "Linearized Identification of Buildings With Cores for Seismic Vulnerability Assessment," by I-K. Ho and A.E. Aktan, 11/1/89, (PB90-251943/AS).

NCEER-90-0001 "Geotechnical and Lifeline Aspects of the October 17, 1989 Loma Prieta Earthquake in San Francisco," by T.D. O'Rourke, H.E. Stewart, F.T. Blackburn and T.S. Dickerman, 1/90, (PB90-208596/AS).

NCEER-90 0002 "Nonnormal Secondary Response Due to Yielding in a Primary Structure," by D.C.K. Chen and L.D. Lutes, 2/28/90, (PB90-251976/AS).

NCEER-90-0003 "Earthquake Education Materials for Grades K-12," by K.E.K. Ross, 4/16/90, (PB91-113415/AS).

NCEER-90-0004 "Catalog of Strong Motion Stations in Eastern North America," by R.W. Busby, 4/3/90, (PB90-251984)/AS.

NCEER-90-0005 "NCEER Strong-Motion Data Base: A User Manuel for the GeoBase Release (Version 1.0 for the Sun3)," by P. Friberg and K. Jacob, 3/31/90 (PB90-258062/AS).

NCEER 90-0006 "Seismic Hazard Along a Crude Oil Pipeline in the Event of an 1811-1812 Type New Madrid Earthquake," by H.H.M. Hwang and C-H.S. Chen, 4/16/90(PB90-258054).

NCEER-90-0007 "Site-Specific Response Spectra for Memphis Sheahan Pumping Station," by H.H.M. Hwang and C.S. Lee, 5/15/90, (PB91-108811/AS).

NCEER-90-0008 "Pilot Study on Seismic Vulnerability of Crude Oil Transmission Systems," by T. Ariman, R. Dobry, M. Grigoriu, F. Kozin, M. O'Rourke, T. O'Rourke and M. Shinozuka, 5/25/90, (PB91-108837/AS).

NCEER-90-0009 "A Program to Generate Site Dependent Time Histories: EQGEN," by G.W. Ellis, M. Srinivasan and A.S. Cakmak, 1/30/90, (PB91-108829/AS).

NCEER-90-0010 "Active Isolation for Seismic Protection of Operating Rooms," by M.E. Talbott, Supervised by M. Shinozuka, 6/8/9, (PB91-110205/AS).

NCEER-90-0011 "Program LINEARID for Identification of Linear Structural Dynamic Systems," by C-B. Yun and M. Shinozuka, 6/25/90, (PB91-110312/AS).

NCEER-90-0012 "Two-Dimensional Two-Phase Elasto-Plastic Seismic Response of Earth Dams," by A.N. Yiagos, Supervised by J.H. Prevost, 6/20/90, (PB91-110197/AS).

NCEER-90-0013 "Secondary Systems in Base-Isolated Structures: Experimental Investigation, Stochastic Response and Stochastic Sensitivity," by G.D. Manolis, G. Juhn, M.C. Constantinou and A.M. Reinhorn, 7/1/90, (PB91-110320/AS).

NCEER-90-0014 "Seismic Behavior of Lightly-Reinforced Concrete Column and Beam-Column Joint Details," by S.P. Pessiki, C.H. Conley, P. Gergely and R.N. White, 8/22/90, (PB91-108795/AS).

NCEER-90-0015 "Two Hybrid Control Systems for Building Structures Under Strong Earthquakes," by J.N. Yang and A. Danielians, 6/29/90, (PB91-125393/AS).

NCEER-90-0016 "Instantaneous Optimal Control with Acceleration and Velocity Feedback," by J.N. Yang and Z. Li, 6/29/90, (PB91-125401/AS).

NCEER-90-0017 "Reconnaissance Report on the Northern Iran Earthquake of June 21, 1990," by M. Mehrain, 10/4/90, (PB91-125377/AS).

NCEER-90-0018 "Evaluation of Liquefaction Potential in Memphis and Shelby County," by T.S. Chang, P.S. Tang, C.S. Lee and H. Hwang, 8/10/90, (PB91-125427/AS).

NCEER-90-0019 "Experimental and Analytical Study of a Combined Sliding Disc Bearing and Helical Steel Spring Isolation System," by M.C. Constantinou, A.S. Mokha and A.M. Reinhorn, 10/4/90, (PB91-125385/AS).

NCEER-90-0020 "Experimental Study and Analytical Prediction of Earthquake Response of a Sliding Isolation System with a Spherical Surface," by A.S. Mokha, M.C. Constantinou and A.M. Reinhorn, 10/11/90, (PB91-125419/AS).

NCEER-90-0021 "Dynamic Interaction Factors for Floating Pile Groups," by G. Gazetas, K. Fan, A. Kaynia and E. Kausel, 9/10/90, (PB91-170381/AS).

NCEER-90-0022 "Evaluation of Seismic Damage Indices for Reinforced Concrete Structures," by S. Rodríguez-Gómez and A.S. Cakmak, 9/30/90, PB91-171322/AS).

NCEER-90-0023 "Study of Site Response at a Selected Memphis Site," by H. Desai, S. Ahmad, E.S. Gazetas and M.R. Oh, 10/11/90, (PB91-196857/AS).

NCEER-90-0024 "A User's Guide to Strongmo: Version 1.0 of NCEER's Strong-Motion Data Access Tool for PCs and Terminals," by P.A. Friberg and C.A.T. Susch, 11/15/90, (PB91-171272/AS).

NCEER-90-0025 "A Three-Dimensional Analytical Study of Spatial Variability of Seismic Ground Motions," by L-L. Hong and A.H.-S. Ang, 10/30/90, (PB91-170399/AS).

NCEER-90-0026 "MUMOID User's Guide - A Program for the Identification of Modal Parameters," by S. Rodríguez-Gómez and E. DiPasquale, 9/30/90, (PB91-171298/AS).

NCEER-90-0027 "SARCF-II User's Guide - Seismic Analysis of Reinforced Concrete Frames," by S. Rodríguez-Gómez, Y.S. Chung and C. Meyer, 9/30/90, (PB91-171280/AS).

NCEER-90-0028 "Viscous Dampers: Testing, Modeling and Application in Vibration and Seismic Isolation," by N. Makris and M.C. Constantinou, 12/20/90 (PB91-190561/AS).

NCEER-90-0029 "Soil Effects on Earthquake Ground Motions in the Memphis Area," by H. Hwang, C.S. Lee, K.W. Ng and T.S. Chang, 8/2/90, (PB91-190751/AS).

NCEER-91-0001 "Proceedings from the Third Japan-U.S. Workshop on Earthquake Resistant Design of Lifeline Facilities and Countermeasures for Soil Liquefaction, December 17-19, 1990," edited by T.D. O'Rourke and M. Hamada, 2/1/91, (PB91-179259/AS).

NCEER-91-0002 "Physical Space Solutions of Non-Proportionally Damped Systems," by M. Tong, Z. Liang and G.C. Lee, 1/15/91, (PB91-179242/AS).

NCEER-91-0003 "Kinematic Seismic Response of Single Piles and Pile Groups," by K. Fan, G. Gazetas, A. Kaynia, E. Kausel and S. Ahmad, 1/10/91, to be published.

NCEER-91-0004 "Theory of Complex Damping," by Z. Liang and G. Lee, to be published.

NCEER-91-0005 "3D-BASIS - Nonlinear Dynamic Analysis of Three Dimensional Base Isolated Structures: Part II," by S. Nagarajaiah, A.M. Reinhorn and M.C. Constantinou, 2/28/91, (PB91-190553/AS).

NCEER-91-0006 "A Multidimensional Hysteretic Model for Plasticity Deforming Metals in Energy Absorbing Devices," by E.J. Graesser and F.A. Cozzarelli, 4/9/91.

NCEER-91-0007 "A Framework for Customizable Knowledge-Based Expert Systems with an Application to a KBES for Evaluating the Seismic Resistance of Existing Buildings," by E.G. Ibarra-Anaya and S.J. Fenves, 4/9/91, (PB91-210930/AS).

NCEER-91-0008 "Nonlinear Analysis of Steel Frames with Semi-Rigid Connections Using the Capacity Spectrum Method," by G.G. Deierlein, S-H. Hsieh, Y-J. Shen and J.F. Abel, 7/2/91, (PB92-113828/AS).

NCEER-91-0009 "Earthquake Education Materials for Grades K-12," by K.E.K. Ross, 4/30/91, (PB91-212142/AS).

NCEER-91-0010 "Phase Wave Velocities and Displacement Phase Differences in a Harmonically Oscillating Pile," by N. Makris and G. Gazetas, 7/8/91, (PB92-108356/AS).

NCEER-91-0011 "Dynamic Characteristics of a Full-Sized Five-Story Steel Structure and a 2/5 Model," by K.C. Chang, G.C. Yao, G.C. Lee, D.S. Hao and Y.C. Yeh," to be published.

NCEER-91-0012 "Seismic Response of a 2/5 Scale Steel Structure with Added Viscoelastic Dampers," by K.C. Chang, T.T. Soong, S-T. Oh and M.L. Lai, 5/17/91 (PB92-110816/AS).

NCEER-91-0013 "Earthquake Response of Retaining Walls; Full-Scale Testing and Computational Modeling," by S. Alampalli and A-W.M. Elgamal, 6/20/91, to be published.

NCEER-91-0014 "3D-BASIS-M: Nonlinear Dynamic Analysis of Multiple Building Base Isolated Structures," by P.C. Tsopelas, S. Nagarajaiah, M.C. Constantinou and A.M. Reinhorn, 5/28/91, (PB92-113885/AS).

NCEER-91-0015 "Evaluation of SEAOC Design Requirements for Sliding Isolated Structures," by D. Theodossiou and M.C. Constantinou, 6/10/91, (PB92-114602/AS).

NCEER-91-0016 "Closed-Loop Modal Testing of a 27-Story Reinforced Concrete Flat Plate-Core Building," by H.R. Somaprasad, T. Toksoy, H. Yoshiyuki and A.E. Aktan, 7/15/91.

NCEER-91-0017 "Shake Table Test of a 1/6 Scale Two-Story Lightly Reinforced Concrete Building," by A.G. El-Attar, R.N. White and P. Gergely, 2/28/91, to be published.

NCEER-91-0018 "Shake Table Test of a 1/8 Scale Three-Story Lightly Reinforced Concrete Building," by A.G. El-Attar, R.N. White and P. Gergely, 2/28/91, to be published.

NCEER-91-0019 "Transfer Functions for Rigid Rectangular Foundations," by A.S. Veletsos, A.M. Prasad and W.H. Wu, 7/31/91, to be published.

NCEER-91-0020 "Hybrid Control of Seismic-Excited Nonlinear and Inelastic Structural Systems," by J.N. Yang, Z. Li and A. Danielians, 8/1/91.

NCEER-91-0021 "The NCEER-91 Earthquake Catalog: Improved Intensity-Based Magnitudes and Recurrence Relations for U.S. Earthquakes East of New Madrid," by L. Seeber and J.G. Armbruster, 8/28/91, to be published.

NCEER-91-0022 "Proceedings from the Implementation of Earthquake Planning and Education in Schools: The Need for Change - The Roles of the Changemakers," by K.E.K. Ross and F. Winslow, 7/23/91.

NCEER-91-0023 "A Study of Reliability-Based Criteria for Seismic Design of Reinforced Concrete Frame Buildings," by H.H.M. Hwang and H-M. Hsu, 8/10/91.

NCEER-91-0024 "Experimental Verification of a Number of Structural System Identification Algorithms," by R.G. Ghanem, H. Gavin and M. Shinozuka, 9/18/91.

NCEER-91-0025 "Probabilistic Evaluation of Liquefaction Potential," by H.H.M. Hwang and C.S. Lee," 11/25/91.

NCEER-91-0026 "Instantaneous Optimal Control for Linear, Nonlinear and Hysteretic Structures - Stable Controllers," by J.N. Yang and Z. Li, 11/15/91.

NCEER-91-0027 "Experimental and Theoretical Study of a Sliding Isolation System for Bridges," by M.C. Constantinou, A. Kartoum, A.M. Reinhorn and P. Bradford, 11/15/91.